UNIVERSIDADE Đ COIMBRA

Joana Almeida Santos

Models of Functional Connectivity as Potential Biomarkers in Multiple Sclerosis using fMRI

Dissertação no âmbito do Mestrado Integrado em Engenharia Biomédica orientada pelo Doutor João Valente Duarte e pelo Doutor Rodolfo Telo Martins de Abreu apresentada ao Departamento de Física da Faculdade de Ciências e Tecnologia da Universidade de Coimbra

outubro de 2021

Resumo

A imagem por ressonância magnética (MRI, do inglês *Magnetic Resonance Imaging*) é a técnica mais utilizada no diagnóstico e monitorização da esclerose múltipla (MS, do inglês *Multiple Sclerosis*). O uso da imagem por ressonância magnética funcional (fMRI, do inglês *functional MRI*) tem sido cada vez mais comum na identificação de padrões de conetividade funcional (FC, do inglês *functional connectivity*) na MS, principalmente com o cérebro em repouso. Padrões de ativação anormais na MS também foram encontrados durante a realização de tarefas, mas não há consenso sobre as mudanças da FC neste contexto.

Esta tese tem como objetivo recolher dados fMRI e explorar as mudanças da FC no cérebro de doentes com MS em relação a controlos saudáveis, durante tarefas de perceção de movimento visual passivo e de movimento biológico, bem como descrever quantitativamente essas alterações. Para cada participante, o sinal fMRI médio de dezasseis regiões do cérebro (oito em cada hemisfério) envolvidas nas tarefas foi calculado, e a FC foi determinada através da Causalidade de Granger (valores F). As matrizes de conetividade foram comparadas entre grupos para identificar quais as ligações alteradas na MS. Além disso, medidas quantitativas de conetividade foram extraídas com base na teoria de grafos. A correlação entre a FC e dados neuropsicológicos dos doentes também foi analisada.

Durante ambas as tarefas, foi observado um aumento geral dos valores F na MS, bem como alterações nas ligações recrutadas pelas tarefas, com mais envolvimento de regiões de alto nível na tarefa de movimento biológico. A disparidade dos valores F entre os grupos indica que uma sobrecompensação pode ocorrer na MS durante o desempenho de tarefas envolvendo regiões críticas. Além disso, a análise com teoria dos grafos revelou que as propriedades topológicas da rede estavam alteradas na MS e que, ao contrário de estudos anteriores, doentes com MS apresentavam valores de eficiência mais elevados. Mudanças significativas na FC foram também encontradas na correlação dos valores F com os dados neuropsicológicos, o que contribui para a compreensão dos mecanismos subjacentes às alterações cognitivas na MS.

Conseguimos reforçar a ideia de que a MS é uma doença de desconexão que afeta a função cerebral e provar que a análise multivariada de dados fMRI pode contribuir para o estudo dos mecanismos anormais e adaptativos da MS.

Palavras-chave

Esclerose múltipla; fMRI em tarefa; Conetividade funcional; Causalidade de Granger; Teoria de grafos

Abstract

Magnetic resonance imaging (MRI) is the gold standard for diagnosing and monitoring Multiple Sclerosis (MS). More recently, functional MRI (fMRI) has been used to identify functional connectivity (FC) patterns in MS, mostly during resting-state. Abnormal fMRI activation patterns have also been found during task performance, but there is no consensus regarding these FC changes in MS.

This thesis aims to collect fMRI data and explore changes of brain directed FC in MS patients relative to healthy controls during visual passive motion and biological motion perception tasks and quantitively describe these alterations. For each participant, the average fMRI signal within sixteen brain regions (8 in each hemisphere) elicited by the task was computed, and the pairwise FC was calculated using Granger Causality (F-values). The connectivity matrices were compared between groups to identify which connections were altered in MS. Furthermore, quantitative connectivity measures were extracted using concepts from graph theory. The correlation between F-values and neuropsychological data of the patients was also analysed.

During both tasks, a general increase of the F-values was observed in MS, as well as alterations in the connections employed in the tasks, with high-order regions being more involved in the biological motion task. The disparity of F-values between groups indicates that overcompensation may occur in MS during task performance involving critical brain regions. Moreover, graph theory analysis revealed that the network's topological properties were altered in MS and that, contrary to previous research, MS presented higher efficiency values. Significant alterations between groups in FC were found when correlating F-values with neuropsychological data, which further contributes to the understanding of the underlying mechanisms of cognitive impairment in MS.

We were able to reinforce that MS is a disconnection disease that affects brain function and prove that multivariate analysis of fMRI data might contribute to the study of the abnormal and adaptive mechanisms of MS.

Keywords

Multiple sclerosis; Task-based fMRI; Functional connectivity; Granger causality; Graph theory

Agradecimentos

Finalizado este percurso de cinco anos, não poderia deixar de agradecer a todos os que dele fizeram parte.

Aos meus orientadores, Doutor João Valente Duarte e Doutor Rodolfo Abreu, pela orientação exemplar, pelo interesse e empenho demonstrado, por todos os conselhos e críticas construtivas e, acima de tudo, pela forma como me fizeram sentir integrada neste projeto desde o primeiro dia.

À Júlia e ao Dani por me terem sempre acompanhado no curso, na minha vida académica e, principalmente, por terem sido os meus guias neste último ano, durante a realização da tese.

A todos os meus amigos, de Seia e os que tive a felicidade de conhecer em Coimbra, um especial 'obrigada' pelo apoio indispensável e por, no meio de tantas horas passadas em cafés, me terem ajudado a crescer.

Aos meus pais, pelos 23 anos de paciência e compreensão. Pelo orgulho que sempre demonstraram e pelo apoio incondicional que sempre tornou tudo possível.

Aos meus avós, longe, mas sempre perto, que foram e serão sempre um exemplo para mim.

À Universidade de Coimbra, e em especial ao Departamento de Física, que me acolheram nesta cidade e mudaram a minha vida.

A todos, *obrigada*.

Contents

List of Tables

List of Figures

List of Acronyms

2D	Two-dimensional
3D	Three-dimensional
4D	Four-dimensional
AD	Alzheimer's disease
AIC	Akaike information criterion
aINS	Anterior insula
BCT	Brain connectivity toolbox
BIC	Bayesian information criterion
BM	Biological motion
BOLD	Blood oxygen level dependent
BVMT	Brief visuospatial memory test
CBF	Cerebral blood flow
CBV	Cerebral blood volume
CIS	Clinically isolated syndrome
CMRO$_2$	Cerebral metabolic rate of oxygen
CNS	Central nervous system
CNT	Healthy controls
CSF	Cerebrospinal fluid
CVLT	California verbal learning test
dHB	Deoxyhemoglobin
DCM	Dynamic causal modelling
DMTs	Disease modifying therapies
EBA	Extrastriate body area
EC	Effective connectivity
EDSS	Expanded disability status scale
EPI	Echo planar imaging
FBA	Fusiform body area
FC	Functional connectivity
FDR	False discovery rate
FFG	Fusiform gyrus
fMRI	Functional magnetic resonance imaging
GC	Granger causality
GCA	Granger causality analysis
GLM	General linear model
GM	Grey matter

HbO$_2$	Oxyhemoglobin
HRF	Hemodynamic response function
IFG	Inferior frontal gyrus
KS	Kolmogorov-Smirnov
LWR	Levinson-Wiggins-Robinson
MFIS	Modified fatigue impact scale
MP2RAGE	Magnetization-prepared 2 rapid acquisition gradient echoes
MRI	Magnetic resonance imaging
MS	Multiple sclerosis
MSC	Multiple sclerosis patients
MVGC	Multivariate Granger causality
OLS	Ordinary least squares
PASAT	Paced auditory serial addition test
PPMS	Primary progressive multiple sclerosis
pSTS	Posterior superior temporal sulcus
PTh	Proportional threshold
RF	Radio frequency
RME	Reading the mind with the eyes
ROI	Region of interest
RRMS	Relapsing-remitting multiple sclerosis
rs-fMRI	Resting-state functional magnetic resonance imaging
RUN V1MT	V1MT localiser run
RUNS BM	Biological motion run
SDMT	Symbol digit modalities test
sMRI	Structural magnetic resonance imaging
SPMS	Secondary progressive multiple sclerosis
TE	Time of echo
TR	Time of repetition
V3	Visual area 3
V5/hMT+	Middle temporal visual area
VAR	Vector autoregressive
WM	White matter

1
Introduction

1.1 Motivation

Multiple sclerosis (MS) is the most common chronic neurological pathology among young adults between 20 and 40 years old (Oh, Vidal-Jordana and Montalban, 2018) (Dobson and Giovannoni, 2019). It primarily affects the central nervous system (CNS), particularly the myelin sheaths around nerve cells, which have a critical role in the transmission of the nervous signal and, thus, in the efficiency of the information exchange between brain regions that will eventually translate into body movements, actions, and thoughts. MS symptoms, depending on where MS lesions develop on the brain and spinal cord, can manifest themselves in several different ways, such as decreased motor coordination, bladder issues, chronic pain, muscle spasms, extreme fatigue, and changes in speech. Overall, cognitive problems and reduced mobility characterize this pathology, which will gradually but inevitably result in the loss of the patient's independence (Rodriguez-Rincon *et al.*, 2019).

The disease is chronic, irreversible, and usually progressive, and there are still no concrete explanations about what causes it. Additionally, the existing treatments do not offer a resolution, focusing mainly on controlling the progression of the disease and diminishing the discomfort of those affected. This uncertainty and incomplete understanding of MS, but also the prospect of a potential severe disability, dramatically affects the patients and everyone who cares for them, not only when considering the socio-economic aspects that it encompasses, but also the psychological and mental-wellness ones, even leading to anxiety and depression (Sousa *et al.*, 2018).

MS also has an extensive impact on society, especially in its economy. Costs of MS involve the healthcare system's support, the loss of productivity at work, informal care time, or medication. According to reports from the United Kingdom, the costs of progressive MS reach about £3 billion per year (Doshi and Chataway, 2017) (Rodriguez-Rincon *et al.*, 2019).

A worrisome aspect of this condition is that its prevalence is rapidly increasing. According to a recent report (Walton *et al.,* 2020), MS diagnosis has increased 30% since 2013, and currently, 2.8 million people suffer from this disease, making its global prevalence an average of 35.9 per 100,000 people worldwide. MS affects females twice as much as males, a difference that is becoming more noticeable with time, and that can be detrimental in the building of careers and planning of families, with the likelihood of women having children being drastically decreased (Walton *et al.,* 2020).

Thus, the need for a better understanding of the aetiology, mechanisms of progression, and possible cures of MS is fundamental. While there is still a long way to go in the search for answers, studies have already shown that a prompt treatment upon diagnosis slows down the progression of the disease, reduces disability, extends lifetime expectancy, which is decreased by approximately ten years in MS (Oh, Vidal-Jordana and Montalban, 2018), and overall provides a better quality of life. Hence, the focus in more recent investigations, in addition to provide an accurate and rapid diagnosis, is to search for biomarkers that provide information about whether a particular characteristic is indicative of disease progression and how it relates to existing treatments. Finding such biomarkers is crucial to reliably assess disease progression to better adjust interventions. This process is progressively facilitated through imaging techniques, such as Magnetic Resonance Imaging (MRI), that allow a better comprehension of the human brain and, even more recently, its functions and connectivity (Walton *et al.,* 2020).

1.2 Proposed Approach

This Master's Thesis aims primarily at understanding multiple sclerosis' hallmarks and discriminative features by implementing models of the brain's functional connectivity during task performance. The proposed approach is to extract quantitative connectivity measures in patients in early phases of MS, particularly Relapsing-Remitting Multiple Sclerosis (RRMS), and compare them to those extracted from a demographically matched healthy control group.

Data is obtained through functional Magnetic Resonance Imaging (fMRI) while the subject performs a visual task. Realistic brain networks are then constructed, and measures of neuronal functional connectivity are obtained through Granger Causality Analysis (GCA) and graph theory analysis. Finally, neuropsychological data collected from the MS patients is correlated with previously attained functional connectivity values. In addition to allowing an overview of the pathophysiology of the disease, these results, by providing an objective observation of the impact of MS on the communication between different regions of the brain, will further help achieve a posterior main goal, the identification of MS progression biomarkers. Hopefully, by investigating new biomarkers of brain connectivity in MS, this is a step forward in providing a more reliable diagnosis as well as tools to quantitatively follow disease progression and clinical improvement during treatment, which might improve the management of this condition.

1.3 Objectives, Hypotheses and Original Contributions

Several neuroimaging studies in multiple sclerosis focus on patterns of brain activation. However, there is still a lack of knowledge regarding quantitative connectivity measures that aim to describe brain function and information processing in MS. In addition, while the literature on brain connectivity is growing, almost all the existing projects in MS examine undirected functional connectivity (simple correlation between pairs of signals) of the brain in its resting state, i.e., when there is no explicit task-related activity. As task performance can provide new types of reliable information, since our brain is constantly performing tasks that allow us to move and think, this thesis intends to investigate brain directed functional connectivity in MS during a visual task with the help of functional imaging techniques.

The specific objectives of this master's thesis are the following:
- Construction of the participant's brain networks, represented by directed functional connectivity matrices, through collected fMRI data and the use of GCA. This data is acquired while the participants are executing two visual perception tasks, as this information can further clarify the importance of the connections between distant brain regions (and its impairment in MS) and may provide new biomarkers for the disease. The visual tasks were chosen as they are very simple and involve an already known network of regions that can be thoroughly studied.
- Analysis of the significantly different connections between healthy controls and patients with multiple sclerosis.
- Extraction of global and local quantitative connectivity measures that describe brain function and efficiency in the information exchange between regions.
- Exploration of the correlation between functional connectivity data, obtained with GCA, and the neuropsychological evaluation of MS patients, to investigate the

relationship between brain connectivity and characteristic clinical symptoms and cognitive difficulties.

Some hypotheses were outlined a priori, based on previous research done in this context. First and foremost, an increase of connectivity in the MS patient's group, as a result of compensatory neuroplasticity, was expected, as well as alterations in the connection patterns in MS patients when performing the tasks. Additionally, alterations in the connectivity measures were also anticipated, with a tendency for a decrease in network efficiency.

1.4 Thesis Outline

This chapter presents the motivation underlying the development of this master's thesis, stating the proposed approach and its main objectives, the outline, and the outputs beyond the thesis. The thesis comprises six main chapters, including Chapter 1 with the Introduction to the topic and the thesis document. Chapter 2 begins by exploring and explaining the fundamentals of multiple sclerosis and concepts regarding fMRI and brain connectivity. The importance of task-related fMRI studies will also be addressed. Chapter 3 discusses the state of the art concerning fMRI and brain connectivity in the context of MS through a comprehensive literature review and provides guidance for the future obtained results. Chapter 4 will present the approach and methodology of the study: the type of data, the experimental setup, the methods for construction of brain networks, and the software used to extract the connectivity measures. Chapter 5 summarizes the results and discusses them extensively. Finally, Chapter 6 will present the take-home messages and conclude with the study's limitations and possible future work.

1.5 Thesis Outputs

The work described in this thesis resulted in one abstract submitted and accepted for poster presentation in the peer-reviewed international conference European Committee for Treatment and Research in Multiple Sclerosis (ECTRIMS), and was "*awarded an abstract grant based on the scientific quality of the abstract*":

Duarte JV, **Santos J**, Abreu R, Soares JF, Batista S, Lima AC, Sousa L, Castelo-Branco M (2021). *Probing brain effective connectivity in early MS patients with Granger causality analysis of task-fMRI (abstract)*. 37th Congress of European Committee for Treatment and Research in Multiple Sclerosis - ECTRIMS 2021.

2

Background and Literature Review

2.1 Multiple Sclerosis

Multiple sclerosis is a neurodegenerative disease that targets the CNS, causing irreversible damage to the brain and spinal cord and leading to an array of debilitating symptoms.

The condition's aetiology is still poorly understood, which is an obstacle in its prevention and prompt treatment. However, studies have shown that its onset may be multifactorial due to a combination of genetic factors, infections by viruses (particularly the Epstein-Barr virus), obesity, smoking, or even influenced by environmental factors, such as lack of vitamin D and exposure to ultraviolet-B light (Goldenberg, 2012) (Doshi and Chataway, 2017) (Dobson and Giovannoni, 2019).

Ultimately, MS is considered an autoimmune disease arising from the response of the adaptive immune system against antigens coming from the CNS: when lymphocytes migrate through the blood-brain barrier, that separates the circulatory and the nervous system in the brain, they will trigger several sources of inflammation, from T- and B-cell clonal expansion to mitochondrial damages that lead to energy failure and oxidative damage (Doshi and Chataway, 2017). This response will damage the myelin sheaths of neurons, a process called *demyelination*. Demyelination, together with infiltrates of inflammatory cells, forms the well-known lesions, also known as scars or plaques, generally in white matter (WM) regions but also in grey matter (GM) (Goldenberg, 2012). As the disease progresses, axonal damage/loss is also observed (Filippi and Rocca, 2009) (Dobson and Giovannoni, 2019).
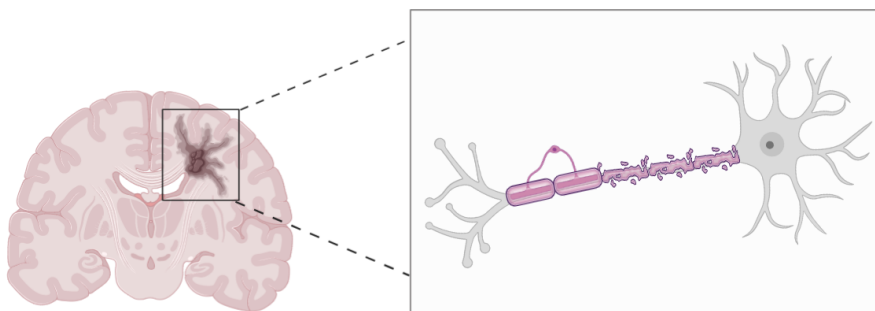
Figure 2.1 - Brain lesions in MS and demyelination of the neuron's axon sheaths (created with BioRender.com).

As myelin surrounds and insulates axons, it has an essential role in the rate at which action potentials (electric impulses) and the nervous signals are propagated and, thus, has a crucial role in the information propagation from one brain region to another. When inflammation and demyelination occur, this process is compromised, and there is an interruption of the nervous stimulus and information flow, i.e., there are connectivity damages. This situation occurs in various degrees and directly affects motor and sensitive functions (Peixoto and Abreu, 2016).
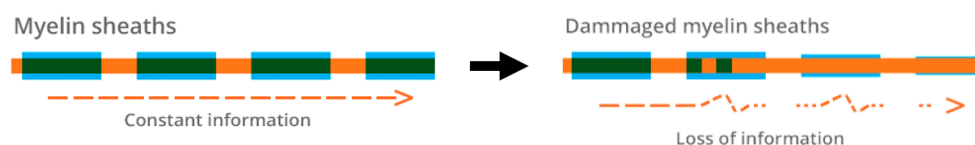
Figure 2.2 - Connectivity damages and loss of information flow (GAEM, 2017, available at:
https://fundaciongaem.org/en/what-is-multiple-sclerosis/).
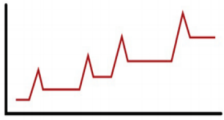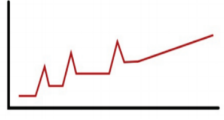
Initial symptoms of MS involve sensory disturbances such as paresthesias (which includes numbness and tingling), dysesthesias (burning and "pins and needles" sensations), bladder disturbances and others. These usually resolve but can eventually develop into chronic neuropathic pain. Moreover, MS patients suffer from severe mobility impairment, visual problems, impaired memory, and disconcerting fatigue (Goldenberg, 2012).
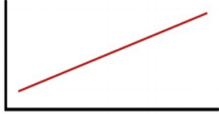
2.1.1 Phenotypes and Clinical Features

In approximately 80% of reported cases, MS is suspected for the first time when a patient presents a set of characteristics known as a *clinically isolated syndrome* (CIS), which is an acute clinical episode/attack of focal neurological changes that suggest demyelination in the CNS and lasts for longer than twenty-four hours, with no signs of infection (Doshi and Chataway, 2017). CIS is always isolated in time, and usually, it is isolated in space, with common lesions in the optical nerve (sometimes originating optical neuritis), spinal cord, brainstem, cerebellum or, in rare cases, in a cerebral hemisphere (Peixoto and Abreu, 2016) (Dobson and Giovannoni, 2019). CIS is not considered a type of MS because it does not fulfil dissemination in time criteria (section 2.1.2); however, it can eventually convert to an early phase of MS (relapsing-remitting MS) (Lublin *et al.*, 2014) (Doshi and Chataway, 2017).

MS is divided into three major types based on the patient's clinical characteristics (Table 2.1). However, there is no characteristic histological distinction between the types. Thus, because MS evolution is usually progressive, it is often assumed that the pathological changes form a continuous spectrum, ranging from relapsing (or 'inflammatory dominant'), in which the patients experience improvement in their symptoms after an attack, to progressive (or 'neurodegenerative dominant'), happening when delayed neurodegeneration ultimately leads to non-relapsing progression (Goldenberg, 2012) (Oh, Vidal-Jordana and Montalban, 2018) (Dobson and Giovannoni, 2019).

Table 2.1 - Types of MS and respective main characteristics. In the graphs describing the progression of MS (left column), the x-axis represents time, and the y-axis represents the level of disability (Goldenberg, 2012) (National Multiple Sclerosis Society, 2013) (Lublin *et al.*, 2014) (Doshi and Chataway, 2017) (Oh, Vidal-Jordana and Montalban, 2018) (Thompson et al., 2018) (Dobson and Giovannoni, 2019) (Rodriguez-Rincon *et al.*, 2019).

Type of MS	Main Characteristics
Relapsing–remitting MS (RRMS)	RRMS is the most common disease course, affecting nearly 85% of MS patients. It is characterized by intercalation of flare-ups (or relapses), which involve worsening of the symptoms, with periods of clinical recovery (or remission) when symptoms disappear, and the progression of the disease is apparently stagnated. Relapses happen due to the demyelination of brain areas and evolve over twenty-four hours, persisting for some time before improving. Even though it is not noticeable, there is an accumulation of disability, including brain atrophy, with every relapse since there is an excess of ongoing inflammation
Secondary progressive MS (SPMS)	Generally, when RRMS patients are not treated, up to 80% of the cases evolve into secondary progressive MS, 10 to 15 years after the initial diagnosis. Relapses cease to exist, and, as the name indicates, there is a progressive worsening of the disease and its symptoms and, thus, an irreversible accumulation of disability and loss of neurologic functions. There may be periods of remission and plateaus of symptom severity. Hallmarks of this type of MS are axonal injury and increased atrophy in white and grey matter, but less inflammation.

Primary progressive MS (PPMS)	PPMS is the only type of MS characterized by progressive disability from the outset, generally due to a disease in the spinal cord. It affects 15% of people with MS, and most of them are only diagnosed after 40 years old. There are no relapses and remissions, and their symptoms will gradually worsen from the moment of diagnosis. Nonetheless, there may be plateaus in disease evolution

The progression of different features of MS and the decrease in the quantity of the relapses (but more difficulty in recovering from them), is described in figure 2.3.
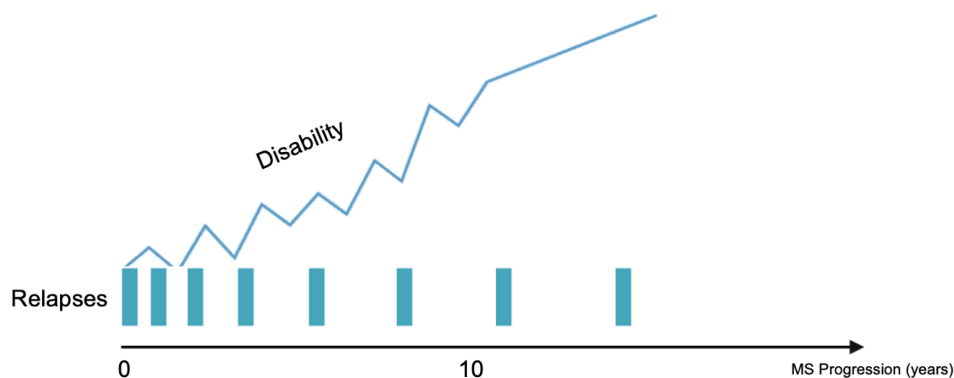
Figure 2.3 - Disability progression and frequency of relapses during MS evolution. The x-axis represents time in years, the top part of the y-axis represents the level of disability and the bottom part of the y-axis represents the quantity of relapses. Accumulation of disability in RRMS eventually leads to severe neurodegeneration and a progressive disease course after 10–15 years of the initial diagnosis. There is less focal inflammation, as seen through the reduction in relapses. (Adapted from (Doshi and Chataway, 2017)) (created with BioRender.com).

2.1.2 Multiple Sclerosis Diagnosis

The diagnosis of MS is mainly made through clinical findings and evidence provided by MRI or the analysis of cerebrospinal fluid (CSF). These techniques can estimate the risk of CIS converting into MS and propel treatment prescription in the earliest stages, hence diminishing morbidity (Goldenberg, 2012) (Peixoto and Abreu, 2016).

Several clinical indicators can predict the conversion of CIS to MS as well as the disease course, such as age, sex, frequency of relapses and accumulation of disability after disease onset, but lesions observed in MRI (both in the brain and spinal cord) and the presence of CSF-specific oligoclonal bands, which are immunoglobulins that suggest inflammation of the CNS, are the primary biomarkers of this pathology (Oh, Vidal-Jordana and Montalban, 2018). Symptoms and examinations are relevant but do not represent the actual number of brain lesions: most of these lesions that can be detected with MRI are clinically silent (Traboulsee *et al.*, 2005). Therefore, MRI is considered the most reliable technique for diagnosing MS, given its higher predictive value (Peixoto and Abreu, 2016).

In a T2-weighted MRI protocol, the hallmarks of MS, determinant in the long-term disease outcome, are the focal lesions in WM, particularly affecting the periventricular regions of the brain, but also in GM regions (Tahedl *et al.*, 2018) (Fleischer *et al.*, 2019).
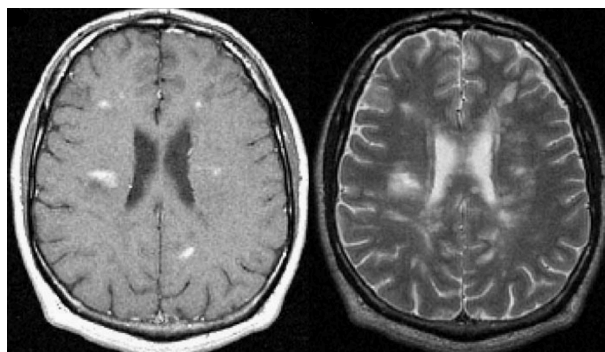
Figure 2.4 - Brain axial MRI scan of an RRMS patient. (Left) T1-weighted image (taken after lesion enhancing through gadolinium administration); (Right) T2-weighted image. The MS lesions are shown in white in both images, mainly in the brain's periventricular regions. In the T1-weighted image the lesions appear as white thanks to gadolinium administration. Adapted from (Trip and Miller, 2005). In MS, myelin, which contains fat tissue, is stripped away from nerve cells, which causes the area to hold more water. This difference between tissues is shown in the MRI scan with either brighter or darker areas depending on the type of scan (Schild and Berlex Laboratories, 1999). T1 and T2 refer to the time between tissue excitation and image capture in MRI (Kashou, 2014). Each method (T1 and T2) can detect different structures or chemicals in the CNS. For example, in a T1-weighted image, fluids and inflamed areas are dark, whereas fat tissues and WM are bright, and this method provides information about disease activity, highlighting actively inflamed areas. In turn, in a T2-weighted image, fluids and inflamed areas are bright, and the disease burden or lesion load (that is, the total amount of lesioned areas) is better analysed (Filippi and Rocca, 2011).

At least one of the following criteria must be met to form a diagnostic with MRI (Goldenberg, 2012):

- *Space Dissemination Criterion* - evidence of at least two lesions in the WM of CNS.
- *Time Dissemination Criterion* - evidence of at least two episodes (relapses) during the course of MS. This criterion must be confirmed by clinical signs on MRI images, at least three months after the previous clinical episode.
- *Inflammatory Criterion* - analysis of CSF is able to prove chronic CNS inflammation.

The McDonald criteria were created to facilitate proving these criteria, particularly dissemination in space and time. The most recent revisions were made in 2017 to anticipate the diagnosis and prevent the progression of the disease. Table 2.2 shows the data needed for a diagnosis, based on the number of relapses that have occurred and the number of lesions (Peixoto and Abreu, 2016) (Thompson et al., 2018).

Table 2.2 - McDonald Criteria, revisions from 2017 (Thompson et al., 2018). These criteria help in the diagnosis of MS.

Number of Relapses	Number of Lesions (with objective clinical evidence)	Additional data needed for a diagnosis
≥ 2	≥ 2	None, since the clinical evidence is sufficient.
≥ 2	1 (and evidence of a previous relapse involving damage in a different location)	None, since the clinical evidence is sufficient.
≥ 2	1	Dissemination in space proven with: • MRI (one or more lesions) **OR** • Additional relapse (which implicates damage at a different CNS site)
1	≥ 2	Dissemination in time proven with: • MRI (new lesion since previous scan) **OR** • Additional relapse **OR** • CSF-specific oligoclonal bands

1 (Clinically isolated syndrome)	1	Dissemination in space proven with: • MRI (one or more lesions) **OR** • Additional relapse **OR** **AND** dissemination in time proven with: • MRI (new lesion since previous scan) • Additional relapse • CSF-specific oligoclonal bands
0 (Primary progressive multiple sclerosis)	—	≥1 year of disability progression (symptoms + ongoing observation) determined with either two of the following: • One or more brain lesions (MRI) • Two or more spinal cord lesions (MRI) • CSF-specific oligoclonal bands

There is no definitive **cure** for MS. Its treatment mainly consists of *disease-modifying therapies* (DMTs) that try to suppress inflammation and disease activity, shortening the duration of relapses and decreasing their frequency, and *symptomatic therapies* that are not MS-specific but instead target each symptom provoked by the disease (such as bladder dysfunction and neuropathic pain) and intend to diminish the patient's discomfort and maintain function, temporarily (Goldenberg, 2012) (Dobson and Giovannoni, 2019).

2.1.3 Expanded Disability Status Scale

Every person suffering from MS has a different disease progression. Therefore, it is relevant to find a quantitative measure or scale to describe it, particularly in terms of physical disability. The Expanded Disability Status Scale (EDSS), represented in figure 2.5, primarily measures how much patients are physically affected by the disease. It is an ordinal rating system ranging from 0, where physical symptoms are practically null, and everything is considered "normal", and 10, which is death due to MS, in 0.5 increments (when EDSS reaches 1). This scale may change during disease progression, given that the higher the EDSS score, the more physically disabled the patient is. Lower EDSS values (less than 4) account for impairments based on neurological examinations, EDSS values between 4 and 6 depend on aspects of walking ability, and EDSS over 6 assesses handicaps of MS patients (JF, 1983) (Meyer-Moock *et al.*, 2014).
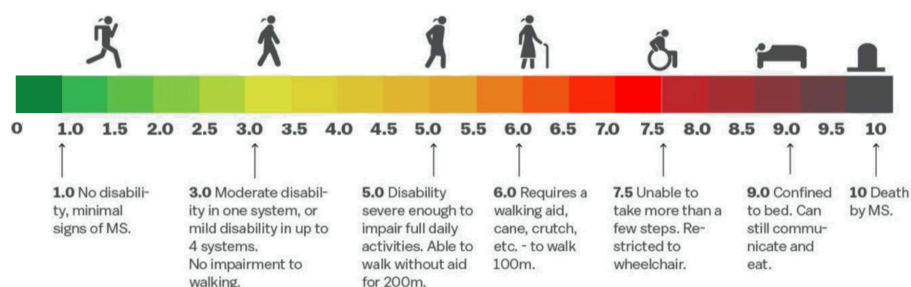
Figure 2.5 - Expanded Disability Status Scale. Adapted from: (Another MS Warrior, 2019, available at: *https://anothermswarrior.com/tag/dmt/*).

This scale is based on aspects such as (JF, 1983):
- Balance and coordination.
- Numbness (or other abnormal physical sensations).
- Bladder issues.
- Eye movement and eyesight.
- Speech and swallowing.
- Way of thinking and memory.

Nonetheless, the EDSS is far from perfect since it does not consider 'invisible' symptoms, including pain, fatigue, or depression. Furthermore, it does not take into account how MS affects the arms, hands and fingers' movements (JF, 1983).

EDSS is also used to evaluate the therapeutic interventions' effectiveness and helps decide which patients may be able to participate in clinical trials of many MS drugs. For example, people with EDSS scores above 6.5 cannot participate in DMTs trials since it is believed that these drugs do not have benefits once this level of disability is surpassed (JF, 1983) (Meyer-Moock *et al.*, 2014).

2.2 Functional MRI

Assessing brain activity and function in a non-invasive, cost-effective manner has been a challenge throughout the history of neuroscience. Therefore, the creation of new, innovative techniques was necessary given the progressive increase of cases related to neurodegenerative diseases (Logothetis, 2003) (Logothetis, 2008).

In the late 1890s, neurophysiologists Roy and Sherrington discovered the relation between cerebral blood flow and neuronal activity (Siero, Bhogal and Jansma, 2013). When John Belliveau showed that cerebral activation could be imaged using high-resolution MRI (and gadolinium administration), functional brain maps' construction was possible. Later, in 1992, Seiji Ogawa developed a technique based on BOLD (Blood Oxygen Level Dependent) imaging that leverages different magnetic properties of oxygenated and deoxygenated blood to detect changes in blood flow elicited by neuronal activation, propelling the beginning of functional Magnetic Resonance Imaging (fMRI) (Ogawa *et al.*, 1992) (Logothetis, 2008).

fMRI measures hemodynamic changes and metabolic demands after enhanced neural activity to evaluate the mechanisms involved in cognitive capacities. These conclusions are possible because fMRI activations in the brain reflect alterations of neural activity. These activations can be detected with MRI via measurements of tissue perfusion, blood oxygenation or blood volume. However, the alterations are best described by analysing the BOLD signal detected when there is neuronal activity in brain areas activated by motor, sensitive or cognitive tasks. This signal mainly depends on the underlying physiological and metabolic brain mechanisms modulating blood flow during functional stimuli, showing imaging differences in blood oxygenation (Logothetis and Wandell, 2004) (Logothetis, 2008) (Filippi and Rocca, 2009).

2.2.1 The Physics Behind Magnetic Resonance Imaging

Magnetic Resonance Imaging is the gold standard for neuroimaging given its non-invasive and non-ionizing nature that allows for the safe acquisition of detailed anatomic information as three-dimensional (3D) datasets that can be easily interpreted and thoroughly studied (Schild and Berlex Laboratories, 1999).

MRI benefits from the high prevalence of the hydrogen atoms in biological tissues, randomly orientated, and each inducing a small magnetic field due to the spin of the atoms' protons. When subjected to an external uniform magnetic field (applied through a magnet in the MRI scanner), the hydrogen protons become aligned to this magnetic field and start to precess around its axis. Posteriorly, a radio frequency (RF) pulse, i.e., a short burst of an electromagnetic wave, is sent to the patient through an RF coil, disturbing the protons and exciting them into a higher energy state. Protons then align to a certain angle with the magnetic field (depending on the RF pulse) and precess in phase with it. This excitation is only achieved if the RF pulse frequency is the same as the proton's precessing frequency, a phenomenon called *resonance*. When the RF pulse is switched off, the protons then return to their previous alignment through relaxation processes, emitting RF energy that is then measured by a receiver coil. This time-varying precession of protons causes variations in the surrounding magnetic field, and induces an electric current in the receiver coil, which in turn

translates into the MRI signal that is later rendered into 3D images of the body (Schild and Berlex Laboratories, 1999) (Logothetis and Wandell, 2004) (Kashou, 2014).
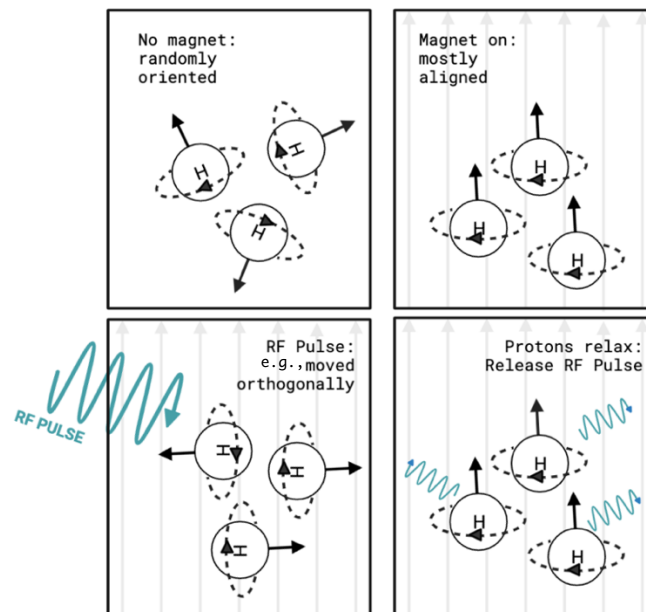
Figure 2.6 - Fundamental principles of MRI. Usually, the hydrogen protons are facing random directions (top left), until the magnetic field created by the MR scanner aligns them in the same direction (top right). A RF pulse is emitted and, consequently, the protons are excited to a higher state (bottom left). Finally, when the protons relax, they emit RF energy which is captured by the receiver coil and is transformed into the MRI signal (bottom right). Adapted from: (Farnsworth, 2019, available at: *https://imotions.com/blog/eeg-vs-mri-vs-fmri-differences*) (created with BioRender.com).

Image contrasts are determined by tissue properties, namely the different relaxation characteristics of different types of tissue and respective relaxation times (T1 and T2). T1, or longitudinal relaxation time, corresponds to the time taken by the excited protons to realign with the applied magnetic field, while T2, or transverse relaxation time, corresponds to the time taken by the protons to de-phase, i.e., lose precessing phase coherence. Different tissues have different T1 and T2 values. The contrast can also be controlled through changes in the pulse sequence. The most relevant parameters are the Time of Repetition (TR), the time taken between successive pulse sequences, and the Time of Echo (TE), the time taken between sending the RF and receiving an echo signal (Schild and Berlex Laboratories, 1999) (Kashou, 2014).

The three main components in the MRI scanner for acquiring an image are the magnet, the RF transmitter/receiver coil, which generates the RF pulse, and three spatial encoding gradient coils. The gradient coils (with x, y, and z directions) generate gradient fields that are secondary time-varying magnetic fields (meaning that they change their strength according to their position) superimposed on the applied external magnetic field to modify the strength of the original magnetic field in different locations. When these gradients are turned on and off, "slices" of the brain can be taken, i.e., two-dimensional (2D) images that are put together to define the 3D brain. Therefore, images of the slices are generated one pixel at a time, according to the location and signal strength received by the corresponding voxel. Finally, through Fourier transformation, the frequency information present in each location's signal is converted into intensity levels, which are then translated into different shades of grey in a matrix of pixels (Schild and Berlex Laboratories, 1999) (Kashou, 2014).

2.2.2 Emergence of Functional MRI

Structural MRI (sMRI) is commonly used to diagnose MS, primarily because of its high sensitivity to detect WM lesions and ease of obtaining the images. The methods applied in the analysis of sMRI are often focused on quantifying lesion load and mainly include lesion counting or volume measurements. Nonetheless, these techniques cannot detect lesions in the normal-appearing WM and GM, since these are structures only diffusely affected in MS (Fleischer *et al.*, 2019), and do not account for damages in the interaction and communication between brain regions, which are also impaired because of WM and GM lesions. These damages in the information exchange processes are particularly worrisome as they lead to altered connectivity and ultimately to physical and cognitive problems. For example, sMRI cannot depict remyelination and repair in some brain regions, as well as structural and functional brain reorganisation that plays an essential role in the progression of disability. Thus a holistic characterisation of all lesions and a detailed topological mapping of the brain is fundamental (Audoin *et al.*, 2003) (Droby *et al.*, 2016) (Fleischer *et al.*, 2019).

Studies have recently focused on the relationship between brain structure and function, and network-based approaches are increasingly used to quantitatively characterise brain organisation and further visualise functional connectivity patterns. The analysis of functional networks is made possible through the BOLD signal obtained from fMRI (Faivre *et al.*, 2016) (Fleischer *et al.*, 2019).

2.2.3 Neural Activity and BOLD Signal

Oxygen (O_2) is transported in the blood via the hemoglobin molecule. When hemoglobin is paired with oxygen molecules, it becomes oxyhemoglobin (HbO_2), and when it is devoid of oxygen, it is called deoxyhemoglobin (dHb). Oxy and deoxyhemoglobin have different magnetic properties, and therefore different effects in the MRI signal: oxyhemoglobin is *diamagnetic*, minimally affecting or distorting the magnetic field because the molecule has no unpaired electrons. On the other hand, because four of its six outer electrons are unpaired, deoxyhemoglobin is *paramagnetic*, leading to a measurable, additive magnetic field, which causes magnetic field distortions in and around the blood vessels and MRI signal loss (figure 2.7). fMRI takes advantage of these molecules' characteristics and bases its technique on detecting perturbations and alterations in the deoxyhemoglobin concentration in areas where there is neuronal activity. Thus, by analysing and comparing the amplitude and time courses of the BOLD signal, fMRI can indirectly measure brain function activity (Logothetis, 2008) (Siero, Bhogal and Jansma, 2013) (Kashou, 2014) (Duarte, 2016).
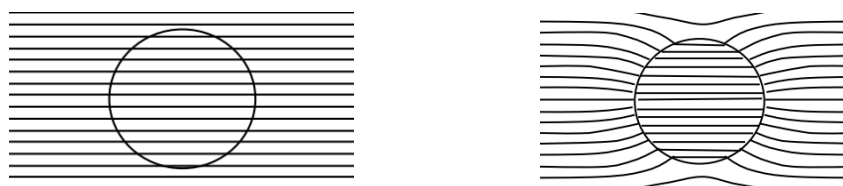
Figure 2.7 - Magnetic effect of oxyhemoglobin (left) and deoxyhemoglobin (right) in the blood vessels. dHb causes more distortions, leading to a measurable magnetic field. Adapted from (Birn, available at: *http://www.humanbrainmapping.org/files/2015/Ed%20Materials/OHBM15_AdvancedFMRI_Birn_Rasmus.pdf*).

Neuronal activity yields oxygen consumption and, consequently, causes the increase of cerebral blood volume (CBV) and cerebral blood flow (CBF) in the activated brain areas. The active process that relates neuronal activity to an increase in blood flow is called *neurovascular coupling*, which can be described as a linear transform model, meaning that for an increase in neuronal activity, there is a proportional increase in blood flow, irrespective of the pathological state, brain development and brain region. As this increase in CBV and CBF consumes energy, the delivery and supply of oxygen and glucose in these brain areas is necessary, so there will be an increase in the cerebral metabolic rate of oxygen ($CMRO_2$) extraction/consumption, which means there will be less oxygen in the blood. Thus, as the magnetic susceptibility effect associated with the paramagnetic dHb causes distortions of the magnetic field, one would expect a decrease in the fMRI signal. However, the increase in CBF overcompensates for the decrease in O_2, and although there is an increase of both CBF and $CMRO_2$, the increase of the latter is not commensurately elevated and not as noticeable as the increase in CBF, causing less O_2 to be removed. Therefore, there is an oversupply of oxygenated blood, i.e., the total delivery of oxygen exceeds consumption demands. Because the increase of the CBF is more significant than the O_2 consumption, the ratio of HbO_2 (diamagnetic) to dHb (paramagnetic) is also increased in the activation site. This drop in the dHb concentration increases the signal strength and originates the BOLD contrast mechanism (Logothetis and Wandell, 2004) (Logothetis, 2008) (Filippi and Rocca, 2009) (Siero, Bhogal and Jansma, 2013) (Filippi and Rocca, 2013) (Hillman, 2014) (Duarte, 2016).
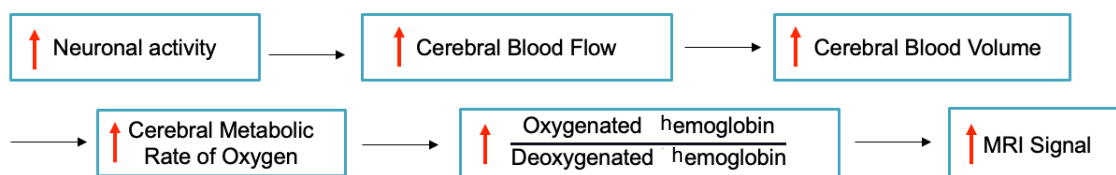
Figure 2.8 - Processes that convert the activation of an area of the brain during a task to an electric signal.

Although these variations in the strength of the signal during neuronal activation are not absolute, they can be compared relative to the signal strength in different conditions. This comparison between conditions creates a contrast. Usually, the BOLD signal is contrasted between one condition that is "active", during which neural activity is elicited by a stimulus, and a "passive" or baseline condition, during which the stimulus-related neural activity is not present (Logothetis and Wandell, 2004) (Siero, Bhogal and Jansma, 2013) (Duarte, 2016).

2.2.4 Hemodynamic Response Function

The vascular response to an increased energy demand is called the *hemodynamic response*. If an isolated brief stimulus (an 'impulse stimulus') is applied in the MRI scanner and the BOLD response is measured, we can estimate the BOLD hemodynamic response function (HRF), which describes the time course of the coupling between neuronal and vascular activity and is represented in figure 2.9. The HRF is helpful because it varies significantly across subjects, experimental conditions, tasks, and brain regions (Logothetis and Wandell, 2004) (Siero, Bhogal and Jansma, 2013) (Duarte, 2016).
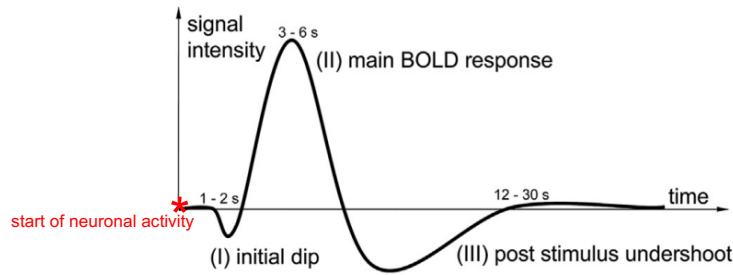
Figure 2.9 - Hemodynamic response function. Adapted from (Siero, Bhogal and Jansma, 2013).

The BOLD time course starts delayed to the start of neuronal activity, and the slight initial dip observed post-stimulus occurs due to the increase of $CMRO_2$ in the capillaries, which leads to an increase in the concentration of dHb and, consequently, to a decrease in signal intensity. This dip is followed by an abrupt increase, culminating in a peak, considered the bulk of the BOLD response. This increase is called "overshoot" due to the increase in the CBF, which overcompensates for the extracted oxygen, the consequent increase in HbO_2 to dHb ratio, and the increase in the MRI signal. Finally, the response returns to the baseline and creates a post-stimulus undershoot, also very variable and caused by an accumulation of dHb in the blood vessels (Logothetis and Wandell, 2004) (Siero, Bhogal and Jansma, 2013) (Duarte, 2016).

2.2.5 Experimental Design - Resting-State and Task-Based fMRI

Resting-state fMRI (rs-fMRI) is commonly used to discover and explore brain connections and their organization. The participant in the MRI scanner does not perform a goal-oriented task, since rs-fMRI only measures changes in brain activity and spontaneous fluctuations in the BOLD signal, which ultimately lead to a better understanding of correlations between brain regions. Nevertheless, there are some limiting factors concerning rs-fMRI, such as influences of other non-neuronal effects (e.g., underlying BOLD fluctuations) and measures that are recorded without any controlled cognitive activity (e.g., physiological noise such as respiration and heartbeat) (Siero, Bhogal and Jansma, 2013).

Contrarily, *task-based fMRI* aims to understand brain function by observing changes in the BOLD signal caused by the performance of goal-oriented tasks (figure 2.10). This is particularly interesting because the execution of a specific task could better highlight particular brain's characteristics, such as efficiency in information exchange between distant brain areas, which could be impaired by structural and functional damage caused by neurodegenerative pathologies. This is possible because as long-range communication generally brings more costs to the network (in energy, for example), brain regions only establish a connection upon task-specific activities and demands (Di *et al.*, 2013).
Because in task-based fMRI an external input (the task) is introduced, a starting point can be set in the signal acquisition, and thus information flow can be traced back to its origin, i.e., the region from where information was sent in the first place can be determined. This is ideal for the study of functional connectivity (FC) and effective connectivity (EC). Studying FC and EC is more difficult in rs-fMRI because the origin of the neurophysiological signal is ambiguous and thus difficult to interpret. (Deshpande and Hu, 2012). Nonetheless, rs-fMRI results are shown to be correlated to task-based fMRI results, i.e., if there is a higher

registered FC in rs-fMRI, the FC in task-based fMRI will most likely be higher as well (Di *et al.*, 2013).

However, it is essential to mention that task-based measurements are not absolute, just an implication that there is either an increase or a decrease in brain activity (Siero, Bhogal and Jansma, 2013).
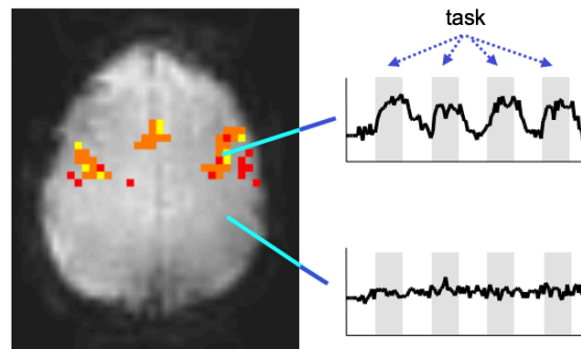
Figure 2.10 - Comparison of the BOLD signal in regions that are activated by a task (top right graph) and regions that are not activated by a task (bottom right graph). An increase in the signal is observed in the regions involved in the task (orange areas). In the y-axis, the back line represents the BOLD signal and its variations, the x-axis represents time, the grey blocks refer to periods of task performance, and the white blocks, periods of rest (or baseline). Adapted from: (Birn, available at: *http://www.humanbrainmapping.org/files/2015/Ed%20Materials/OHBM15_AdvancedFMRI_Birn_Rasmus.pdf*).

Two experimental designs are commonly used within task-based paradigms: blocked design and event-related design (represented in figure 2.11). In a *blocked design*, tasks are presented in long and fixed periods of about 15-60 seconds, the 'blocks'. These task blocks are intercalated with periods of a baseline task (that does not concern the function of interest) or resting-state. The blocked design leverages the fact that the BOLD signal in task-activated regions shows a relatively constant amplitude and accumulates over the period during which the task is performed. The most significant advantage of this type of design is the statistical power to detect brain activations. In an *event-related design*, short events (of a few hundred milliseconds) of one or more conditions or tasks are presented to the subject in single trials, usually separated by 12-14 seconds (Siero, Bhogal and Jansma, 2013). This type of design is better suited to investigate the HRF at the cost of lower statistical power.
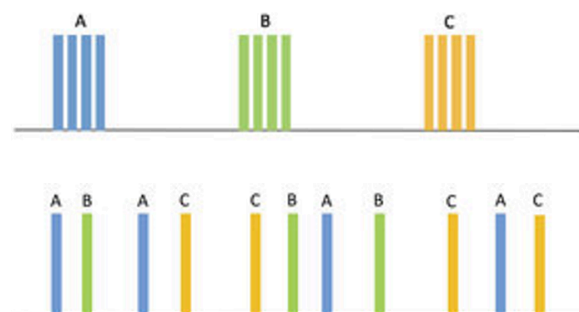
Figure 2.11 - Experimental designs within task-based fMRI paradigms: (top) blocked design and (bottom) event-related design. Adapted from: (Arco *et al.*, 2018).

2.2.6 Processing of the fMRI Data

Typically, one MRI dataset is acquired in one or more sessions. Each session collects one or more anatomical images and one or more functional runs (task or resting-state), each consisting of a timeseries of 3D functional volumes of data, which means one functional run is a four-dimensional volume (4D, space and time dimensions). Each functional volume is composed of 2D slices acquired at different points in time within the TR. All slices stacked together form a 3D image of the brain, i.e., a volume, composed of voxels (Duarte, 2016).

Processing of fMRI data consists of two phases: pre-processing and statistical analysis.

2.2.6.1 Pre-processing

Differences in brain activity between experimental conditions can be due to factors unrelated to the task, such as the parallel functioning of the brain and noise produced through the course of the imaging process. In pre-processing, these effects and outlier data are recognized and corrected, including variations in the average signal intensity that may result from physiological sources (patient motion, respiration, cardiac pulsations, anxiety) or from the scanner itself (field inhomogeneities, electronics). Thus, the typical pre-processing steps include (Chen and Glover, 2015):

- *Slice timing correction*: fMRI sequences acquire slices one at a time, meaning that the brain volume will not be covered simultaneously. This situation may lead to the signal from one slice being offset in time one or two seconds compared to another, which can be a problem in statistical analysis. Slice timing correction corrects this limitation and compensates for the time differences by time-shifting a slice to the same point where a reference slice is scanned. This will mathematically resemble the total brain volume measured at the same moment (Chen and Glover, 2015).

- *Realignment and motion correction*: head motion is the primary source of error in fMRI acquisition, which causes significant changes in the signal over time and decreases data quality. Usually, this correction method describes head motion through six parameters: three translation and three rotation parameters. A volume is chosen as a reference and an iterative process is used to align each volume with the reference volume (Chen and Glover, 2015).

- *Geometric distortions correction:* the echo planar imaging (EPI) acquisition pulse sequence is often used to obtain fMRI images. However, static field inhomogeneities may cause geometric distortions, leading to the obtained EPI functional data not being spatially aligned with the structural MRI scans, a necessary process to locate the functional images to their underlying anatomical structure (Jezzard, 2012). This correction fixes the problem by, for example, mapping the static magnetic field through phase difference measurements between two images with different TE (Chen and Glover, 2015) (Schallmo *et al.*, 2021).

- *Bias field correction*: fMRI images sometimes present intensity non-uniformities resulting from magnetic field variations. These variations will provoke changes in the signal and confuse tissue classifiers since they will assume that each tissue has a uniform intensity. Bias field correction methods estimate this bias field and make the signal intensities homogeneous (BrainSuite, n.d.).

- *Coregistration:* alignment of the functional images with the reference anatomical images (Chen and Glover, 2015).

- *Segmentation of structural image:* process that divides the structural images of the brain into images of different tissues classes (usually GM, WM, and CSF), to better measure and visualise the brain's structures.

- *Physiological noise correction*: respiration and cardiac pulsations possibly induce artefacts in the fMRI images, and sometimes they generate time-varying signals that, if uncorrected, can be associated with neuronal activity, creating confounds in the data and obscuring signals of interest. Thus, to minimize the influence of the physiological noise (or provide information that allows for a correction) techniques that are based on cardiac and respiratory cycles are used (Brooks *et al.*, 2013) (Chen and Glover, 2015).

- *Smoothing*: the application of low-pass filters averages signals from adjacent voxels and "blurs" the image. This improves the signal-to-noise ratio (SNR) but decreases spatial resolution and smears activated areas into adjacent voxels. This can be used mainly because neighbouring brain voxels are usually inherently correlated in their function and blood supply (Chen and Glover, 2015).

- *High-pass filtering:* fMRI images have noise related to low temporal frequencies (e.g., scanner temporal drift). High-pass filtering can detect these frequencies and remove them, only allowing high-frequency signals in the images (Chen and Glover, 2015).

2.2.6.2 Statistical Analysis - General Linear Model

The statistical analysis of fMRI data identifies regions in the brain that show significant increased or decreased responses linked to the task, highlighting them. This analysis is achieved through the General Linear Model (GLM), which is a matrix algebra approach that, in this case, aims to explain the variation of the observed fMRI time course of a voxel, y_i, in terms of a linear combination of predictors, x_i. The predictors are a group of reference functions that include experimental design variables, such as stimulus information and the expected shape of the HRF, and possible confounding variables (e.g., motion parameters). The GLM estimates a beta weight, β_i, associated with each predictor x_i, which quantifies how much each predictor influences the data y_i (i.e., the voxel's time course), plus an error term, ε_i, that accounts for the data that is not fitted in the model (Monti, 2011) (Poline and Brett, 2012) (Kashou, 2014) (Duarte, 2016).

$$y_i = x_i.\beta_i + \varepsilon_i \tag{1}$$

This equation can be translated into matrix form:

$$
\begin{aligned}
y_1 &= x_1.\beta_1 + \varepsilon_1 \\
y_2 &= x_2.\beta_2 + \varepsilon_2 \\
y_3 &= x_3.\beta_3 + \varepsilon_3 \\
&\vdots \\
y_i &= x_i.\beta_i + \varepsilon_i
\end{aligned}
\quad\longrightarrow\quad
\begin{bmatrix} y_1 \\ y_2 \\ y_3 \\ \vdots \\ y_i \end{bmatrix}
=
\begin{bmatrix} x_1 \\ x_2 \\ x_3 \\ \vdots \\ x_i \end{bmatrix}
\begin{bmatrix} \beta_1 \\ \beta_2 \\ \beta_3 \\ \vdots \\ \beta_i \end{bmatrix}
+
\begin{bmatrix} \varepsilon_1 \\ \varepsilon_2 \\ \varepsilon_3 \\ \vdots \\ \varepsilon_i \end{bmatrix}
\quad\longrightarrow\quad
\mathbf{Y} = \mathbf{X}.\beta + \varepsilon
$$

Figure 2.12 - Matrix form of the GLM model.

The predictor variables constitute the *design matrix*, X (figure 2.13). The GLM intends to estimate the β values to minimize the error term and generate contrasts between conditions. If this β weight is statistically different from zero, it is considered that the voxel shows a strong activation or deactivation, depending on whether it is positive or negative, during the time period in which the corresponding predictor was "active". The application of GLM to fMRI data ultimately results in the construction of a 3D map that represents brain regions or voxels that have "statistically significant" values of neuronal (de)activation, given that a contrast between conditions of interest (for example, task and baseline) is established (figure 2.14) (Monti, 2011) (Poline and Brett, 2012) (Kashou, 2014) (Duarte, 2016).
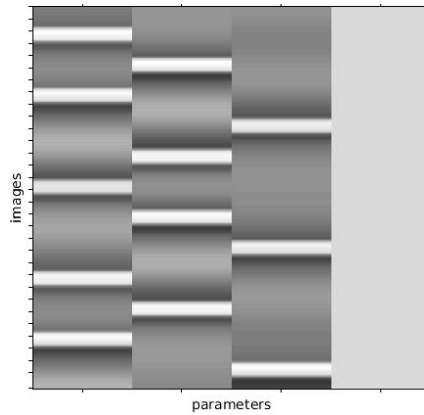
Figure 2.13 - Design matrix. Obtained using the SPM software, during the performance of a visual task.
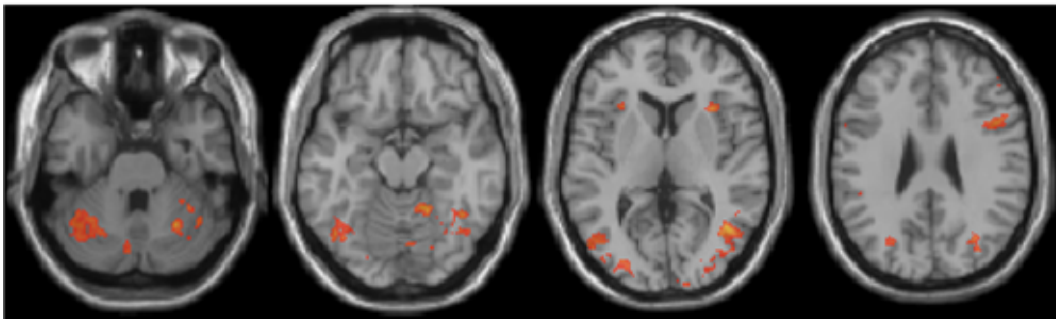
Figure 2.14 - Statistical map obtained with GLM. It shows brain activation during the performance of a visual task (group analysis, 29 participants), using the SPM software.

2.3 Brain Connectivity

Neuroimaging, exceptionally fMRI, has become the gold standard for comprehending and disclosing the brain's architecture, how it processes information, and how a given task can modulate its activity, and to better comprehend concepts that regulate cognition, behaviour, and perception. However, to further understand its principles, it is fundamental to first distinguish between functional segregation and integration (figure 2.15) (Friston, 2011).

Functional segregation concerns the brain's ability to cluster into connected areas where there is specialized information processing. *Functional integration* characterizes the brain's performance by evaluating how quickly specialized information from different brain areas is combined and how the "segregated clusters" coordinate and couple. Functional segregation is an already established principle of human brain organization and it is typically investigated in fMRI activation studies. However, integration of these segregated brain areas is more challenging to assess. To better characterize the functional integration principle and, thus, interactions between activated brain areas, research often turns to connectivity analysis (Roebroeck, Formisano and Goebel, 2005) (Friston, 2011) (Friston, Moran and Seth, 2013).

functional segregation   functional integration
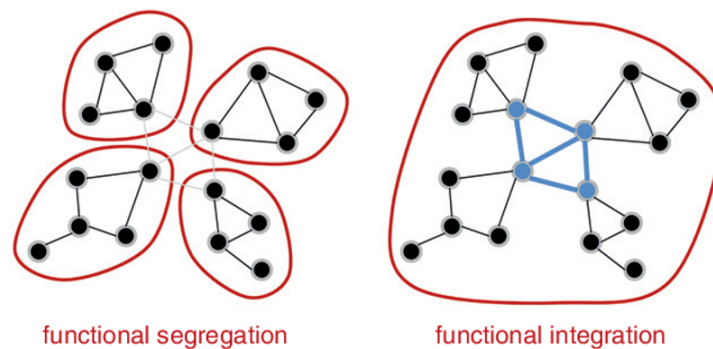
Figure 2.15 – Brain's functional segregation and integration. Brain segregation divides the brain into specialized sections, or 'clusters', and brain integration connects these clusters. Adapted from (Sporns, 2013a).

2.3.1 Types of Brain Connectivity

Structural connectivity models and characterizes the brain as a group of distributed cortical regions connected by WM tracts and evaluates these pathways' integrity. It is usually measured with diffusion-weighted MRI using tractography (Uddin, 2013) (Pagani *et al.*, 2020).

Functional connectivity (FC) represents the statistical dependencies between timeseries of neurophysiological events without knowing their exact causes. This type of connectivity subdivides into undirected and directed FC, depending on whether one considers the dependencies as spontaneous or as reflecting dynamical processes with causes and consequences, respectively. Techniques that assess undirected functional connectivity are, for example, correlation-based approaches (e.g., independent components analysis (ICA) and Pearson Correlation), which only determine the pairwise relationship of the variables (in this case, brain regions) without taking into consideration directional and multivariate information prevalent in brain networks (Abidin *et al.*, 2017) (Miri Ashtiani *et al.*, 2019). Directed FC can solve this problem and is primarily assessed through Granger Causality

Analysis (GCA), explained in detail in the next section (Roebroeck, Formisano and Goebel, 2005) (Friston, Moran and Seth, 2013).

On the other hand, *effective connectivity* (EC) refers to how one neuronal system can influence another. In this case, causation is assessed, i.e., if the activation in one brain area is known to cause the activation of another area. EC is always directed because causality is inherent in the model (Friston, 2011). The primary technique that assesses EC is Dynamic Causal Modelling (DCM).
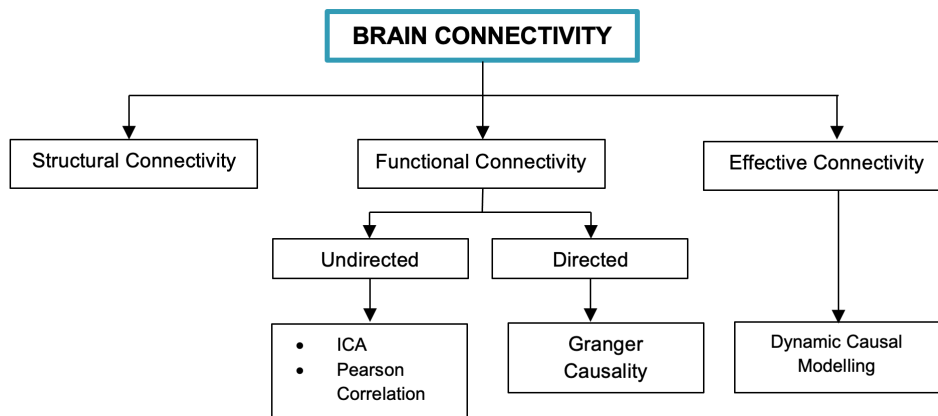
Figure 2.16 - Types of brain connectivity and methods with which they are analysed.

There is still controversy in the scientific community regarding if GCA is a method that studies functional or effective connectivity. GCA and DCM are both fMRI-based connectivity methods that are gaining popularity in the study of brain connectivity. They have some characteristics in common as they both assess directed influences between activated brain regions through the BOLD signal. Nevertheless, the two methods answer fundamentally different questions, so choosing one of them depends on whether there is interest in describing the data in terms of information flow (GCA) or rather in understanding the underlying brain mechanisms (DCM).

Unlike DCM, GCA is a more exploratory approach that does not consider the underlying causality between brain interactions but rather the temporal correlations between the time courses of the regions to predict certain behaviours (like the activation of brain regions involved in the task). It makes minimal assumptions about the data, namely, what are the connections between brain regions, before applying the model. DCM, on the contrary, models the hemodynamic processes and neuronal dynamics; thus, it can be known whether brain activity of a region (a cause) induces the activation of another region (a consequence). This method is more prone to suffer from model misspecifications and inaccurate results (Roebroeck, Formisano and Goebel, 2011) (Friston, Moran and Seth, 2013) (Seth, Barrett and Barnett, 2015).

The distinction between effective and functional connectivity supports the assertion that GCA and DCM are complementary rather than competitive methods as their assumptions are different, thus permitting different interpretations of brain function (Friston, Moran and Seth, 2013) (Seth, Barrett and Barnett, 2015).

2.3.2 Granger Causality Analysis

Granger Causality (GC) was first described in the Economy field in 1969 by Clive Granger (Granger, 1969). However, it has been commonly applied in neuroscience due to its versatility, easiness, and simplicity to apply to neurophysiological models, albeit with some restrictions (Seth, Barrett and Barnett, 2015).

GC is a framework for multivariate timeseries analysis based on autoregressive models. With this method, a BOLD signal timeseries can be predicted from another BOLD signal timeseries based on the time lag between the two (figure 2.17), thus identifying brain regions that are functionally connected and that possibly exchange information (Roebroeck, Formisano and Goebel, 2005) (Seth, Barrett and Barnett, 2015). In this thesis, Granger causality analysis was applied to the fMRI BOLD signal to assess the directed functional connections between brain regions during task performance, based on the assumption that the 'cause' (the activation of a region) precedes and helps predict the 'consequence' (the activation of another region) (Azarmi *et al.*, 2019).
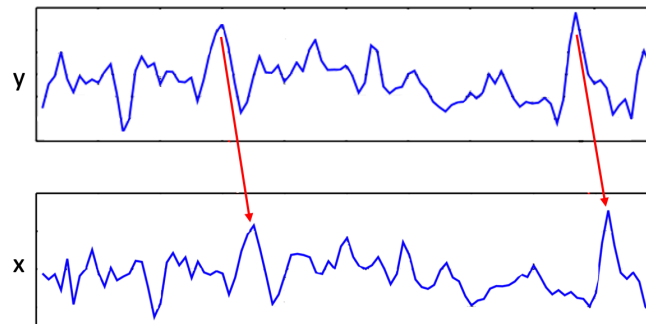
Figure 2.17 - Temporal precedence of timeseries Y in relation to X.

The basic principle of GC is that variable (or timeseries) Y is said to "Granger-cause" another variable X if its past information can help predict the future of X over and above the information provided by X's own past (Seth, Barrett and Barnett, 2015).

The workflow of GCA is simple since it is based on vector autoregressive (VAR) modelling, which is a multivariate timeseries modelling that finds the relation between a variable's current observations with its own past observations as well as with the past observations of other variables. Therefore, the primary goal of GCA is to fit a VAR model to the data to find optimal weights and minimise estimation errors (Roebroeck, Formisano and Goebel, 2005) (Barnett and Seth, 2014).

Firstly, the timeseries X is predicted from the autoregression of its past, omitting the potential influence of other variables (Seth, Barrett and Barnett, 2015). This is called the 'restricted model' because only information related to X is considered, described by equation 2.

$$X_t \ = \ \sum_{i=1}^{p} A_i \, . \, X(t \, - \, i) \ + \ \varepsilon_1(t) \tag{2}$$

If the timeseries *Y* is available, this new information, thought to help predict the timeseries *X*, is added and an unrestricted model is also formulated (equation 3).

$$X_t \; = \; \sum_{i=1}^{p} A_i \cdot X(t - i) \; + \; \sum_{j=1}^{p} B_j \cdot Y(t - j) \; + \; \varepsilon_2(t) \tag{3}$$

In equations 2 and 3, X_t and Y_t are the averages of the BOLD time courses of each brain region, the parameter p is the model order, A_i and B_j are the coefficients of the model, i and j represent the lags (i.e., the past time points that are included in the model) and ε_1 and ε_2 represent the prediction errors for the restricted and unrestricted model, respectively. In conclusion, it all comes down to the prediction errors: if $\varepsilon_1 > \varepsilon_2$, then the new information from timeseries Y helps in the prediction of X, i.e., timeseries X's values are improved in the unrestricted model, and it is assumed that Y "Granger-causes" X (Azarmi *et al.*, 2019).

GCA can also provide information about the direction of the interaction between timeseries. Geweke, based on the observed temporal precedence between variables, formulated equation 4 that represents the directed Granger Causality between X and Y (Geweke, 1982) (Roebroeck, Formisano and Goebel, 2005).

$$F_{x,y} \; = \; F_{x \to y} + \; F_{y \to x} \; + \; F_{x.y} \tag{4}$$

In this equation, $F_{x,y}$ represents the temporal dependence between the two timeseries. If there is no dependence between them, $F_{x,y} = 0$. $F_{y \to x}$ represents the linear dependence from Y to X. If the past values of Y improve the prediction of the value of X, then $F_{y \to x} > 0$. $F_{x \to y}$ represents the linear dependence from X to Y. $F_{x.y}$ denotes indirect instantaneous influences that direct causal influences cannot explain (Roebroeck, Formisano and Goebel, 2005).

In turn, $F_{y \to x}$ can be described by equation 5 (Geweke, 1982).

$$F_{y \to x} \; = \; log \frac{var(\varepsilon_1(t))}{var(\varepsilon_2(t))} \tag{5}$$

This equation considers the linear dependence from Y to X to be the logarithm of the ratio between the variance of the prediction error of the restricted model (which only uses past time points of X) and the variance of the prediction error of the unrestricted model, where information from both variables is used to predict X. If the past of Y can improve the prediction of X, then the variance of the error ε_2 is smaller, meaning that the coefficients are reliably estimated and that this prediction is reasonable. This also implies that the ratio of the error variances is higher than 1, and the overall value of the logarithm is higher than 0. If it does not improve the prediction of X, then the logarithm and, consequently, $F_{y \to x}$ is 0 (Seth, Barrett and Barnett, 2015) (Abidin *et al.*, 2017).

When a GC relationship between variables is found, it is assumed that there is "information flow" from Y to X. This general assumption can be made because GC is considered to be an approximation of *transfer entropy* (the statistics are equivalent for Gaussian variables), which characterizes directed statistical dependencies and shared information between variables (Friston, Moran and Seth, 2013) (Seth, Barrett and Barnett, 2015).

2.3.2.1 GCA's Limitations

The application of GCA to fMRI data remains controversial primarily because the BOLD signal derived from fMRI is an indirect measure of neural activity (Friston, Moran and Seth, 2013) (Seth, Barrett and Barnett, 2015) (Seth, Chorley and Barnett, 2013).

One of the most problematic characteristics of fMRI when applying GCA is the sampling rate (or TR), generally in the order of seconds. This is a complication because neuronal responses are in the order of milliseconds, and such a discrepancy in the timescales can originate inexact results and inaccuracies in the analysis. Other limitations involve assumptions that need to be fulfilled in GCA. To apply GCA (Deshpande and Hu, 2012) (Friston, Moran and Seth, 2013) (Seth, Barrett and Barnett, 2015):

- The modelled variables are stochastic.
- The data are stationary.
- The interaction between variables is linear. This is not the case in the human brain; however, the equivalence with transfer entropy allows linear VAR modelling and GC to be sensitive to the linear parts of the data.

Thus, thorough treatment and interpretation of the data are required when using GCA.

2.3.3 Graph Theory

Focal but also diffuse lesions in the brain and spinal cord are a hallmark of MS (Fleischer *et al.*, 2019). Thus, to evaluate connectivity disruption, a holistic model that describes this distributed nature of the damage is appropriate (Welton *et al.*, 2020). How does the network structure affect how the brain functions, and how can a pathological state disturb network organization? These questions can only be answered through network analysis, made possible by the mathematical concept of *graph theory*.

Because the brain has many elements interacting functionally to exchange information, it can be viewed as a complex network and hence, represented as a connectivity graph. A graph can be defined by a set of nodes (vertices) and edges (links) between pairs of nodes. Nodes in brain networks usually represent brain regions, and edges represent connections between nodes: the edges are anatomical if they have a direct physical connection, functional if they have a correlation in their activity pattern (BOLD signal) or effective if a node's activity modulates another node's activity and there is a causal interaction between them (Rubinov and Sporns, 2010) (Kaiser, 2011). The nature of nodes and edges can be determined by brain mapping methods, such as anatomical parcellation schemes (or atlases), as well as measures of connectivity (Rubinov and Sporns, 2010). The functional association between the nodes can be determined through previously mentioned connectivity methods, such as Granger Causality.
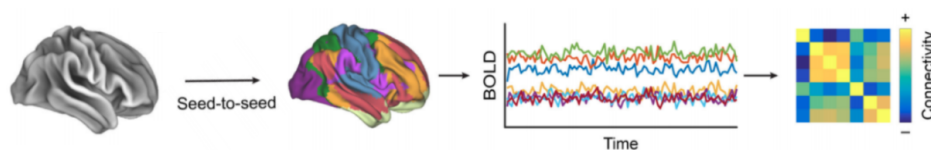
Figure 2.18 - Brain parcellation and connectivity analysis. Usually, parcellation schemes are applied to fMRI data, which help define nodes (brain regions). Then, the time course of each node is extracted, and connectivity matrices are constructed bases on the relationship between the nodes' time courses. From these matrices, graph theory analysis can be performed, and connectivity measures extracted. Adapted from (Tahedl *et al.*, 2018).

fMRI and other neuroimaging techniques can be used to assess if and which nodes are connected and if there is information exchange between them. All this information can be represented by connectivity matrices, where rows and columns denote nodes (or brain regions), and each matrix entry (a_{ij}) represents an edge (or connection between brain regions). In an unweighted graph, all edges weigh the same, i.e., $a_{ij} = 1$. In a weighted graph, each element a_{ij} reflects the strength of the connection (Rubinov and Sporns, 2010).

Graphs can also be classified as directed and undirected. In undirected graphs, all the edges are bidirectional (for example, an edge between nodes i and j means that $a_{ij} = 1$ and $a_{ji} = 1$). If the graph is directed, then the element a_{ij} represents a connection from node i to node j, and the element a_{ji} represents the information flow in the opposite way, from node i to node j, and these connections can have different strengths (Rubinov and Sporns, 2010).
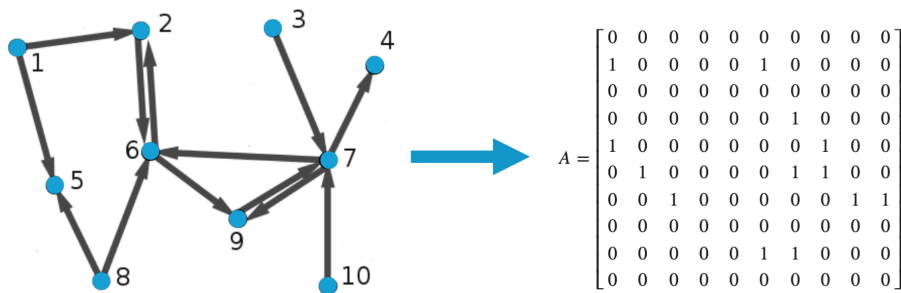
Figure 2.19 - Example of an unweighted directed graph and corresponding connectivity matrix. Each matrix's element represents a connection between nodes in the graph on the left (Nykamp, available at *https://mathinsight.org/network_introduction*).

2.3.4 Graph Measures of Connectivity

Given the brain networks' inherent complexity, the comparison of properties between individuals and groups is difficult. A method that can capture the graph's topology and architecture is, therefore, necessary. Using graph theory and ensuing network construction, a set of metrics can be calculated to quantify its specific organizational properties that focus on, for example, degree of segregation, degree of integration and efficiency of information transfer, the centrality of the nodes within the network and general resilience. Significant diverging values of these neuro-biologically meaningful measures between the two groups are indicative of differences between control and MS patients' brain networks (Abidin *et al.*, 2017).

Segregation measures are assessed to find and quantify clusters/modules (groups of brain regions that are densely interconnected and specialized). Integration measures evaluate how the regions communicate and how efficient is this communication, depending mainly on the paths (sequence of nodes) within the network; the shorter the path, the stronger the potential for integration is. An established principle of healthy human brain organization is *small-worldness*, which combines and balances functionally specialized clusters with many robust connections that allow for efficient communication (Rubinov and Sporns, 2010).

Measures of centrality find the importance of specific brain regions within the network. It is assumed that the more central a node is, the more it participates in short paths and, consequently, the more it influences the information flow and node communication in the network. These brain regions are usually referred to as *hubs* of the network. They actively

27

interact with many brain regions, facilitating functional integration and contributing to the network's resilience (Bullmore and Sporns, 2009) (Rubinov and Sporns, 2010). Finally, quantifying resilience assesses the network's vulnerability to insults, and in this case, can evaluate the influence of neuropathological lesions in brain activity.

A summary of the graph theory connectivity measures that can be calculated from fMRI (and other neuroimaging modalities) data is presented in Table 2.3.

Table 2.3 - Definition of the connectivity metrics.

Segregation	**Mean clustering coefficient**	All the nodes that are connected to another node are denominated *neighbours* of that node (Kaiser, 2011). The mean clustering coefficient represents the node's neighbours that are also neighbours of each other. A high mean clustering coefficient between nodes indicates that these nodes form a cluster (Bullmore and Sporns, 2009) (Rubinov and Sporns, 2010).
	Modularity	Degree to which the network can be divided into delineated and nonoverlapping groups of nodes. (Rubinov and Sporns, 2010)
Integration	**Characteristic path length**	Average shortest path length (i.e., minimum number of edges) between all network's nodes (Bullmore and Sporns, 2009) (Rubinov and Sporns, 2010). It measures the ease with which the information traverses the entire graph (Welton *et al.*, 2015).
	Global efficiency	Inverse of the characteristic path length (Rubinov and Sporns, 2010). It measures how the network nodes are connected and how efficient is the information exchanged between them (Kaiser, 2011).
	Local efficiency	Global efficiency calculated on a given node's neighbourhood. It assesses the efficiency of information exchange of a subnetwork constituted by a node and its neighbours if the node is extracted from the network (Stanley *et al.*, 2015) (J. Liu *et al.*, 2017).
	Small-worldness index	Quantifies the network's balance between functional integration and segregation (Rubinov and Sporns, 2010).
Centrality	**Degree**	Number of links connected to a node. It measures the significance of a node within the network because a high degree node means that the node interacts with many others (Bullmore and Sporns, 2009) (Rubinov and Sporns, 2010). • mean degree - measures the network density and total wiring cost. • in-degree - number of inward links of a node. • out-degree - number of outward links of a node.
	Strength	Total sum of the links' weights connected to a given node. In-strength represents the sum of the inward links' weights and out-strength the sum of the outward links' weights (Rubinov and Sporns, 2010).
	Eccentricity	Longest shortest path between a given node and all other nodes in the network. Measures the easiness of a node to be functionally reached by all of the other nodes, reflecting the efficiency of information exchange (Su *et al.*, 2017) (Weisstein, n.d.). • radius - minimum eccentricity. • diameter - maximum eccentricity, i.e., the largest distance between any two nodes.
	Within-module degree	Determines the nodes that establish many connections but only within the module in which they are included (Rubinov and Sporns, 2010).
	Participation coefficient	Measure of the distribution and diversity of a node's links in the modules of a graph (Rubinov and Sporns, 2010). For exemple, if a node has the same number of edges with all of the network's modules, then the participation coefficient = 1. If all the node's edges are only within its own module, then the participation coefficient = 0.
	Betweenness centrality	Number of paths with the shortest length that go through a given node. A high value means that the node connects disparate parts of the network and therefore carries more information. It measures both the network's compactness and the efficiency of communication between nodes (Rubinov and Sporns, 2010).
	Subgraph centrality	Sum of the closed walks in the network starting and ending at a particular node, hence characterizing its participation in the network's subgraphs. A smaller value means that the length of the closed walk is shorter and, thus, the node has more influence on centrality (Rubinov and Sporns, 2010).
	K-coreness centrality	A k-core is the largest subgraph within the network that contains nodes with at least a *k* degree. The k-coreness centrality identifies these subgraphs that are densely connected (Rubinov and Sporns, 2010).

	Eigenvector centrality	Measures a node's level of influence within a network through a scoring system based on the number of connections that the node establishes. A high eigenvector centrality means that nodes are linked to nodes that also have high degree values. So, the higher the score, the more influence the node exerts over the network (Shaw, 2019).
	Pagerank centrality	Directed variant of eigenvector centrality. Each node has a score based on the number of incoming links (in-degree). Thus, generally nodes with high in-degree (and the nodes they are connected to) are influential in the network (Shaw, 2019).
	Local flow coefficient	Number of paths of length two that link the neighbours of a node and that pass through that node, divided by the number of possible paths that can be established between the node's neighbours. It represents the node's ability to conduct information flow (Sacchet *et al.*, 2015).
	Global flow coefficient	Average of the network's local flow coefficients over the network (Sacchet *et al.*, 2015).
Resilience	**Assortativity coefficient**	Correlation coefficient between all the node's degrees on opposite ends of an edge. Positive assortativity means that high-degree nodes connect with other high-degree nodes, creating a resilient core. A negative value means that the nodes are widely distributed and are, thus, vulnerable hubs (Bullmore and Sporns, 2009) (Rubinov and Sporns, 2010).

3

State of the Art

3.1 Functional Connectivity Alterations in Multiple Sclerosis

There is evidence of pathological-provoked changes in function, communication, and organization of the brain in patients with multiple sclerosis (Reddy *et al.*, 2002) (Audoin *et al.*, 2003) (Filippi and Rocca, 2009) (Faivre *et al.*, 2012) (Shu *et al.*, 2016) (Basile *et al.*, 2014) (Fleischer *et al.*, 2019) (Azarmi *et al.*, 2019). The analysis of these changes is of utmost importance and aims to turn the resultant functional connectivity measures into biomarkers of this condition. However, a question that remains unsolved is how FC changes occur in multiple sclerosis. Some argue that the overall brain connectivity is decreased because of structural modifications and the presence of demyelinating lesions that consequently cause breaks in communication and information exchange. Others argue that compensatory mechanisms that lead to an increase in FC are involved in maintaining and restore functionalities in the early phases of MS, and may even become maladaptive and contribute to clinical impairment during the progression of the disease (Rocca and Filippi, 2017) (Schoonheim, 2017) (Tahedl *et al.*, 2018) (Fleischer *et al.*, 2019).

In fact, many studies observed a compensatory mechanism in patients with MS, particularly in the early phases of the condition, when the disability is minimal (Reddy *et al.*, 2002) (Basile *et al.*, 2014). This phenomenon, also called *neuroplasticity*, consists of a general increase in the brain's FC and it represents the brain's capacity to preserve function and adapt its behaviour and connections in response to insults or dysfunction that causes impairment in brain activation, ultimately limiting cognitive impairment expression. It's mainly mediated by alterations in synaptic efficiency and emergence of new connections and pathways of information (Parry *et al.*, 2003). Although it is a popular concept and recent research focused on proving it in various disconnection diseases, its definition remains ambiguous and controversial since the underlying neural mechanisms are still relatively unknown and defining its characteristics is complex (Behfar *et al.*, 2020).

Various studies reported evidence of this compensation using local activation measures. For example, Audoin and colleagues (Audoin *et al.*, 2003) noticed significant differences between the formation of lesions and the clinical expression of MS that could be explained by neuroplasticity. The participants, which included MS patients in an early phase of the disease, performed a Paced Auditory Serial Addition Test (PASAT) task to evaluate information processing speed. They concluded that a compensatory mechanism led to higher activation in regions involved in executive processing and that fMRI was a great tool to evidence neuroplasticity. Staffen and colleagues (Staffen *et al.*, 2002) also observed this overcompensation during a similar cognitive task (Paced Visual Serial Addition Test, PVSAT) in RRMS patients, where there was more recruitment of brain regions that participated in these attentional processes.

Regarding compensation effects in functional connectivity, this phenomenon is proven again, in resting-state condition, by Droby and colleagues (Droby *et al.*, 2016), who observed that, in patients with RRMS, the levels of FC did not change drastically, which indicated preservation of the brain function in an early phase of MS. Furthermore, they observed that FC increased substantially during a relapse, which usually indicates the development of a new lesion, and concluded that this could denote the recruitment of intact brain regions to compensate for the ones damaged by the lesions, thus limiting clinical consequences.

Finally, Faivre and colleagues (Faivre *et al.*, 2016) argue that there are indeed compensatory adaptive phenomena in MS which translate into an increased recruitment of areas, to

compensate for brain injuries. However, these mechanisms are also saturable, i.e., they function during the disease course, but they may reach a maximal level, after which there is only disability progression.

3.2 Graph Theory in Multiple Sclerosis

There is a lack of studies that explore functional or effective connectivity using graph theory in multiple sclerosis. Besides, the use of graph theory in the neuroscience context has only gained attention in 2009, after the launch of the Human Connectome Project (Farahani, Karwowski and Lighthall, 2019), so its application is still relatively recent. Most of the research on MS focuses mainly on studying structural MRI connectivity or resting-state fMRI connectivity, which is not the objective of this thesis. Another common aspect between most studies is that they apply graph theory connectivity measures to the whole brain, contrary to what was done in this project (section 4. Methodology). Nonetheless, a comprehensive review of the existing work in this area will be given.

Structural connectivity was the first approach used to study connectivity in MS in combination with graph theory (Solana *et al.*, 2019) (Fleischer *et al.*, 2019) (Pagani *et al.*, 2020). Research on this topic has shown that network metrics in MS patients were indeed significantly altered and that, generally, the efficiency of the information transfer between regions was the most affected aspect. Overall, graph measures of segregation were increased, while measures of integration were decreased (Welton *et al.*, 2020). However, researchers noticed that structural connectivity was insufficient to explain cognitive alterations in MS patients since it was shown that there is not a direct mapping between structural and functional connectivity. Furthermore, sometimes brain regions may be activated in a task even when they are not structurally connected, which could reflect the brain's ability to coordinate pathways involving different nodes to perform a given task. The conclusion was that brain function and connections should be analysed from a dynamic perspective, so functional connectivity approaches started being utilised (Ford and Kensinger, 2014) (Shu *et al.*, 2016).

Rocca and colleagues (Rocca *et al.*, 2016) developed an rs-fMRI-focused study that aimed to prove that disruption of functional connectivity in MS plays a significant role in the disease's clinical manifestations by analysing the topological organisation of functional brain networks. Their main conclusions were that changes in the global network properties do indeed distinguish healthy controls from MS patients, although they did not find significant differences between MS clinical phenotypes. They also showed that changes happen in the network hubs (either formation, loss, or different lateralisation), which could indicate a decrease of the FC of certain strategic regions that define the correct functioning of the network. Moreover, they verified a decrease in global integration, which demonstrated a less competent information exchange between distant brain regions and is strongly associated with cognitive impairment, and a preservation of segregation, which infers that transfer and processing of information are only efficient when executed locally. All these modifications ultimately lead to physical disability, cognitive impairment, and phenotypic variability in MS.

In (Shu *et al.*, 2016), the topological aspects and changes of both structural and functional connectivity were investigated in CIS and MS patients, with rs-fMRI. They proved that functional changes were only observed in the MS stage and that they were only correlated with disability (physical and cognitive) in MS patients, not CIS patients, which suggests that

these alterations were not as evident in a (possible) very early stage of MS, which could be due to the balance between neuroplasticity and disconnection.

Abidin and colleagues (Abidin *et al.*, 2017) also focused on CIS patients and the conversion of CIS to MS to analyse the probability of long-term disability. They used rs-fMRI data and a multivariate analysis using large-scale Granger Causality. Differences at a global and regional level were detected, mainly an increase of clustering and modularity, which could imply that there is an efficient exchange of information within specific networks and processes of reorganization as a compensatory response to the tissue damage.

Welton and colleagues (Welton *et al.*, 2020) also used rs-fMRI to conclude about brain network organisation in MS patients with cognitive impairment. Their results were that there were longer average path lengths, increased modularity, increased clustering, reduced global efficiency, and lower small-worldness in MS patients' brains. These results again demonstrate more network segregation and a decrease in efficiency.

Overall, in rs-fMRI, the primary differences in network organisation in MS seem to be longer characteristic path lengths, increased modularity, and decreased global efficiency (Rocca *et al.*, 2016) (Shu *et al.*, 2016). This implies that the network is more clustered, which could be the brain's response to the damages in WM tracts provoked by focal lesions, i.e., long-range connections become impaired, so, as a result, networks become even more connected to their neighbours (figure 3.1). Another aspect that seems recurrent in MS is that the network's nodes have fewer connections, thus fewer hubs (Welton *et al.*, 2020) (Rocca *et al.*, 2016).
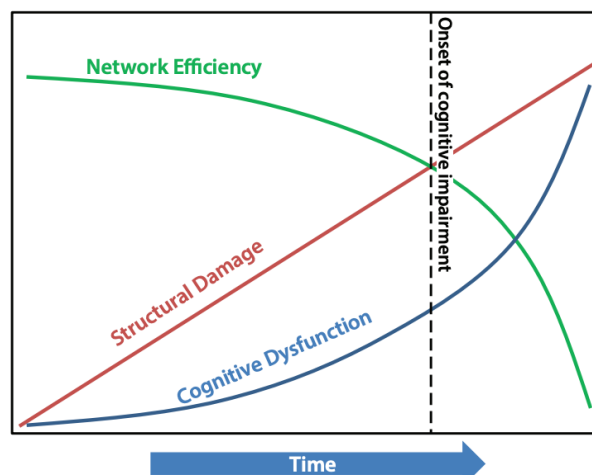
Figure 3.1 - Evolution of cognitive decline. The x-axis represents time and the y-axis represents the evolution of network efficiency, structural damage and cognitive dysfunction. As the structural damage increases and the network's efficiency decreases, the cognitive dysfunction also increases. This becomes more noticeable when the structural damage surpasses the network's efficiency (Benedict *et al.*, 2016).

Task-related fMRI studies are not as common as structural MRI or rs-fMRI studies. This is due mainly to the difficulties these task processes bring, such as the increase in signal noise which could be detrimental to data analysis.

Nonetheless, Ashtiani and colleagues (Miri Ashtiani *et al.*, 2018) used correlation analysis to examine whole-brain connectivity changes between healthy controls and RRMS patients during a PASAT task that required some level of attention, working memory and processing information speed. They employed graph theory analysis to determine the quantitative

topological characteristics of the brain networks that could explain the cognitive damage seen in the patients. They analysed the global measures mean clustering coefficient, modularity, transitivity, characteristic path length, global efficiency, assortativity and small-worldness index, and the local measures, degree, participation coefficient, diversity centrality, betweenness centrality, subgraph centrality, k-coreness centrality, pagerank centrality and eigenvector centrality. There were no statistically significant differences between healthy controls and MS patients in the global measures, except for the mean clustering coefficient, which showed a decrease in MS, and modularity, which also decreased. Both groups showed a small-world characteristic (balance between functional segregation and integration); however, this value decreased with the wiring costs and structural damage. They proposed that these changes could be explained by the increase of the WM lesion load. Most local measures also revealed significant differences between groups in several regions, particularly those involved in the PASAT task.

More recently, Azarmi and colleagues (Azarmi *et al.*, 2019) employed the same approach as (Miri Ashtiani *et al.*, 2018) but used Granger Causality instead of Pearson's Correlation to determine the directed network measures. They analysed global measures, such as mean clustering coefficient, modularity, transitivity, characteristic path length, global efficiency, global flow coefficient, and assortativity, and local measures such as degree (total, in- and out-degree), participation coefficient, betweenness centrality, subgraph centrality, k-coreness centrality, pagerank centrality, and local flow coefficient. On one hand, only the global flow coefficient showed significant differences between controls and MS patients among global measures. On the other hand, regarding local measures, only subgraph centrality was not significantly different between groups. These results suggest that an approach focusing on smaller task-related networks might have higher sensitivity than whole-brain resting-state paradigms to detect functional connectivity changes in MS, particularly in early phases. This study also validated GC as a method capable of determining changes in brain networks in MS.

Despite the limitations in analysing data provided by task-based fMRI, the performance of goal-oriented tasks, as mentioned in section 2.2.5, could emphasize the brain's characteristics involved in information exchange between brain regions that otherwise might not be connected, given that executing tasks in MS has a higher cost (in energy, for example) in brain networks.

Table 3.1 - Summary with the main results obtained in graph theory studies applied to MS.

Study	Participants	Parcellation	fMRI	Network Construction	Threshold	Global Metrics	Local Metrics	Results
Shu *et al.*, 2016	35 Controls 41 CIS 32 MS	90 ROIs, AAL, whole brain	Resting-state	Pairwise Pearson Correlation	Significance Threshold: p<0.05, Bonferroni correction	Clustering coefficient, characteristic path length, global efficiency, mean local efficiency, small-worldness index, mean strength	Nodal efficiency	No significant changes between groups in global measures. Lower values of mean strength, global efficiency, mean local efficiency, clustering coefficient in MS patients. Higher values of characteristic path length in MS patients 21 regions showed differences between groups. Overall, there was a reduction in nodal efficiency in MS patients.
Rocca *et al.*, 2016	55 Controls 246 MS	116 ROIs, AAL, whole brain	Resting-state	Bivariate Correlation Analysis	Absolute Threshold: 0 - 0.2; increments of 0.01	Clustering coefficient, characteristic path length, global efficiency, assortativity, mean degree, hierarchy	Nodal degree, betweenness centrality	Higher values of characteristic path length and assortativity in MS patients. Lower values of global efficiency and hierarchy in MS patients. Lower degree in the bilateral caudate nucleus and right cerebellum.
Abidin *et al.*, 2017	9 Controls 9 CIS	90 ROIs, AAL, whole brain	Resting-state	Large-Scale Granger Causality Analysis	Proportional Threshold: 0.45	Clustering coefficient, modularity, global efficiency, assortativity, mean degree (in- and out-degree)	Strength, degree, local efficiency, nodal clustering coefficient	Higher values of clustering coefficient and modularity in MS patients. Several metrics changed in precentral, frontal gyrus and some portions of parietal lobe.
Miri Ashtiani *et al.*, 2018	12 Controls 8 RRMS	116 ROIs, AAL, whole brain	Task-based, PASAT	Pairwise Pearson Correlation	Proportional Threshold: 0.01 - 0.5; increments of 0.01	Clustering coefficient, modularity, transitivity, characteristic path length, global efficiency, assortativity, mean local efficiency, small-worldness index	Degree, participation coefficient, centralities: diversity; betweenness; subgraph; k-coreness; pagerank; eigenvector	Clustering coefficient and modularity had lower values in MS patients. Almost all the local measures were different between groups in several regions.
Azarmi *et al.*, 2019	12 Controls 8 RRMS	116 ROIs, AAL, whole brain	Task-based, PASAT	Granger Causality Analysis	Proportional Threshold: 0.06 - 0.3; increments of 0.01	Clustering coefficient, modularity, transitivity, characteristic path length, global efficiency, assortativity, global flow coefficient	Total, in- and out-degree, participation coefficient, local flow coefficient, centralities: betweenness; subgraph; k-coreness; pagerank	Only the global flow coefficient was significantly different between groups. Only subgraph centrality didn't have significantly different regions between groups.
Miri Ashtiani *et al.*, 2019	12 Controls 8 RRMS	116 ROIs, AAL, whole brain	Task-based, PASAT	Modular Structures Sparse Weights	Proportional Threshold: 0.1 - 0.5; increments of 0.01	Clustering coefficient, modularity, transitivity, characteristic path length, global efficiency, mean local efficiency	Nodal clustering coefficient, local efficiency, eccentricity, node strength, within-module degree, participation coefficient, centralities: betweenness; diversity; eigenvector	Lower values of modularity in MS patients. Eccentricity, strength, within-module degree, eigenvector centrality identified the greatest number of significantly different regions (between groups). In participation coefficient only the right putamen was significant between groups. No significant regions between groups in diversity centrality.
Welton *et al.*, 2020	23 Controls 37 MS	164 ROIs, Destrieux Atlas, whole brain	Resting-state	Pairwise Pearson Correlation	Proportional Threshold: 0.2 - 0.5; increments of 0.02	Clustering coefficient, modularity, characteristic path length, global efficiency, small-worldness index	—	Higher values of characteristic path length, clustering coefficient and modularity in MS patients. Lower values of global efficiency in MS patients. No changes in small-worldness index.

4
Methodology

The data analysed in this thesis were collected in the context of the funded scientific project BIOMUSCLE (PTDC/MEC-NEU/31973/2017). Patients were recruited and clinically evaluated by the members of the project at the Neurology Department of the University Hospital of Coimbra and met the criteria for MS diagnosis according to McDonald Criteria (Thompson et al., 2018).
All the participants filled out written informed consent forms before the experiment.

4.1 Experimental Setup

4.1.1 Participants

Twenty-nine participants were recruited for this fMRI study: fifteen patients recently diagnosed with RRMS and fourteen demographically matched healthy controls. The demographic characteristics of the participants are detailed in Table 4.1.
The time from diagnosis of the MS patients ranged from 8 to 68 months (median = 18 months), and the EDSS score was less or equal to 3.0 (the controls did not perform this clinical evaluation). All the participants had a normal or corrected-to-normal vision and no known cognitive impairments.

Table 4.1 - Demographic characteristics of the participants.

	Mean Age	No. of Females	No. of Males	Handedness	Mean EDSS
Healthy Controls	32.93 ± 8.64	8	6	All right-handed	—
Multiple Sclerosis Patients	32.33 ± 8.59	8	7	All right-handed	2.05 ± 0.5*

* - EDSS data only available for 11 of the 15 MS patients

4.1.2 Neuropsychological Evaluation

Patients with MS, even in the early phases of the disease, might show signs of cognitive impairment in aspects such as memory, attention, verbal fluency, visual perception, and a slowed processing of information (Sousa et al., 2018) (Miri Ashtiani et al., 2018). In this study, eleven of the fifteen patients performed a neuropsychological evaluation, which consisted of diverse tests that allowed for an in-depth assessment of their brain function and cognitive status.

Six assessments were included in this evaluation. The first two are scales that measure physical disability and fatigue, four assessments are cognitive tests, namely those composing the Brief Cognitive Assessment for MS (BICAMS) (Langdon et al., 2011), which study brain performance during processing speed, auditory, visuospatial, and verbal memory tasks, and the last assessment is a social cognition test. A brief description of each test is presented below.

- **Expanded Disability Status Scale (EDSS)** is a scale ranging from 0 (normal neurological status) to 10 (death due to MS) that may change throughout the progression of the disease according to the patient's physical impairment evolution (JF, 1983) (Meyer-Moock *et al.*, 2014).

- **Modified Fatigue Impact Scale (MFIS)** is a self-reported questionnaire that assesses the impact and severity of fatigue on the daily lives of patients with MS (Gomes, 2011) (Fisk et al., 1994). The MS patients had scores between 3 and 54 (mean score: 30.55 ± 15.51).

- **Symbol Digit Modalities Test (SDMT)** is a written/oral task that measures cognitive processing speed (Sousa *et al.*, 2018).The MS patients had scores between 35 and 71 (mean score: 53.18 ± 11.33).

- **California Verbal Learning Test (CVLT)** is an oral task that assesses auditory and verbal memory (Sousa *et al.*, 2018). The MS patients had scores between 45 and 73 (mean score: 52.27 ± 8.95).

- **Brief Visuospatial Memory Test (BVMT)** is a visual and written task that measures visuospatial learning and memory abilities (Sousa *et al.*, 2018). The MS patients had scores between 16 and 36 (mean score: 26.91 ± 6.83).

- **Reading the Mind in the Eyes (RME)** assesses subtle cognitive dysfunction through identification of the mental state of other people through photographs of their eyes (Baron-Cohen et al., 2001). The MS patients had scores between 18 and 29 (mean score: 24.18 ± 3.52).

Spearman correlation analysis was then performed between the values of FC of every connection in the network and the results in the neuropsychological tests, obtained for the eleven MS patients.

4.1.3 MRI Acquisition

MRI acquisition was done in a 3T Siemens MRI system, at the Institute of Nuclear Sciences Applied to Health (ICNAS), in Coimbra, Portugal.
Each participant's scanning session consisted of an anatomical scan, with a T1-weighted magnetization-prepared 2 rapid acquisition gradient echoes (MP2RAGE) sequence, a functional run of a localiser task (of visual regions V1 and hMT+) and two functional runs of a biological motion (BM) perception task, collected using a 2D-EPI sequence with TR/TE = 1000/37 ms, voxel size = 2 mm isotropic.

Table 4.2 - Main characteristics and parameters of the fMRI acquisition.

Type of Run	Name of Sequence	TR (seconds)	No. runs	Duration (minutes)
Anatomical	MP2RAGE	—	1	10.00
Localiser	2D-EPI	1	1	3.20
BM task		1	2	8.37 each total = 16.74

4.1.4 fMRI Experimental Design

One of the first symptoms of MS is optic neuritis, which affects the patient's visual abilities. Detecting functional changes in the visual system in the context of MS through specifically designed tasks is thus fundamental, and it enables a more feasible comprehension of the compensatory mechanisms that may be happening in this disconnection disease (Martínez-Lapiscina *et al.*, 2014) (Kale, 2016). In this study, two tasks were employed, one passive task of visual motion of kinetic dot patterns and one visual biological motion perception task, which can provide new insights into the brain pathways involved in movement perception.

Passive visual motion task

This task is a passive visualisation of dots in motion, which is commonly used by the neuroimaging community to localise brain regions V1 and hMT+, which are involved in visual motion processing. Hereafter this task will be referred to as *V1MT*.
This functional localiser consists of ten blocks of 18 seconds each. Each block comprises three periods. The first period is a 'fixation period' lasting for 6 seconds, in which the participant looks at a red cross that is located at the centre of the screen. The second period, lasting 6 seconds, involves a pattern of stationary dots. Finally, in the third period, dots that are moving at a constant speed (5 deg/sec), radially, inward and outward from fixation, are shown for 6 seconds (Huk and Heeger, 2002) (Chang *et al.*, 2018). These stimuli are represented schematically in figure 4.1.
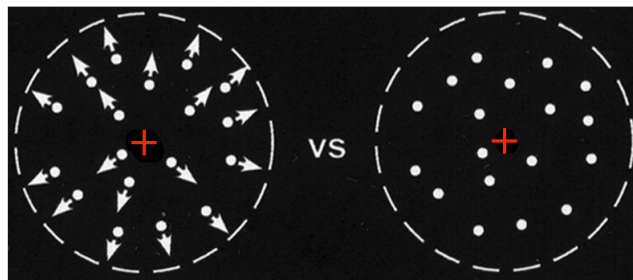

Figure 4.1 - Representation of the stimuli presented during the localiser V1MT task. (Left) Moving dots. (Right) Stationary dots. This task allows the localisation of area hMT+, which is identified based on the responses that are registered to different stimuli: moving dot patterns and stationary dot patterns. These stimuli are presented while the subject fixates a red cross in the centre of the figure. (adapted from (Huk and Heeger, 2002))

Biological Motion perception task

This task was designed to be a more cognitively demanding task than V1MT, by recruiting not only the same V1 and hMT+ regions, but also a network of regions involved in perception of specific patterns of biological motion of humans. Hereafter this task will be referred to as *BM*. Biological motion stimuli are based on human motion. In this task, 12 point-lights are placed at the main joints of a human walker. Each biological motion run has twelve blocks of 40 seconds each. These are divided into 4 or 5 blocks ('body blocks') with the walker facing left or right, 4 or 5 blocks ('foot blocks') with the point-light only in the right ankle (moving to left or to the right), and 3 blocks ('random blocks') of the 12 point-lights positioned in random locations across the y-axis, at the same time maintaining their trajectory across the x-axis. In this acquisition, two biological motion runs are performed which will result in nine body, nine foot and six random blocks being collected. Also, after the stimuli, the participants were asked to report the direction of the dot motion (i.e., if they were moving to the left or to the right), by pressing one of the two available buttons (Soares *et al.*, 2021). These stimuli are represented schematically in figure 4.2.
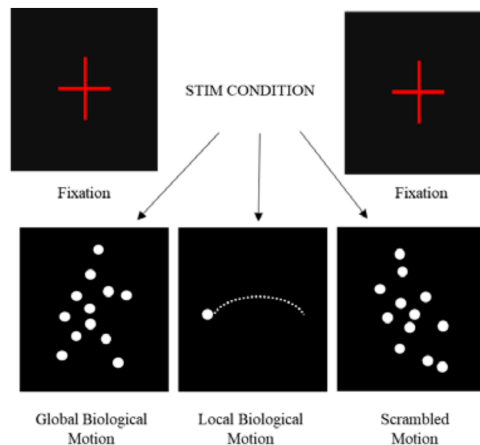
Figure 4.2 - Representation of the stimuli presented during the biological motion task (Soares *et al.*, 2021).

4.1.5 Pre-processing of fMRI Data

Pre-processing fMRI data allows for the identification and correction of artefacts and noise in the BOLD signal (section 2.2.6.1). This process is done with software that can analyse sequences of brain images acquired with fMRI, namely MATLAB®, SPM12, the PhysIO toolbox (Kasper *et al.*, 2017), but also FMRIB Software Library (FSL) that is used for image distortion correction.

In this thesis, the pre-processing pipeline of the fMRI data includes the following steps in the first part: (1) slice timing correction, (2) realignment and motion correction (relative to the first volume), (3) geometric distortions correction and (4) bias field correction (Soares *et al.*, 2021).

The second part of pre-processing consists of the regression of the non-neuronal fluctuations, namely, WM and ventricular CSF BOLD fluctuations, cardiac signals, respiratory signals, and head motion: (1) coregistration (anatomical to functional), (2) segmentation of structural image and extraction of the WM and ventricular CSF masks, (3) computation of the physiological noise fluctuations, including 6 motion parameters, with PhysIO toolbox, which were then regressed out of the BOLD signal, (4) with framewise displacement the volumes with motion outliers were identified and interpolated, (5) the "clean images" obtained from the 4 previous steps were brain masked, (6) spatial smoothing (3 mm full-width-at-half-maximum (FWHM) isotropic Gaussian kernel), (7) high-pass temporal filtering (cut-off period of 12 seconds for the localiser run and 80 seconds for the biological motion runs) (Soares *et al.*, 2021).

4.2 Network Construction

4.2.1 ROI Selection

The connectivity metrics were calculated in a restricted network of brain regions of interest (ROIs) known to be involved in the processing of visual biological motion stimuli based on existing literature. Early-level visual regions V3A and hMT+ and four additional extrastriate regions that have been previously implicated for biological motion perception were included (Chang *et al.*, 2018). The ROIs were calculated using MarsBaR toolbox (Brett *et al.*, 2002) and each was defined as a sphere (5 mm radius) centered on [x y z] MNI coordinates of: [±26, -91, 6] for V3A and [±44, -73, 5] for hMT+ (Tootell *et al.,* 1997) (Castelo-Branco *et al.,* 2002) (Aspell, Tanskanen and Hurlbert, 2005) (Koyama *et al.*, 2005) (Duarte *et al.*, 2017), [±58, -46, 6] for the posterior superior temporal sulcus (pSTS) (Sunaert *et al.*, 1999), [±37, 10, 28] for the inferior frontal gyrus (IFG) (Saygin *et al.*, 2004) (Saygin, 2007) [left -46, -75, -4; right 47, -71, -4] for the extrastriate body area (EBA) (Peelen, Wiggett and Downing, 2006) (Jastorff and Orban, 2009), as well as [left -38, -38, -27; right 43, -43, -28] for the fusiform body area (FBA) (Peelen, Wiggett and Downing, 2006) (Jastorff and Orban, 2009). Two additional ROIs recently found to be functionally synchronized during different stages of biological motion processing were considered (Pavlova *et al.*, 2017) (Sokolov *et al.*, 2018) these were located at [±42, -56, -14] for the fusiform gyrus (FFG) (Grossman *et al.,* 2000) (Vaina *et al.*, 2001) (Grossman, Blake and Kim, 2004) (Peelen, Wiggett and Downing, 2006) and [±36, 24, 2] for the anterior insula (Saygin *et al.*, 2004) (Freitag *et al.*, 2008).

In summary, the ROIs involved in this BM task and defining our network are:
- Anterior Insula (aINS)
- Extrastriate Body Area (EBA)
- Fusiform Body Area (FBA)
- Fusiform Gyrus (FFG)
- Inferior Frontal Gyrus (IFG)
- Posterior Superior Temporal Sulcus (pSTS)
- Visual Area 3 (V3)
- Middle Temporal Visual Area (V5/hMT+)

More information about these (functional) regions, including location and function, is listed in Table 4.3.

Table 4.3 - Location and main functions of the regions involved in the BM task.

Region of Interest	Location in the Brain	Main functions
aINS	Part of the insular cortex that is situated within the lateral sulcus and separates the temporal lobe from the parietal and frontal lobes (Uddin et al., 2017).	Controls emotional responses and empathic processes. Takes part in the high-level cognitive control and attentional processes during social decision making, as well as in risk evaluation and memory processing (Uddin et al., 2017).
EBA	Extrastriate visual cortex, which is located at the posterior inferior temporal sulcus/middle temporal gyrus, in the temporal lobe (Amoruso, Couto and Ibáñez, 2011).	Responsible for visual perception of static and moving images of the human body and its parts (Amoruso, Couto and Ibáñez, 2011).
FBA	Found ventrally in the fusiform gyrus in the temporal lobe (Amoruso, Couto and Ibáñez, 2011).	Responsible for visual processing of human bodies in contrast to body parts (more holistic image of the human body). Distinguishes human bodies from other objects, such as human-like stick figures (Amoruso, Couto and Ibáñez, 2011).
FFG	Temporal and occipital lobe between the lingual gyrus and parahippocampal gyrus (above), and the inferior temporal gyrus (below) (Palejwala *et al.*, 2020).	Related to face and body recognition, communicating with the visual pathway. The left FFG recognizes "face-like" features in objects that may or may not be actual faces, whereas the right FFG determines if that recognized face-like feature is, in fact, a face (Palejwala *et al.*, 2020).
IFG	Frontal gyri, in the frontal lobe, being a part of the prefrontal cortex (Ishkhanyan *et al.*, 2020).	Contains the Broca's area, involved in language processing, comprehension and production, and speech production (Ishkhanyan *et al.*, 2020). Entertains connectivity with the right STS and exerts substantial BM-specific top-down influences on the early visual cortex (Sokolov *et al.*, 2018).
pSTS	Between the superior temporal gyrus and the middle temporal gyrus in the temporal lobe (Beauchamp, 2015).	Involved in social perception and cognition, including the perception of faces and biological motion, as well understanding others' actions, mental states, and language (Beauchamp, 2015).
V3	Visual cortex (Tootell et al., 1997).	Visual processing of global motion. (Tootell et al., 1997).
hMT+	Extrastriate visual cortex, in the temporal lobe (Born and Bradley, 2005).	Visual perception of motion (speed and direction of moving stimuli) and eye movement (Born and Bradley, 2005).

In total, sixteen brain regions, eight in each brain hemisphere, were chosen to construct the network, represented in a 3D brain in figure 4.3. The corresponding ROIs were saved as whole-brain masks. The mask will have zeros where the location of the voxel does not correspond to the ROI and ones when it does. These masks were then transformed into the same space as the functional images of each participant and used to compute the FC between each pair of regions. Hence, this resulted in 16x16 ROI-to-ROI connectivity matrices.
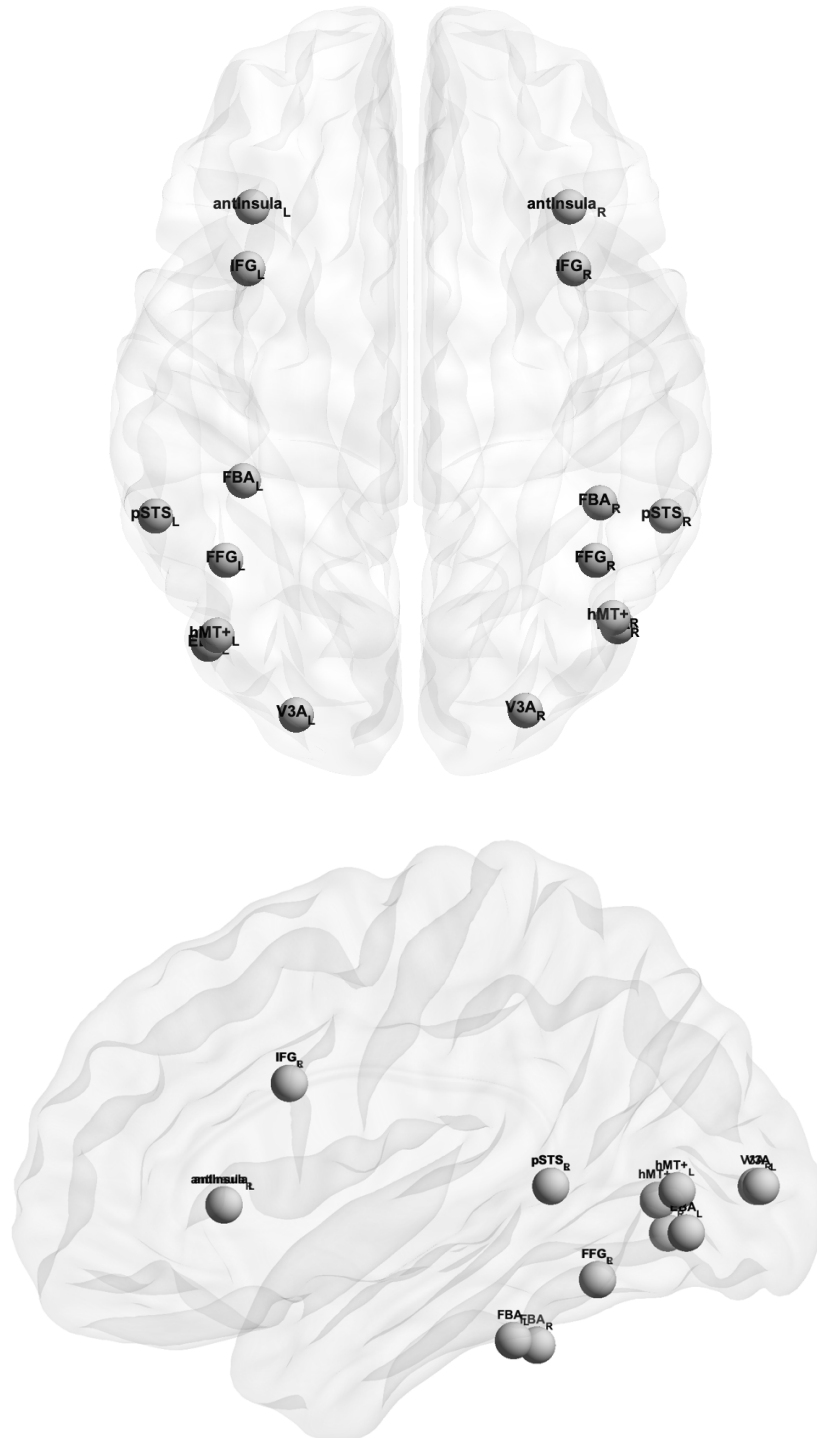
Figure 4.3 - Network with the location of the brain regions involved in the biological motion task. Visualised with the BrainNet Viewer (Xia, Wang and He, 2013), http://www.nitrc.org/projects/bnv/

4.2.2 Average Time Course Export

For each functional run and participant, the BOLD signal (time course) within each of these ROIs was averaged and considered as the region's representing time series for the following sections of the study.

The function will first reshape the 4D fMRI file into a 2D matrix, in which each column is a brain volume, and the rows represent all the voxels that exist in that volume. Then, it reshapes the 3D ROI mask into a vector, in which each row represents the voxels in the mask, only keeping the voxels equal to 1 (true), which indicates that the voxel location corresponds to the ROI. The '*timecourse*' variable stores the average of the time courses of all voxels within the ROI. This is done for all the 16 ROIs in the network.

4.2.3 Granger Causality

GCA was implemented in Matlab through the Multivariate Granger Causality (MVGC) toolbox (Barnett and Seth, 2014). This choice was based on how this toolbox implements GCA through several Matlab routines with optimised computational efficiency and accuracy. It provides a simple way to estimate several important aspects, such as the model order, the model parameters, and statistical inferences, with constant error checking throughout (Barnett and Seth, 2014).

It is based on VAR modelling, which makes it a perfect fit for the temporal predictive behaviour of Granger Causality between multiple variables.

The toolbox provides a *mvgc_demo* script that implements a function that determines pairwise GC, serving as a basis for constructing the connectivity matrices. This function was adapted to receive a set of parameters as input, which intend to define and optimize the model's performance, and all the previously calculated average BOLD time courses of the sixteen ROIs, obtained from the fMRI data.

4.2.3.1 Pipeline of the MVGC Toolbox

After some testing, the following input algorithmic parameters were set regarding the design of the experimental task:

- **Number of trials** - Number of task blocks. Each run in which a task is performed is evaluated individually, hence this parameter is always equal to 1.

- **Number of observations per trial** - Number of volumes per run. For the localiser run, the total number of brain volumes is 192 (equivalent to the seconds that the run lasts for since the TR is equal to 1 second), while for the BM run, the total number of volumes is 502. The two BM runs were concatenated so that the number of observations was higher (the number of observations will then be equal to 1004).

This increase will allow a more precise calculation of the matrices since a small number of points can be detrimental to the calculations although it will make the process more computationally intensive. This is only possible because the two BM tasks are identical.

- **Model order estimation method** - Model order estimation is necessary to choose the number of parameters used to obtain the best model fit and moderate the complexity, while simultaneously avoiding overfitting (Barnett and Seth, 2014). A low model order decreases the model's accuracy, while a high model order causes overfitting and thus makes the process computationally long and intensive (Azarmi *et al.*, 2019). Two criteria were available in the toolbox to estimate the optimal model order: Akaike information criterion (AIC) and Bayesian information criterion (BIC). The BIC was chosen because it is the most accurate when the number of data points is not very large, which is the case in this fMRI study (Azarmi *et al.*, 2019). The model order estimation is defined by the data, so a low sampling rate in fMRI (for example, TR = 1 second), and thus a low number of observations, is usually associated with low model orders (Seth, Barrett and Barnett, 2015).

- **Maximum model order for model order estimation** - Twenty was chosen as a random number to be the highest possible model order (default).

- **VAR model estimation regression model** – Model to calculate the VAR parameters (regression coefficients, A_i, and residuals covariance matrix, $cov(\varepsilon_t)$). The Levinson-Wiggins-Robinson (LWR) algorithm was chosen. The other available choice is the ordinary least squares (OLS) algorithm. However, the LWR algorithm is considered to be the most stable in this context. Also, in the OLS algorithm, the parameters A_i and $cov(\varepsilon_t)$ need to be recomputed separately for each model order, while in the LWR algorithm this is done recursively, which makes this algorithm highly efficient in model selection criteria (Barnett and Seth, 2014).

- **Information criteria regression mode** - Calculation of the model order with AIC and BIC for VAR models. The LWR algorithm is also used.

- **Maximum autocovariance lags** – Lags for the autocovariance sequence. This parameter is empty for automatic calculation (default).

- **Statistical test for MVGC** - The F-test was chosen for statistical analysis of the connectivity matrices. The null hypothesis in this test is that past values of timeseries Y do not explain the variation in timeseries X, i.e., Y does not Granger-cause X. The toolbox alternative for this statistical test is the chi-square test, but this test is usually used only when there is a large number of variables and lags, which is not the case in this study. The F-test has higher statistical power when dealing with small samples, and it is also easier to run (Barnett and Seth, 2014).

- **Multiple hypothesis test correction** – If a given test is repeated many times, it will probably give some false positives (the null hypothesis is incorrectly rejected). In order to control the proportion of these erroneous results and increase the statistical power, a multiple hypothesis test correction is applied. Between all of the offered corrections in the MVGC toolbox (Bonferroni, Sidak, Holm), the False Discovery Rate (FDR) approach was chosen because it is not as strict as the others, thus decreasing

the risk of missing exciting findings. Instead, it controls for a low proportion of false positives (Colquhoun, 2014).

After defining the input parameters mentioned above, the VAR data is also defined, which will correspond to the average BOLD signals (time courses) within each of the 16 ROIs. Then, the model order, i.e, the number of past observations that are going to be included in the VAR model, will be estimated with both methods (AIC and BIC), through the *tsdata_to_infocrit* function, but only the model order provided by the BIC is chosen as the best model order for the reasons explained previously. After this estimation, a VAR model is fitted to the timeseries, through the *tsdata_to_var* function, and the restricted and unrestricted model parameters (regression coefficients, A_i, and residuals covariance matrix, $\text{cov}(\varepsilon_t)$) will be determined to be used in the subsequent calculations. Next, the autocovariance sequence, G, is calculated, as it drives many GC calculations, through the *var_to_autocov* function. Finally, the pairwise GC is determined in the time domain through the *autocov_to_pwcgc* function (Barnett and Seth, 2014) (Seth, Barrett and Barnett, 2015). This function will thus return time-domain pairwise causalities in a square matrix, in this case ROIs x ROIs, of Granger F-values. It also performs a significance test using a theoretical null distribution, which identifies which causalities are statistically significantly different from zero on a matrix with zeros, for non-significant connectivity, and ones, for significant connectivity (figure 4.4).
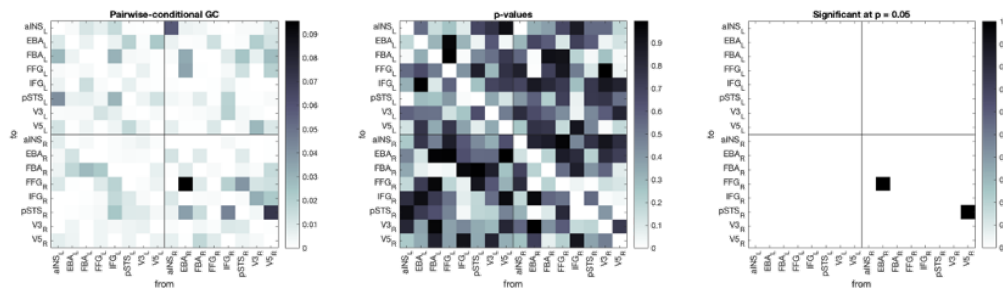
Figure 4.4 - Matrices obtained with the MVGC toolbox. (Left) Matrix with pairwise GC and respective F-values. (Middle) Matrix with the calculated p-values after statistical analysis with the F-test. (Right) Matrix with the statistically significantly connections different from zero (p-value < 0.05).

It is relevant to clarify that the magnitude of the F-values is essentially meaningless since it is only a hypothesis-test statistic. However, it may have an interpretation because Granger Causality can be seen as an approximation to transfer entropy when analysing Gaussian data, and thus the F-values, as measures of directed information flow, can be compared within experimental conditions (Barnett and Seth, 2014) (Seth, Barrett and Barnett, 2015).

4.2.4 Influence of ROI Size

After a remodelling of the methodology, an experiment regarding ROI size was done to possibly draw conclusions about this parameter's influence on the network's connectivity and on the statistically significant differences between groups.

Two radiuses with 5 mm and 10 mm were explored to define the ROIs in 20 participants: 11 MS patients and 9 healthy controls. The regions' definition and the process used to obtain the connectivity matrices is the same for both ROI sizes.

4.2.5 Connectivity Measures

The connectivity measures were calculated with the Brain Connectivity Toolbox (BCT). This toolbox is implemented in Matlab and can perform network analysis of functional connectivity datasets, based on graph theory (Rubinov and Sporns, 2010).

In section 2.3.4, twenty connectivity measures were described. These measures are primarily used in whole-brain analyses and rs-fMRI studies, such as those reviewed in the state of the art. Because we have a more restricted network of 16 regions (8 per hemisphere) that are involved specifically in connections when a visual task is performed, it is not intuitively reasonable to compute some of these measures. Thus, the following rationale (described below) was used to decide on which measures to use in our context, also considering their reliability (Welton *et al.*, 2020) and frequency with which they are used in the literature.

Segregation measures (mean clustering coefficient, transitivity, modularity) were excluded since it is assumed that the restricted network with 16 regions is already segregated, as it is specifically recruited when the participants are presented with the task. Segregation means the separation of the brain regions into functionally specialized groups, but this network is already specialized in this particular visual BM task. Similarly, the small-worldness index (i.e., the balance between functional segregation and integration) was excluded. Also, all measures that include calculations involving creation of groups/modules/subgraphs are excluded because of the reasons mentioned above (within-module degree, participation coefficient, subgraph centrality and k-coreness centrality). Finally, eigenvector centrality was excluded because its calculation only applies to undirected networks, which is not the case in these matrices obtained with GC. However, there is a directed variant - pagerank centrality - which was used instead.

Therefore, the connectivity measures calculated in this study were the characteristic path length, global efficiency, local efficiency, global flow coefficient, local flow coefficient, total flow, assortativity, eccentricity, radius, diameter, total degree, in-degree, out-degree, mean network strength, total strength, in-strength, out-strength, betweenness centrality and pagerank centrality. Some of these measures are represented in figure 4.5.
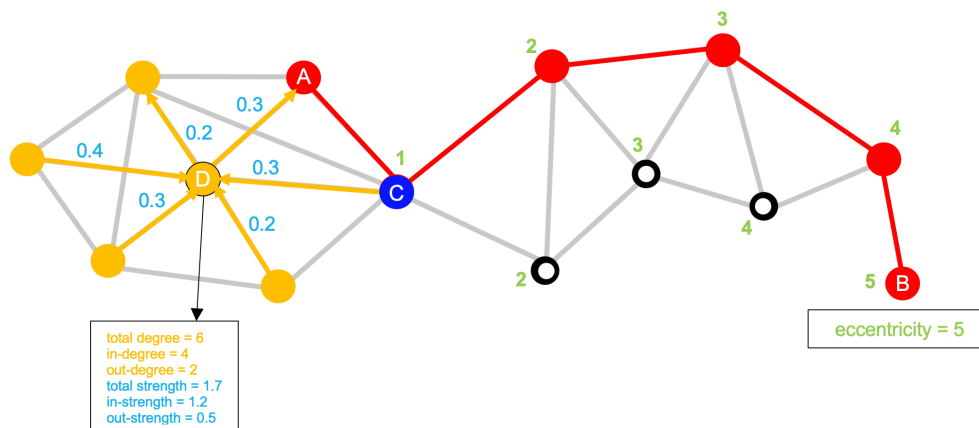
Figure 4.5 - Schematic representation of some of the used connectivity measures. In red is represented the characteristic path length from node A to node B (shortest path length, or minimum number of edges, between the nodes). In dark blue is node D with the highest betweenness centrality (number of times that the node lies on the shortest paths between every node). In yellow are the edges that connect node C to the neighbour nodes – total degree; the incoming connections to node C represent the in-degree and the outgoing represent the out-degree. In light blue is the weight of each of these edges: their sum represents the total strength of the node; the sum of the incoming connections represents the in-strength, and the sum of the outgoing connections represents the out-strength. In green is the eccentricity of node A: first, all of the shortest paths between node A and every other node are calculated (green numbers represent the number of nodes in these paths), and then the longest one of all of these node's paths is chosen (in this case, the path reaching node B) (Rubinov and Sporns, 2010).

4.2.5.1 Matrix Thresholding

Thresholding is often applied after network construction to remove spurious connections that do not contain relevant information and to, consequently, obtain sparsely connected matrices, which are essential for the calculation of the connectivity metrics. Despite this, some studies argue that this process could potentially ignore valuable information within the matrix (Fornito et al., 2016) (Hallquist and Hillary, 2019).

There are several methods for network thresholding, but the most commonly used (and the ones available in the BCT) are the absolute thresholding, which is a weight-based approach, and the proportional thresholding, a density-based approach. The choice between the two methods depends on whether or not a difference in connection density is viewed as a confound (Kaiser, 2011) (Fornito et al., 2016).

The absolute thresholding is the most straightforward approach because it thresholds by absolute weight of the connections, i.e., it applies a single threshold value to the whole matrix. Therefore, all elements above that threshold are maintained, and the rest below the threshold are set to zero. Several criteria may be adopted to choose a threshold such as using a significance level, thus omitting values that can be expected by chance; using an arbitrary value that can keep a certain average degree of the network; or using a large value so that it is guaranteed that all of the network's nodes are connected. The main limitation of this absolute thresholding approach is that topological properties generally vary as a function of the number of edges in a network, and usually, the obtained thresholded matrices have a different number of edges, which can be problematic in the analysis of differences between groups (Fornito et al., 2016) (Hallquist and Hillary, 2019).

The proportional thresholding approach aims to keep a fixed network density, i.e., the number of connections (or edges) is the same across all individuals. This solves the problem of the

network density's influence in the metrics' calculation and their comparison between groups since the threshold can vary from person to person. This approach consists of choosing a proportion (PTh) between 0 and 1, thus preserving only the strongest weights (Fornito et al., 2016) (Hallquist and Hillary, 2019). Proportional thresholding is commonly applied in disease connectome studies because removing the bias in the number of edges results in more stable and reliable connectivity measures. However, if the proportion is elevated and a high density is chosen, spurious connections may have a negative impact on the calculations, as they add noise to the signal (Hallquist and Hillary, 2019).

In this thesis, we opted for proportional thresholding, as it is the most used in research, particularly related to MS, and generates the most reliable results compared to the absolute threshold.

4.2.6 Methodology - Summary
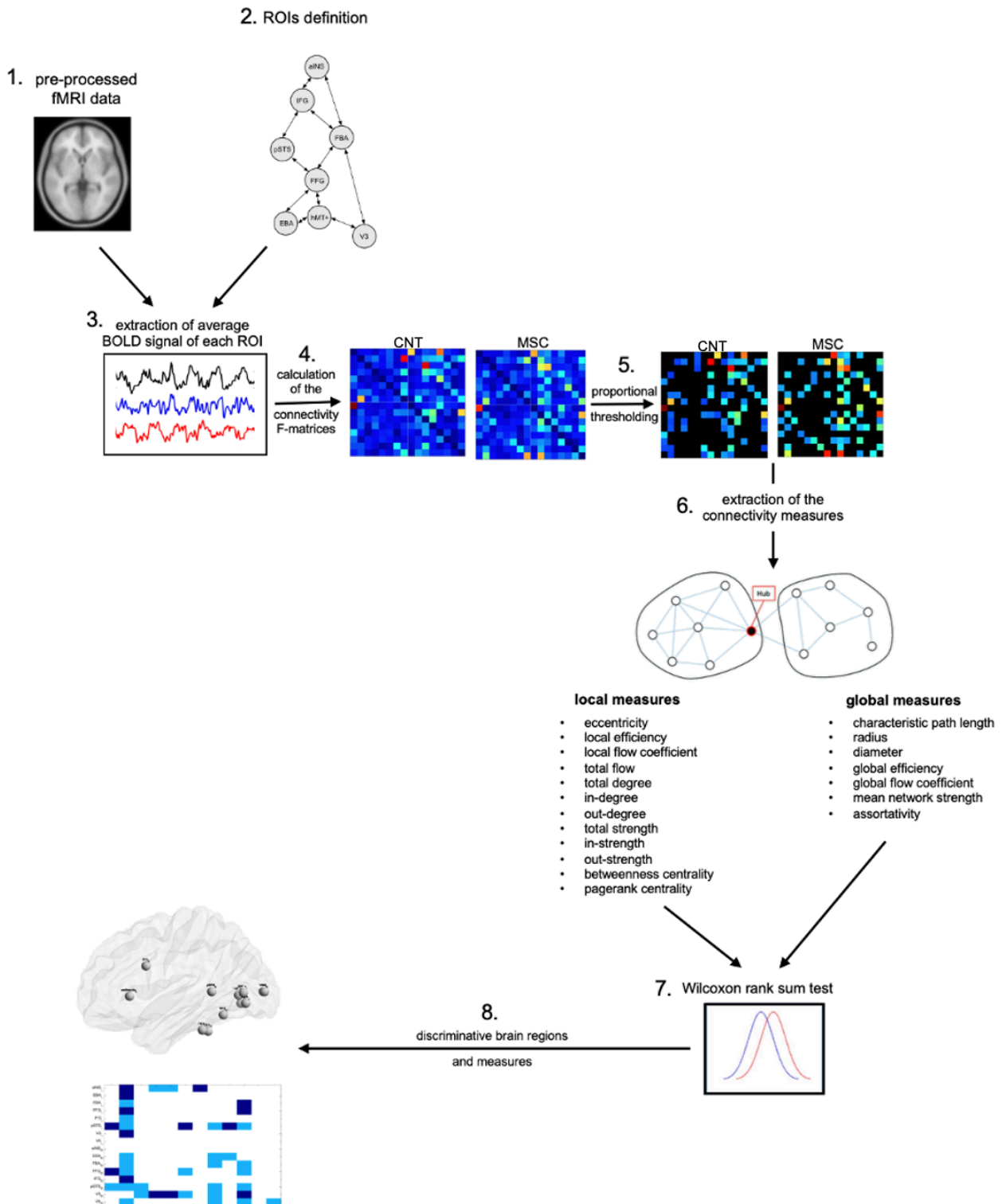
Figure 4.6 - Schematic representation of the steps followed in this study. (1) Pre-processing of the fMRI data; (2) ROIs definition; (3) Extraction of the average BOLD signal for each ROI; (4) Calculation of the F-matrices with GC; (5) Proportional thresholding of the F-matrices; (6) Extraction of the local and global connectivity measures; (7) Between-groups statistical analysis with the Wilcoxon rank sum test (significantly different metrics between groups when p<0.05); (8) Analysis of the discriminative regions and measures between healthy controls and MS patients. Adapted from (Sporns, 2013b) (Miri Ashtiani *et al.*, 2018) (Azarmi *et al.*, 2019)

5

Results and Discussion

5.1 Individual MVGC Matrices

With the MVGC toolbox, the ROI x ROI matrices with the pairwise Granger causalities are calculated. Each element a_{ij} of the matrix represents the F-value between every two regions involved in the visual tasks, which will be our measure of functional connectivity (FC) between ROIs (sections 2.3.2 and 4.2.3.1), even though it does not have yet a known biological meaning (regarding the underlying mechanism). The statistical testing is performed with the F-test, and its results are also presented in matrix form in which each coloured square represents a statistically significant connection (with p-value < 0.05, FDR corrected) between two regions. The null hypothesis of the F-test, in this case, is that the activation of a region Y does not Granger-cause the activation of a region X, i.e., $F_{y \rightarrow x}$ of the connections is significantly different from zero (section 2.3.2). If the null hypothesis if rejected (at p-value < 0.05) then Y Granger-causes X.

The matrices from figures 5.1 and 5.2 are a sample of the obtained individual matrices, taken for two age-matched participants (control 9 and patient 14). All fifty-eight calculated matrices (twenty-nine for each task: V1MT and BM) for each participant are in Appendix I.

Henceforth, in graphics and tables, the experimental run with task V1MT run will be designated by RUN V1MT, and the two concatenated experimental runs with the biological motion perception task will be named RUNS BM. The group of healthy controls will be named CNT, and the group of MS patients will be named MSC.
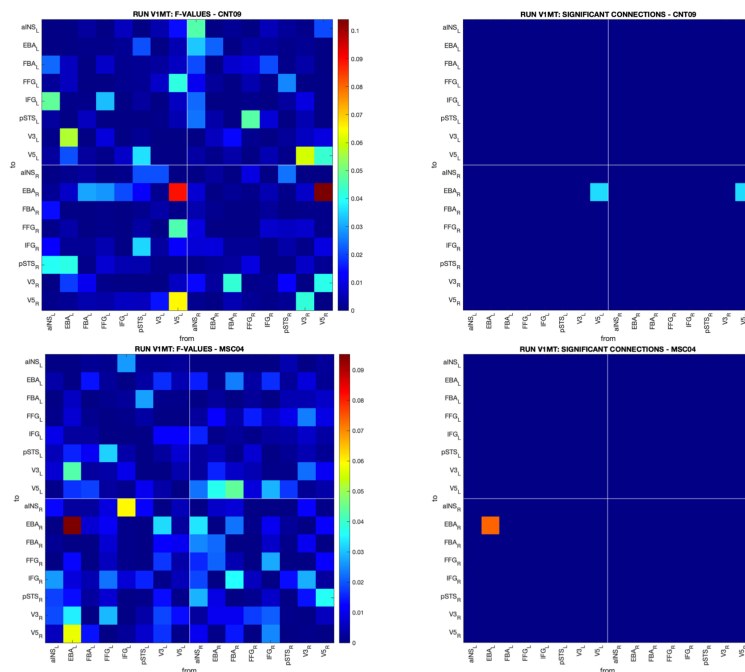
Figure 5.1 - Individual ROI x ROI matrices for two age-matched participants: healthy control 9 and MS patient 4, in the V1MT run. (Top left) Matrix with the pairwise Granger F-values for each connection between every two regions involved in the task, for CNT09. (Top right) Statistically significant connections, after performing the F-test (p<0.05) for CNT09. (Bottom left) Matrix with the Granger F-values for each connection for MSC04. (Bottom right) Statistically significant connections, after performing the F-test (p<0.05) for MSC04. The colorbars in the left matrices represent the F-values.
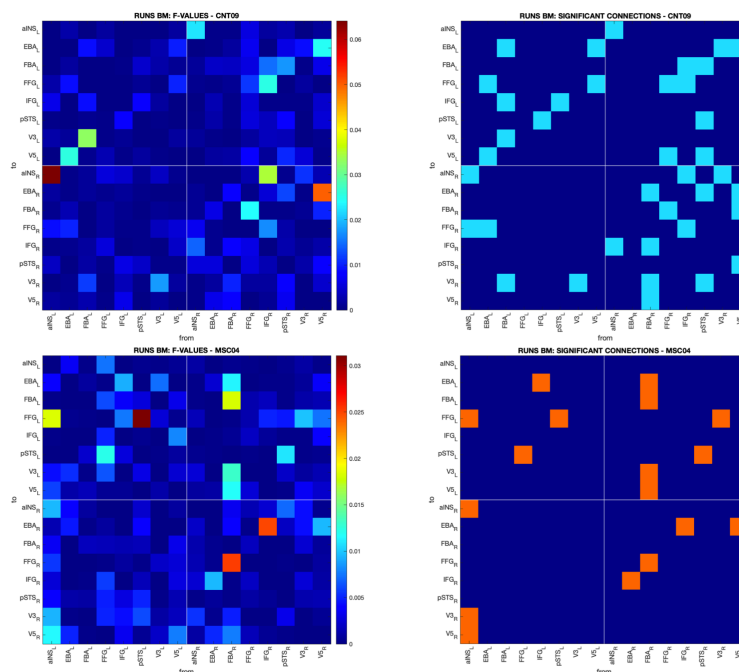
Figure 5.2 - Individual ROI x ROI matrices for two age-matched participants: healthy control 9 and MS patient 4, in the BM runs. (Top left) Matrix with the pairwise Granger F-values for each connection between every two regions involved in the task, for CNT09. (Top right) Statistically significant connections, after performing the F-test ($p<0.05$) for CNT09. (Bottom left) Matrix with the Granger F-values for each connection for MSC04. (Bottom right) Statistically significant connections, after performing the F-test ($p<0.05$) for MSC04. The colorbars in the left matrices represent the F-values.

The major distinction between the two runs, observed through the individual matrices, is that in the V1MT run, there are considerably less statistically significant connections than in the BM runs, both in controls and MS patients. This is expected because it is easier to find significant differences with a larger sample size (BM runs are much longer) as small differences become more detectable. Furthermore, we should also consider that the BM task is more demanding and recruits more heavily the connections of the restricted network than the passive task performed during the V1MT run. This might originate as well that more significant connections emerge in the BM runs.

Interestingly, the observation that MS patients and age-matched healthy controls display different significant connections between the brain regions involved in either task (V1MT and BM) and different F-values of connectivity implies different brain organization, despite similar task performance.

After the calculation of the individual matrices, each matrix's total mean connectivity value was determined. The mean values for CNT and MSC are presented in Table 5.1.

Table 5.1 - Mean values of the individual F-matrices of runs V1MT and BM, for CNT and MSC.

	Participant	Mean F-Value	
		Run V1MT	Runs BM
CNT	1	0.0063	0.0048
	2	0.0066	0.0020
	3	0.0071	0.0035
	4	0.0075	0.0033
	5	0.0075	0.0018
	6	0.0061	0.0017
	7	0.0075	0.0033
	8	0.0062	0.0033
	9	0.0079	0.0038
	10	0.0069	0.0019
	11	0.0060	0.0037
	12	0.0063	0.0036
	13	0.0062	0.0020
	14	0.0059	0.0031
MSC	1	0.0072	0.0041
	2	0.0070	0.0032
	3	0.0071	0.0032
	4	0.0082	0.0024
	5	0.0071	0.0041
	6	0.0080	0.0045
	7	0.0074	0.0022
	8	0.0072	0.0029
	9	0.0075	0.0032
	10	0.0080	0.0036
	11	0.0058	0.0016
	12	0.0069	0.0025
	13	0.0068	0.0040
	14	0.0069	0.0030
	15	0.0073	0.0027

The F-values are higher in the V1MT localiser run than in the BM runs. However, because the F-value has no known direct biological meaning (section 4.2.3.1), we should only compare values obtained in the same experimental condition (i.e., within the same run).

Moreover, although the F-values seem slightly more elevated in the MS patients (in each run), it is difficult to compare the groups relying only on individual connectivity matrices or their mean F-values. Hence, to better analyse differences between MS patients and healthy controls, the mean connectivity matrices for each group were calculated.

5.2 Mean Matrices

The mean matrices for both runs (V1MT and BM) and both groups of participants (CNT and MSC) were determined and are represented in figure 5.3. In each run, the F-values of the two groups were normalized to the maximum value. The total mean F-value of each of these matrices was also calculated and is displayed in the figure.

	CNT	MSC
RUN V1MT	Mean F-value: 0.0067	Mean F-value: 0.0072
RUNS BM	Mean F-value: 0.0030	Mean F-value: 0.0032
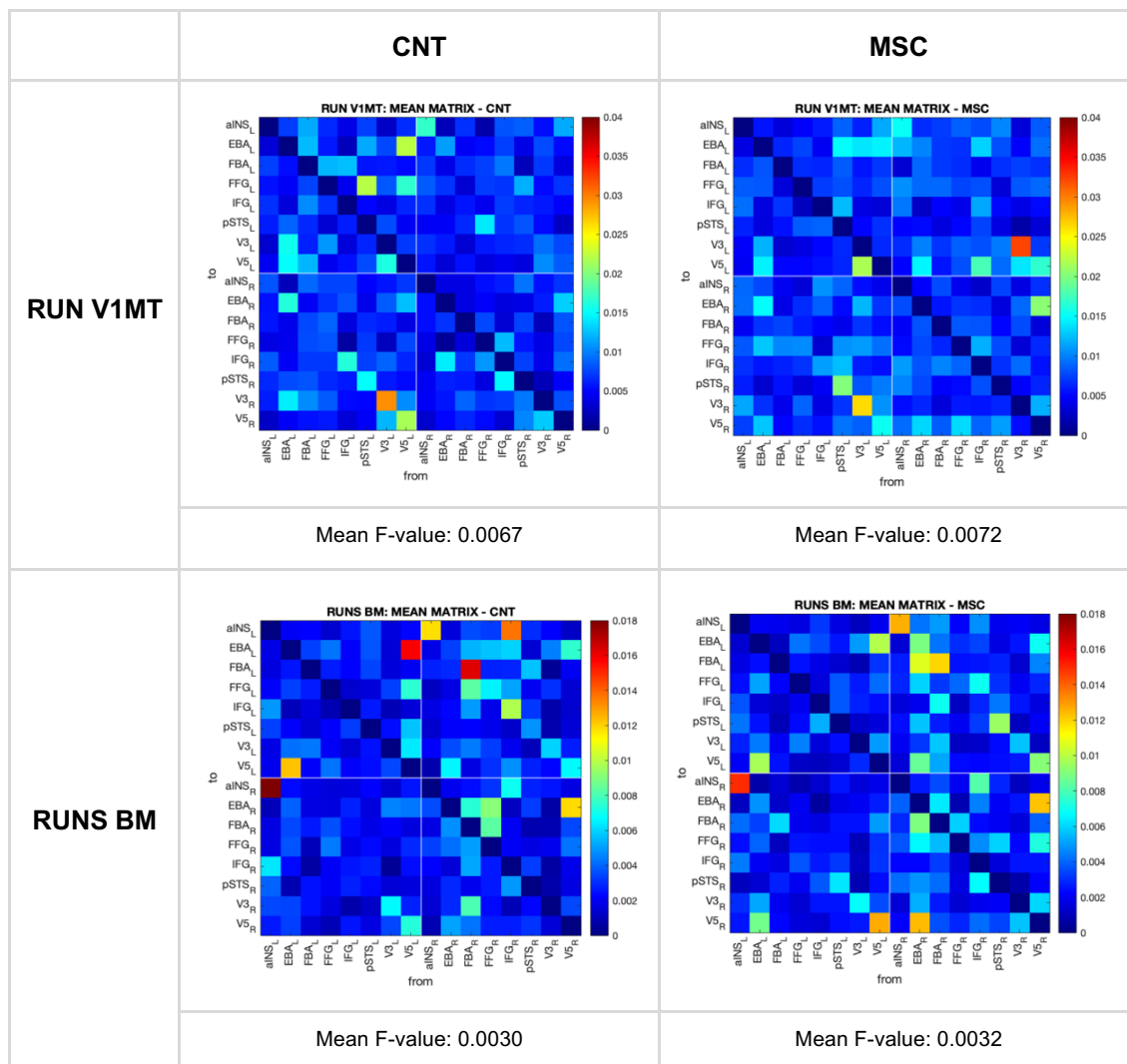
Figure 5.3 - Mean matrices for both groups (CNT and MSC) and both runs (V1MT and BM) and respective mean total F-value. The F-values in each matrix's element represent the mean F-value of that specific connection for all of the participants in the group. The colorbars represent the F-values.

From these data, it can be observed that there is an increase (of 0.0005 units) in the mean F-value, in patients with MS, in the V1MT localiser run. This aspect can also be observed in the BM runs, where there is an increase in the mean F-value in the patients' group, although not as noticeable as the one seen in the V1MT run (increase of 0.0002).

To further validate this finding of the increase in the F-values in MS patients, in both runs, histograms with the distribution of the F-values for each of the groups of participants were constructed separately for each run and represented in figure 5.4.
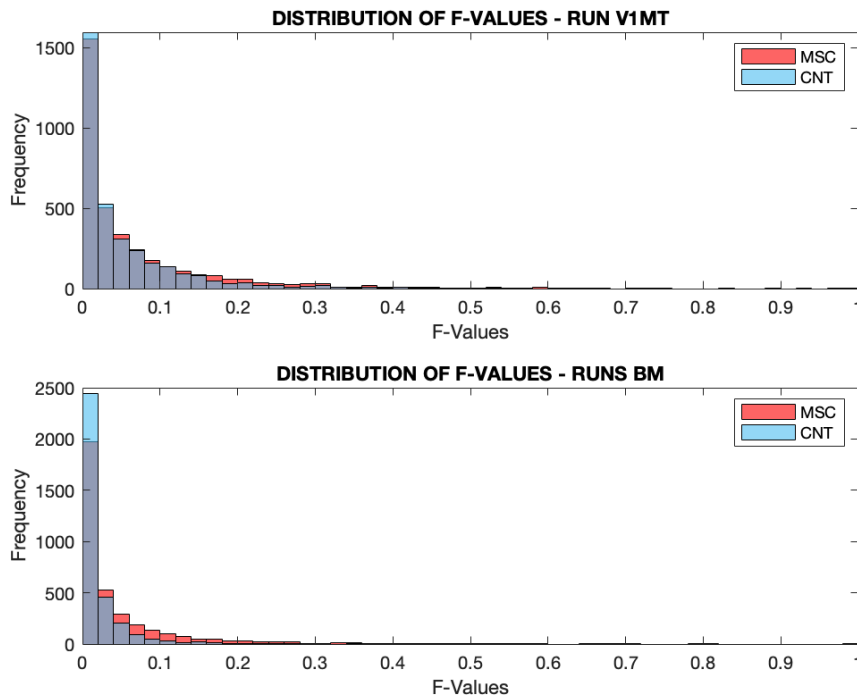
Figure 5.4 - Histogram with the distribution of the F-values for both groups and runs. (Top) Histogram with the distribution of the F-values for both groups (MSC in red and CNT in blue) in the V1MT run. (Bottom) Histogram with the distribution of the F-values for both groups (MSC in red and CNT in blue) in the BM runs.

The distributions of both groups, in the two runs, are skewed right, and generally, most of the F-values are very low. However, there is a slight increase of the F-values in the MSC group, also for both runs, as shown by the increased height of the red bars in higher F-values.

These results suggest that the F-values, and consequently FC, generally increase in MS patients in both visual tasks. This may be due to brain neuroplasticity, the compensatory response described in disconnection conditions, often characterised by an increase in connectivity (more information in Chapter 3) (Audoin *et al.*, 2003) (Droby *et al.*, 2016) (Faivre *et al.*, 2016). The rise in connectivity in both the localiser and biological motion runs also implies that this could be a generalized mechanism of the brain of MS patients that does not depend on the complexity of the task.

Nonetheless, although the nature of F-values does not allow us to compare them between different experimental conditions directly, we can, theoretically, compare the number of significant connections between conditions and/or groups. We observe that there are more connections with elevated values of FC during the biological motion task, which could be explained due to the slightly heightened complexity of the task, that also includes decision-making and will inherently involve more brain regions in information exchange and processing.

5.3 Within-Group Statistical Analysis

Within-group statistical analysis can reveal the significant connections between regions in each group (CNT and MSC) in both tasks. The analysis was performed with the F-test, available in the MVGC Toolbox. If the null hypothesis is rejected ($p < 0.05$), it means that the F-values of the connection are significantly different from zero. The results of this analysis are shown in figure 5.5, in which the F-values of only the statistically significant connections are represented.
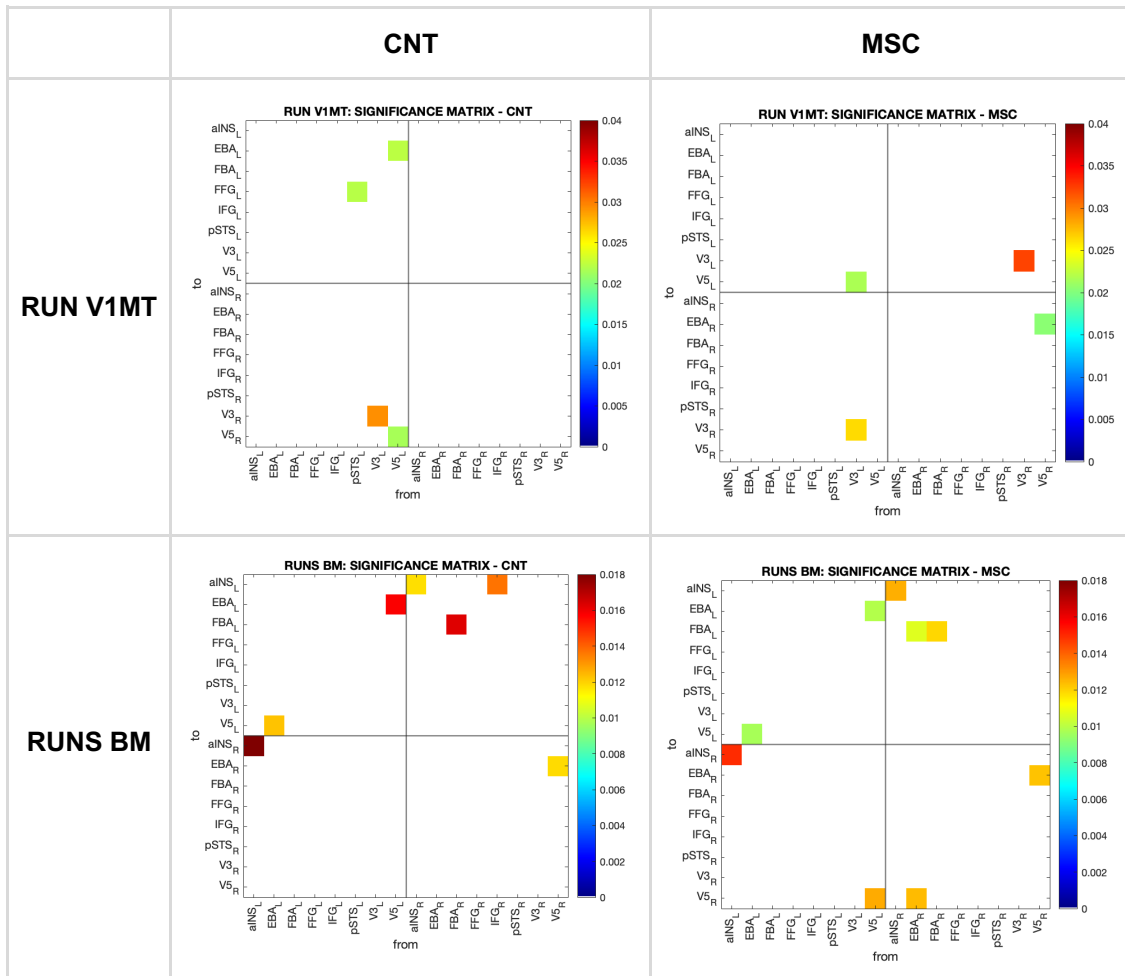
Figure 5.5 - Matrices with the F-values of the statistically significant connections for both groups (CNT and MSC) and both runs (V1MT and BM). Significant connections in run V1MT: $p < 0.05$, no correction for multiple comparisons (because there would be no connections left). Significant connections in runs BM: $p < 0.05$, FDR correction. The colorbars represent the F-values.

With the BrainNet Viewer toolbox, a 3D representation of the matrices from figure 5.5 is obtained.
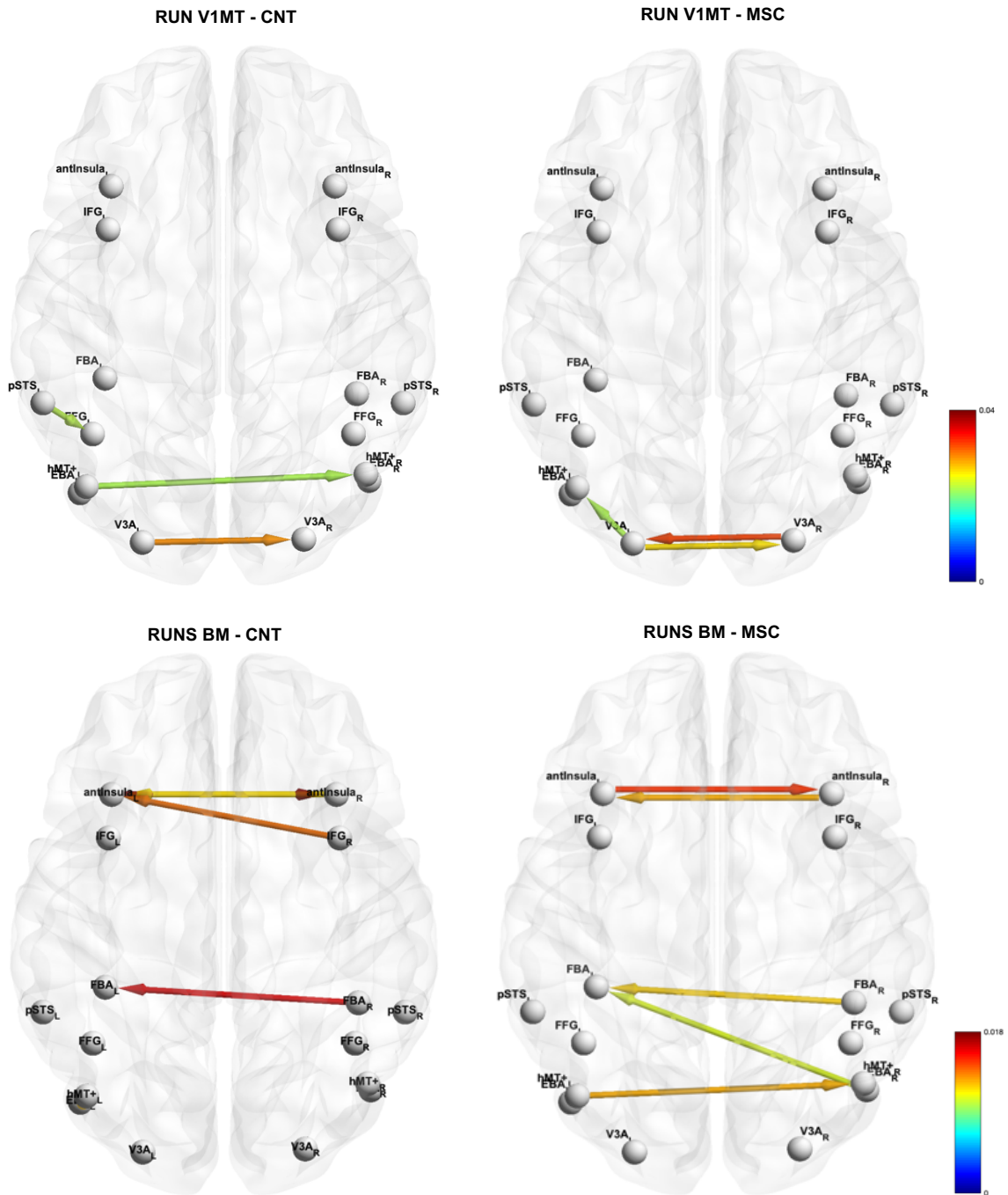
Figure 5.6 - 3D representation of the significant connections within the mean matrices of figure 5.5. (Top left) 3D representation of the significant connections within the mean matrix for the CNT group, in the V1MT run. (Top right) 3D representation of the significant connections within the mean matrix for the MSC group, in the V1MT run. (Bottom left) 3D representation of the significant connections within the mean matrix for the CNT group, in the BM runs. (Bottom right) 3D representation of the significant connections within the mean matrix for the MSC group, in the BM runs. The colorbars represent the F-values of the significant connections in the brain. The 3D representations were created with the BrainNet Viewer (67) (Xia, Wang and He, 2013), http://www.nitrc.org/projects/bnv/.

The within-group analysis shows more connections with high F-values in the BM runs (mainly corresponding to red, orange, and yellow elements in the mean matrices) than in the V1MT run. In the localiser run, the significant FC connections are mainly between visually related regions (V3 and hMT+) as this task primarily requires the visual cortex's activation (Huk and Heeger, 2002) (Chang *et al.*, 2018), whereas in the biological motion runs, there are more significant FC connections between regions specifically involved in biological motion (aINS, FBA, EBA, hMT+) (Chang *et al.*, 2018). This is in line with (Cardin, Friston and Zeki, 2011) that demonstrated that recognizable stimuli (BM runs) result in larger activations in anterior visual and frontal regions and that random stimuli, such as in the localiser run, activate more posterior visual areas.

Noteworthy, hMT+ seems to have a determinant role in both runs, which fits in with the idea that this region appears as an intermediate between the primary visual cortex and higher-order regions (Born and Bradley, 2005) (Sokolov *et al.*, 2018). Surprisingly, pSTS is not involved in the significant connections in the BM runs, although it is assumed in the literature to be the region with the most relevance in the performance of this kind of task since it has a major role in the perception of biological motion (Sokolov *et al.*, 2018) (Chang *et al.*, 2018).

Regarding the significant connections in each group during each task, the MS patients exhibited connectivity pattern alterations of four types: decreased and increased shared connections with CNT, a gain of new connections that CNT did not show, and loss of connections that were observed in CNT.

- In the V1MT run, the only shared connection between CNT and MSC was $V3_L \rightarrow V3_R$, which showed a decreased FC in MSC compared to CNT.
  MSC attained three extra connections, mainly between visual areas: $V3_L \rightarrow V5_L$, $V3_R \rightarrow V3_L$ (which is an inversion of the shared connection $V3_L \rightarrow V3_R$) and $V5_R \rightarrow EBA_R$. MS patients also lost the $V5_L \rightarrow EBA_L$ connection seen in CNT: it appears that the patients did not lose this connection in the left hemisphere, but instead, it was shifted to the right (opposite) hemisphere. This could be yet another form of validation of the brain's adaptive response when facing an insult (a change of a function or connection to the other brain hemisphere). They also lost the $pSTS_L \rightarrow FFG_L$ and $V5_L \rightarrow V5_R$ connections.

- In the BM runs, there are several different significant connections between groups and new connectivity patterns. Most of the shared connections have lower FC values, and are thus weaker, in MSC: $aINS_L \rightarrow aINS_R$, $EBA_L \rightarrow V5_L$ and its inverted form $V5_L \rightarrow EBA_L$ and $FBA_R \rightarrow FBA_L$. It seems that the connections with a higher FC in MSC also shifted hemispheres: the $aINS_L \rightarrow aINS_R$ connection that had higher FC in CNT now starts in the right hemisphere ($aINS_R \rightarrow aINS_L$), and the $V5_L \rightarrow EBA_L$ in CNT now appears with higher FC values in MSC in the right hemisphere ($V5_R \rightarrow EBA_R$). MSC lost the connection $IFG_R \rightarrow aINS_L$ and attained the connections $V5_L \rightarrow V5_R$, $EBA_R \rightarrow V5_R$ and $EBA_R \rightarrow FBA_L$. In general, MSC has more significant connections, which could imply the recruitment of additional brain regions during task performance and suggest that this is an adaptive response to disease-associated brain injury (Parry *et al.*, 2003).

Summarizing, Table 5.2 shows the connections with statistically significant connectivity values in the V1MT localiser run and Table 5.3 shows the connections with statistically significant connectivity values, in the BM runs.

Table 5.2 - Statistically significant connections in the V1MT run (within-group analysis with F-test). They are divided into shared connections between CNT and MSC (and subdivided in higher or lower values of FC in MSC) and connections only existent in CNT and MSC.

SHARED CONNECTIONS		ONLY CNT CONNECTIONS	ONLY MSC CONNECTIONS
Lower values in MSC	Higher values in MSC		
$V3_L \rightarrow V3_R$	—	$V5_L \rightarrow EBA_L$	$V3_L \rightarrow V5_L$
		$pSTS_L \rightarrow FFG_L$	$V5_R \rightarrow EBA_R$
		$V5_L \rightarrow V5_R$	$V3_R \rightarrow V3_L$

Table 5.3 - Statistically significant connections in the BM runs (within-group analysis with F-test). They are divided into shared connections between CNT and MSC (and subdivided in higher or lower values of FC in MSC) and connections only existent in CNT and MSC.

SHARED CONNECTIONS		ONLY CNT CONNECTIONS	ONLY MSC CONNECTIONS
Lower values in MSC	Higher values in MSC		
$aINS_L \rightarrow aINS_R$	$aINS_R \rightarrow aINS_L$		$V5_L \rightarrow V5_R$
$EBA_L \rightarrow V5_L$		$IFG_R \rightarrow aINS_L$	$EBA_R \rightarrow V5_R$
$V5_L \rightarrow EBA_L$	$V5_R \rightarrow EBA_R$		
$FBA_R \rightarrow FBA_L$			$EBA_R \rightarrow FBA_L$

A noteworthy aspect is that in the BM runs, the connection from IFG_R ($IFG_R \rightarrow aINS_L$) in the frontal lobe disappears in MSC. Instead, connections from EBA_R ($EBA_R \rightarrow V5_R$, $EBA_R \rightarrow FBA_L$) in the temporal lobe emerge. This is in concordance with research in Alzheimer's Disease (AD) that showed that one of the hallmarks of neuroplasticity is the over-recruitment of extrastriate areas (EBA, for example) (Rytsar *et al.*, 2011).

Another interesting result to consider is that the connections between homologous interhemispheric regions, i.e., same regions but in opposite hemispheres (L → R, R → L), are prevalent in MSC. This may be a result of *homologous area adaptation*, in which if a given region (or module) becomes damaged, its function is shifted to a homologous region that is unimpaired (Grafman, 2000) (Stephan *et al.*, 2007). When the neural resources of the hemisphere that is receiving the stimulus are insufficient for optimal processing, there is a distribution of the established connections across both hemispheres, which implies a task-dependent increase in interhemispheric connectivity (Stephan *et al.*, 2007). This is further supported by the consistent observation in the two runs that, in run V1MT, $V5_L \rightarrow EBA_L$ is only present in CNT, and $V5_R \rightarrow EBA_R$ is only present in MSC, and in runs BM, although they are shared connections in controls and MS patients, $V5_L \rightarrow EBA_L$ has a higher FC in CNT, and $V5_R \rightarrow EBA_R$ has higher FC in MSC. It is not difficult to believe that this might result from interhemispheric homologous "connection" adaptation.

5.4 Between-Groups Statistical Analysis

The within-group statistical analysis of the previous section intended to find the significant differences within each group (CNT and MSC) for each run. The resulting connections were, thus, statistically different from zero and allowed a qualitative comparison between groups and the more active connections elicited by the two tasks. In this between-groups analysis, only connections that are statistically different between the two groups are assessed.

The data (F-values for each group and run) were tested for normality using the Kolmogorov-Smirnov (KS) test and through visual inspection of the histograms. As the data are not normal, a statistical group analysis using a two-tail, two-sample Wilcoxon rank sum test was performed to determine the differences in the directed FC between CNT and MSC. In this statistical test, the null hypothesis is that the two independent group samples have an equal median. The alternative hypothesis is that they do not. The result (the test decision), h, is equal to 1 if the null hypothesis is rejected at a 5% significance level, and 0 otherwise. The results are not corrected for multiple hypothesis testing, a decision made to decrease the probability of missing potentially interesting effects and justified with the reasonably low number of connections considered in this restricted network (compared to typical whole-brain analysis).

In figures 5.7 and 5.8, there are two matrices. The first matrix in each figure, in the left, has the p-values of the connections that are statistically significantly different between groups (p < 0.05), and the second matrix, in the right, shows the difference between the medians of the F-values of the two groups for each significantly different connection (since the data is not normally distributed, the median was calculated instead of the mean). This value of the difference in medians between the groups gives information about which group's median is higher. If the value is positive, the median of the MS patients' group is higher (represented in red colours in the second matrix), meaning that F-values are generally greater in MS patients. If the value is negative, the median of the controls' group is higher (represented in blue colours), and the F-values are generally greater in healthy controls.

RUN V1MT
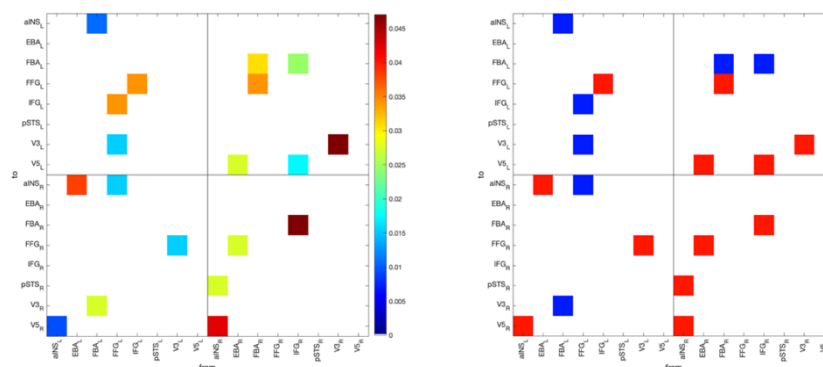
Figure 5.7 - Results of the between-groups statistical analysis, for run V1MT. (Left) p-values obtained with between-groups statistical analysis performed with the Wilcoxon rank sum test (only statistically significantly different connections between groups are shown, p < 0.05). The colorbar represents the p-values, ranging from 0 (blue) to 0.05 (red). (Right) Difference in the medians of F-values in the same significantly different connections between the two groups (CNT and MSC). Red colours represent a higher median in the MS patients' group and blue colours represent a higher median in the healthy control group.

Table 5.4 - Statistically significantly different connections between groups in the V1MT run. They are divided into connections with higher F-values in MSC (red connections in the matrices) and connections with higher F-values in CNT (blue connections in the matrices).

HIGHER F-VALUES IN MSC			HIGHER F-VALUES IN CNT		
aINS$_L$	→	V5$_R$	FBA$_L$	→	V3$_R$
EBA$_L$	→	aINS$_R$	FBA$_L$	→	aINS$_L$
IFG$_L$	→	FFG$_L$	FFG$_L$	→	IFG$_L$
V3$_L$	→	FFG$_R$	FFG$_L$	→	V3$_L$
aINS$_R$	→	V5$_R$	FFG$_L$	→	aINS$_R$
aINS$_R$	→	pSTS$_R$	FBA$_R$	→	FBA$_L$
EBA$_R$	→	FFG$_R$	IFG$_R$	→	FBA$_L$
EBA$_R$	→	V5$_L$			
FBA$_R$	→	FFG$_L$			
IFG$_R$	→	V5$_L$			
IFG$_R$	→	FBA$_R$			
V3$_R$	→	V3$_L$			

In run V1MT, the number of connections with higher F-values in the MS patients group (red connections) is larger than the inverse case of higher F-values in healthy controls (blue connections).

RUNS BM
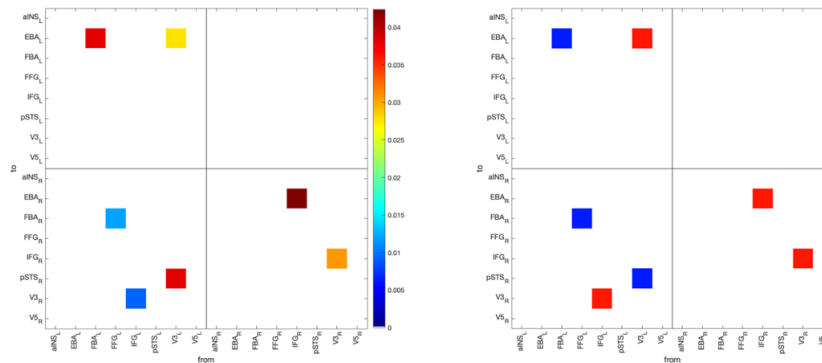
Figure 5.8 - Results of the between-groups statistical analysis, for runs BM. (Left) p-values obtained with between-groups statistical analysis performed with the Wilcoxon rank sum test (only statistically significantly different connections between groups are shown, $p < 0.05$). The colorbar represents the p-values, ranging from 0 (blue) to 0.05 (red). (Right) Difference in the medians of F-values in the same significantly different connections between the two groups (CNT and MSC). Red colours represent a higher median in the MS patients' group and blue colours represent a higher median in the healthy control group.

Table 5.5 - Statistically significantly different connections between groups in the BM runs. They are divided into connections with higher F-values in MSC (red connections in the matrices) and connections with higher F-values in CNT (blue connections in the matrices).

HIGHER F-VALUES IN MSC			HIGHER F-VALUES IN CNT		
IFG$_L$	$\rightarrow$	V3$_R$	FBA$_L$	$\rightarrow$	EBA$_L$
V3$_R$	$\rightarrow$	EBA$_L$	FFG$_L$	$\rightarrow$	FBA$_R$
IFG$_R$	$\rightarrow$	EBA$_R$	V3$_L$	$\rightarrow$	pSTS$_R$
V3$_R$	$\rightarrow$	IFG$_R$			

There are fewer connections that are significantly different between groups in the BM runs in comparison to the V1MT run. However, the number of connections with higher F-values in the MS patients' group is again larger than the number of connections with increased F-values in the CNT group.

The 3D representation of the connections that are significantly different between groups and the direction of the difference (red: higher F-values in MSC; blue: higher F-values in CNT) is shown below for each run (V1MT and BM).
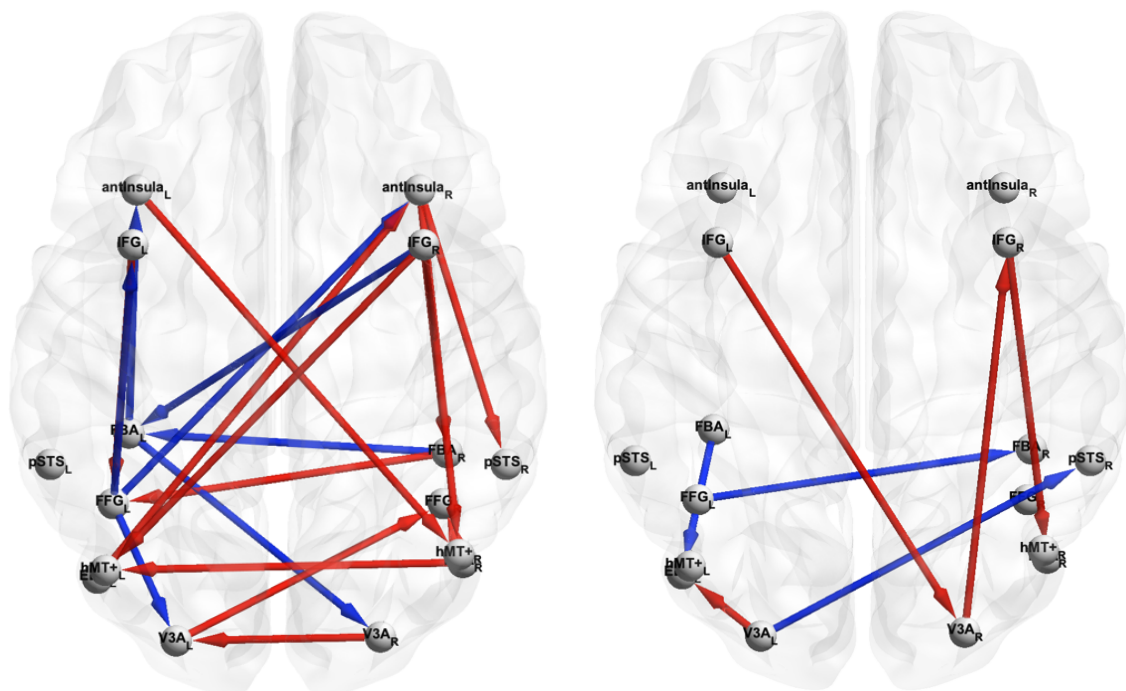
Figure 5.9 - 3D representation of the difference in medians of F-values between groups for the V1MT run (on the left image (corresponding to the matrix from figure 5.7)) and for the BM runs (on the right image (corresponding to the matrix from figure 5.8)). Red connections represent higher F-values in MSC, and blue connections represent higher F-values in CNT. The 3D representations were created with the BrainNet Viewer (Xia, Wang and He, 2013), http://www.nitrc.org/projects/bnv/.

The between-group statistical analysis once more supports the suggestion that there is neuroplasticity in the early phases of MS. This is observed through the larger number of significantly different (between groups) connections with higher F-values in MSC than in CNT, which may represent new connections between ROIs that in CNT were not activated by the task, as a compensation effect. In turn, the connections with higher F-values in CNT can reflect a deficit in their connectivity strength in MS patients.

Regarding the connections, in the localiser run, the involvement of several regions is altered in MSC:
- FBA and FFG do not send as much information as in the CNT group.
- aINS, IFG (frontal regions), EBA and V3 send more information than in CNT.
- FFG and V5 receive more information than in CNT.

In CNT, in the run V1MT, the number of significantly stronger (relative to MSC) forward and backward connections is balanced, whereas the stronger connections in MSC (relative to CNT) are mostly backwards connections, specifically from the frontal to temporal regions. Studies in schizophrenia (Fogelson *et al.*, 2014) (Rolls *et al.*, 2020), which is also considered a disconnection disease that shows a neural compensatory response, have demonstrated that the connectivity of backward connections is greater in patients than in healthy controls during target detection, particularly from inferotemporal regions (FFG and FBA, for example) to the temporoparietal region hMT+, and from hMT+ to V1, an early visual region. This is further verified by Cardin and colleagues (Cardin, Friston and Zeki, 2011) which argue that high-order visual form (with recognizable stimulus, for example) recruits more high-order visual areas, which specialize in processing specific attributes (such as collinearity and meaning), that will, in turn, generate top-down signals to lower-level regions, in order to encode visual information more efficiently.

This tendency for backward connectivity is not observed in the BM runs, but there are still more connections with higher F-values in MSC than in CNT. There is a reduction in connections which involve FBA in MSC, as well as an increase in the participation of IFG, V3 and EBA and the disappearance of the $V3_L \rightarrow pSTS_R$ connection. Despite the disappearance of this connection in MSC, four of the seven statistically different connections in this run ($V3_L \rightarrow pSTS_R$ in CNT and $IFG_L \rightarrow V3_R$, $V3_L \rightarrow EBA_L$, $IFG_R \rightarrow EBA_R$ in MSC) are characteristically involved in biological motion, which further verifies their involvement in this movement perception task. This is proven by Sokolov and colleagues (Sokolov *et al.*, 2018), which employed DCM to observe the behaviour of the regions and their connections involved in BM. According to them, pSTS does not have a gatekeeper role in the functional integration of the occipitotemporal and frontal regions, i.e., it is not the only region with communication with higher-order regions, but that FFG and the middle temporal cortex (MTC), which contains hMT+ and EBA, are also able to communicate with these regions. Moreover, the authors claim that the most sensitive connections in the perception of biological motion are IFG → early visual cortex (OCC), insula → OCC, insula → MTC, pSTS → OCC, FFG → pSTS and insula → FFG, most of them being top-down connections (connections from higher-level regions to, in case, OCC).

Deficits in cortical function, evaluated through cerebral perfusion techniques (Vitorino *et al.*, 2016), in cognitively impaired RRMS patients, were found in the inferior frontal gyrus, inferior parietal lobule, fusiform gyrus, and lingual gyrus. Although the participants in our study are not cognitively impaired, we observed altered connections involving IFG and FFG,

suggesting that these regions could be the first to be affected by MS and have a major impact on cognitive decline.

Furthermore, these results, both in the V1MT run and in the BM runs, are in concordance with previous research which argues that MS patients have higher levels of connectivity and more recruited areas in the frontal lobe of the brain (in this case, aINS and IFG), in comparison to CNT, in order to maintain an adequate task performance (Leavitt et al., 2011) (Rocca *et al.*, 2016).

5.5 Shift in Brain Lateralisation

When a task is performed, information transfer should flow from the non-specialized to the specialised hemisphere, which entails that connections towards the dominant hemisphere are stronger than those away from it. In this case, as all of the participants are right-handed, connections should be stronger and thus have higher values of connectivity in the left hemisphere, which is considered the dominant one (Stephan *et al.*, 2007).

However, there is evidence of a shift in functional hemispheric lateralisation and a subsequent decrease in FC of the left hemisphere in the brain of MS patients (Tahedl *et al.*, 2018). In fact, this could be a result of GM and WM atrophy in the left hemisphere, supported by (Preziosa *et al.*, 2017), which further concludes that the two brain hemispheres have different vulnerabilities to structural damages induced by MS. Filippi and colleagues (Filippi *et al.*, 1995) also associated hand dominance and interhemispheric lesion distribution by proving that there was a higher lesion burden in the dominant hemisphere. As the dominant hemisphere (for handedness and language), for right-handed people, is the left, this hemisphere may be more susceptible to damage and accumulation of lesions.

In the context of neuroplasticity and its relationship with brain lateralisation, Agcaoglu and colleagues (Agcaoglu et al., 2018) studied aging in the brain and concluded that there was a decreased lateralisation in some networks, namely the frontal and the attentional, in the left hemisphere, but a preservation of the right, which could reflect compensatory mechanisms when the brain starts to lose function.

In our study, we hypothesized that, as a result of this adaptive shift in hemispheric lateralisation, there could be an increased presence of intra-hemispheric connections in the right hemisphere (R → R) and interhemispheric connections to the right hemisphere (L → R) and from the right hemisphere (R → L), as well as heightened connectivity values of these connections. In fact, the results showed that both in the within-group and between-groups analyses, and in both runs, there was a considerable increase in the connections seen in the right hemisphere and a decrease in the MSC's connections in the left hemisphere, which is in agreement with previous research in AD, which is also characterized by neuroplasticity mechanisms (Rytsar *et al.*, 2011).

Specifically, in the between-groups analysis, in the run V1MT, there is an increase in the number of R → L, L → R and R → R connections with higher F-values in MSC, being that the right hemisphere sends most of them (8 out of the 12 connections). In the BM runs, there is an increase in the R → R intra-hemispheric connections in MSC, and the right hemisphere now receives more connections.

Moreover, a decrease in the FC of intra-hemispheric connections in the left hemisphere, L → L, and an increase of the FC in intra-hemispheric connections in the right hemisphere, R → R, and interhemispheric connections, L → R and R → L, in MS patients is expected. These values can be evaluated through the mean F-values for each quadrant of the mean F-matrices, shown in Table 5.6.

Table 5.6 - Matrices with the F-values of each quadrant of the mean F-matrices of figure 5.3 for both groups (CNT and MSC) and both runs (V1MT and BM).

	CNT		MSC	
RUN V1MT	L → L	R → L	L → L	R → L
	0.0068	0.0066	0.0063	0.0081
	L → R	R → R	L → R	R → R
	0.0078	0.0056	0.0080	0.0065
RUNS BM	L → L	R → L	L → L	R → L
	0.0028	0.0036	0.0024	0.0038
	L → R	R → R	L → R	R → R
	0.0029	0.0026	0.0030	0.0033

These results demonstrate that there is indeed an increase in the FC of the connections that involve the right hemisphere. Although the values are not statistically significantly different ($p > 0.05$), this tendency further corroborates the hypothesis of compensatory processes in MS and a change in brain lateralisation.

5.6 Influence of ROI Size

In an initial phase of the study, we used a radius of 10 mm to define the ROIs for just 20 of the 29 participants. Then, after a revision in the methodology, we understood it would be reasonable (and consistent with the literature) to use a smaller radius of 5 mm. Therefore, when extracting the average BOLD time course of the regions, two ROI radiuses were tested in 20 participants: 5 mm and 10 mm. The resulting connectivity matrices after between-groups statistical analysis with Wilcoxon rank sum test for both ROI sizes and runs are presented in figures 5.10 and 5.11, for run V1MT, and figures 5.12 and 5.13, for runs BM.

RUN V1MT

Radius of ROIs = 10 mm
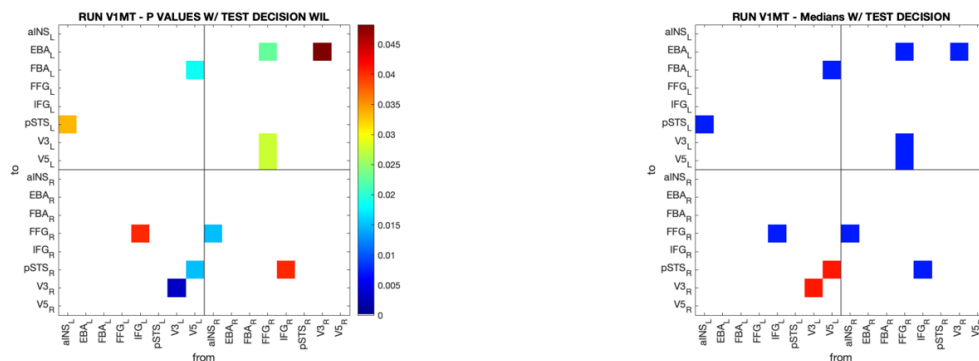
Figure 5.10 - Results of the between-group statistical analysis, for run V1MT, for a radius of 10 mm. (Left) p-values obtained with between-groups statistical analysis performed with the Wilcoxon rank sum test (only statistically significantly different connections between groups are shown, p < 0.05). The colorbar represents the p-values, ranging from 0 (blue) to 0.05 (red). (Right) Difference in the medians of F-values in the same significantly different connections between the two groups (CNT and MSC). Red colours represent a higher median in the MS patients' group and blue colours represent a higher median in the healthy control group.

Radius of ROIs = 5 mm
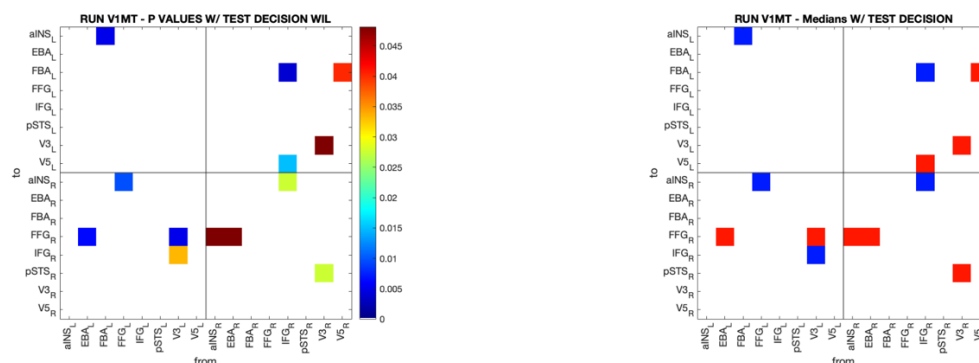
Figure 5.11 - Results of the between-group statistical analysis, for run V1MT, for a radius of 5 mm. (Left) p-values obtained with between-groups statistical analysis performed with the Wilcoxon rank sum test (only statistically significantly different connections between groups are shown, p < 0.05). The colorbar represents the p-values, ranging from 0 (blue) to 0.05 (red). (Right) Difference in the medians of F-values in the same significantly different connections between the two groups (CNT and MSC). Red colours represent a higher median in the MS patients' group and blue colours represent a higher median in the healthy control group.

The main conclusion taken from this exploration, in the localiser run, was that with the smaller radius' ROIs (5 mm), more connections that are significantly different between groups show higher F-values in MS patients, in contrast to using a bigger radius with 10 mm. This can be supported by observing that there are more red coloured connections in the matrix for the 5 mm ROIs. There are also more specific connections, i.e., the p-values were lower with 5 mm ROIs (more blue coloured connections in the left matrix).

RUNS BM

Radius of ROIs = 10 mm
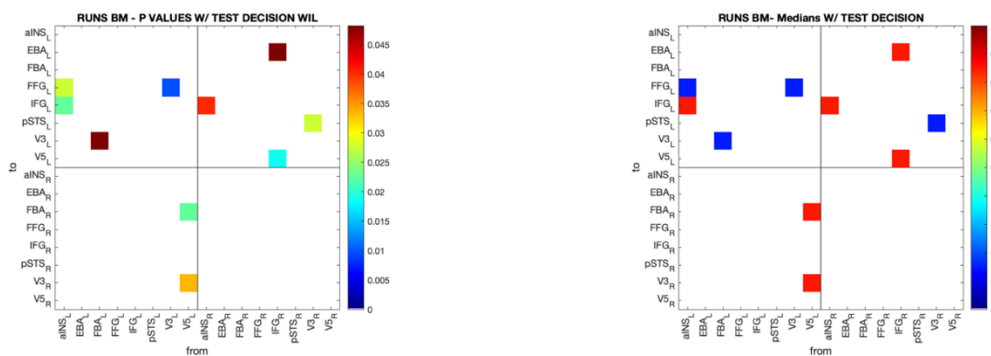
Figure 5.12 - Results of the between-group statistical analysis, for runs BM, for a radius of 10 mm. (Left) p-values obtained with between-groups statistical analysis performed with the Wilcoxon rank sum test (only statistically significantly different connections between groups are shown, p < 0.05). The colorbar represents the p-values, ranging from 0 (blue) to 0.05 (red). (Right) Difference in the medians of F-values in the same significantly different connections between the two groups (CNT and MSC). Red colours represent a higher median in the MS patients' group and blue colours represent a higher median in the healthy control group.

Radius of ROIs = 5 mm
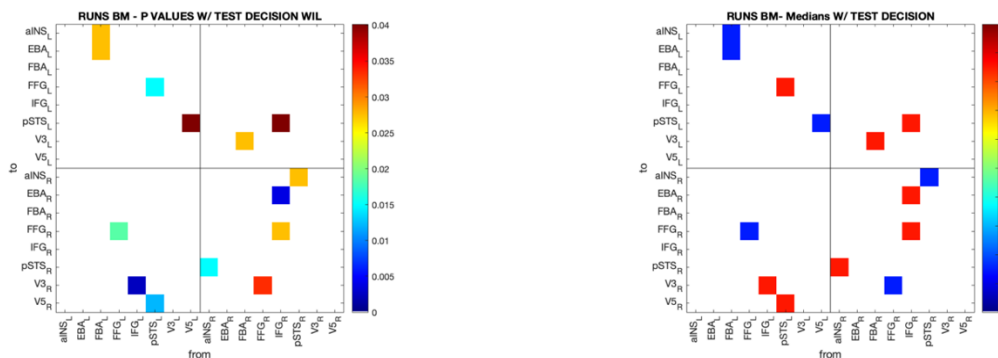
Figure 5.13 - Results of the between-group statistical analysis, for runs BM, for a radius of 5 mm. (Left) p-values obtained with between-groups statistical analysis performed with the Wilcoxon rank sum test (only statistically significantly different connections between groups are shown, p < 0.05). The colorbar represents the p-values, ranging from 0 (blue) to 0.05 (red). (Right) Difference in the medians of F-values in the same significantly different connections between the two groups (CNT and MSC). Red colours represent a higher median in the MS patients' group and blue colours represent a higher median in the healthy control group.

In the biological motion concatenated runs, the 5 mm ROIs led to an increase in the number of blue coloured connections (higher F-value connections in the healthy controls) in comparison to the 10 mm ROIs, but also to an increase in the number of red coloured connections (higher F-value connections in the MS patients). The proportion of red coloured connections is approximately the same in both matrices with both ROI sizes (6/10 in the 10mm radius and 8/14 in the 5mm radius), which means that are no significant changes in the proportion of significantly different connections with higher/lower F-values in each group with the alteration of the ROI's size. Despite this, in the 5 mm ROIs, there are more specific different connections since p-values were generally lower.

In conclusion, it was observed that the ROI radius chosen to extract the average time course of each ROI's BOLD signal influenced the results. The primary observation is that a 5 mm radius can define a more specific space for the region, ultimately leading to better and more accurate results when extracting the time courses and performing statistical analysis. This occurs partly because bigger sized ROIs comprise the intended brain region and some surrounding voxels, which may lead to the inclusion of noise in the calculations that inevitably contributes to this difference in results. Using a 5 mm radius may be a better choice because the included noise is significantly less than when using 10 mm ROIs, and thus the signal-to-noise ratio increases. Therefore, we opted to re-run the analyses with the complete dataset using the ROIs with a radius of 5mm. The results presented in this thesis so far are indeed those obtained using 5 mm ROIs, we just presented this ROI size exploration here to allow the reader to be already familiar with the connectivity matrices at this point and focus easily on the comparison between ROI sizes in this section. The definition of the ROIs proves to be an important factor in the study of functional connectivity, and we suggest that a more exact definition of the regions leads to more accurate results.

5.7 Optimal Threshold

The connectivity measures are calculated from the F-value matrices, with BCT (Rubinov and Sporns, 2010). Proportional thresholding, which maintains a fixed density between the participants' networks, and thus the same number of edges, is advised in order to obtain more sparsely connected matrices and, therefore, more stable network metrics. However, the choice of a specific threshold remains unclear, and the literature often shows studies that investigate connectivity measures for a large range of thresholds, generally from 5% to 50% network density. This means that only 5 to 50% of the original edges are maintained. For example, (Miri Ashtiani *et al.*, 2019) argues that selecting a range between 10% and 50% for proportional thresholding prevents matrices from being too sparse (less than 10% density can lead to the elimination of important connections within the network) and too dense (more than 50% density may include noise and insignificant information). (Welton *et al.*, 2020) concludes that a threshold between 20% and 50% produces reliable results, and (Abidin *et al.*, 2017) chooses a density of 45% as the threshold for their research.

In this study, an exploration of different threshold values and their impact in connectivity measures was performed, and one specific threshold for each run was chosen to calculate the connectivity measures and to analyse which regions could be more involved in each task and those which could have a particularly important role within the defined network. Nonetheless, we emphasise that this is a merely exploratory approach, as calculating the measures with several thresholds may bring new and relevant information.

In order to choose an 'optimal' threshold, the procedure described below was followed for each run (figure 5.14).
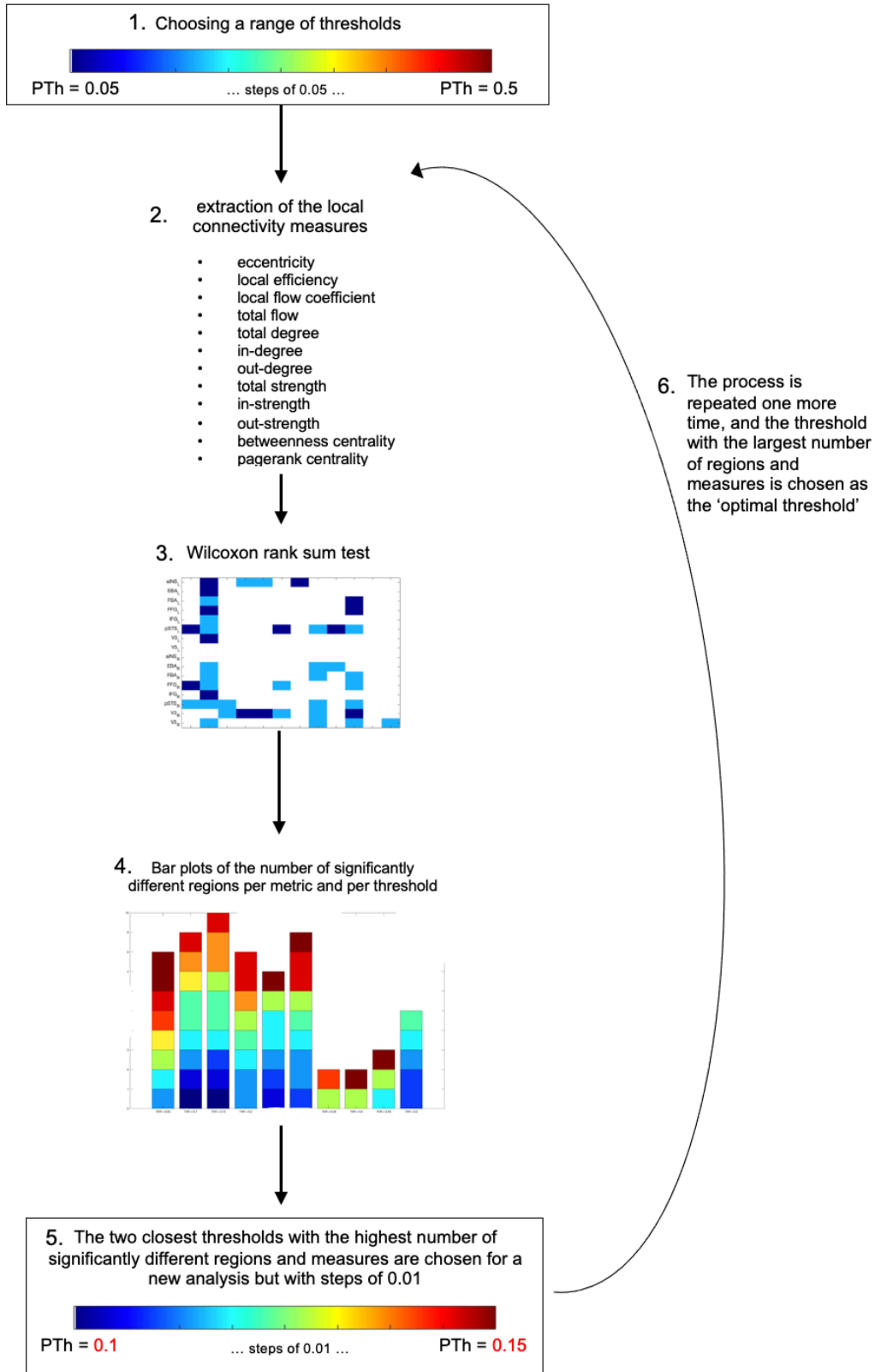
Figure 5.14 - Schematic representation of the steps followed to choose the 'optimal' threshold for calculation and representation of the global and local connectivity measures. (1) A range of thresholds was chosen: 0.05 < PTh < 0.5, with steps of 0.05. (2) Calculation of the local metrics for each threshold. (3) Statistical analysis with Wilcoxon Rank Sum test to find significantly different nodes between groups in each local measure (p < 0.05). (4) Construction of the bar plot, with the ten thresholds in the x-axis and significantly different nodes in the y-axis. (5) The two closest thresholds which had the largest number of significantly different connectivity measures and nodes (between groups) were chosen to repeat the above procedure, but with steps of 0.01. (6) The threshold with the largest number of significantly different nodes local measures is chosen as the 'optimal threshold'.

RUN V1MT

Firstly, a range of thresholds was chosen. In this case, we used densities from 5% to 50% (or a proportion of 0.05 and 0.5, respectively) as they are the most common thresholds used in the literature. All connectivity measures mentioned in section 4.2.5 were calculated for that range of thresholds with a 5% (or 0.05) step, i.e, the values of PTh are equal to 0.05, 0.1, 0.15, 0.2, 0.25, 0.3, 0.35, 0.4, 0.45 and 0.5. The weights of the connections below these thresholds were set to 0.

After calculating the metrics for each threshold, statistical analysis with the Wilcoxon Rank Sum test was performed to find significant differences between groups in global measures and significantly different nodes in each local measure (p < 0.05). The significantly different nodes in the local measures will be used as guidance for choosing the threshold, as they convey more information concerning the importance of the regions within the network. This statistical analysis is represented in matrix form with all local measures in the x-axis and respective significantly different nodes between groups in the y-axis. Figure 5.15 is an example of these matrices with PTh = 0.1, and in Appendix II, all of the matrices, for all of the thresholds, are represented.
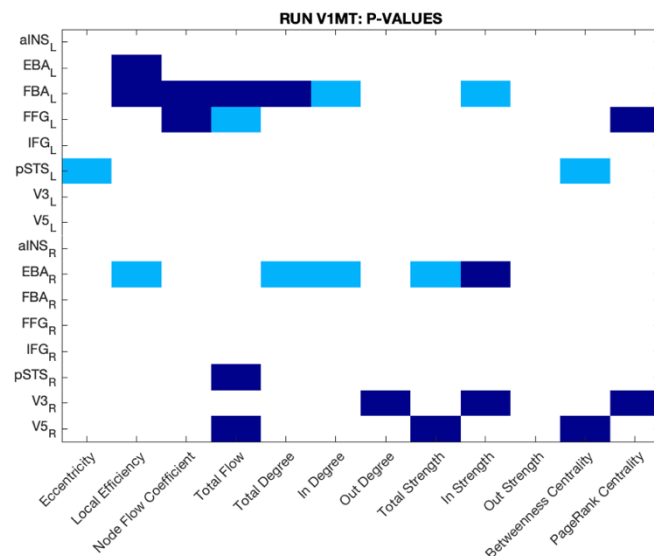
Figure 5.15 - Matrix with the nodes and corresponding local measures that are statistically significantly different between groups, with PTh = 0.1, in the V1MT run. Wilcoxon rank sum test was performed and the nodes with a p-value < 0.05 are represented in light blue. The nodes in dark blue have a p-value < 0.1 (tendency for statistical significance).

The data was analysed to conclude which thresholds could yield the greatest number of significantly different connectivity metrics between groups for at least one node and the largest number of statistically significant different nodes involved in general (for all metrics). Thus, a bar plot was constructed (figure 5.16), in which the ten thresholds are represented in the x-axis and the number of nodes presenting significantly different metrics in the y-axis.
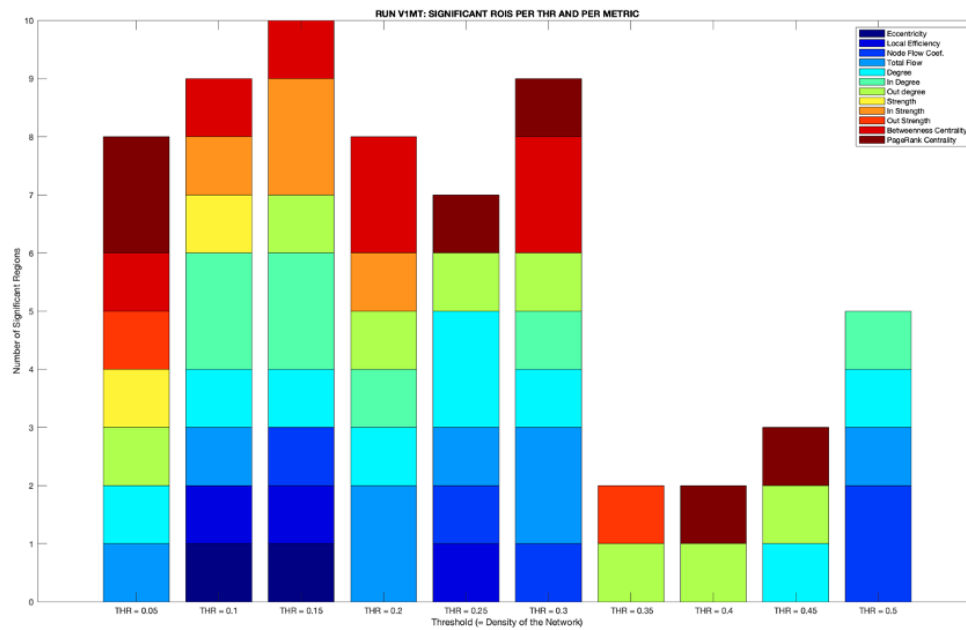
Figure 5.16 - Bar plot of the number of nodes and corresponding local measures that are statistically significantly different between groups (PTh = 0.05 to 0.5, with steps of 0.05), for the V1MT run. Each bar is divided into colours, each one representing a local connectivity metric that is significantly different between groups in each threshold.

In this run (V1MT), the two closest thresholds which yielded the largest number of significantly different connectivity measures and nodes were PTh = 0.1 (8 metrics and 9 nodes) and PTh = 0.15 (8 metrics and 10 nodes). These thresholds were chosen to repeat the above procedure, but now with smaller steps of 0.01. This subdivision will make the threshold more specific, thus allowing for a more selective choice.

The new thresholds to be investigated are PTh = 0.1, 0.11, 0.12, 0.13, 0.14 and 0.15.
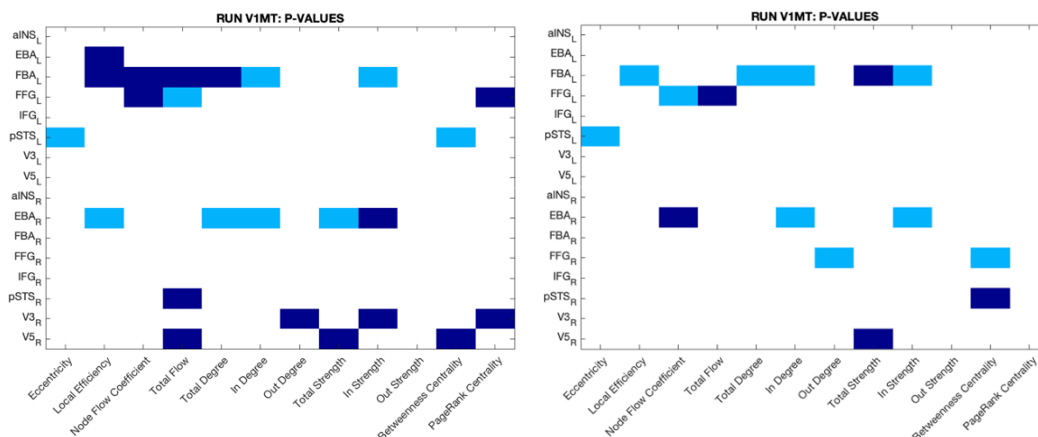
Figure 5.17 - Matrix with the nodes and corresponding local measures that are statistically significantly different between groups, PTh = 0.1 (left) and PTh= 0.15 (right), in the V1MT run. Wilcoxon rank sum test was performed and the nodes with a p-value < 0.05 are represented in light blue. The nodes in dark blue have a p-value < 0.1 (tendency for statistical significance).

A new bar plot with the new significantly different local metrics between groups for each threshold was constructed.

74
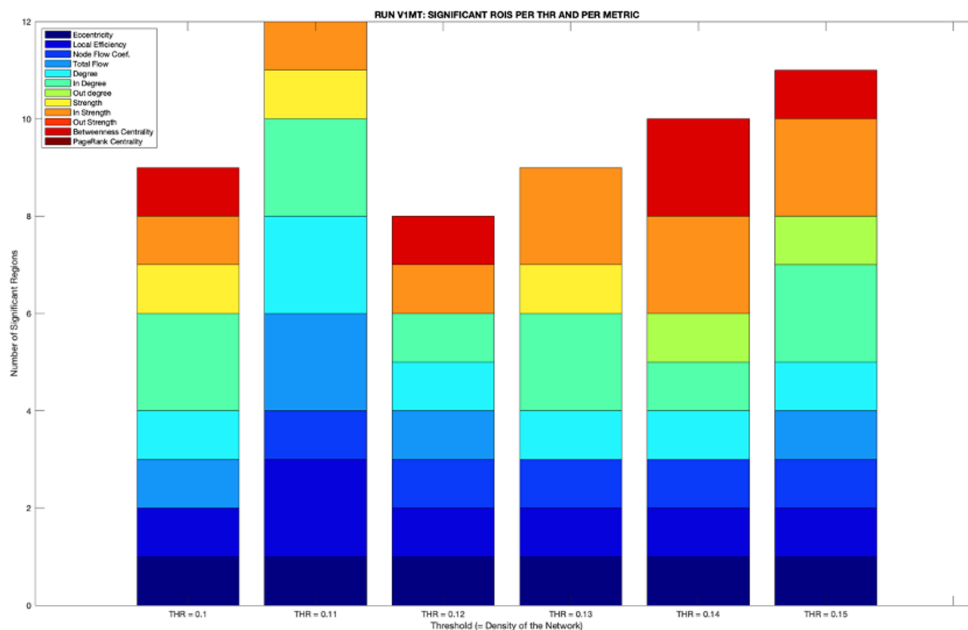
Figure 5.18 - Bar plot of the number of nodes and corresponding local measures that are statistically significantly different between groups (PTh = 0.1 to 0.15, with steps of 0.01), for the V1MT run. Each bar is divided into colours, each one representing a local connectivity metric that is significantly different between groups in each threshold.

We observed that PTh = 0.11 is the threshold which yielded the highest number of significantly different nodes and local measures between groups, so it was considered the 'optimal threshold' for the localiser run. The matrix of the significantly different nodes and local measures for this threshold is represented in figure 5.19.
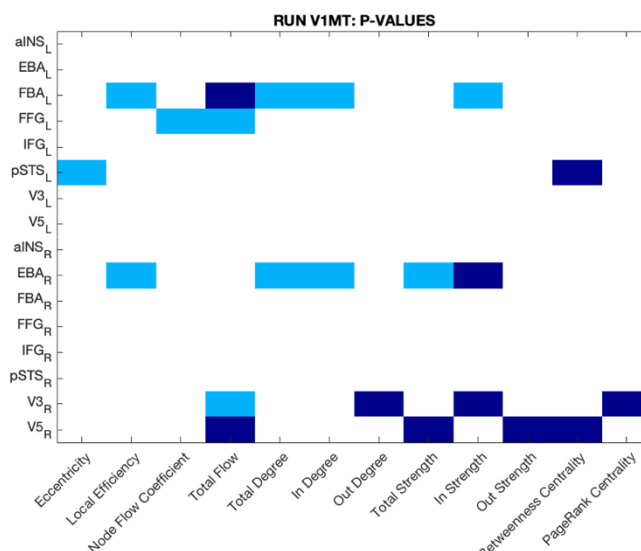
Figure 5.19 - Matrix with the nodes and corresponding local measures that are statistically significantly different between groups, with PTh = 0.11, in the V1MT run. Wilcoxon rank sum test was performed and the nodes with a p-value < 0.05 are represented in light blue. The nodes in dark blue have a p-value < 0.1 (tendency for statistical significance).

RUNS BM

For the BM runs, the same procedure was followed.
The significantly different metrics between groups for each threshold were represented in a bar plot (figure 5.20).
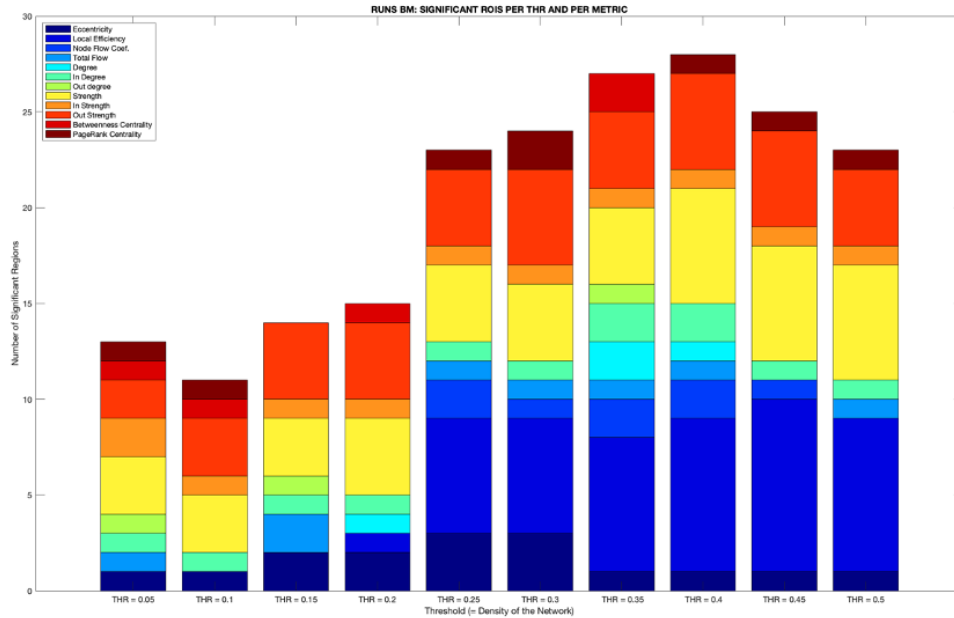
Figure 5.20 – Bar plot of the number of nodes and corresponding local measures that are statistically significantly different between groups (PTh = 0.05 to 0.5, with steps of 0.05), for the BM runs. Each bar is divided into colours, each one representing a local connectivity metric that is significantly different between groups in each threshold.

In the BM runs, the range of thresholds with the largest number of significantly different connectivity measures and nodes was between PTh = 0.35 (which has the highest number of significantly different metrics: 11 metrics, 27 nodes) and PTh = 0.4 (which has the highest number of significantly different nodes: 10 metrics, 28 nodes).
These thresholds were chosen to repeat the above procedure, but now with smaller steps of 0.01. Hence, the new thresholds to be studied are 0.35, 0.36, 0.37, 0.38, 0.39 and 0.4.
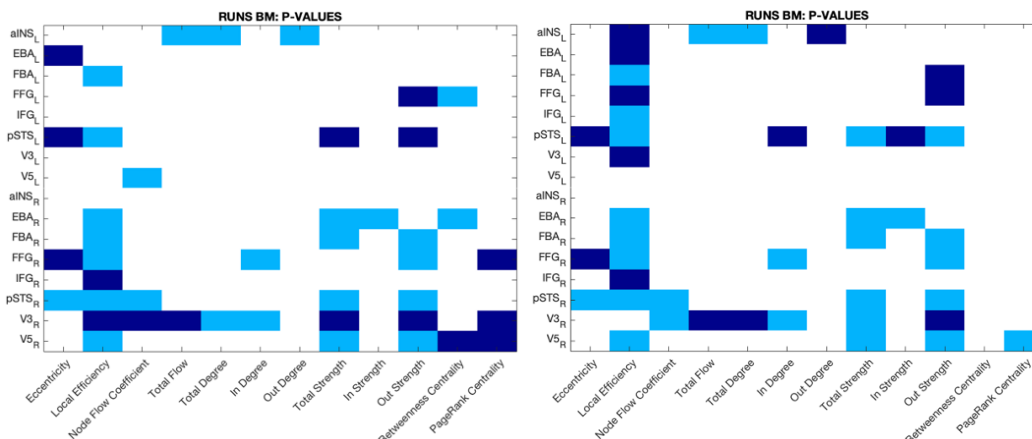
Figure 5.21 – Matrix with the nodes and corresponding local measures that are statistically significantly different between groups, PTh = 0.35 (left) and PTh= 0.4 (right), in the BM runs run. Wilcoxon rank sum test was performed and the nodes with a p-value < 0.05 are represented in light blue. The nodes in dark blue have a p-value < 0.1 (tendency for statistical significance).

A new bar plot with the new significantly different metrics between groups for each new threshold was constructed (figure 5.22).
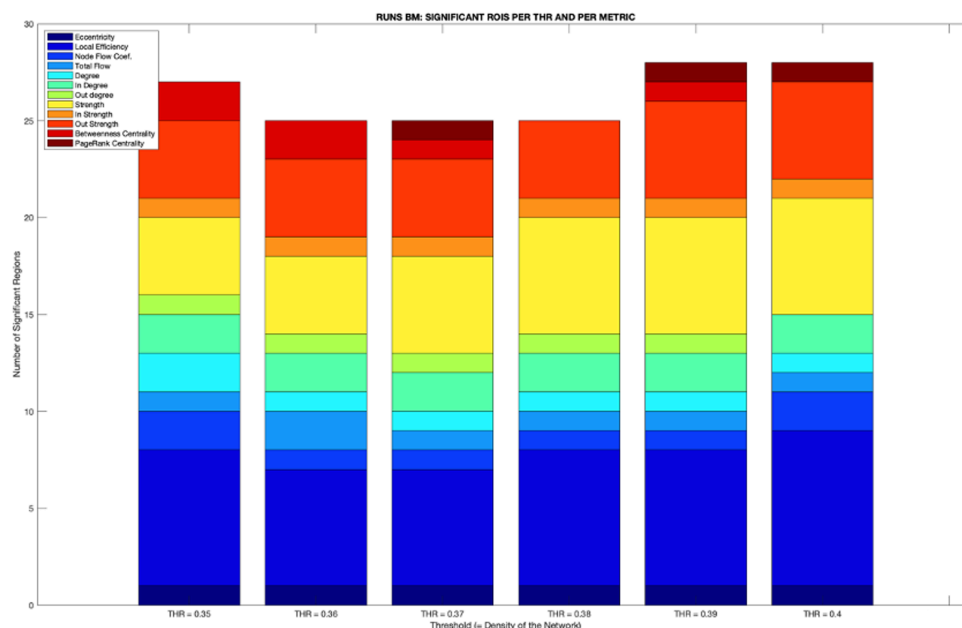
Figure 5.22 – Bar plot of the number of nodes and corresponding local measures that are statistically significantly different between groups (PTh = 0.35 to 0.4, with steps of 0.01), for the BM runs. Each bar is divided into colours, each one representing a local connectivity metric that is significantly different between groups in each threshold.

PTh = 0.39 was the threshold which yielded the highest number of significantly different nodes and local measures, so it is considered the 'optimal threshold' for the biological motion runs. The matrix of the significantly different nodes and local measures for this threshold is represented in figure 5.23.
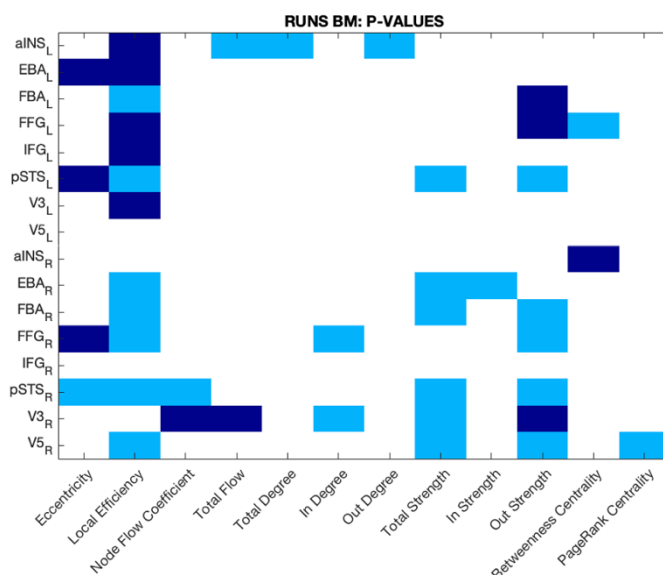
Figure 5.23 – Matrix with the nodes and corresponding local measures that are statistically significantly different between groups, with PTh = 0.39, in the BM runs. Wilcoxon rank sum test was performed and the nodes with a p-value < 0.05 are represented in light blue. The nodes in dark blue have a p-value < 0.1 (tendency for statistical significance).

5.8 Connectivity Measures

After choosing an 'optimal' threshold, the connectivity measures were calculated: characteristic path length, global efficiency, local efficiency, global flow coefficient, local flow coefficient, total flow, assortativity, eccentricity, radius, diameter, total degree, in-degree, out-degree, mean network strength, total strength, in-strength, out-strength, betweenness centrality and pagerank centrality.

As we are using a multivariate approach in a restricted network, composed of only 16 nodes (regions) and two different visual tasks, which have not been yet studied in the context of MS, we expected different outcomes about the connectivity metrics in relation to what is reported in previous research.

5.8.1 Global Measures

The global connectivity measures characterize and describe global graph properties of the network, such as efficiency and resilience, that can be used to analyse the global topology, looking beyond the local changes of each region. Global network metrics have been insightful regarding brain organization and function, describing network segregation (dense, within-subnetwork connectivity) and integration (communication across distinct subnetworks (Rubinov and Sporns, 2010) (Welton *et al.*, 2020).

The calculated global connectivity measures were the characteristic path length, global efficiency, diameter, radius, global flow coefficient, assortativity and average strength. The representation of the global measures individually in each group for each run is shown below.

RUN V1MT
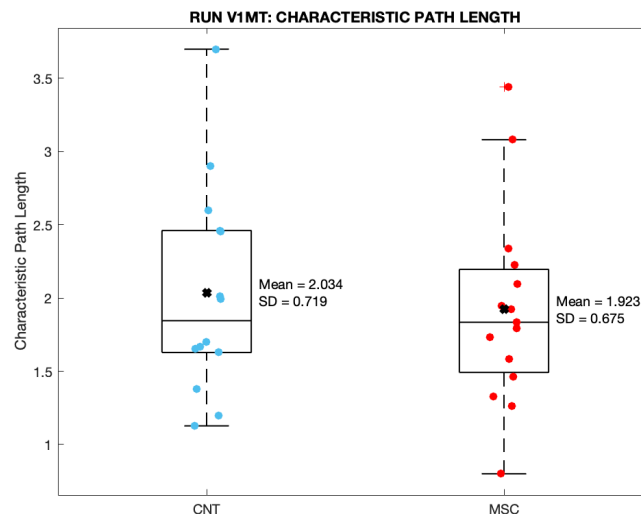
Figure 5.24 - Box plots with the distribution of the values of the characteristic path length in both groups, for the run V1MT. The values of the measures for CNT are in blue, and for MSC are in red. The mean and standard deviation are also indicated.
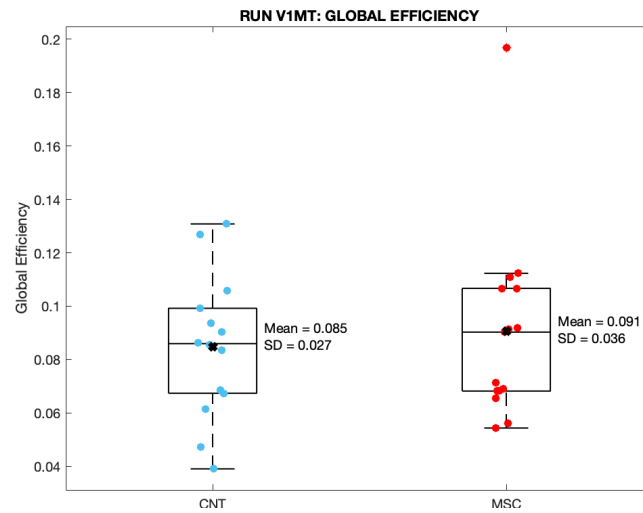
Figure 5.25 - Box plots with the distribution of the values of the global efficiency in both groups, for the run V1MT. The values of the measures for CNT are in blue, and for MSC are in red. The mean and standard deviation are also indicated.
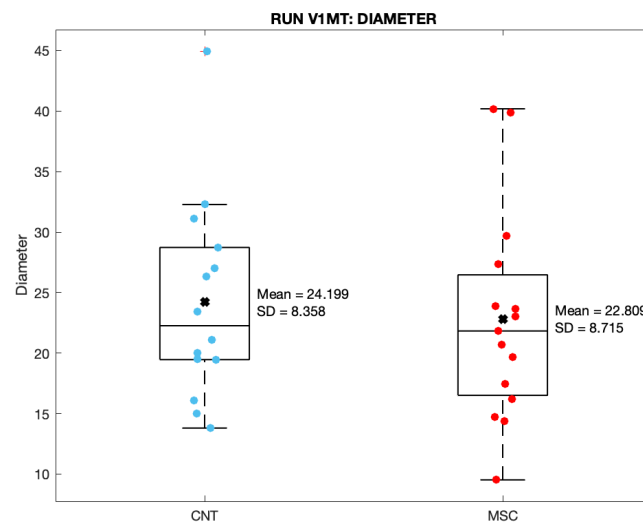
Figure 5.26 - Box plots with the distribution of the values of the diameter in both groups, for the run V1MT. The values of the measures for CNT are in blue, and for MSC are in red. The mean and standard deviation are also indicated.
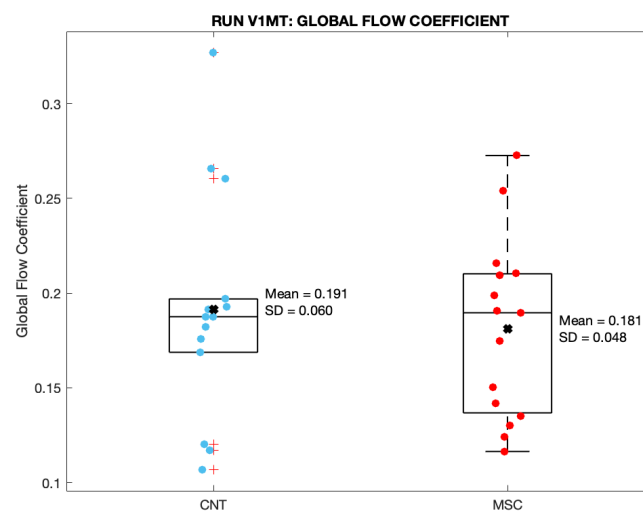
Figure 5.27 - Box plots with the distribution of the values of the global flow coefficient in both groups, for the run V1MT. The values of the measures for CNT are in blue, and for MSC are in red. The mean and standard deviation are also indicated.
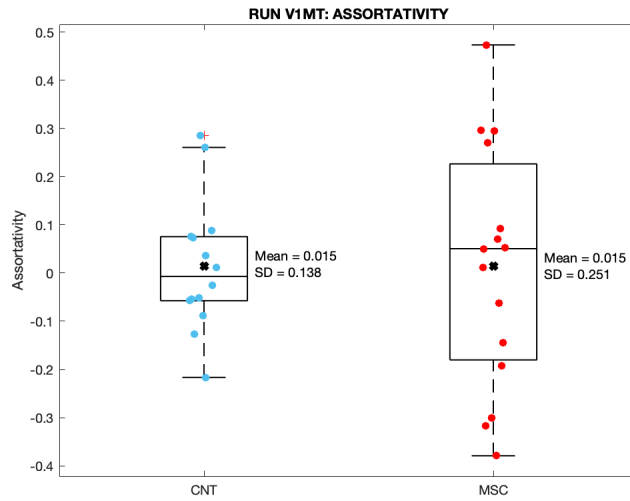
Figure 5.28 - Box plots with the distribution of the values of the assortativity in both groups, for the run V1MT. The values of the measures for CNT are in blue, and for MSC are in red. The mean and standard deviation are also indicated.
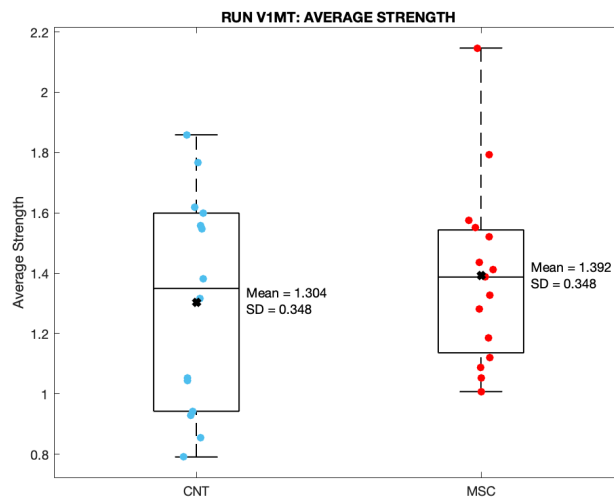
Figure 5.29 - Box plots with the distribution of the values of the average strength in both groups, for the run V1MT. The values of the measures for CNT are in blue, and for MSC are in red. The mean and standard deviation are also indicated.

In the V1MT run, the median values of the characteristic path length and diameter are decreased in MS patients, whereas the median values of global efficiency, global flow coefficient, assortativity and average strength are increased in MS patients.

RUNS BM
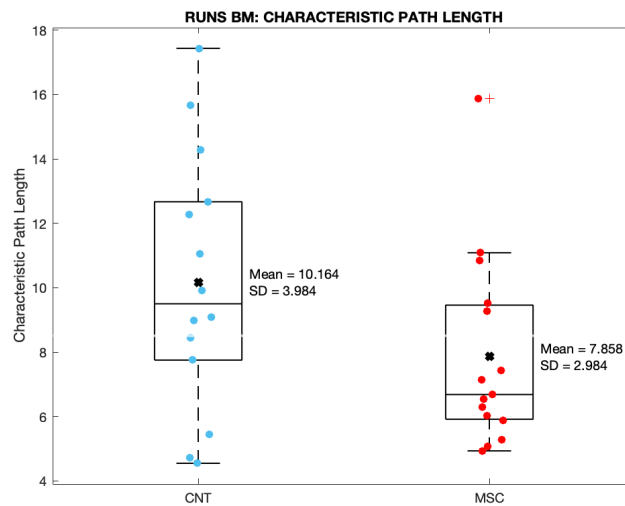
Figure 5.30 - Box plots with the distribution of the values of the characteristic path length in both groups, for the runs BM. The values of the measures for CNT are in blue, and for MSC are in red. The mean and standard deviation are also indicated.
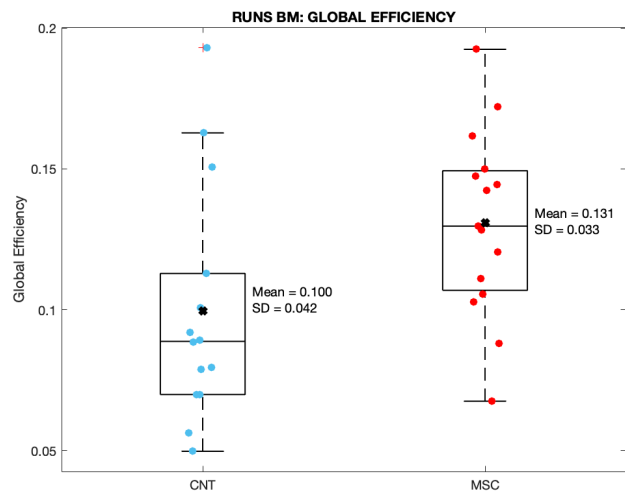
Figure 5.31 - Box plots with the distribution of the values of the global efficiency in both groups, for the runs BM. The values of the measures for CNT are in blue, and for MSC are in red. The mean and standard deviation are also indicated.
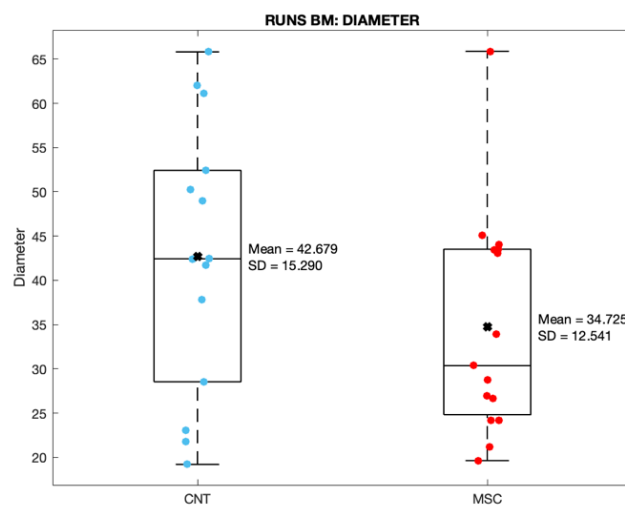
Figure 5.32 - Box plots with the distribution of the values of the diameter in both groups, for the runs BM. The values of the measures for CNT are in blue, and for MSC are in red. The mean and standard deviation are also indicated.
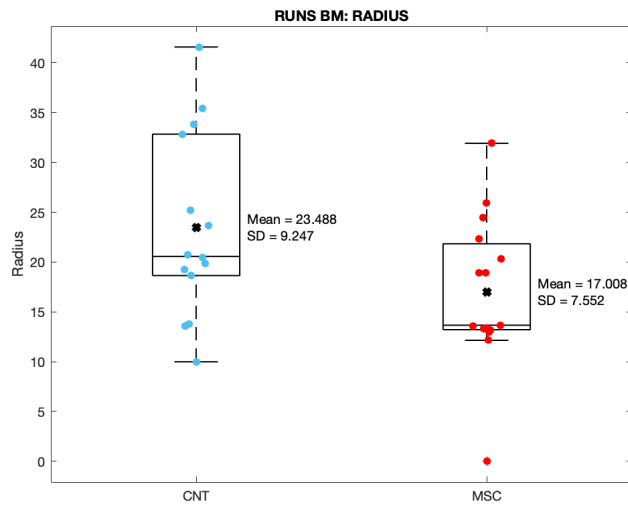
Figure 5.33 - Box plots with the distribution of the values of the radius in both groups, for the runs BM. The values of the measures for CNT are in blue, and for MSC are in red. The mean and standard deviation are also indicated.
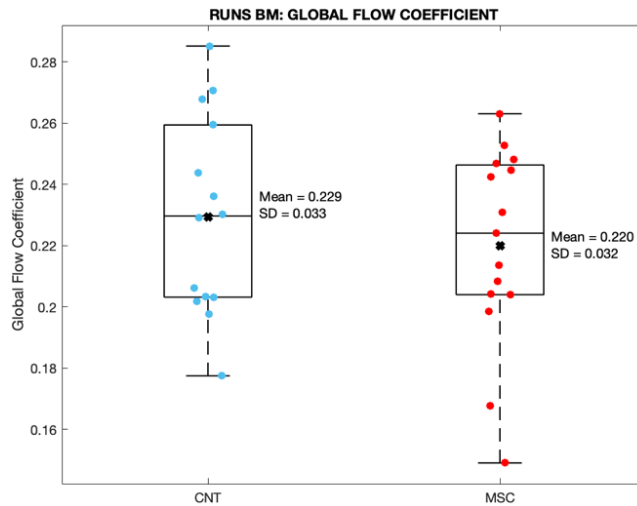
Figure 5.34 - Box plots with the distribution of the values of the global flow coefficient in both groups, for the runs BM. The values of the measures for CNT are in blue, and for MSC are in red. The mean and standard deviation are also indicated.
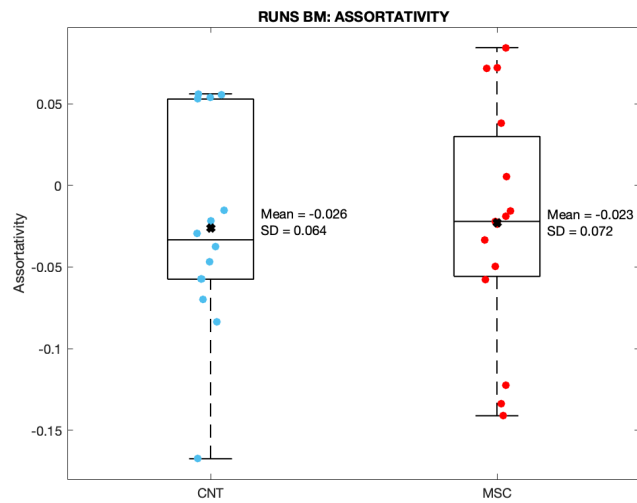
Figure 5.35 - Box plots with the distribution of the values of the assortativity in both groups, for the runs BM. The values of the measures for CNT are in blue, and for MSC are in red. The mean and standard deviation are also indicated.
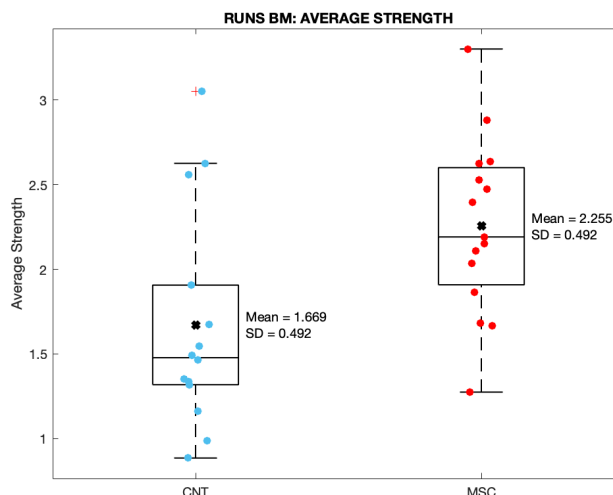
Figure 5.36 - Box plots with the distribution of the values of the average strength in both groups, for the runs BM. The values of the measures for CNT are in blue, and for MSC are in red. The mean and standard deviation are also indicated.

In BM runs, the characteristic path length, radius, diameter, and global flow coefficient decreased in MS patients, whereas global efficiency, assortativity, and average strength increased in MS patients.

The values of the global connectivity measures for both runs in each group are summarized in Table 5.7, which contains the median values of each connectivity measure (the median is chosen instead of the mean because the data are not normal, verified with the KS test).

Table 5.7 - Median values of each global connectivity measure, for each group (CNT and MSC) and each run (V1MT and BM). The blue values are those which are increased in comparison to the other group (within the same run). * indicates statistically significant differences between-groups.

	MEDIAN VALUES			
	RUN V1MT		RUNS BM	
	CNT	MSC	CNT	MSC
Characteristic Path Length	1.845	1.835	9.50	6.68
Global Efficiency	0.086	0.0903	0.089*	0.13*
Diameter	22.26	21.83	42.44	30.37
Radius	—	—	20.57*	13.67*
Assortativity	- 0.0072	0.051	- 0.033	- 0.022
Mean Network Strength	1.35	1.39	1.48	2.19
Global Flow Coefficient	0.1875	0.1896	0.23	0.22

A statistical Wilcoxon rank sum test was performed to evaluate which measures were significantly different between the two groups (significance at $p < 0.05$). In the V1MT run, none of the global measures was statistically significantly different (all p-values > 0.05). In the BM runs, two global measures (global efficiency and radius) were statistically significantly different between groups (p-value of global efficiency = 0.0382; p-value of radius = 0.0471). It is then important to analyse the behaviour of the measures in MSC, particularly if they increase or decrease in the network in comparison with the CNT group.

The *characteristic path length* calculates the average shortest distance between every pair of nodes in the graph, hence relating to efficiency in information transfer since a shorter path length implies more speed in information exchange and processing. These values were decreased in MS patients in both runs. Accordingly, the *global efficiency*, which is considered to be the inverse of the characteristic path length and measures the general efficiency of the information transfer between the network's nodes, is increased in MSC in both runs. The results of these two metrics indicate that there is an overall increase in efficiency within the network.

The *radius* and *diameter* are derived from eccentricity, a local connectivity measure that first calculates all shortest paths between a node and every other node in the network and then chooses the longest one of all of these node's paths. The radius represents the minimum eccentricity, i.e., the smaller value of all nodes' eccentricities, and the diameter represents the maximum eccentricity. These measures describe the ease with which a node can be reached by other nodes, reflecting the network's efficiency (Su *et al.*, 2017). In the V1MT run, the radius is 0 for all participants, except for MSC07. This might be the result of incidentally using a threshold that is too restrictive in this situation (only 11% of the connections are retained and the others are set to 0), and the minimum values of the longest shortest path between the nodes tend to be 0 because most of the connections involved in these paths are eliminated. In the BM runs, the radius decreases in MSC. The diameter is also decreased in MSC in both runs. Since the radius and the diameter are related to the efficiency in global brain network organisation, i.e., the lower the radius and diameter, the more efficient is information processing between remote brain regions, this decrease may support the idea of a more efficient network (Su *et al.*, 2017).

The *average network* strength is the total average of each node's strength (local connectivity measure), and it is increased in MSC in both runs. It assesses the overall strength of the relationship between the nodes, so an increase in this measure implies stronger connectivity between regions, and thus there is a more facilitated information exchange and functional integration (Joseph *et al.*, 2012).

Assortativity measures the network's resilience when facing disruptions, that in the case of MS, can be WM and GM lesions. It assesses the likelihood of a node to be connected to another node with a similar degree; therefore, a positive assortativity value suggests that high-degree nodes connect and build a resilient and robust core (Rubinov and Sporns, 2010). The majority of biological networks are disassortative, i.e., the nodes are distributed and vulnerable, but sometimes this can change as networks display assortative hubs when faced with targeted attacks as a defence (Thedchanamoorthy *et al.*, 2014). Assortativity increases in MSC in both runs, which could be another indication of an adaptive response to lesions caused by MS, which was also shown by Rocca and colleagues (Rocca *et al.*, 2016).

The only global measure that is contradictory between runs is the global flow coefficient, the overall nodes' ability to conduct information flow, which increases in V1MT run and decreases in the BM runs in MSC. However, this measure it is not statistically significantly different between groups, and the changes are relatively small between the groups.

Most of the studies in MS, using task-based or resting-state paradigms, argue that, generally, there is a decrease in the efficiency of information transfer and in the strength and resilience of the network, even in the early phases of MS. However, what we found is conflicting with the literature: we see an increase in the quality and efficiency of information flow as well as an increase in the strength of the network. However, a study in the context of Gilles de la Tourette syndrome, studying structural connectivity, also found higher values of global efficiency and concluded that this increase of structural integration was associated with the syndrome's severity and could reflect potential adaptive plasticity (Schlemm *et al.*, 2017). If we analyse the obtained results from that point of view, all the results are in agreement: efficiency, resilience and strength increases could be yet another proof of the compensatory mechanism in MS in the early phases of the disease. These results may be possible in our study because we are analysing a very task-specific network, associated with visual perception, and ignoring the whole-brain connectivity during its performance, i.e., we can observe an increase in efficiency in this task in a small network, but that does not mean that overall brain efficiency is also increased.

5.8.2 Local Measures

The local connectivity metrics reflect the importance of a node (or a brain region) within the network and allow us to understand its role and what might happen if it is compromised. Moreover, an alteration of these local measures between groups might imply an altered network topology in the patient's group (Schlemm *et al.*, 2017).

The local measures that were studied are eccentricity, local efficiency, local flow coefficient, total flow, total degree, in-degree, out-degree, total strength, in-strength, out-strength, betweenness centrality and pagerank centrality. These are shown below for each participant, along with the median value for each node in each group, in the V1MT run.
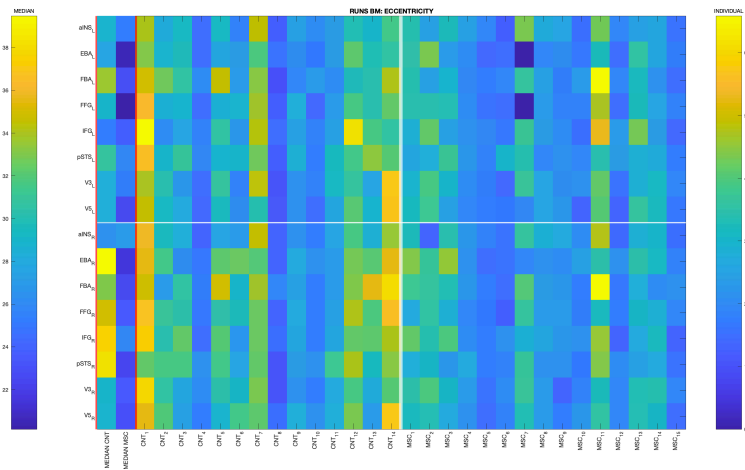
RUN V1MT
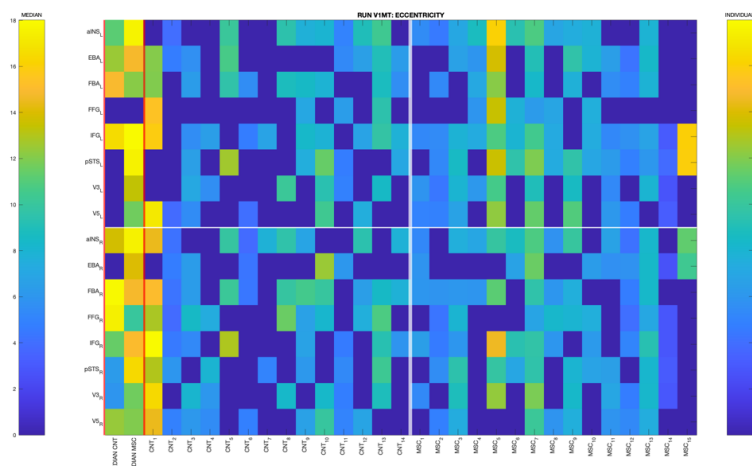
Figure 5.37 - Matrix representing the values of the eccentricity for each node (y-axis) and for each participant (x-axis), in the V1MT run. The two first columns of the matrix represent the median of the eccentricity values of the two groups (CNT and MSC) for each node. The first colorbar (on the left) represents the metric's median values and the second colorbar (on the right) represents the metric's individual values for each node.
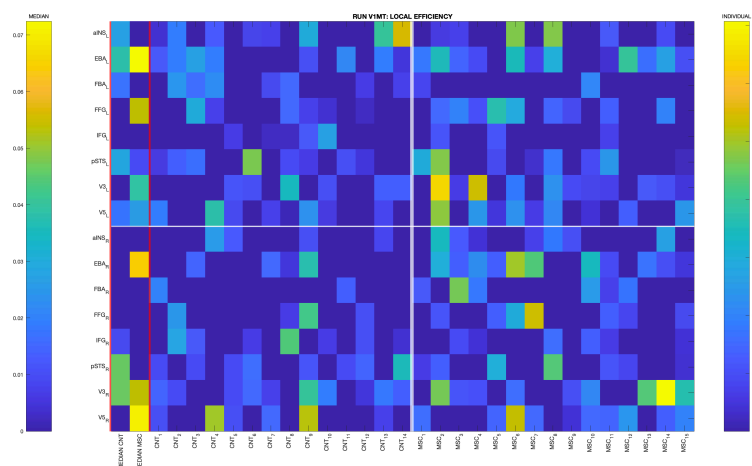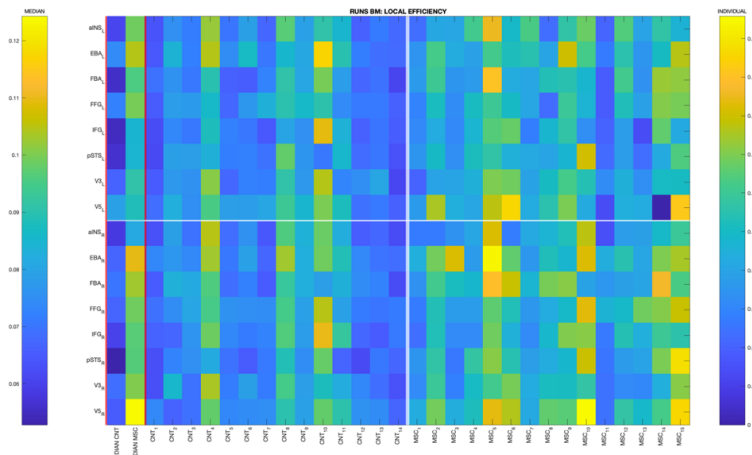

Figure 5.38 - Matrix representing the values of the local efficiency for each node (y-axis) and for each participant (x-axis), in the V1MT run. The two first columns of the matrix represent the median of the local efficiency values of the two groups (CNT and MSC) for each node. The first colorbar (on the left) represents the metric's median values and the second colorbar (on the right) represents the metric's individual values for each node.
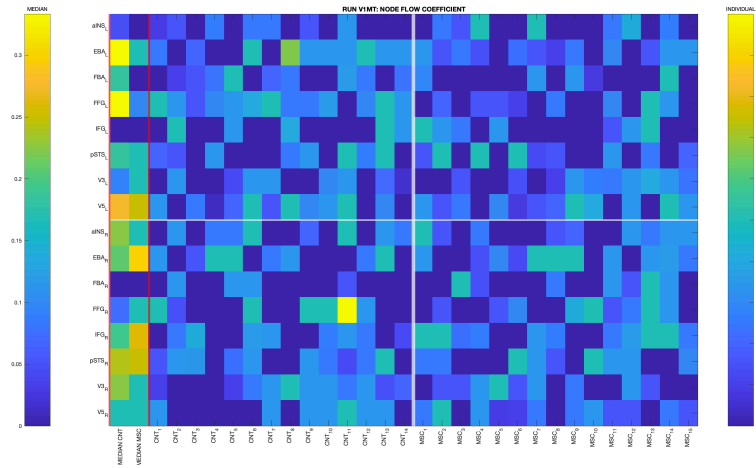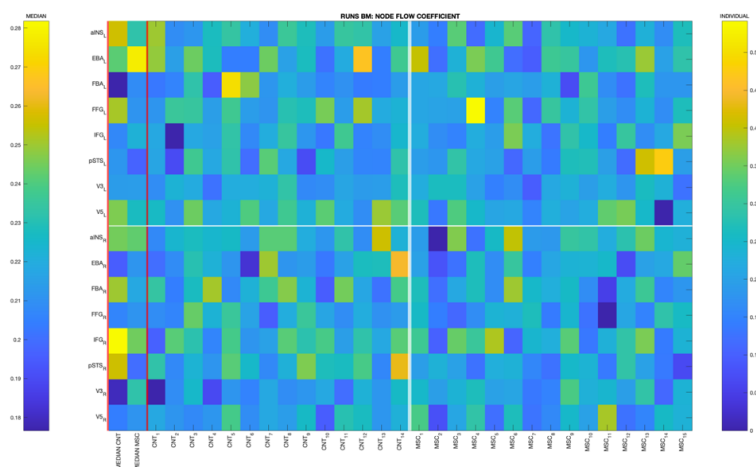
Figure 5.39 - Matrix representing the values of the local flow coefficient for each node (y-axis) and for each participant (x-axis), in the V1MT run. The two first columns of the matrix represent the median of the local flow coefficient values of the two groups (CNT and MSC) for each node. The first colorbar (on the left) represents the metric's median values and the second colorbar (on the right) represents the metric's individual values for each node.
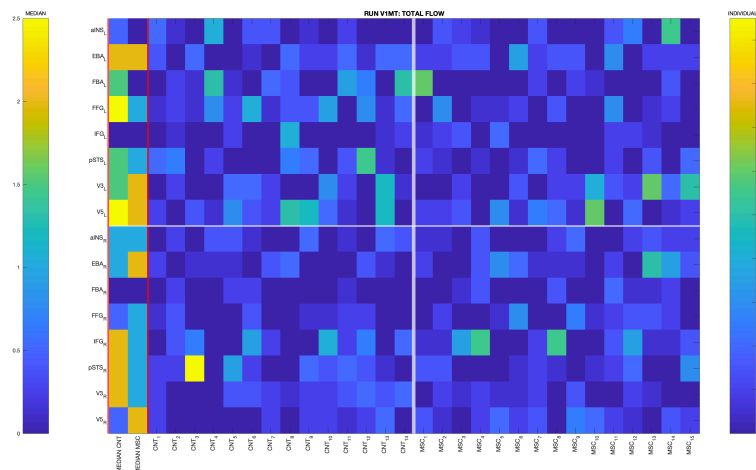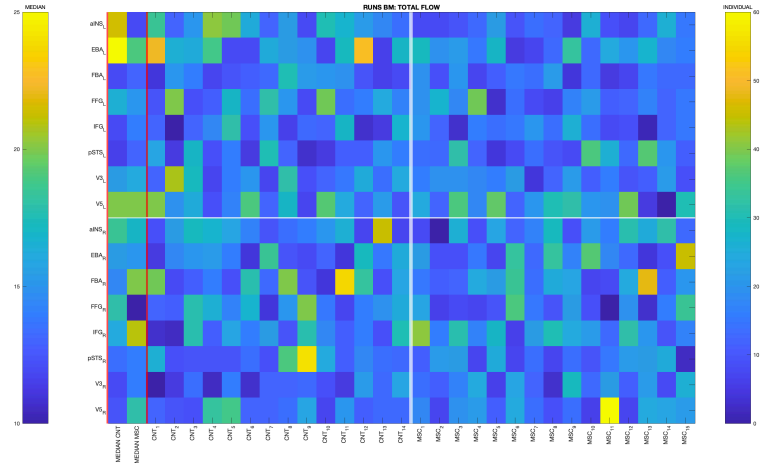

Figure 5.40 - Matrix representing the values of the total flow for each node (y-axis) and for each participant (x-axis), in the V1MT run. The two first columns of the matrix represent the median of the total flow values of the two groups (CNT and MSC) for each node. The first colorbar (on the left) represents the metric's median values and the second colorbar (on the right) represents the metric's individual values for each node.
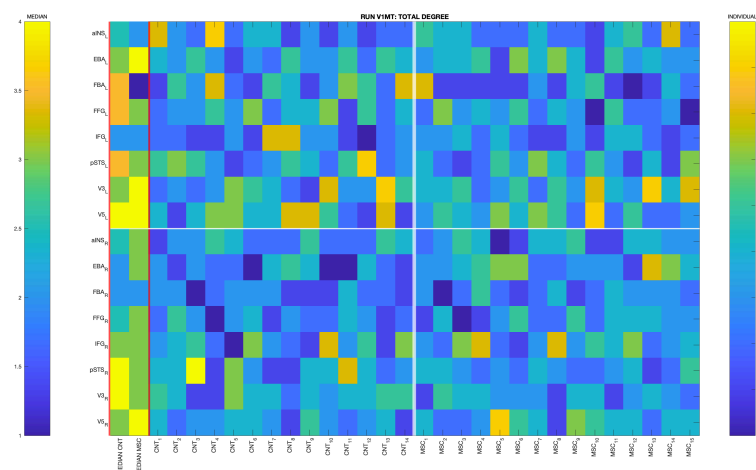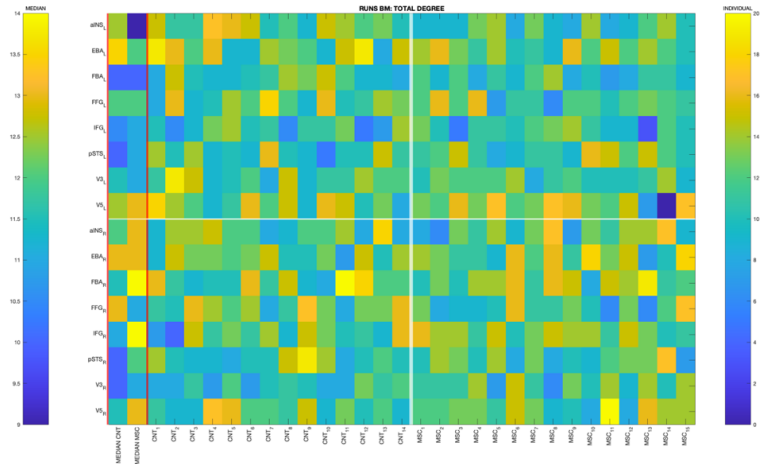

Figure 5.41 - Matrix representing the values of the total degree for each node (y-axis) and for each participant (x-axis), in the V1MT run. The two first columns of the matrix represent the median of the total degree values of the two groups (CNT and MSC) for each node. The first colorbar (on the left) represents the metric's median values and the second colorbar (on the right) represents the metric's individual values for each node.
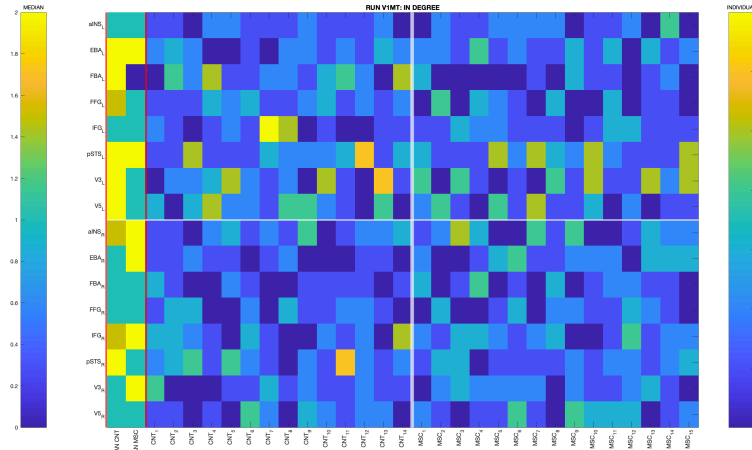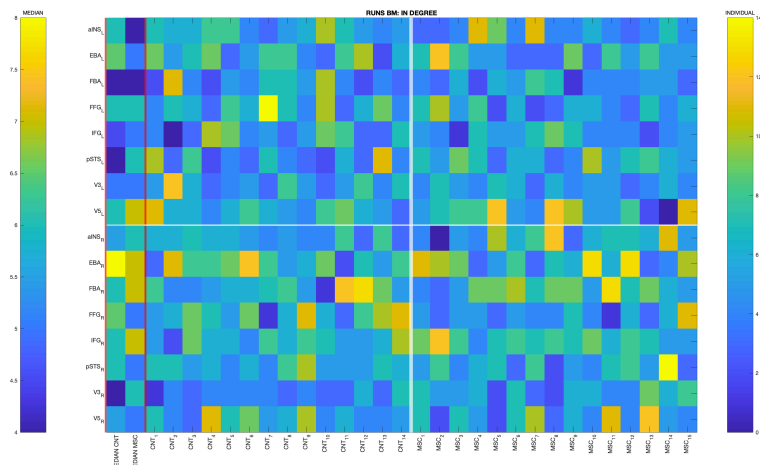
Figure 5.42 - Matrix representing the values of the in-degree for each node (y-axis) and for each participant (x-axis), in the V1MT run. The two first columns of the matrix represent the median of the in-degree values of the two groups (CNT and MSC) for each node. The first colorbar (on the left) represents the metric's median values and the second colorbar (on the right) represents the metric's individual values for each node.
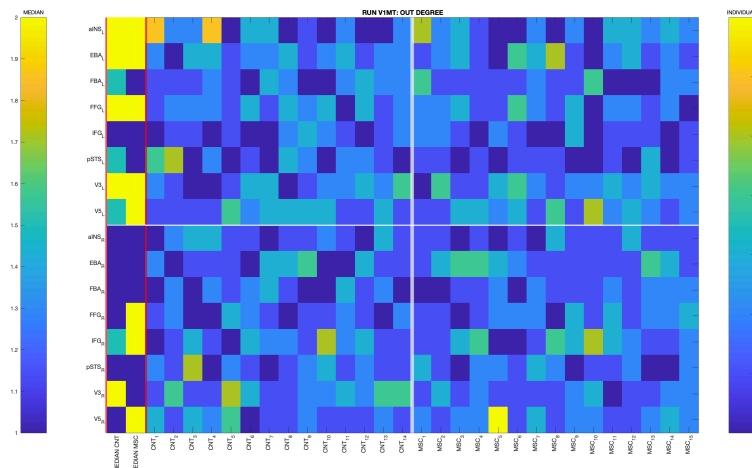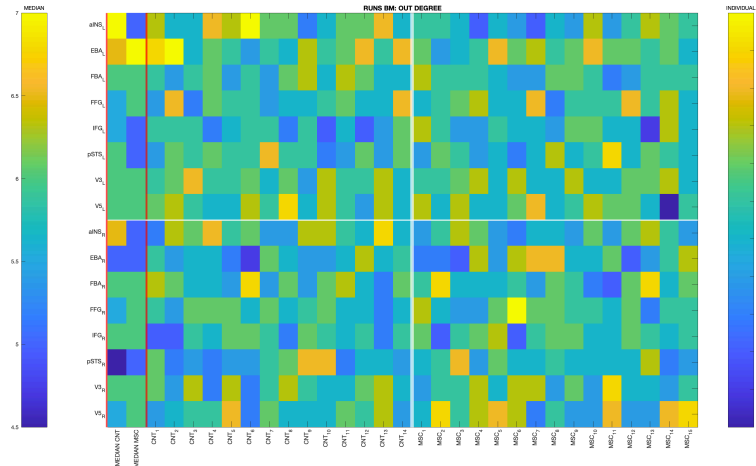

Figure 5.43 - Matrix representing the values of the out-degree for each node (y-axis) and for each participant (x-axis), in the V1MT run. The two first columns of the matrix represent the median of the out-degree values of the two groups (CNT and MSC) for each node. The first colorbar (on the left) represents the metric's median values and the second colorbar (on the right) represents the metric's individual values for each node.
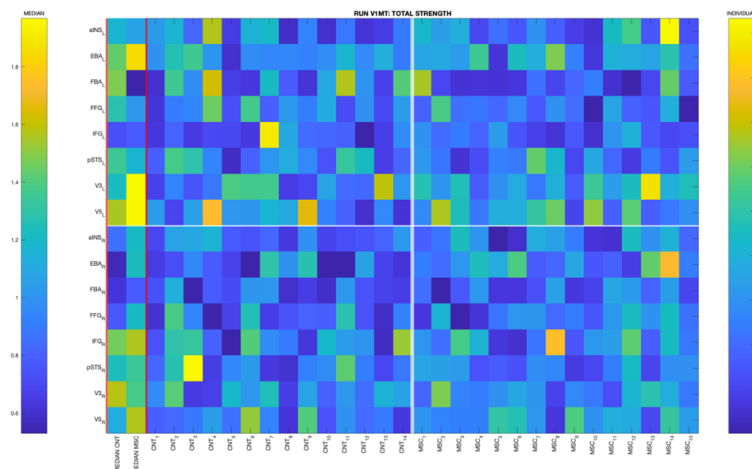
Figure 5.44 - Matrix representing the values of the total strength for each node (y-axis) and for each participant (x-axis), in the V1MT run. The two first columns of the matrix represent the median of the total strength values of the two groups (CNT and MSC) for each node. The first colorbar (on the left) represents the metric's median values and the second colorbar (on the right) represents the metric's individual values for each node.
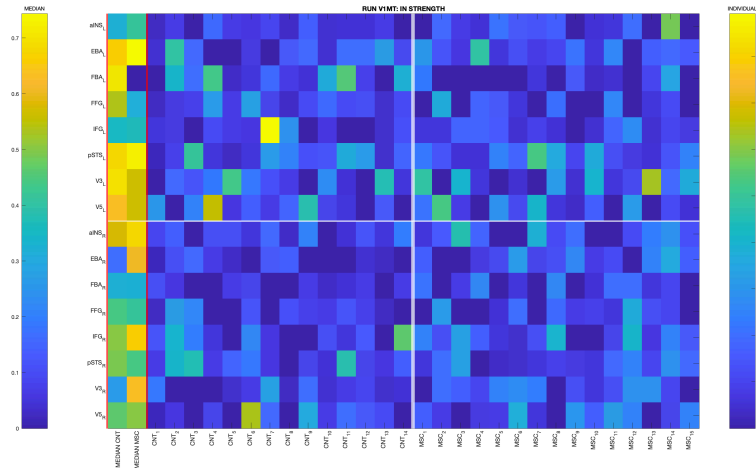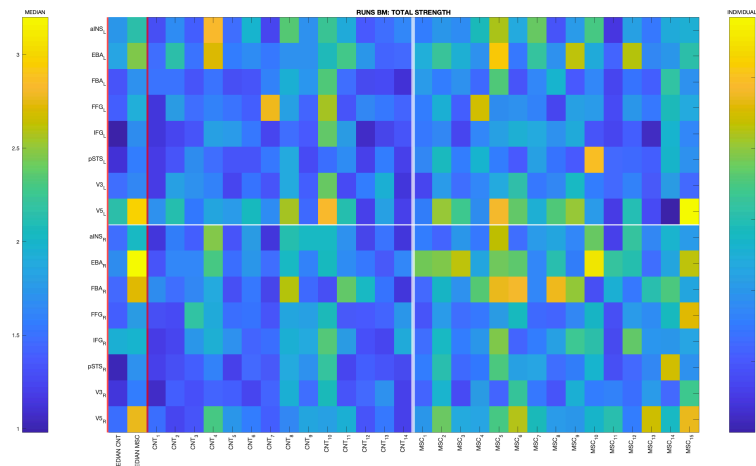
Figure 5.45 - Matrix representing the values of the in-strength for each node (y-axis) and for each participant (x-axis), in the V1MT run. The two first columns of the matrix represent the median of the in-strength values of the two groups (CNT and MSC) for each node. The first colorbar (on the left) represents the metric's median values and the second colorbar (on the right) represents the metric's individual values for each node.
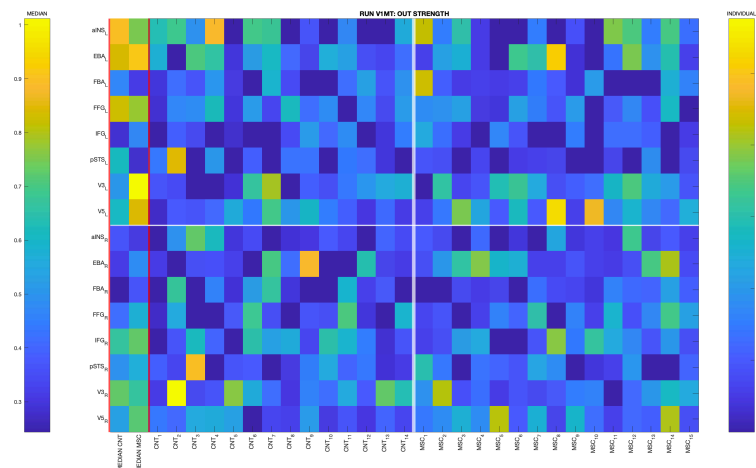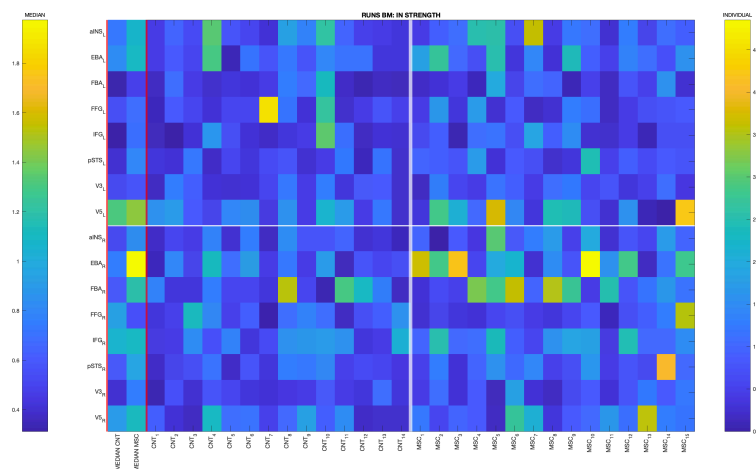

Figure 5.46 - Matrix representing the values of the out-strength for each node (y-axis) and for each participant (x-axis), in the V1MT run. The two first columns of the matrix represent the median of the out-strength values of the two groups (CNT and MSC) for each node The first colorbar (on the left) represents the metric's median values and the second colorbar (on the right) represents the metric's individual values for each node.
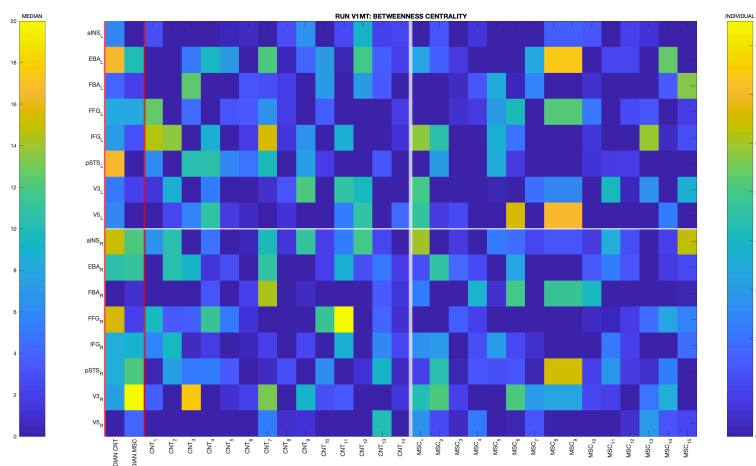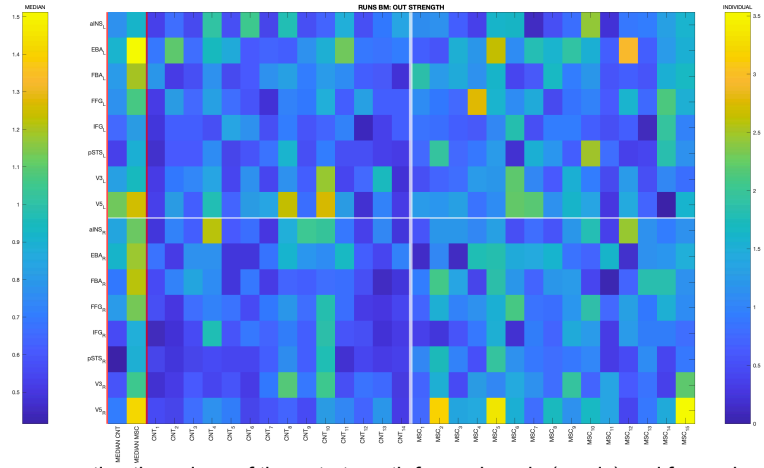

Figure 5.47 - Matrix representing the values of the betweenness centrality for each node (y-axis) and for each participant (x-axis), in the V1MT run. The two first columns of the matrix represent the median of the betweenness centrality values of the two groups (CNT and MSC) for each node. The first colorbar (on the left) represents the metric's median values and the second colorbar (on the right) represents the metric's individual values for each node.
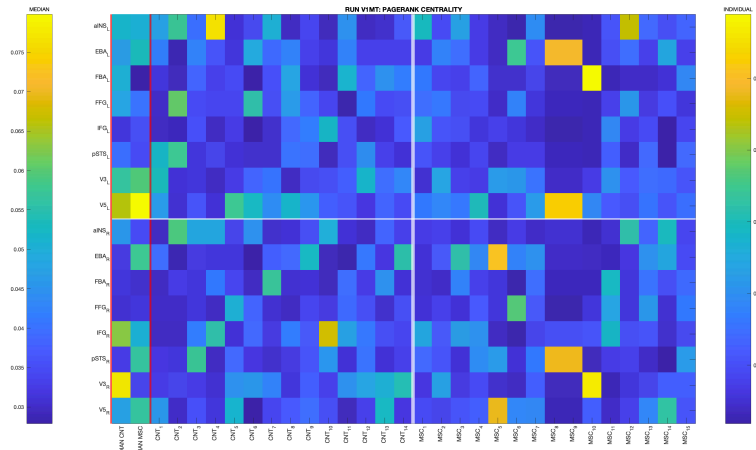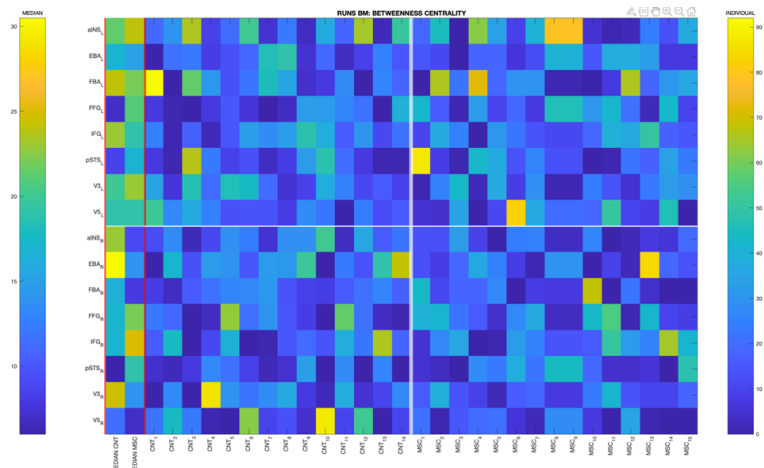
Figure 5.48 - Matrix representing the values of the pagerank centrality for each node (y-axis) and for each participant (x-axis), in the V1MT run. The two first columns of the matrix represent the median of the pagerank centrality values of the two groups (CNT and MSC) for each node. The first colorbar (on the left) represents the metric's median values and the second colorbar (on the right) represents the metric's individual values for each node.
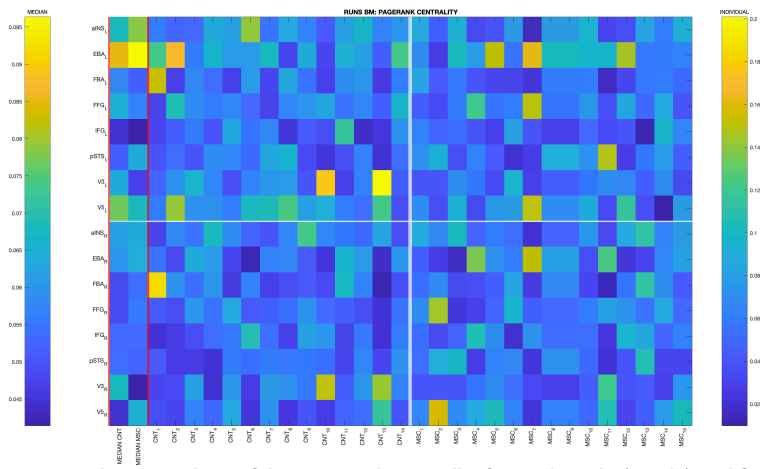
A statistical Wilcoxon rank sum test was performed to evaluate which nodes and which connectivity metrics were significantly different between groups (p < 0.05). This statistical analysis is represented in matrix form with all significantly different local measures (x-axis) and respective significantly different nodes between groups (y-axis).
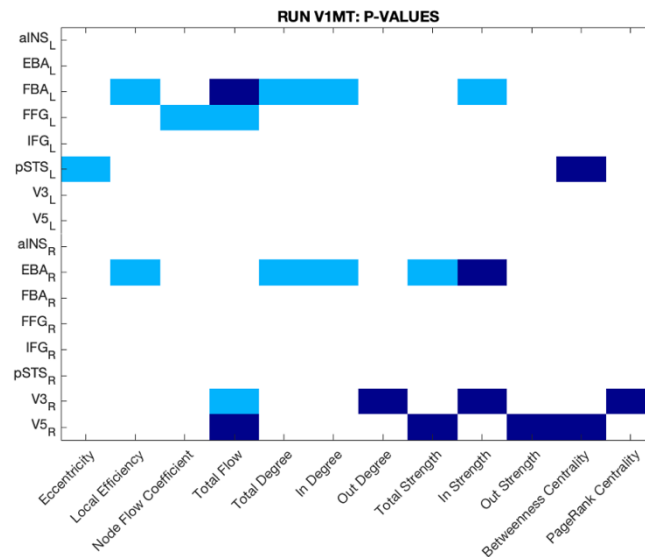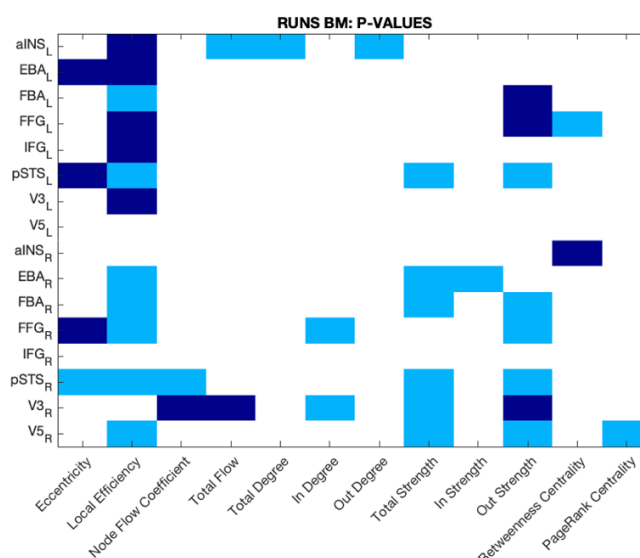

Figure 5.49 - Matrix with the nodes and corresponding local measures that are statistically significantly different between groups, with PTh = 0.11, in the V1MT run. Wilcoxon rank sum test was performed and the nodes with a p-value < 0.05 are represented in light blue. The nodes in dark blue have a p-value < 0.1 (tendency for statistical significance).

RUNS BM

Figure 5.50 - Matrix representing the values of the eccentricity for each node (y-axis) and for each participant (x-axis), in the BM runs. The two first columns of the matrix represent the median of the eccentricity values of the two groups (CNT and MSC) for each node. The first colorbar (on the left) represents the metric's median values and the second colorbar (on the right) represents the metric's individual values for each node.

Figure 5.51 - Matrix representing the values of the local efficiency for each node (y-axis) and for each participant (x-axis), in the BM runs. The two first columns of the matrix represent the median of the local efficiency values of the two groups (CNT and MSC) for each node. The first colorbar (on the left) represents the metric's median values and the second colorbar (on the right) represents the metric's individual values for each node.

Figure 5.52 - Matrix representing the values of the local flow coefficient for each node (y-axis) and for each participant (x-axis), in the BM runs. The two first columns of the matrix represent the median of the local flow coefficient values of the two groups (CNT and MSC) for each node. The first colorbar (on the left) represents the metric's median values and the second colorbar (on the right) represents the metric's individual values for each node.

Figure 5.53 - Matrix representing the values of the total flow for each node (y-axis) and for each participant (x-axis), in the BM runs. The two first columns of the matrix represent the median of the total flow values of the two groups (CNT and MSC) for each node. The first colorbar (on the left) represents the metric's median values and the second colorbar (on the right) represents the metric's individual values for each node.

Figure 5.54 - Matrix representing the values of the total degree for each node (y-axis) and for each participant (x-axis), in the BM runs. The two first columns of the matrix represent the median of the total degree values of the two groups (CNT and MSC) for each node. The first colorbar (on the left) represents the metric's median values and the second colorbar (on the right) represents the metric's individual values for each node.

Figure 5.55 - Matrix representing the values of the in-degree for each node (y-axis) and for each participant (x-axis), in the BM runs. The two first columns of the matrix represent the median of the in-degree values of the two groups (CNT and MSC) for each node. The first colorbar (on the left) represents the metric's median values and the second colorbar (on the right) represents the metric's individual values for each node.

Figure 5.56 - Matrix representing the values of the out-degree for each node (y-axis) and for each participant (x-axis), in the BM runs. The two first columns of the matrix represent the median of the out-degree values of the two groups (CNT and MSC) for each node. The first colorbar (on the left) represents the metric's median values and the second colorbar (on the right) represents the metric's individual values for each node.

Figure 5.57 - Matrix representing the values of the total strength for each node (y-axis) and for each participant (x-axis), in the BM runs. The two first columns of the matrix represent the median of the total strength values of the two groups (CNT and MSC) for each node. The first colorbar (on the left) represents the metric's median values and the second colorbar (on the right) represents the metric's individual values for each node.

Figure 5.58 - Matrix representing the values of the in-strength for each node (y-axis) and for each participant (x-axis), in the BM runs. The two first columns of the matrix represent the median of the in-strength values of the two groups (CNT and MSC) for each node. The first colorbar (on the left) represents the metric's median values and the second colorbar (on the right) represents the metric's individual values for each node.

93

Figure 5.59 - Matrix representing the values of the out-strength for each node (y-axis) and for each participant (x-axis), in the BM runs. The two first columns of the matrix represent the median of the out-strength values of the two groups (CNT and MSC) for each node. The first colorbar (on the left) represents the metric's median values and the second colorbar (on the right) represents the metric's individual values for each node.

Figure 5.60 - Matrix representing the values of the betweenness centrality for each node (y-axis) and for each participant (x-axis), in the BM runs. The two first columns of the matrix represent the median of the betweenness centrality values of the two groups (CNT and MSC) for each node. The first colorbar (on the left) represents the metric's median values and the second colorbar (on the right) represents the metric's individual values for each node.

Figure 5.61 - Matrix representing the values of the pagerank centrality for each node (y-axis) and for each participant (x-axis), in the BM runs. The two first columns of the matrix represent the median of the pagerank centrality values of the two groups (CNT and MSC) for each node. The first colorbar (on the left) represents the metric's median values and the second colorbar (on the right) represents the metric's individual values for each node.

A new statistical Wilcoxon rank sum test was performed to evaluate which nodes and which connectivity metrics were significantly different between groups (p < 0.05), in the BM runs. This statistical analysis is represented in matrix form with all significantly different local measures (x-axis) and respective significantly different nodes between groups (y-axis).

Figure 5.62 - Matrix with the nodes and corresponding local measures that are statistically significantly different between groups, with PTh = 0.39, in the BM runs. Wilcoxon rank sum test was performed and the nodes with a p-value < 0.05 are represented in light blue. The nodes in dark blue have a p-value < 0.1 (tendency for statistical significance).

Eccentricity is the "longest" shortest path that the information from a node 'travels' to reach any other node and is interpreted as the ease of a region to be functionally reached by all of the other regions in the network, which also reflects how efficient is the information exchange (Su *et al.*, 2017). The smaller the eccentricity, the more central the node is located in the network because the paths to reach other nodes are inherently smaller as well. Hence, a node with low values of eccentricity will influence and/or be more influenced by the activity of other nodes. In turn, a node with high values of eccentricity could have a marginal functional role in the network. (Tewarie *et al.*, 2014) and (Miri Ashtiani *et al.*, 2019) argue that the eccentricity can significantly change in early MS.

In the V1MT localiser run, pSTS$_L$'s eccentricity value is significantly different between groups and increased in MSC, indicating that this node could have a marginal role in the network and therefore be damaged in MSC. In the BM runs, the pSTS$_R$'s eccentricity value is different between groups and increased in CNT, which could mean that in MSC it becomes more influent in the network, as a compensation.

These results could also reflect damages in the left hemisphere and compensation in the right hemisphere, which further supports the hypothesis of a shift in brain lateralization.

Local efficiency measures the efficiency of information exchange within the direct neighbourhood of a node (J. Liu *et al.*, 2017), which means that nodes with high values of local efficiency effectively share information with their immediate local neighbours (Stanley *et al.*, 2015).

In the V1MT localiser run, there are two nodes that are significantly different between groups: FBA$_L$, with a higher local efficiency in CNT, and EBA$_R$ with a higher local efficiency in MSC.

In the BM runs, several nodes are significantly different between groups: V5$_R$, pSTS$_R$, FFG$_R$, FBA$_R$, EBA$_R$, pSTS$_L$ and FBA$_L$. All of them have higher local efficiency values in MSC. These

nodes may have important roles in their respective sub-networks and their removal from the network may have harmful consequences in information processing. These results further reinforce the idea that the right hemisphere is more recruited in MS, as a consequence of adaptive phenomena.

Local (or node) flow coefficient represents the ability of the node to conduct information flow (Sacchet *et al.*, 2015). Therefore, the higher is the local flow coefficient of a node, the more is the node's ability to conduct information.
In the V1MT localiser run, only FFG_L is significantly different between groups, having higher values in CNT. In the BM runs, the values of $pSTS_R$'s local flow coefficient are different between groups with higher values in CNT.
This could indicate that these nodes might have lost the ability to conduct information flow in an efficient manner in the MSC group (at least as efficiently as in the control group), and thus their function might be compromised due to the effect of the disease.

Total flow measures the number of information paths that flow across the node (Sacchet *et al.*, 2015). A higher total flow of a node could mean that more information flow passes through that node.
In the V1MT localiser run, FFG_L and $V3_R$ are significantly different between groups, and they have higher values in CNT. FFG_L has also a higher local flow coefficient in CNT, which adds up to the idea that its functions in transmitting information become damaged in MS.
In the BM runs, $aINS_L$ is the only node significantly different between groups, having higher values in CNT. $aINS_L$'s role in managing information flow may also be compromised in MS.

Total degree represents the number of links connected to a given node and provides information about each ROI's significance: the higher the degree of a node, the more it interacts with others and creates pathways for information flow. Nodes with high degree can be considered hubs, which are known to have a critical role in the network, integrating and distributing information (Khazaee, Ebrahimzadeh and Babajani-Feremi, 2017).
In the V1MT localiser run, the two nodes that are significantly different between groups are FBA_L, with a higher degree in CNT, and EBA_R with a higher degree in MSC.
In the BM runs, $aINS_L$ has a higher degree in CNT. Its role and influence in the network may be compromised in MSC, as seen previously with the total flow measure.

The in- and out-degree measures are related to the degree, but they only account for the node's number of inward and outward connections, respectively, in a directed network (Rubinov and Sporns, 2010). These measures might seem redundant at first glance since the degree already describes the total number of neighbours of the node; however, the correlation between in- and out-degree can bring new information about the network and its nodes. Nodes with higher in-degree are seen as *integrators* within the networks, i.e, more information converges to them. Nodes with higher out-degree are seen as *distributors*, i.e, they send more information to the rest of the network. If one of these measures is altered, this might mean that the function of the node is also altered. For example, the node might have the same total degree in CNT and MSC, but the node's in-degree in MSC is lower, and the out-degree is higher. This can mean that the node's functions in MS, particularly when receiving information, are damaged.

In *in-degree*, in the V1MT localiser run, and similarly to the total degree, the two nodes that are different between groups are FBA_L, with a higher in-degree in CNT, and EBA_R with a

higher in-degree in MSC. In the BM runs, the two nodes different between-groups are V3$_R$, which has a higher in-degree in MSC, and FFG$_R$, which has a higher in-degree in CNT.

In *out-degree*, there are no nodes that are significantly different between groups in the V1MT localiser run. In the BM runs, aINS$_L$ is the only node that is significantly different between groups with increased out-degree values in CNT, again reinforcing that this node's function is damaged in MS.

Total strength is a metric related to degree, but, in weighted networks, it instead considers the sum of weights of links connected to the node (Rubinov and Sporns, 2010). Therefore, the outcomes of degree and strength are different: while degree focuses on the number of connections of the node, strength considers the relationship between the node and its neighbours. Moreover, strength only considers the general involvement of the node within the network, failing to account for the number of links. This might be problematic when analysing the centrality of the node, since it is usually measured by the number of connections it has, not by the strength of the connections. Thus, having a higher strength doesn't mean that the node has influence over many other nodes in the network, it only means that more information passes through it (Opsahl, Agneessens and Skvoretz, 2010).
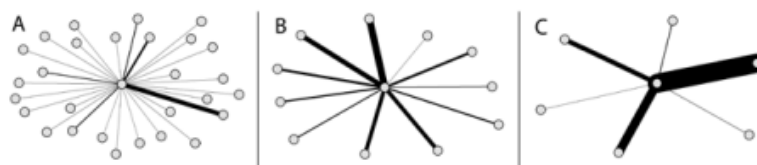
Figure 5.63 - Representation of the difference between the strength and degree of a node. Node A has more neighbours, thus, a higher degree; Node C has less neighbours but the strength of the connections is higher than in node A; Node B is an intermediate between nodes A and C, in terms of strength and degree (Opsahl, Agneessens and Skvoretz, 2010).

Despite this, strength is usually preferred when analysing weighted graphs (Opsahl, Agneessens and Skvoretz, 2010).
In the V1MT localiser run, the strength of EBA$_R$ is significantly different between groups and has higher values in MSC. In the BM runs, several nodes are significantly different between groups: V5$_R$, V3$_R$, pSTS$_R$, FBA$_R$, EBA$_R$ and pSTS$_L$. All of them have higher values of strength in MSC, again highlighting the importance of the right hemisphere in MS networks.

In-strength is related to the total strength, but it represents the sum of the weights of the incoming connections of a node (Rubinov and Sporns, 2010).
In the V1MT localiser run, FBA$_L$ is significantly different between groups and has higher in-strength values in CNT. In the BM runs, EBA$_R$ is significantly different between groups and has higher in-strength values in MSC, meaning that the incoming flux of information to this node is higher in MS.

Out-strength is the sum of the weights of the outcoming connections of a node (Rubinov and Sporns, 2010).
There are no nodes that are significantly different between groups in the V1MT localiser run. In the BM runs, several nodes are significantly different between groups: V5$_R$, FFG$_R$, pSTS$_R$, FBA$_R$ and pSTS$_L$. All of them have higher values of strength in MSC, meaning that the outcoming flux of information from these nodes in MS is high.

Betweenness centrality measures the number of paths with the shortest length that go through a given node. A high value of betweenness centrality means that the node connects

disparate parts of the networks and plays an important role in information exchange (Rubinov and Sporns, 2010).

There are no nodes that are significantly different between groups in the V1MT localiser run. In the BM runs, FFG_L is significantly different between groups and has higher values in MSC, which could mean that this node participates in a large number of shortest paths and intercedes in the information flow of the network, carrying more information.

Pagerank centrality measures the importance and level of influence of a node within a network, considering the quality of the connections. Ashtiani and colleagues (Miri Ashtiani *et al.*, 2019) described eigenvector centrality, the undirected version of pagerank centrality, as effective in the detection of main brain hubs, which are usually altered in MSC.

There are no nodes that are significantly different between groups in the V1MT localiser run. In the BM runs, $V5_R$ is significantly different between groups and has higher values in MSC. This could imply that $V5_R$ has a major impact in the network, in these runs, and it communicates with many other nodes (more connections). Also, as pagerank centrality can detect brain hubs, $V5_R$ could potentially represent one, given its significance in other metrics such as local efficiency, strength, and out-strength, always having higher values in MSC, which again supports the hypothesis that it is a hub in the network, and could emerge in MS.

The significantly different nodes between groups are summarized in Table 5.8.

Table 5.8 - Significantly different nodes between groups within each connectivity measure for runs V1MT and BM. The red nodes represent the nodes with the median values of the metrics increased in the MS patients' group.

Local connectivity measure	Significantly different node(s) between groups	
	RUN V1MT	**RUNS BM**
Eccentricity	$pSTS_L$	$pSTS_R$
Local Efficiency	EBA_R	$V5_R$
		$pSTS_R$
		FFG_R
		FBA_R
	FBA_L	EBA_R
		$pSTS_L$
		FBA_L
Node Flow Coefficient	FFG_L	$pSTS_R$
Total Flow	$V3_R$	$aINS_L$
	FFG_L	
Total Degree	EBA_R	$aINS_L$
	FBA_L	
In-Degree	EBA_R	$V3_R$
	FBA_L	FFG_R
Out-Degree	---	$aINS_L$
Strength	EBA_R	$V5_R$
		$V3_R$
		$pSTS_R$
		FBA_R
		EBA_R
		$pSTS_L$

In-Strength	FBA$_L$	EBA$_R$
Out-Strength	---	V5$_R$
		pSTS$_R$
		FFG$_R$
		FBA$_R$
		pSTS$_L$
Betweenness Centrality	---	FFG$_L$
Pagerank Centrality	---	V5$_R$

The four local graph metrics that presented the largest number of between-group differences in run V1MT, highlighting the ROIs' importance and role, are local efficiency, total flow, degree, and in-degree, which had two significantly different nodes each. There are no statistically significant nodes in out-degree, out-strength, betweenness centrality and pagerank centrality (at $p < 0.05$) in this run.

The three local graph metrics that presented the greatest number of between-group differences in the BM runs are local efficiency, strength, and out-strength, which had seven, six and five significantly different nodes, respectively.

The general conclusion from this analysis is that the number of the significantly different nodes and the values of the local connectivity metrics generally increase in the MS patient's group. This again supports the hypothesis of neuroplasticity in early phases of MS as compensation for damages in some specific brain regions during the performance of tasks.

Noteworthy, there is a difference in the significantly different nodes in the tasks. In the run V1MT, only five different nodes are significant, primarily involved in lower-level visual perception. In the BM runs, which involve a more complex task, more regions are significantly different between groups, namely pSTS and aINS, which are higher-level regions associated with the perception of biological motion and decision making. It is also worth mentioning that aINS in the left hemisphere always has higher values of the metrics in CNT, indicating that its function and influence over the MS network is compromised. Nonetheless, we observe cases in which the same node appears to have decreased efficiency during the V1MT run and increased efficiency during the BM runs. This might seem counter-intuitive, but it highlights the importance of using appropriate tasks when investigating these kinds of measures. There might be subtle differences that are relevant from the clinical point of view but only revealed if the network(s) involving these regions are sufficiently recruited.

In run V1MT, two particular ROIs (nodes) stand out in the statistical analysis given their active presence in several metrics: FBAL, which has increased values in CNT, and EBAR that has increased values in MSC. These observations regarding the involvement of EBA in the right hemisphere in MSC, while the involvement of FBA on the left hemisphere seems to be diminished or lost (relative to the CNT group), might further relate and support the hypothesis of a shift in brain lateralization described earlier (section 5.5). Overall, these results of the significantly different nodes in the calculation of local connectivity metrics seem to back up this idea of lateralization: we observe more involvement of the right hemisphere in the MSC group (as they have higher values of the metrics) and a decrease in the activity of the left hemisphere (they have higher values of the metrics in the CNT group).

It is important to note that the interpretation and discussion of the involvement of nodes and connectivity metrics is based on differences between groups. This means that a particular node that appears to have an increase/decrease in a specific connectivity metric in the group of patients with MS (relative to healthy controls) is not necessarily participating in the processing of the task(s) at hand or is not necessarily completely replacing the function or role of another node in the network. It shows that its participation in the network is somehow different in the context of MS due to, e.g., deterioration of its function, deterioration of its connectivity, or neuroplasticity. Furthermore, we recall that the whole analysis is done with a very restricted and specific network (in contrast to many studies of rs-fMRI and whole-brain connectivity analysis). The nature of the analysis reveals alterations in the functioning of the network at the level of communication between brain regions while participants maintained task performance. Thus, between-groups differences probably reflect a reorganization of the same system (the restricted network of interest) to fight against the effect of the disease and maintain efficiency in brain function and communication.

Finally, an important note to make is that, even if we cannot find a homogeneous pattern of differences between groups (e.g., all metrics are decreased in MS patients), this does not mean the information is not relevant. A pattern of altered connectivity measures in a group of patients might reveal connections that are preserved (these would be connections or nodes with no differences), connections that are somehow physiologically adapting and compensating effects of the disease connections/nodes (these would be those with increased connectivity measures), and connections/nodes that are damaged and not able to compensate (those are the ones showing decreased connectivity). The last in particular are candidates for further exploration and early intervention, if possible.

5.9 Neuropsychological Evaluation

Cognitive dysfunction is also a hallmark in MS, even in the early phases of the disease: some studies estimate that 43 to 70% of RRMS patients have signs of cognitive deficits (Parry *et al.*, 2003) (Du *et al.*, 2019). These damages involve several domains such as memory, attention, decision making and processing speed (section 4.1.2) (Miri Ashtiani *et al.*, 2019). However, most RRMS patients do not show noticeable signs of cognitive impairment, and these evaluations tend not to have significant correlations with MRI measures such as lesion burden. A possible explanation for this is neuroplasticity, which allows the brain to adapt and reorganize, compensating for impairments in the brain network's function (Parry *et al.*, 2003). Thus, investigating early cognitive alterations and their relationship with brain connectivity may be helpful in the prevention of irreversible damages in the cognition of MS patients.

Functional connectivity and its correlation with neuropsychological evaluations has been studied previously, but this thesis' approach considers a more specific (visual) network and the directed functional connectivity between the brain regions involved in the tasks. Hence, these results could shed light on the alteration of cognitive functions in an early stage of MS.

The data were tested for normality using the KS test. Therefore, Spearman correlation analysis was performed between the F-values of every connection in the network and the results in the six neuropsychological tests: Expanded Disability Status Scale (EDSS), Modified Fatigue Impact Scale (MFIS), Symbol Digit Modalities Test (SDMT), California Verbal Learning Test (CVLT), Brief Visuospatial Memory Test (BVMT) and Reading the Mind with the Eyes (RME), whose results were obtained from eleven MS patients.

The results of the analysis for each test are presented in the subsections below, and in each of them, three matrices are shown with: (1) the p-values of the statistically significant ($p < 0.05$) correlations between connectivity F-values in each pairwise connection and the test score (i.e., the correlation is significantly different from 0), (2) the Spearman r-values ranging from -1 to 1, representing the correlation between the F-values and the test scores, for those connections that were statistically significant (shown in the first matrix), and (3) the pairwise connections that were different between groups (section 5.4) and had at the same time a significant correlation with the clinical/neuropsychological test. The last matrix thus shows a conjunction analysis that reveals the connections that are simultaneously significantly different between groups and correlated with the test in MS patients.

5.9.1 Expanded Disability Status Scale

The Expanded Disability Status Scale is an ordinal scale ranging from 0 to 10 that describes disease progression in MS patients, mainly focusing on physical impairment (section 2.1.4) (JF, 1983) (Meyer-Moock *et al.*, 2014).
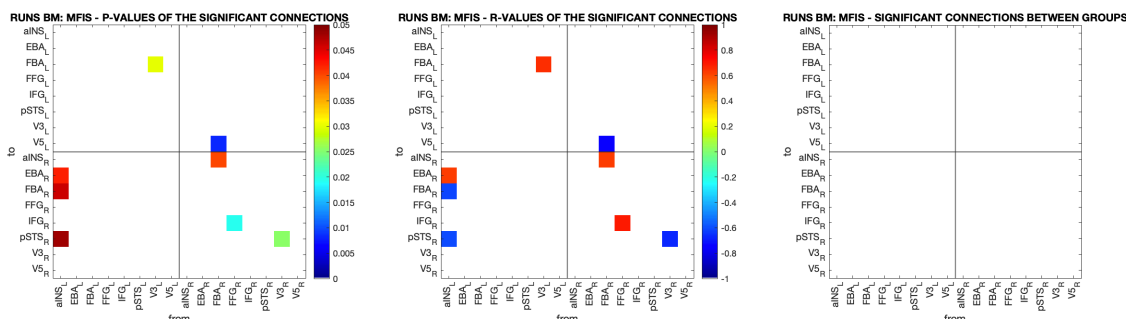
RUN V1MT
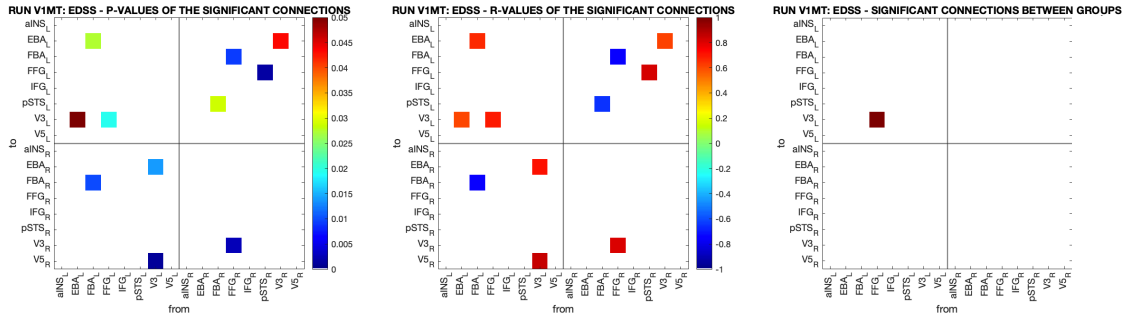
Figure 5.64 - Results of the Spearman correlation for EDSS data, in the V1MT run. (Left) Matrix with the p-values of the significant correlations ($p < 0.05$) between pairwise connectivity and test scores. The colorbar represents p-values. (Middle) Matrix with the r-values of the correlation of F-values and EDSS scores for the connections with significant correlations ($p < 0.05$) (the same as on the matrix on the left). Red/orange/yellow represents a positive correlation, blue represents negative correlations. The colorbar represents the Spearman r-values. (Right) Connections with a significant correlation between F-values and the test score, among those previously found to be significantly different between groups.

There are eleven connections with significant correlation between the F-values and the results for EDSS, with a predominance for positive correlations. The most robust connections ($p < 0.01$) are $V3_L \rightarrow V5_R$, $V3_L \rightarrow EBA_R$, $FFG_R \rightarrow V3_R$, $pSTS_R \rightarrow FFG_L$, which have positive correlations with EDSS, and $FBA_L \rightarrow FBA_R$ and $FFG_R \rightarrow FFG_L$, which have negative correlations with EDSS.

The only connection correlated with EDSS that is significantly different between groups is $FFG_L \rightarrow V3_L$, with a correlation p-value of 0.0193 and a Spearman r-value of 0.688, having higher F-values in CNT. The scatter plot of F-values of this connection and the EDSS scores is represented in figure 5.65.
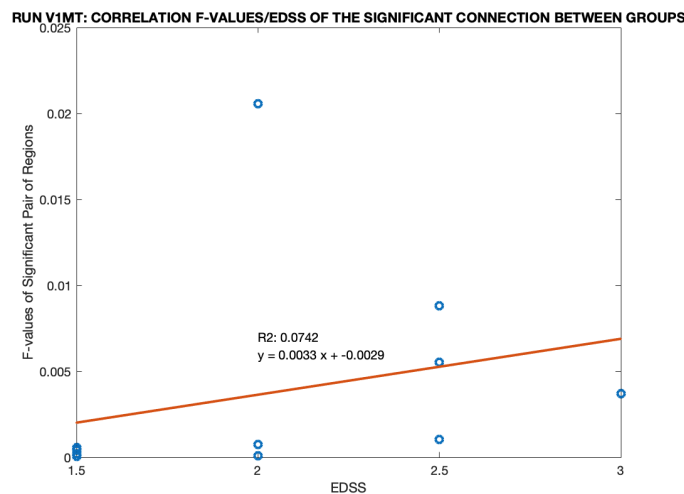
Figure 5.65 - Graphic representation of the correlation between the F-values of the connection $FFG_L \rightarrow V3_L$ (in the run V1MT) and the EDSS results.
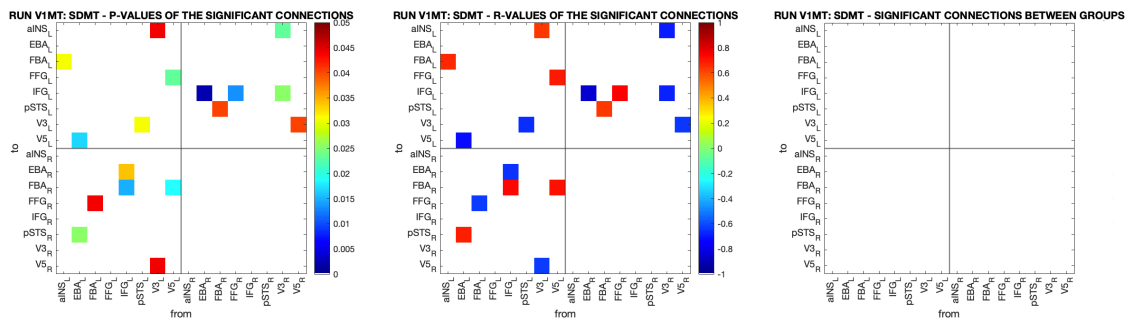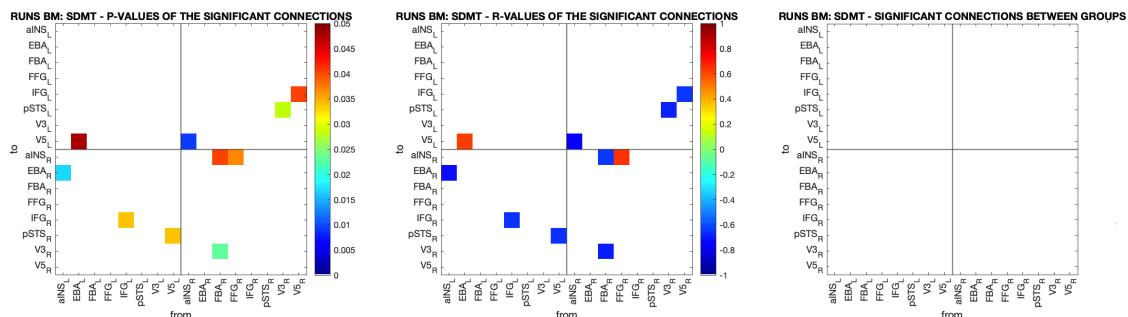
RUNS BM
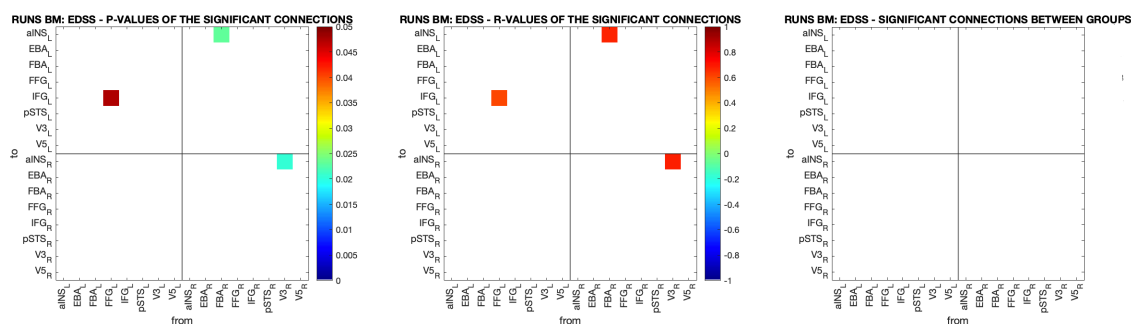
Figure 5.66 - Results of the Spearman correlation for EDSS data, in the BM runs. (Left) Matrix with the p-values of the significant correlations (p < 0.05) between pairwise connectivity and test scores. The colorbar represents p-values. (Middle) Matrix with the r-values of the correlation of F-values and EDSS scores for the connections with significant correlations (p < 0.05) (the same as on the matrix on the left). Red/orange/yellow represents a positive correlation, blue represents negative correlations. The colorbar represents the Spearman r-values. (Right) Connections with a significant correlation between F-values and the test score, among those previously found to be significantly different between groups.

In the BM runs, there are three connections with significant correlation between the F-values and the results for EDSS, although they are not very specific (p-values are higher than 0.01). Moreover, all connections have positive correlations with the EDSS values and none of them have been found to be statistically significantly different between groups.

Discussion of the EDSS results

The ROIs used in this study might be non-optimal to investigate the correlation of functional connectivity with physical disability evaluated with EDSS because they are mainly involved in visual performance and body and social perception. This may explain why this is the test with less statistically significant correlations with the F-values of connectivity.

Nevertheless, most of the significant connections seem to have a positive correlation with the EDSS data, i.e., increases in the FC of these connections may lead to a higher EDSS and, thus, to a higher disability. Connections to and from V3 seem to be very correlated with EDSS in both runs, suggesting that visual tests (almost every one of them involves V3 since this region is activated in the majority of visual tasks) can be an early detector for physical and cognitive impairment. FFG (and particularly FFG$_L$) and FBA (which is a part of the FFG) also seem to stand out in the more specific connections, generally having positive correlations with EDSS. This can be explained because these are regions that communicate with the visual pathway. FFG is also part of the only discriminative connection between groups in the V1MT run. Further studies with more data are needed to confirm the relationship of these metrics during visual tasks with EDSS scores and disability. If such a correlation were found to be robust, it would place this visual network as a candidate for the investigation of novel biomarkers for predicting EDSS scores and disease progression in patients with RRMS.

5.9.2 Modified Fatigue Impact Scale

Fatigue, a feeling of lack of energy and physical tiredness, is experienced by approximately 90% of the MS patients, and two-thirds of these patients report that it is one of the most disabling symptoms of the disease (DeLuca *et al.*, 2008). Its impact on their daily lives is evaluated through the self-administered MFIS questionnaire, consisting of questions related to fatigue's influence on physical, cognitive, and psychosocial aspects of the patient's life. A higher score represents a higher level of fatigue (Fisk et al., 1994) (Gomes, 2011).
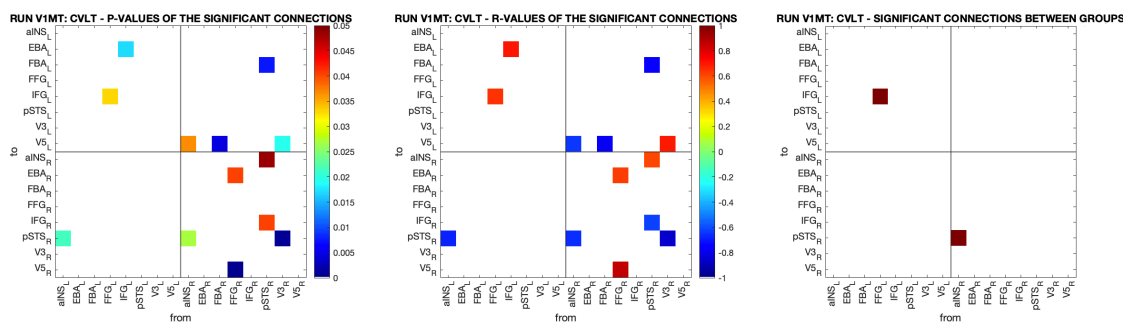
RUN V1MT
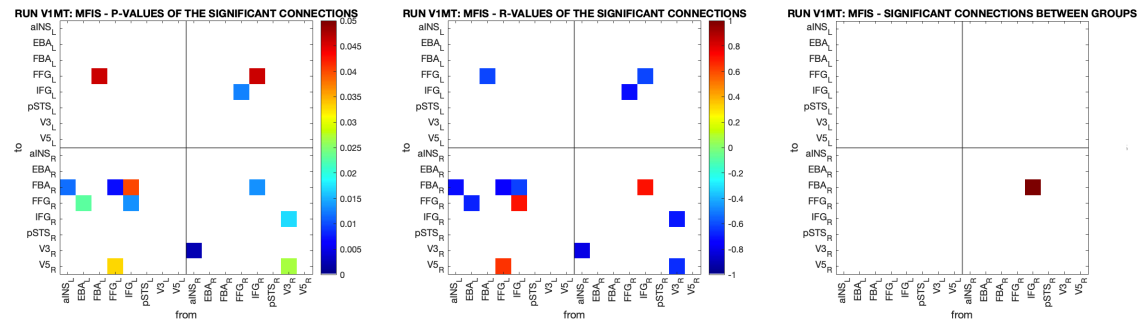
Figure 5.67 - Results of the Spearman correlation for MFIS data, in the V1MT run. (Left) Matrix with the p-values of the significant correlations ($p < 0.05$) between pairwise connectivity and test scores. The colorbar represents p-values. (Middle) Matrix with the r-values of the correlation of F-values and MFIS scores for the connections with significant correlations ($p < 0.05$) (the same as on the matrix on the left). Red/orange/yellow represents a positive correlation, blue represents negative correlations. The colorbar represents the Spearman r-values. (Right) Connections with a significant correlation between F-values and the test score, among those previously found to be significantly different between groups.

There are thirteen connections with significant correlation between the F-values and the results for MFIS, with a predominance for negative correlations. However, it is worth noting that the most robust connections ($p < 0.015$) are $IFG_L \rightarrow FFG_R$ and $IFG_R \rightarrow FBA_R$, which have positive correlations with the MFIS values, followed by $aINS_L \rightarrow FBA_R$, $aINS_R \rightarrow V3_R$, $FFG_L \rightarrow FBA_R$, and $FFG_R \rightarrow IFG_L$, which have negative correlations with the MFIS values.

The only connection significantly different between groups is $IFG_R \rightarrow FBA_R$, with a p-value of 0.0133 and a Spearman r-value of 0.715, having higher F-values in MSC. The scatter plot of F-values of this connection and MFIS scores is represented in figure 5.68.
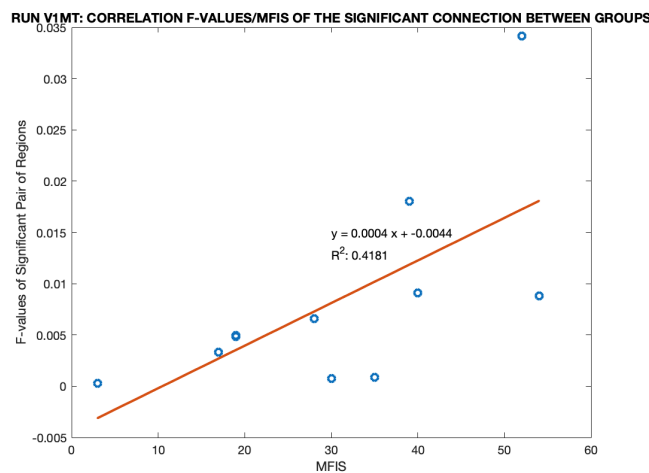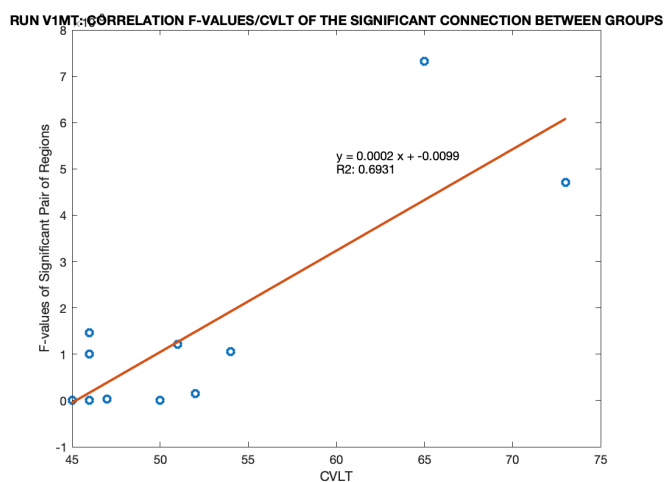

Figure 5.68 - Graphic representation of the correlation between the F-values of the connection $IFG_R \rightarrow FBA_R$ (in the run V1MT) and the MFIS results.

This suggests an intuitive correlation of higher functional connectivity (more brain activity) with more fatigue, probably as a result of higher energetic demands during task performance.

RUNS BM

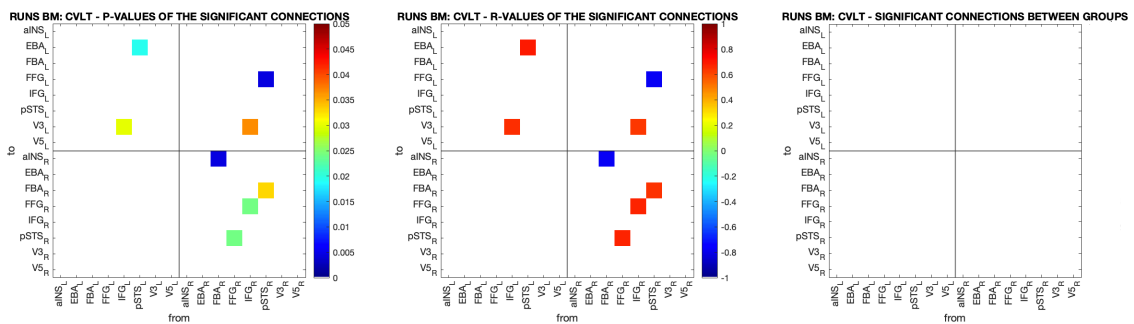

Figure 5.69 – Results of the Spearman correlation for MFIS data, in the BM runs. (Left) Matrix with the p-values of the significant correlations (p < 0.05) between pairwise connectivity and test scores. The colorbar represents p-values. (Middle) Matrix with the r-values of the correlation of F-values and MFIS scores for the connections with significant correlations (p < 0.05) (the same as on the matrix on the left). Red/orange/yellow represents a positive correlation, blue represents negative correlations. The colorbar represents the Spearman r-values. (Right) Connections with a significant correlation between F-values and the test score, among those previously found to be significantly different between groups.

There are eight connections with significant correlation between the F-values and the results for MFIS, with an equal number of positive and negative correlations. The most robust connection is $FBA_R \rightarrow V5_L$, which has a negative correlation with the MFIS results.
None of the connections that have a correlation with the test's scores are significantly different between groups.

Discussion of the MFIS results

The processes that induce fatigue in MS are still poorly understood. It is argued that it is caused by WM structural damage and demyelination that impair the propagation of information flow between regions and consequently disrupt brain function and restrict activities such as motor planning and execution. Neuroplasticity is also pointed to as a possible cause for fatigue since maladaptive compensatory recruitment of additional brain regions during the execution of a task may excessively activate the brain beyond its capacity to properly function (DeLuca *et al.*, 2008) (Manjaly *et al.*, 2019). Because there is no certainty about these mechanisms, this study can be of particular help.

In our study, the insula (particularly $aINS_L$) participates in some connections related to MFIS. Stefancin and colleagues (Stefancin *et al.*, 2019) also reported that a connection between the left insula and posterior cingulate significantly correlated with the MFIS scores, showing reduced connectivity.

FBA_R also has an important role in these results, being the only connection that is significantly different between groups in the run V1MT and the most specific connection in the BM runs. Hence, it could be an informative region when exploring predictors of fatigue in MS patients. This connection with higher levels of connectivity in MS patients in the V1MT run, which also has a positive correlation with the MFIS values (the higher is the FC of the connection, the

higher are the levels of fatigue), could argue in favour of the maladaptive effect that neuroplasticity has on fatigue (DeLuca *et al.*, 2008) (Manjaly *et al.*, 2019).

However, as there are more connections with a negative correlation with the MFIS data, it can also be argued that their lowered FC value contributes to an increase in the MS patients' fatigue. This may be in disagreement with the hypothesis that a higher activation of some brain regions or augmented recruitment of certain (or new) connections, as a compensatory response in MS, contributes to higher levels of fatigue. However, it must be noted that this is a study with cognitively preserved patients in an early stage of the disease that might not experience high levels of fatigue. On the other hand, these negative correlations might as well be a result of an efficient adaptive neuroplasticity phenomenon, i.e., the brain reorganization leads to increased FC, which in turn originates lower levels of fatigue.

Therefore, although these results suggest that connectivity measures during simple visual tasks might be a proxy for fatigue levels, further investigation is needed to completely understand the underlying mechanisms. In the future, this knowledge might guide intervention strategies to prevent cognitive decline and disease progression in MS.

5.9.3 Symbol Digit Modalities Test

The SDMT measures the cognitive processing speed, which is believed to be slowed in MS patients. This test involves writing or orally reporting (in 90 seconds) a 'key' that associates nine symbols with single digits from 1 to 9. It is assumed that the higher the score in SDMT, the less cognitively impaired the MS patient is in this domain (Sousa *et al.*, 2018).
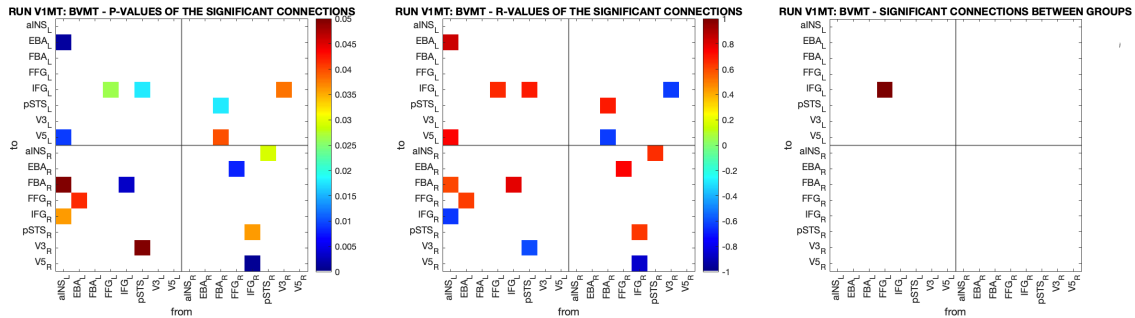
RUN V1MT

Figure 5.70 – Results of the Spearman correlation for SDMT data, in the V1MT run. (Left) Matrix with the p-values of the significant correlations ($p < 0.05$) between pairwise connectivity and test scores. The colorbar represents p-values. (Middle) Matrix with the r-values of the correlation of F-values and SDMT scores for the connections with significant correlations ($p < 0.05$) (the same as on the matrix on the left). Red/orange/yellow represents a positive correlation, blue represents negative correlations. The colorbar represents the Spearman r-values. (Right) Connections with a significant correlation between F-values and the test score, among those previously found to be significantly different between groups.

There are seventeen connections with significant correlation between the F-values and the results for SDMT, with nine negative correlations and eight positive correlations. The most robust connections ($p < 0.015$) are $IFG_L \rightarrow FBA_R$, $FFG_R \rightarrow IFG_L$, which have a positive correlation with the SDMT scores, and $EBA_R \rightarrow IFG_L$, which has a negative correlation with the SDMT values.

None of the connections that have a correlation with the test's results are significantly different between groups.
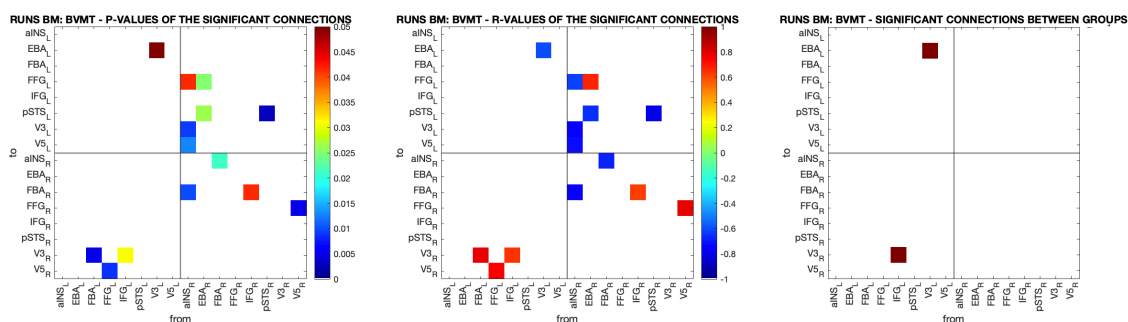
RUNS BM

Figure 5.71 – Results of the Spearman correlation for SDMT data, in the BM runs. (Left) Matrix with the p-values of the significant correlations ($p < 0.05$) between pairwise connectivity and test scores. The colorbar represents p-values. (Middle) Matrix with the r-values of the correlation of F-values and SDMT scores for the connections with significant correlations ($p < 0.05$) (the same as on the matrix on the left). Red/orange/yellow represents a positive correlation, blue represents negative correlations. The colorbar represents the Spearman r-values. (Right) Connections with a significant correlation between F-values and the test score, among those previously found to be significantly different between groups.

There are ten connections with significant correlation between the F-values and the results for SDMT, with a predominance for negative correlations, in the BM runs. The most robust connection is $aINS_R \rightarrow V5_L$, which has a negative correlation with the SDMT scores. None of the connections that have a correlation with the test's results are significantly different between groups.

Discussion of the SDMT results

aINS, IFG, FBA, V5 and V3, seem to be regions (especially IFG and V5) significantly involved in this neuropsychological test. This is expected as IFG and aINS are regions involved in high-level cognitive control, attentional processes, and working memory, thus influencing information processing speed (Tops and Boksem, 2011). In turn, FBA, V5 and V3 have visual perception and processing functions, which are also fundamental in this test.

Like with the MFIS, in the SDMT, there are more connections with a negative correlation with the data in both runs, meaning that higher FC values in these connections are accompanied by lower scores in SDMT. This is in line with the neuroplasticity hypothesis that argues that an increase in FC in the brain may be maladaptive and eventually lead to cognitive impairment and, consequently, to lower scores in information processing speed tests (Rocca and Filippi, 2017). However, we should recall that the recruited MS patients are cognitively preserved. Thus, it is not very likely that the observation of this negative correlation is already a manifestation of this maladaptation. Further investigation is needed to determine if damage in the FC between these significant connections may be an informative factor for monitoring impairment in cognitive functions.

5.9.4 California Verbal Learning Test

CVLT is a test that consists of memorising words (given orally) grouped into different semantic categories, and later reciting as many as possible. It involves auditory and verbal memory, which are also impaired in MS. It is assumed that the higher the score in CVLT, the less cognitively impaired the MS patient is in this domain (Sousa *et al.*, 2018).

RUN V1MT

Figure 5.72 - Results of the Spearman correlation for CVLT data, in the V1MT run. (Left) Matrix with the p-values of the significant correlations ($p < 0.05$) between pairwise connectivity and test scores. The colorbar represents p-values. (Middle) Matrix with the r-values of the correlation of F-values and CVLT scores for the connections with significant correlations ($p < 0.05$) (the same as on the matrix on the left). Red/orange/yellow represents a positive correlation, blue represents negative correlations. The colorbar represents the Spearman r-values. (Right) Connections with a significant correlation between F-values and the test score, among those previously found to be significantly different between groups.

There are thirteen connections with significant correlation between the F-values and the results for CVLT, with seven negative correlations and six positive correlations. The most robust connections ($p < 0.01$) are $FFG_R \rightarrow V5_R$, which has a positive correlation with the CVLT values, $V3_R \rightarrow pSTS_R$, $FBA_R \rightarrow V5_L$ and $pSTS_R \rightarrow FBA_L$, which have a negative correlation with the CVLT scores.

There are two statistically significant connections between groups: $FFG_L \rightarrow IFG_L$, with a p-value of 0.033 and a Spearman r-value of 0.64, having higher values in CNT (figure 5.73), and $aINS_R \rightarrow pSTS_R$, with a p-value of 0.027 and a Spearman r-value of -0.66, with higher values in MSC (figure 5.74).

Figure 5.73 - Graphic representation of the correlation between the F-values of the connection $FFG_L \rightarrow IFG_L$ (in the run V1MT) and the CVLT results.
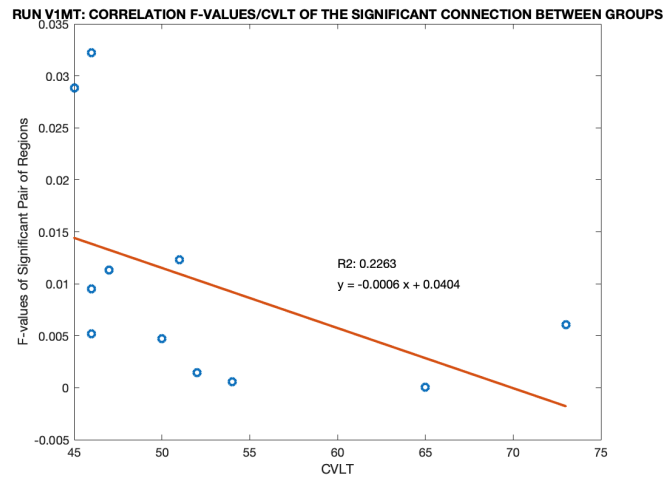
Figure 5.74 - Graphic representation of the correlation between the F-values of the connection aINS$_R$ → pSTS$_R$ (in the run V1MT) and the CVLT results.
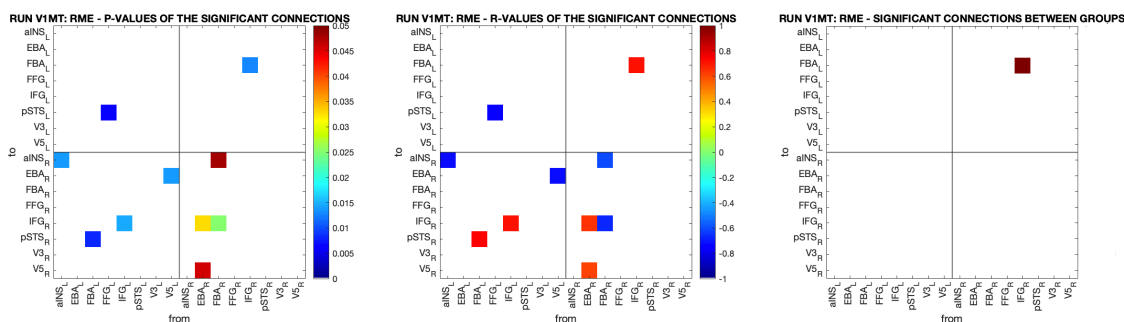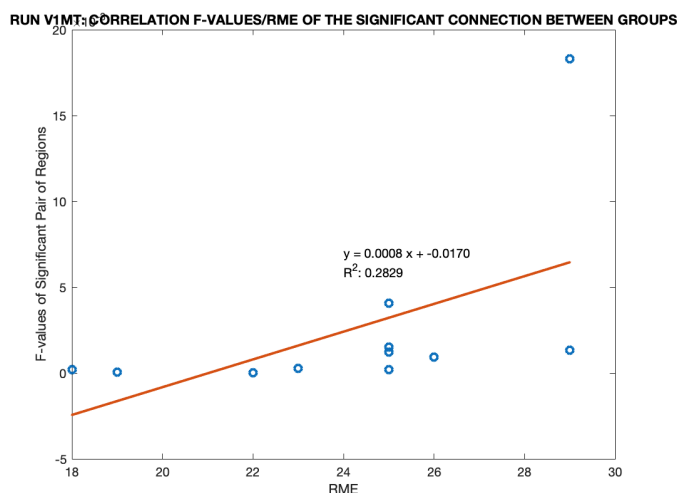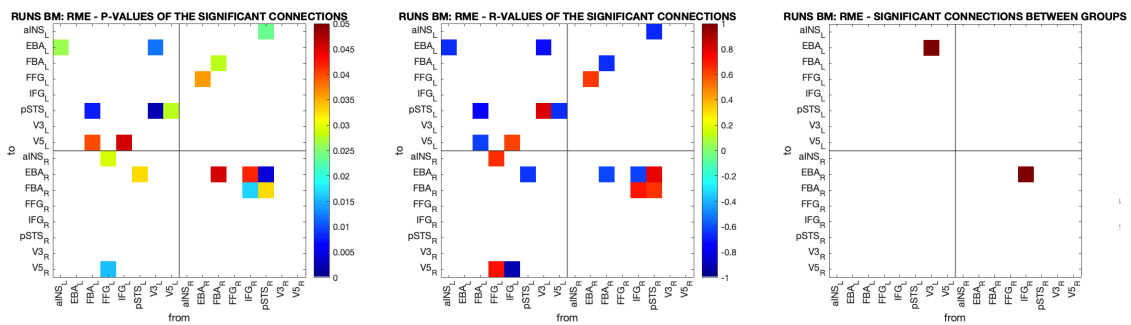
RUNS BM

Figure 5.75 - Results of the Spearman correlation for CVLT data, in the BM runs. (Left) Matrix with the p-values of the significant correlations (p < 0.05) between pairwise connectivity and test scores. The colorbar represents p-values. (Middle) Matrix with the r-values of the correlation of F-values and CVLT scores for the connections with significant correlations (p < 0.05) (the same as on the matrix on the left). Red/orange/yellow represents a positive correlation, blue represents negative correlations. The colorbar represents the Spearman r-values. (Right) Connections with a significant correlation between F-values and the test score, among those previously found to be significantly different between groups.

There are eight connections with significant correlation between the F-values and the results for CVLT, with a predominance for positive correlations. The most robust connections (p < 0.01) are FBA$_R$ → aINS$_R$ and pSTS$_R$ → FFG$_L$, both with negative correlations with the CVLT scores. There are no significantly different connections between groups.

Discussion of the CVLT results

The main regions that are involved in the connections with significant correlation with the CVLT test, in both runs, are aINS, IFG, FFG and especially pSTS. aINS and IFG are high-order regions involved in high-level cognitive control, attentional processes and working memory, and IFG, in particular, is involved in language comprehension and production, which are expected to be activated in this particular test. FFG and pSTS are involved in visual perception. However, the correlation between connections involving pSTS with this test's

110

scores, in the V1MT run, is surprising because this specific task does not include visual biological motion perception.

In run V1MT, the connection $FFG_L \rightarrow IFG_L$ is significantly different between groups, with higher connectivity values in the CNT and a positive correlation with the CVLT scores, i.e, the higher the FC is in this connection in MSC, the higher are the scores in CVLT. Contrarily, the connection $aINS_R \rightarrow pSTS_R$ has higher connectivity values in MSC and a negative correlation with CVLT scores, which means that higher connectivity in this connection leads to lower scores in CVLT.

This divergence of results, one connection leads to better CVLT results, and the other leads to worse results, makes it impossible not to question whether increases in functional connectivity in MS, which are often associated with neuroplasticity, are adaptive and contribute to the patient's recovery, or maladaptive and lead to clinical or cognitive impairment. This is still an open debate in the scientific community, since increases in FC have been related to both improvements and declines in task performance (Rocca and Filippi, 2017) (Schoonheim, 2017). Tahedl and colleagues (Tahedl *et al.*, 2018) discuss that FC changes may actually result from both adaptive and maladaptive processes: there is an adaptive change in the domains and regions that are directly related to the task (in this case $FFG_L \rightarrow IFG_L$), and a maladaptive change when the region/connection does not relate directly to the task ($aINS_R \rightarrow pSTS_R$), which could imply that a higher connectivity in this connection can be harmful to the correct performance of task. This is compatible with these specific regions' functions (for example pSTS is more involved in perception of biological motion than in the performance of auditory/verbal memory and processing tasks).

5.9.5 Brief Visuospatial Memory Test

Brief Visuospatial Memory Test measures visuospatial learning as well as memory abilities. In this test, six figures are shown to the patients, and they have to recreate the design as accurately as possible two times, separated by 25 minutes, with other distractor tasks in between. It is assumed that the higher the score in BVMT, the less cognitively impaired the MS patient is in this domain (Sousa *et al.*, 2018).

RUN V1MT

Figure 5.76 - Results of the Spearman correlation for BVMT data, in the V1MT run. (Left) Matrix with the p-values of the significant correlations (p < 0.05) between pairwise connectivity and test scores. The colorbar represents p-values. (Middle) Matrix with the r-values of the correlation of F-values and BVMT scores for the connections with significant correlations (p < 0.05) (the same as on the matrix on the left). Red/orange/yellow represents a positive correlation, blue represents negative correlations. The colorbar represents the Spearman r-values. (Right) Connections with a significant correlation between F-values and the test score, among those previously found to be significantly different between groups.

There are sixteen connections with significant correlation between the F-values and the results for BVMT, with a predominance for positive correlations. The most robust connections (p < 0.01) are $aINS_L \rightarrow V5_L$, $aINS_L \rightarrow EBA_L$, $IFG_L \rightarrow FBA_R$, $FFG_R \rightarrow EBA_R$, which have positive correlations with the BVMT values, and $IFG_R \rightarrow V5_R$, which has a negative correlation with BVMT scores.

The connection that is statistically significant between groups is $FFG_L \rightarrow IFG_L$, with a p-value of 0.026, and a Spearman r-value of 0.66 (figure 5.77), having higher F-values in CNT.
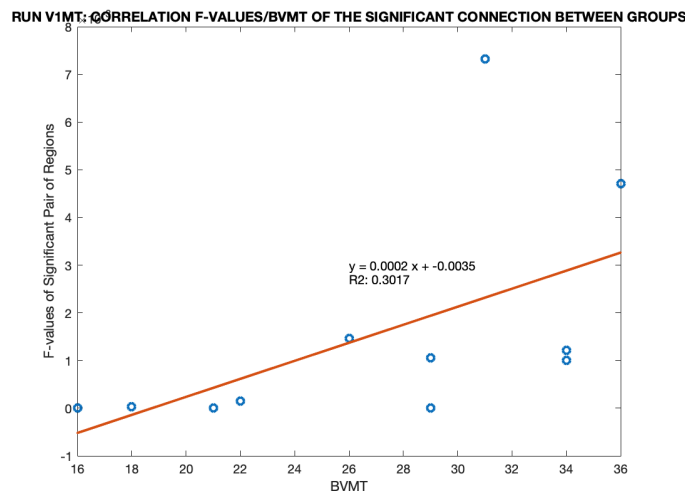
Figure 5.77 - Graphic representation of the correlation between the F-values of the connection $FFG_L \rightarrow IFG_L$ (in the run V1MT) and the BVMT results.

RUNS BM

Figure 5.78 - Results of the Spearman correlation for BVMT data, in the BM runs. (Left) Matrix with the p-values of the significant correlations (p < 0.05) between pairwise connectivity and test scores. The colorbar represents p-values. (Middle) Matrix with the r-values of the correlation of F-values and BVMT scores for the connections with significant correlations (p < 0.05) (the same as on the matrix on the left). Red/orange/yellow represents a positive correlation, blue represents negative correlations. The colorbar represents the Spearman r-values. (Right) Connections with a significant correlation between F-values and the test score, among those previously found to be significantly different between groups.

There are fourteen connections with significant correlation between the F-values and the results for BVMT, with a predominance for negative correlations. The most robust connections (p < 0.01) are $V5_R \rightarrow FFG_R$, $FBA_L \rightarrow V3_R$, $FFG_L \rightarrow V5_R$, which have a positive correlation with the BVMT values, and $aINS_R \rightarrow FBA_R$, $aINS_R \rightarrow V5_L$, $aINS_R \rightarrow V3_L$, $pSTS_R \rightarrow pSTS_L$, which have a negative correlation with the BVMT values.

There are two connections that are significant between groups: $IFG_L \rightarrow V3_R$, with a p-value of 0.031 and a Spearman r-value of 0.65 (figure 5.79) and $V3_L \rightarrow EBA_L$, with a p-value of 0.050 and a Spearman r-value of -0.603 (figure 5.80). Both connections have higher F-values in MSC.
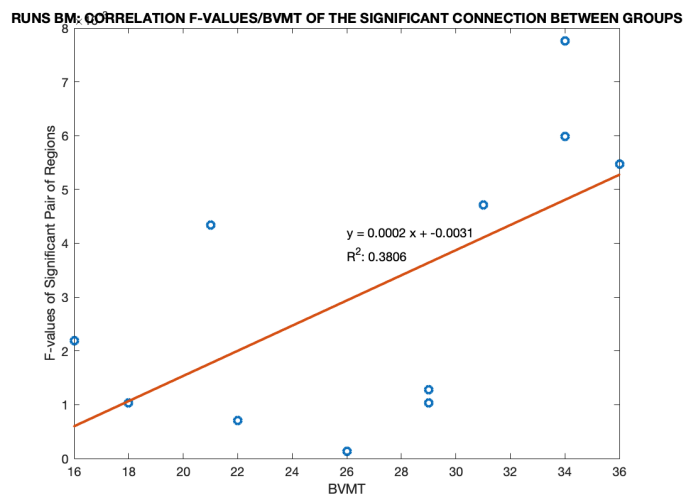
Figure 5.79 - Graphic representation of the correlation between the F-values of the connection $IFG_L \rightarrow V3_R$ (in the runs BM) and the BVMT results.
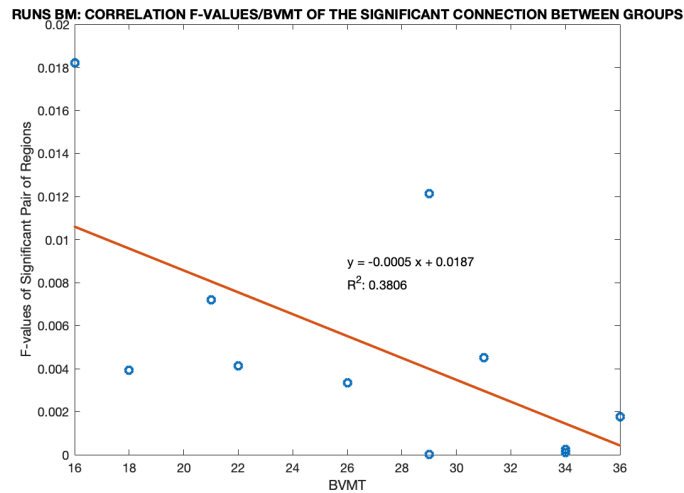
Figure 5.80 - Graphic representation of the correlation between the F-values of the connection $V3_L \rightarrow EBA_L$ (in the runs BM) and the BVMT results.

Discussion of the BVMT results

aINS, IFG, pSTS and FBA are the regions involved in the visual tasks (performed during fMRI measurement) which are more correlated with the performance of the BVMT test. While aINS is the region sending more connections, IFG is the region receiving more connections. It makes sense that connections involving these regions are correlated with this test, as these are high-order ROIs that engage in many cognitive processes, namely attention and memory, which are required to complete this test. In turn, pSTS and FBA are linked to visual functions which are also necessary, although they are usually more related with biological motion perception.

In the V1MT localiser run, a connection involving IFG ($FFG_L \rightarrow IFG_L$) is different between groups, having higher values of functional connectivity in controls and a positive correlation with the BVMT data in MS patients, i.e, a higher connectivity in this connection in MSC leads to a higher score in BVMT and thus to a preservation of the cognitive functions in this domain.

In the BM runs, $IFG_L \rightarrow V3_R$ and $V3_L \rightarrow EBA_L$ are also discriminative connections between groups, both having higher FC values in MSC. But while $IFG_L \rightarrow V3_R$ has a positive correlation with the data (higher values of connectivity lead to higher BVMT scores), $V3_L \rightarrow EBA_L$ has a negative correlation (higher values of connectivity lead to lower BVMT scores). These connections may be another proof of the existence of both adaptive and maladaptive neuroplasticity in MS, as seen before with the CVLT results. In the case of the BVMT, $IFG_L \rightarrow V3_R$ increase in FC could be adaptive, as it leads to a better performance, and $V3_L \rightarrow EBA_L$ could be maladaptive, leading to a worse performance. In fact, IFG and V3 are regions associated with functions that are recruited in this test, and for that reason they need a higher FC to maintain function, while EBA might not be as related since its functions are mainly associated with body movement perception.

These connections in the two runs may be good candidates to further explore neuroplasticity, namely, to confirm that changes in connectivity can affect brain communication and information processing already in early stages of MS.

5.9.6 Reading the Mind with the Eyes

RME is a neuropsychological test that evaluates subtle cognitive dysfunction, in the domain of social cognition. The patient must choose two words that describe the mental state and feelings of 25 photographs of the eye-region of different people. It is assumed that the higher the score in RME, the less cognitively impaired the MS patient is in this domain (Baron-Cohen et al., 2001).

RUN V1MT

Figure 5.81 - Results of the Spearman correlation for RME data, in the V1MT run. (Left) Matrix with the p-values of the significant correlations ($p < 0.05$) between pairwise connectivity and test scores. The colorbar represents p-values. (Middle) Matrix with the r-values of the correlation of F-values and RME scores for the connections with significant correlations ($p < 0.05$) (the same as on the matrix on the left). Red/orange/yellow represents a positive correlation, blue represents negative correlations. The colorbar represents the Spearman r-values. (Right) Connections with a significant correlation between F-values and the test score, among those previously found to be significantly different between groups.

There are ten connections with significant correlation between the F-values and the results for RME, with the same number of positive and negative correlations. The most robust connections ($p < 0.01$) are $IFG_R \rightarrow FBA_L$, $FBA_L \rightarrow pSTS_R$ and $IFG_L \rightarrow IFG_R$, which have a positive correlation with RME scores, and $aINS_L \rightarrow aINS_R$, $FFG_L \rightarrow pSTS_L$, $V5_L \rightarrow EBA_R$, which have a negative correlation with RME results.

The only connection that is statistically significant between groups is $IFG_R \rightarrow FBA_L$, with a p-value of 0.013 and a Spearman r-value of 0.72 (figure 5.82), having higher F-values in CNT.

Figure 5.82 - Graphic representation of the correlation between the F-values of the connection $IFG_R \rightarrow FBA_L$ (in the run V1MT) and the RME results.

RUNS BM

Figure 5.83 - Results of the Spearman correlation for RME data, in the BM runs. (Left) Matrix with the p-values of the significant correlations (p < 0.05) between pairwise connectivity and test scores. The colorbar represents p-values. (Middle) Matrix with the r-values of the correlation of F-values and RME scores for the connections with significant correlations (p < 0.05) (the same as on the matrix on the left). Red/orange/yellow represents a positive correlation, blue represents negative correlations. The colorbar represents the Spearman r-values. (Right) Connections with a significant correlation between F-values and the test score, among those previously found to be significantly different between groups.

There are eighteen connections with significant correlation between the F-values and the results for RME, with a predominance for negative correlations. The most robust connections (p < 0.01) are $V3_L \rightarrow EBA_L$, $pSTS_R \rightarrow EBA_R$, which have a positive correlation with RME scores, and $FBA_L \rightarrow pSTS_L$ and $V3_L \rightarrow pSTS_L$, which have a negative correlation with RME results.

There are two connections that are significant between groups: $V3_L \rightarrow EBA_L$, with a p-value of 0.012 and a Spearman r-value of -0.72 (figure 5.84), and $IFG_R \rightarrow EBA_R$, with a p-value of 0.042 and a Spearman r-value of -0.62 (figure 5.85). Both have higher F-values in MSC.
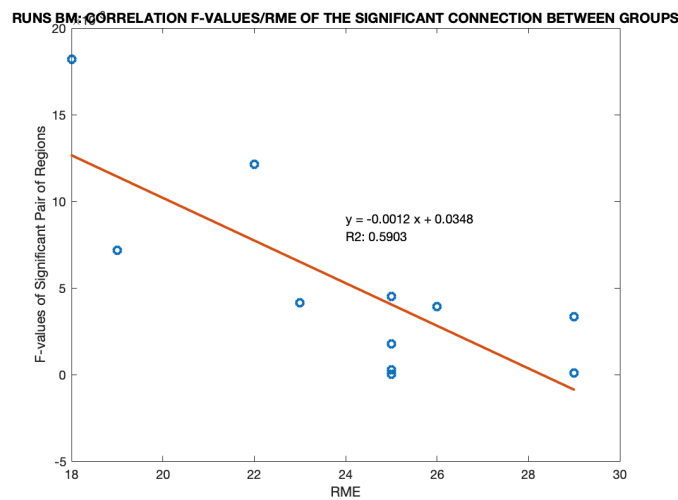
Figure 5.84 - Graphic representation of the correlation between the F-values of the connection $V3_L \rightarrow EBA_L$ (in the runs BM) and the RME results.
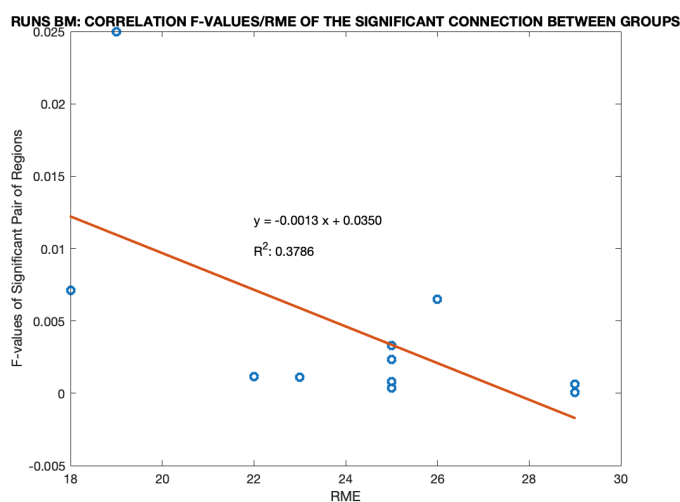
Figure 5.85 - Graphic representation of the correlation between the F-values of the connection IFG$_R$ → EBA$_R$ (in the runs BM) and the RME results.

Discussion of the RME results

It is surprising that there are so many significant connections with correlations with RME scores, because this test better evaluates patients with a higher and more severe degree of cognitive disability that already involves and impairs social perception. Because the patients that participate in this study are cognitively preserved, these results are unexpected.

IFG, EBA, FBA and pSTS are, expectably, the regions that are more involved in the tasks performed in the MR scanner and also recruited with the performance of this test. IFG is also involved in some statistically different between-group connections, thus potentially serving as a region predictive of the RME test score. FBA and EBA are part of the network subserving visual perception of the human body and its parts. pSTS is also involved in many connections with significant correlation with RME scores (it appears as sender and receiver in three connections in the BM runs), which might be expected since it is associated with social perception and cognition, including perception of faces. On the other hand, aINS's presence, however, is not as noticeable, which is surprising given its importance in emotional processing and social perception.

Regarding the connections that are significantly different between groups, in run V1MT, IFG$_R$ → FBA$_L$ has a positive correlation with the RME data and has higher FC values in the controls' group. The significant connection in run V1MT suggests that an increase in connectivity in these regions may lead to a preservation of social cognition and perception of faces and mental states, providing further support for the compensatory mechanism in MS.

In the BM runs, IFG$_R$ → EBA$_R$ and V3$_L$ → EBA$_L$ have a negative correlation with the RME data and higher FC values in the MS patients' group. An increase in FC in these connections can lead to worse results and might be indicative of the development of social cognitive impairment. This could also be a proof of maladaptive neuroplasticity, where a higher FC can lead to worse cognitive performance.

5.9.7 General Discussion of the Correlation Between Connectivity and Neuropsychology

When analysing the correlation of functional connectivity values with the scores of clinical and neuropsychological tests, we must bear in mind that not only different tests provide information about different domains, but also that the test's outcomes might be in two directions: the higher scores, the better, or the other way around.

Thus, determining if positive or negative correlations are supportive of adaptive or maladaptive neuroplasticity depends on the output of each specific test being "the higher the score, the better" or "the lower the score, the better". As an example, a positive correlation of functional connectivity with MFIS (the higher the score, the worse are the levels of fatigue) probably reflects a maladaptive compensatory phenomenon that leads to worse symptoms. Particularly if MS patients show increased connectivity relative to healthy controls, this positive correlation means that abnormally higher connectivity results in undesired higher levels of fatigue. Conversely, a positive correlation of connectivity with (e.g.) the BVMT, in which the higher the score, the more cognitively preserved the patient is in the domain, probably reflects an efficient and adaptive compensation effect (the higher the connectivity the higher the score in the test, which is the desired output).
We observed cases of tests for which there is a divergence in the results (increased connectivity in one connection correlates with better test results, whereas increased connectivity in another correlates with worse test results). This could support the idea that neuroplasticity can be adaptive and contribute to the patient's recovery, or maladaptive and lead to clinical or cognitive impairment. Tahedl and colleagues (Tahedl *et al.*, 2018) further argue that FC changes may actually result from both adaptive and maladaptive processes and that they may be related to the specific recruited connections/regions in the task.

Either way, in the future we should look in detail at every significant correlation to evaluate if increasing/decreasing FC is associated with higher or lower scores in each test, and then better assess the relationship between both, regarding an underlying efficient or maladaptive compensatory mechanism. Furthermore, we must have caution when interpreting these correlations, because we do not have support of causality between altered FC and neuropsychological scores.

It is also worth noting that this is a study with patients who are clinically and cognitively preserved, in an early stage of the disease. It is not unlikely that correlations of connectivity with neuropsychological tests that are significant might change during the progression of the disease, either because the connectivity patterns change or because the neuropsychological characterization changes. Therefore, although these results suggest that connectivity measures during simple visual tasks might be a proxy for clinical and neuropsychological assessment, further investigation is needed to completely understand the underlying mechanisms and to determine its ability to track disease progression and guide intervention strategies to prevent cognitive decline and disease progression in MS.

6
Conclusion

Neuroplasticity has been the focus of many investigations in the context of MS. It reflects the brain's ability to reorganize and adapt to structural damage and there are several theories about it being adaptive, and contributing to a better physical and cognitive performance, or maladaptive, leading to a worse condition (Rocca and Filippi, 2017) (Schoonheim, 2017) (Tahedl *et al.*, 2018). Nevertheless, a consensus has never been reached about the existence of functional plasticity in MS. Therefore, a holistic model encompassing both the analysis of the brain's connectivity and the extraction of quantitative measures that describe the brain's functioning in MS was needed. The ability of fMRI to provide non-invasive measures of brain function and the development of methods to compute connectivity measures bring encouraging opportunities. However, these approaches, especially graph-based studies in MS are currently scarce, and most of them use resting-state fMRI, which doesn't consider the connections the brain elicits when performing a task. Moreover, the few that used task-based designs did not aim for visual networks like the one we used.

The main purpose of this thesis was to obtain models that could describe and compare the (directed) functional connectivity between early multiple sclerosis patients and healthy controls and to construct brain networks that reflected patterns of connectivity underlying brain activation during two types of visual task performance, one more complex than the other. We adopted an exploratory approach for network construction with Granger Causality and graph theory and performed analyses on a restricted number of brain regions specifically involved in the tasks, in order to improve the power in the detection of significant effects.

The main a priori hypotheses were that (i) the connectivity (represented by the F-values) increases in the MS patient's group, as a result of compensatory neuroplasticity, which has been described in studies using fMRI (ii) the neuronal connection patterns differed between groups and unique connections in the MS group were revealed, another reflection of adaptive changes, and (iii) that the quantitative measures of connectivity obtained with graph theory, global and local, were altered in the MS patient's group, with a tendency for the decrease in network efficiency.

Through the analysis of between-group differences in pairwise connectivity strengths and of graph-theoretical topological properties derived from the functional networks, we were able to prove that there are indeed connections which can differentiate CNT from MSC and that these connections could be a demonstration of the brain's neuroplasticity in the early phases of MS. This is observed in the two visual tasks (V1MT localiser and BM), which could indicate that this mechanism exists independently of the complexity of the performed task, although different brain regions with different functions are recruited in each task. A different brain lateralisation was also observed, supported by the increased connectivity in the connections in which the right hemisphere (non-dominant) is involved.

However, the efficiency in the MS networks was elevated which contradicts previous research that argues that even in the early stages of MS the integrity and efficiency of the networks is impaired. These results could be due to differences in methodology, for example, number of participants or differences in the size of the network. Moreover, we observed that the involvement of certain nodes in the network was changed in MS, as proven by differences in local connectivity metrics. Overall, a general assumption that can be made is that MS is a disconnection disease that affects the communication of the brain regions and leads to changes, and sometimes impairments, in functional connectivity.

We also studied the correlation between the functional connectivity values of the MS patients and the results derived from neuropsychological tests. The main conclusions were that different connections were involved in different tests since distinct cognitive domains are involved and recruited. These results also supported the possibility that functional neuroplasticity can be both adaptive and maladaptive and that these phenomena may depend on which connections are recruited in the task that is performed.

We successfully constructed a functional connectivity model that is able to identify differences in the network topological organization between MS patients and controls and allows for the detection of compensatory effects in early phases of the disease. This altered functional connectivity and over-recruitment of cortical areas are among the features of early MS and it is possible they may constitute exploitable candidate biomarkers of developing MS. Besides, the development of metrics capable of providing measures of brain's neuroplasticity might be used to guide the creation of new methods to monitor MS progression and to possibly identify new options of treatment. With this study, we also obtained discriminative quantitative features and regions that could help improve the understanding of deficits in early stages of brain disorders and improve the diagnosis and early treatment of MS patients.

Limitations and Future Work

This study is not without limitations. Firstly, the number of participants is relatively small, which could give rise to some inaccurate results and interpretations, eventually due to lack of statistical power. The recruitment of new participants is therefore advised for validation of the results. The application of Granger Causality in neuroscience (and particularly in fMRI studies) remains a controversial topic, due to the limitations it imposes on the data, such as linearity which is hardly verified in the human brain. The approximation to transfer entropy to characterize information flow also has to be carefully interpreted, under the assumption that the data and the time courses of the regions extracted from the BOLD signal are normal. However, because we only adopted this study as an exploratory approach that needs more methods and data in order to be validated, we employed a less conservative consideration of these assumptions and adopted the principles used by the MVGC toolbox, which is reliably implemented and used by many other researchers. Moreover, the existent studies generally adopt whole brain networks and rs-fMRI acquisition, which is very different from what we did. To the best of our knowledge, our approach has never been adopted before, especially the use of these specific functional brain regions in visual tasks, thus the results are not validated through other studies. Future research may be helpful in testing the reliability of our findings. Regarding the neuropsychological tests' results and their correlation with the F-values of connectivity, the interpretation needs to be careful as well. The interpretation was based on each region's known primary functions, which are believed to be recruited (at least in part) during the performance of the tests, but we did not measure their activity or connectivity actually during the tests. Furthermore, our results in a non-cognitively impaired population may be less comparable to existing literature, since most studies analyse more severe cognitive impairment in more advanced phases of MS (Welton et al., 2020). It is also important to consider that the obtained functional connectivity patterns are largely shaped by structural pathways, as argued by previous research (Y. Liu et al., 2017). Therefore, functional compensation needs to be validated with a decline of the brain's integrity and with changes in cognitive performance. Further in-depth investigations, perhaps involving structural connectivity and the association of structural damages with functional connectivity

are warranted. Finally, our study is cross sectional and although we were able to provide strong evidence of compensatory brain responses, we didn't demonstrate how functional brain networks reorganize as they dynamically change with MS progression (Y. Liu et al., 2017). Future longitudinal studies are thus needed as well.

References

Abidin, A. Z. *et al.* (2017) 'Using large-scale Granger causality to study changes in brain network properties in the Clinically Isolated Syndrome (CIS) stage of multiple sclerosis', *Medical Imaging 2017: Biomedical Applications in Molecular, Structural, and Functional Imaging*, 10137, p. 101371B. doi: 10.1117/12.2254395.

Agcaoglu, O., Miller, R., Mayer, A.R., Hugdahl, K. and Calhoun, V.D. (2018). Corrigendum to "Lateralization of resting state networks and relationship to age and gender" [NeuroImage 104 (2015) 310–325]. *NeuroImage*, 167, p.504.

Amoruso, L., Couto, B. and Ibáñez, A. (2011) 'Beyond extrastriate body area (EBA) and fusiform body area (FBA): Context integration in the meaning of actions', *Frontiers in Human Neuroscience*, 5(November), pp. 1–3. doi: 10.3389/fnhum.2011.00124.

Arco, J. E. *et al.* (2018) 'Influence of activation pattern estimates and statistical significance tests in fMRI decoding analysis', *Journal of Neuroscience Methods*, 308(2013), pp. 248–260. doi: 10.1016/j.jneumeth.2018.06.017.

Aspell, J. E., Tanskanen, T. and Hurlbert, A. C. (2005) 'Neuromagnetic correlates of visual motion coherence', *European Journal of Neuroscience*, 22(11), pp. 2937–2945. doi: 10.1111/j.1460-9568.2005.04473.x.

Audoin, B. *et al.* (2003) 'Compensatory cortical activation observed by fMRI during a cognitive task at the earliest stage of MS', *Human Brain Mapping*, 20(2), pp. 51–58. doi: 10.1002/hbm.10128.

Azarmi, F. *et al.* (2019) 'Granger causality analysis in combination with directed network measures for classification of MS patients and healthy controls using task-related fMRI', *Computers in Biology and Medicine*. Elsevier Ltd, 115, p. 103495. doi: 10.1016/j.compbiomed.2019.103495.

Barnett, L. and Seth, A. K. (2014) 'The MVGC multivariate Granger causality toolbox: A new approach to Granger-causal inference', *Journal of Neuroscience Methods*, 223, pp. 50–68. doi: 10.1016/j.jneumeth.2013.10.018.

Baron-Cohen, S., Wheelwright, S., Hill, J., Raste, Y. and Plumb, I. (2001). The "Reading the Mind in the Eyes" Test Revised Version: A Study with Normal Adults, and Adults with Asperger Syndrome or High-functioning Autism. *Journal of Child Psychology and Psychiatry*, 42(2), pp.241–251.

Basile, B. *et al.* (2014) 'Functional connectivity changes within specific networks parallel the clinical evolution of multiple sclerosis', *Multiple Sclerosis Journal*, 20(8), pp. 1050–1057. doi: 10.1177/1352458513515082.

Beauchamp, M.S. (2015). The social mysteries of the superior temporal sulcus. *Trends in Cognitive Sciences*, 19(9), pp.489–490.

Behfar, Q. *et al.* (2020) 'Graph theory analysis reveals resting-state compensatory mechanisms in healthy aging and prodromal Alzheimer's disease', *Frontiers in Aging Neuroscience*, 12(October), pp. 1–13. doi: 10.3389/fnagi.2020.576627.

Benedict, R.H., DeLuca, J., W. Foley, F., Langdon, D., W. Motl, R., Rocca, M.A. and Till, C. (2016). *AIMS ADVANCES IN MULTIPLE SCLEROSIS - Cognitive Issues in Multiple Sclerosis.* [online] Available at: https://www.cmeaims.org/resources/AIMS-cognitive-primer.pdf.

Born, R. T. and Bradley, D. C. (2005) 'Structure and function of visual area MT', *Annual Review of Neuroscience*, 28, pp. 157–189. doi: 10.1146/annurev.neuro.26.041002.131052.

Brooks, J. C. W. *et al.* (2013) 'Physiological noise in brainstem fMRI', *Frontiers in Human Neuroscience*, c(OCT), pp. 1–13. doi: 10.3389/fnhum.2013.00623.

Bullmore, E. and Sporns, O. (2009) 'Complex brain networks: Graph theoretical analysis of structural and functional systems', *Nature Reviews Neuroscience*, 10(3), pp. 186–198. doi: 10.1038/nrn2575.

Cardin, V., Friston, K. J. and Zeki, S. (2011) 'Top-down modulations in the visual form pathway revealed with dynamic causal modeling', *Cerebral Cortex*, 21(3), pp. 550–562. doi: 10.1093/cercor/bhq122.

Castelo-Branco, M., Formisano, E., Backes, W., Zanella, F., Neuenschwander, S., Singer, W. and Goebel, R. (2002). Activity patterns in human motion-sensitive areas depend on the interpretation of global motion. *Proceedings of the National Academy of Sciences*, 99(21), pp.13914–13919.

Chang, D. H. F. *et al.* (2018) 'Cortical and subcortical responses to biological motion', *NeuroImage*. Elsevier Ltd, 174(October 2017), pp. 87–96. doi: 10.1016/j.neuroimage.2018.03.013.

Chen, J. E. and Glover, G. H. (2015) 'Functional Magnetic Resonance Imaging Methods', *Neuropsychology Review*, 25(3), pp. 289–313. doi: 10.1007/s11065-015-9294-9.

Colquhoun, D. (2014) 'An investigation of the false discovery rate and the misinterpretation of p-values', *Royal Society Open Science*, 1(3). doi: 10.1098/rsos.140216.

DeLuca, J. *et al.* (2008) 'Neural correlates of cognitive fatigue in multiple sclerosis using functional MRI', *Journal of the Neurological Sciences*, 270(1–2), pp. 28–39. doi: 10.1016/j.jns.2008.01.018.

Deshpande, G. and Hu, X. (2012) 'Investigating Effective Brain Connectivity from fMRI Data: Past Findings and Current Issues with Reference to Granger Causality Analysis', *Brain Connectivity*, 2(5), pp. 235–245. doi: 10.1089/brain.2012.0091.

Di, X. *et al.* (2013) 'Task vs. rest-different network configurations between the coactivation and the resting-state brain networks', *Frontiers in Human Neuroscience*, 7(SEP), pp. 1–9. doi: 10.3389/fnhum.2013.00493.

Dobson, R. and Giovannoni, G. (2019) 'Multiple sclerosis – a review', *European Journal of Neurology*, 26(1), pp. 27–40. doi: 10.1111/ene.13819.

Doshi, A. and Chataway, J. (2017) 'Multiple sclerosis, a treatable disease', *Clinical Medicine, Journal of the Royal College of Physicians of London*, 17(6), pp. 530–536. doi: 10.7861/clinmedicine.17-6-530.

Droby, A. *et al.* (2016) 'Changes in brain functional connectivity patterns are driven by an individual lesion in MS: a resting-state fMRI study', *Brain Imaging and Behavior*, 10(4), pp. 1117–1126. doi: 10.1007/s11682-015-9476-3.

Du, X. F. *et al.* (2019) 'Relapsing-Remitting Multiple Sclerosis Is Associated With Regional Brain Activity Deficits in Motor- and Cognitive-Related Brain Areas', *Frontiers in Neurology*, 10(November). doi: 10.3389/fneur.2019.01136.

Duarte, J. V. (2016) 'The role of long-range neural oscillatory synchrony as a mechanism underlying in perceptual coherence'. Available at: http://hdl.handle.net/10316/31083.

Duarte, J. V. *et al.* (2017) 'Pivotal role of hMT+ in long-range disambiguation of interhemispheric bistable surface motion', *Human Brain Mapping*, 38(10), pp. 4882–4897. doi: 10.1002/hbm.23701.

Faivre, A. *et al.* (2012) 'Assessing brain connectivity at rest is clinically relevant in early multiple sclerosis', *Multiple Sclerosis Journal*, 18(9), pp. 1251–1258. doi: 10.1177/1352458511435930.

Faivre, A. *et al.* (2016) 'Depletion of brain functional connectivity enhancement leads to disability progression in multiple sclerosis: A longitudinal resting-state fMRI study', *Multiple Sclerosis*, 22(13), pp. 1695–1708. doi: 10.1177/1352458516628657.

Farahani, F. V., Karwowski, W. and Lighthall, N. R. (2019) 'Application of graph theory for identifying connectivity patterns in human brain networks: A systematic review', *Frontiers in Neuroscience*, 13(JUN), pp. 1–27. doi: 10.3389/fnins.2019.00585.

Filippi, M. *et al.* (1995) 'Does hemispheric dominance influence brain lesion distribution in multiple sclerosis?', *Journal of Neurology Neurosurgery and Psychiatry*, 58(6), pp. 748–749. doi: 10.1136/jnnp.58.6.748.

Filippi, M. and Rocca, M. A. (2009) 'Functional MR Imaging in Multiple Sclerosis', *Neuroimaging Clinics of North America*. Elsevier Ltd, 19(1), pp. 59–70. doi: 10.1016/j.nic.2008.08.004.

Filippi, M. and Rocca, M. A. (2011) 'MR imaging of multiple sclerosis', *Radiology*, 259(3), pp. 659–681. doi: 10.1148/radiol.11101362.

Filippi, M. and Rocca, M. A. (2013) 'Present and future of fMRI in multiple sclerosis', *Expert Review of Neurotherapeutics*, 13(12 SUPPL.), pp. 27–31. doi: 10.1586/14737175.2013.865871.

Fisk, J.D., Pontefract, A., Ritvo, P.G., Archibald, C.J. and Murray, T.J. (1994). The Impact of Fatigue on Patients with Multiple Sclerosis. *Canadian Journal of Neurological Sciences / Journal Canadien des Sciences Neurologiques*, 21(1), pp.9–14.

Fleischer, V. *et al.* (2019) 'Graph Theoretical Framework of Brain Networks in Multiple Sclerosis: A Review of Concepts', *Neuroscience*, 403, pp. 35–53. doi: 10.1016/j.neuroscience.2017.10.033.

Fogelson, N. *et al.* (2014) 'The functional anatomy of schizophrenia: A dynamic causal modeling study of predictive coding', *Schizophrenia Research*. The Authors, 158(1–3), pp. 204–212. doi: 10.1016/j.schres.2014.06.011.

Ford, J. H. and Kensinger, E. A. (2014) 'The relation between structural and functional connectivity depends on age and on task goals', *Frontiers in Human Neuroscience*, 8(MAY), pp. 1–12. doi: 10.3389/fnhum.2014.00307.

Fornito, A., Zalesky, A., Bullmore, E.T. and Elsevier (Amsterdam (2016). *Fundamentals of brain network analysis*. Amsterdam Etc.: Elsevier, Cop.

Freitag, C. M. *et al.* (2008) 'Perception of biological motion in autism spectrum disorders', *Neuropsychologia*, 46(5), pp. 1480–1494. doi: 10.1016/j.neuropsychologia.2007.12.025.

Friston, K. J. (2011) 'Functional and Effective Connectivity: A Review', *Brain Connectivity*, 1(1), pp. 13–36. doi: 10.1089/brain.2011.0008.

Friston, K., Moran, R. and Seth, A. K. (2013) 'Analysing connectivity with Granger causality and dynamic causal modelling', *Current Opinion in Neurobiology*. Elsevier Ltd, 23(2), pp. 172–178. doi: 10.1016/j.conb.2012.11.010.

Geweke, J. (1982) 'Measurement of linear dependence and feedback between multiple time series', *Journal of the American Statistical Association*, 77(378), pp. 304–313. doi: 10.1080/01621459.1982.10477803.

Gomes, L. dos R. (2011) 'Validação da versão portuguesa da escala de impacto da fadiga modificada e da escala de severidade da fadiga na esclerose múltipla', *Universidade do Minho*, pp. 1–38. Available at: http://repositorium.sdum.uminho.pt/handle/1822/17841.

Goldenberg, M. M. (2012). Multiple sclerosis review. Pharmacy and Therapeutics, 37(3), 175.

Grafman, J. (2000) 'Conceptualizing functional neuroplasticity', *Journal of Communication Disorders*, 33(4), pp. 345–356. doi: 10.1016/S0021-9924(00)00030-7.

Granger, C. W. J. (1969). Investigating Causal Relations by Econometric Models and Cross-Spectral Methods. Econometrica, 37, 424-438.

Grossman, E. D., Blake, R. and Kim, C. Y. (2004) 'Learning to see biological motion: Brain activity parallels behavior', *Journal of Cognitive Neuroscience*, 16(9), pp. 1669–1679. doi: 10.1162/0898929042568569.

Grossman, E., Donnelly, M., Price, R., Pickens, D., Morgan, V., Neighbor, G. and Blake, R. (2000). Brain Areas Involved in Perception of Biological Motion. *Journal of Cognitive Neuroscience*, 12(5), pp.711–720.

Hallquist, M.N. and Hillary, F.G. (2019). Graph theory approaches to functional network organization in brain disorders: A critique for a brave new small-world. *Network Neuroscience*, 3(1), pp.1–26.

Hillman, E.M.C. (2014). Coupling Mechanism and Significance of the BOLD Signal: A Status Report. *Annual Review of Neuroscience*, 37(1), pp.161–181.

Huk, A. C. and Heeger, D. J. (2002) 'Pattern-motion responses in human visual cortex', *Nature Neuroscience*, 5(1), pp. 72–75. doi: 10.1038/nn774.

Ishkhanyan, B. *et al.* (2020) 'Anterior and Posterior Left Inferior Frontal Gyrus Contribute to the Implementation of Grammatical Determiners During Language Production', *Frontiers in Psychology*, 11(April), pp. 1–13. doi: 10.3389/fpsyg.2020.00685.

Jastorff, J. and Orban, G. A. (2009) 'Human functional magnetic resonance imaging reveals separation and integration of shape and motion cues in biological motion processing', *Journal of Neuroscience*, 29(22), pp. 7315–7329. doi: 10.1523/JNEUROSCI.4870-08.2009.

Jezzard, P. (2012) 'Correction of geometric distortion in fMRI data', *NeuroImage*. Elsevier Inc., 62(2), pp. 648–651. doi: 10.1016/j.neuroimage.2011.09.010.

JF, K. (1983) 'Rating neurologic impairment in multiple sclerosis: an expanded disability status scale (EDSS).', *Neurology.*, Nov;33(11), pp. 1444–52.

Joseph, J.E., Swearingen, J.E., Clark, J.D., Benca, C.E., Collins, H.R., Corbly, C.R., Gathers, A.D. and Bhatt, R.S. (2012). The changing landscape of functional brain networks for face processing in typical development. *NeuroImage*, 63(3), pp.1223–1236.

Kaiser, M. (2011) 'A tutorial in connectome analysis: Topological and spatial features of brain networks', *NeuroImage*. Elsevier Inc., 57(3), pp. 892–907. doi: 10.1016/j.neuroimage.2011.05.025.

Kale, N. (2016) 'Optic neuritis as an early sign of multiple sclerosis', *Eye and Brain*, 8, pp. 195–202. doi: 10.2147/EB.S54131.

Kashou, N. (2014) 'A Practical Guide to an fMRI Experiment', *Advanced Brain Neuroimaging Topics in Health and Disease - Methods and Applications*, pp. 3–28. doi: 10.5772/58260.

Kasper, L. *et al.* (2017) 'The PhysIO Toolbox for Modeling Physiological Noise in fMRI Data', *Journal of Neuroscience Methods*. Elsevier B.V., 276, pp. 56–72. doi: 10.1016/j.jneumeth.2016.10.019.

Khazaee, A., Ebrahimzadeh, A. and Babajani-Feremi, A. (2017) 'Classification of patients with MCI and AD from healthy controls using directed graph measures of resting-state fMRI', *Behavioural Brain Research*, 322, pp. 339–350. doi: 10.1016/j.bbr.2016.06.043.

Koyama, T. *et al.* (2005) 'The subjective experience of pain: Where expectations become reality', *Proceedings of the National Academy of Sciences of the United States of America*, 102(36), pp. 12950–12955. doi: 10.1073/pnas.0408576102.

Langdon, D., Amato, M., Boringa, J., Brochet, B., Foley, F., Fredrikson, S., Hämäläinen, P., Hartung, H-P., Krupp, L., Penner, I., Reder, A. and Benedict, R. (2011). Recommendations for a Brief International Cognitive Assessment for Multiple Sclerosis (BICAMS). *Multiple Sclerosis Journal*, 18(6), pp.891–898.

Leavitt, V.M., Wylie, G., Genova, H.M., Chiaravalloti, N.D. and DeLuca, J. (2011). Altered effective connectivity during performance of an information processing speed task in multiple sclerosis. *Multiple Sclerosis Journal*, 18(4), pp.409–417.

Liu, J. *et al.* (2017) 'Complex Brain Network Analysis and Its Applications to Brain Disorders: A Survey', *Complexity*, 2017. doi: 10.1155/2017/8362741.

Liu, Y. *et al.* (2017) 'Functional brain network alterations in clinically isolated syndrome and multiple sclerosis: A graph-based connectome study', *Radiology*, 282(2), pp. 534–541. doi: 10.1148/radiol.2016152843.

Logothetis, N. K. (2008) 'What we can do and what we cannot do with fMRI', *Nature*, 453(7197), pp. 869–878. doi: 10.1038/nature06976.

Logothetis, N. K. and Wandell, B. A. (2004) 'Interpreting the BOLD signal', *Annual Review of Physiology*, 66, pp. 735–769. doi: 10.1146/annurev.physiol.66.082602.092845.

Logothetis, N.K. (2003). The Underpinnings of the BOLD Functional Magnetic Resonance Imaging Signal. *The Journal of Neuroscience*, 23(10), pp.3963–3971.

Lublin, F. D. *et al.* (2014) '<MS clinical definitions.pdf>', *Neurology*. Available at: https://www.ncbi.nlm.nih.gov/pmc/articles/PMC4117366/pdf/NEUROLOGY2013555623.pdf.

Manjaly, Z. M. *et al.* (2019) 'Pathophysiological and cognitive mechanisms of fatigue in multiple sclerosis', *Journal of Neurology, Neurosurgery and Psychiatry*, 90(6), pp. 642–651. doi: 10.1136/jnnp-2018-320050.

Martínez-Lapiscina, E. H. *et al.* (2014) 'The visual pathway as a model to understand brain damage in

multiple sclerosis', *Multiple Sclerosis Journal*, 20(13), pp. 1678–1685. doi: 10.1177/1352458514542862.

Matthew Brett, Jean-Luc Anton, Romain Valabregue, Jean-Baptiste Poline. Region of interest analysis using an SPM toolbox [abstract] Presented at the 8th International Conference on Functional Mapping of the Human Brain, June 2-6, 2002, Sendai, Japan. Available on CD-ROM in NeuroImage, Vol 16, No 2.

Meyer-Moock, S. *et al.* (2014) 'Systematic literature review and validity evaluation of the Expanded Disability Status Scale (EDSS) and the Multiple Sclerosis Functional Composite (MSFC) in patients with multiple sclerosis', *BMC Neurology*. BMC Neurology, 14(1), pp. 1–10. doi: 10.1186/1471-2377-14-58.

Miri Ashtiani, S. N. *et al.* (2018) 'Altered topological properties of brain networks in the early MS patients revealed by cognitive task-related fMRI and graph theory', *Biomedical Signal Processing and Control*. Elsevier Ltd, 40, pp. 385–395. doi: 10.1016/j.bspc.2017.10.006.

Miri Ashtiani, S. N. *et al.* (2019) 'Analysis of brain functional connectivity network in MS patients constructed by modular structure of sparse weights from cognitive task-related fMRI', *Australasian Physical and Engineering Sciences in Medicine*. Springer International Publishing, 42(4), pp. 921–938. doi: 10.1007/s13246-019-00790-1.

Monti, M. M. (2011) 'Statistical analysis of fMRI time-series: A critical review of the GLM approach', *Frontiers in Human Neuroscience*, 5(MARCH), pp. 1–13. doi: 10.3389/fnhum.2011.00028.

Ogawa, S. *et al.* (1992) 'Intrinsic signal changes accompanying sensory stimulation: Functional brain mapping with magnetic resonance imaging', *Proceedings of the National Academy of Sciences of the United States of America*, 89(13), pp. 5951–5955. doi: 10.1073/pnas.89.13.5951.

Oh, J., Vidal-Jordana, A. and Montalban, X. (2018) 'Multiple sclerosis: Clinical aspects', *Current Opinion in Neurology*, 31(6), pp. 752–759. doi: 10.1097/WCO.0000000000000622.

Opsahl, T., Agneessens, F. and Skvoretz, J. (2010) 'Node centrality in weighted networks: Generalizing degree and shortest paths', *Social Networks*. Elsevier B.V., 32(3), pp. 245–251. doi: 10.1016/j.socnet.2010.03.006.

Pagani, E. *et al.* (2020) 'Structural connectivity in multiple sclerosis and modeling of disconnection', *Multiple Sclerosis Journal*, 26(2), pp. 220–232. doi: 10.1177/1352458518820759.

Palejwala, A. H. *et al.* (2020) 'Anatomy and white matter connections of the fusiform gyrus', *Scientific Reports*. Nature Publishing Group UK, 10(1), pp. 1–12. doi: 10.1038/s41598-020-70410-6.

Parry, A. M. M. *et al.* (2003) 'Potentially adaptive functional changes in cognitive processing for patients with multiple sclerosis and their acute modulation by rivastigmine', *Brain*, 126(12), pp. 2750–2760. doi: 10.1093/brain/awg284.

Pavlova, M. A. *et al.* (2017) '"wrong Way Up": Temporal and Spatial Dynamics of the Networks for Body Motion Processing at 9.4 T', *Cerebral Cortex*, 27(11), pp. 5318–5330. doi: 10.1093/cercor/bhx151.

Peelen, M. V., Wiggett, A. J. and Downing, P. E. (2006) 'Patterns of fMRI activity dissociate overlapping functional brain areas that respond to biological motion', *Neuron*, 49(6), pp. 815–822. doi: 10.1016/j.neuron.2006.02.004.

Peixoto, S. and Abreu, P. (2016) 'Alterações na Ressonância Magnética Preditoras da Conversão da Síndrome Clinicamente Isolada em Esclerose Múltipla Magnetic Resonance Imaging Conversion Predictors of Clinically Isolated Syndrome to Multiple Sclerosis', pp. 742–748.

Poline, J. B. and Brett, M. (2012) 'The general linear model and fMRI: Does love last forever?', *NeuroImage*. Elsevier Inc., 62(2), pp. 871–880. doi: 10.1016/j.neuroimage.2012.01.133.

Preziosa, P. *et al.* (2017) 'Progression of regional atrophy in the left hemisphere contributes to clinical and cognitive deterioration in multiple sclerosis: A 5-year study', *Human Brain Mapping*, 38(11), pp. 5648–5665. doi: 10.1002/hbm.23755.

Reddy, H. *et al.* (2002) 'Functional brain reorganization for hand movement in patients with multiple sclerosis: Defining distinct effects of injury and disability', *Brain*, 125(12), pp. 2646–2657. doi: 10.1093/brain/awf283.

Rocca, M. A. *et al.* (2016) 'Impaired functional integration in multiple sclerosis: a graph theory study', *Brain Structure and Function*, 221(1), pp. 115–131. doi: 10.1007/s00429-014-0896-4.

Rocca, M. A. and Filippi, M. (2017) 'Functional reorganization is a maladaptive response to injury - YES', *Multiple Sclerosis*, 23(2), pp. 191–194. doi: 10.1177/1352458516667242.

Rodriguez-Rincon, D. *et al.* (2019) 'Exploring the societal burden of multiple sclerosis: A study into the non-clinical impact of the disease, including changes with progression', *Exploring the societal burden of multiple sclerosis: A study into the non-clinical impact of the disease, including changes with progression*. doi: 10.7249/rr4262.

Roebroeck, A., Formisano, E. and Goebel, R. (2005) 'Mapping directed influence over the brain using Granger causality and fMRI', *NeuroImage*, 25(1), pp. 230–242. doi: 10.1016/j.neuroimage.2004.11.017.

Roebroeck, A., Formisano, E. and Goebel, R. (2011) 'The identification of interacting networks in the brain using fMRI: Model selection, causality and deconvolution', *NeuroImage*. Elsevier Inc., 58(2), pp. 296–302. doi: 10.1016/j.neuroimage.2009.09.036.

Rolls, E. T. *et al.* (2020) 'Beyond the disconnectivity hypothesis of schizophrenia', *Cerebral Cortex*, 30(3), pp. 1213–1233. doi: 10.1093/cercor/bhz161.

Rubinov, M. and Sporns, O. (2010) 'Complex network measures of brain connectivity: Uses and interpretations', *NeuroImage*. Elsevier Inc., 52(3), pp. 1059–1069. doi: 10.1016/j.neuroimage.2009.10.003.

Rytsar, R. *et al.* (2011) 'Inhibition in early Alzheimer's disease: An fMRI-based study of effective connectivity', *NeuroImage*. Elsevier Inc., 57(3), pp. 1131–1139. doi: 10.1016/j.neuroimage.2011.05.029.

Sacchet, M. D. *et al.* (2015) 'Support vector machine classification of major depressive disorder using diffusion-weighted neuroimaging and graph theory', *Frontiers in Psychiatry*, 6(FEB), pp. 1–10. doi: 10.3389/fpsyt.2015.00021.

Saygin, A. P. *et al.* (2004) 'Point-light biological motion perception activates human premotor cortex', *Journal of Neuroscience*, 24(27), pp. 6181–6188. doi: 10.1523/JNEUROSCI.0504-04.2004.

Saygin, A. P. (2007) 'Superior temporal and premotor brain areas necessary for biological motion perception', *Brain*, 130(9), pp. 2452–2461. doi: 10.1093/brain/awm162.

Schallmo, M. P. *et al.* (2021) 'Assessing methods for geometric distortion compensation in 7 T gradient echo functional MRI data', *Human Brain Mapping*, 42(13), pp. 4205–4223. doi: 10.1002/hbm.25540.

Schild, H.H. and Berlex Laboratories (1999). *MRI made easy : (... well almost)*. Wayne, Nj: Berlex Laboratories.

Schlemm, E. *et al.* (2017) 'Altered topology of structural brain networks in patients with Gilles de la Tourette syndrome', *Scientific Reports*. Springer US, 7(1), pp. 1–12. doi: 10.1038/s41598-017-10920-y.

Schoonheim, M. M. (2017) 'Functional reorganization is a maladaptive response to injury - Commentary', *Multiple Sclerosis*, 23(2), pp. 194–196. doi: 10.1177/1352458516677593.

Seth, A. K., Barrett, A. B. and Barnett, L. (2015) 'Granger causality analysis in neuroscience and neuroimaging', *Journal of Neuroscience*, 35(8), pp. 3293–3297. doi: 10.1523/JNEUROSCI.4399-14.2015.

Seth, A. K., Chorley, P. and Barnett, L. C. (2013) 'Granger causality analysis of fMRI BOLD signals is invariant to hemodynamic convolution but not downsampling', *NeuroImage*. Elsevier Inc., 65, pp. 540–555. doi: 10.1016/j.neuroimage.2012.09.049.

Shu, N. *et al.* (2016) 'Disrupted topological organization of structural and functional brain connectomes in clinically isolated syndrome and multiple sclerosis', *Scientific Reports*. Nature Publishing Group, 6(April), pp. 1–11. doi: 10.1038/srep29383.

Siero, J.C.W., Bhogal, A. and Jansma, J.M. (2013). Blood Oxygenation Level–dependent/Functional Magnetic Resonance Imaging. PET Clinics, 8(3), pp.329–344.

Soares, J. F. *et al.* (2021) 'On the optimal strategy for tackling head motion in fMRI data', *BIOSIGNALS 2021 - 14th International Conference on Bio-Inspired Systems and Signal Processing; Part of the 14th*

International Joint Conference on Biomedical Engineering Systems and Technologies, BIOSTEC 2021, (March), pp. 306–313. doi: 10.5220/0010327803060313.

Sokolov, A. A. *et al.* (2018) 'Structural and effective brain connectivity underlying biological motion detection', *Proceedings of the National Academy of Sciences of the United States of America*, 115(51), pp. E12034–E12042. doi: 10.1073/pnas.1812859115.

Solana, E. *et al.* (2019) 'Modified connectivity of vulnerable brain nodes in multiple sclerosis, their impact on cognition and their discriminative value', *Scientific Reports*. Springer US, 9(1), pp. 1–8. doi: 10.1038/s41598-019-56806-z.

Sousa, C. *et al.* (2018) 'Validation of the brief international cognitive assessment for multiple sclerosis (BICAMS) in the Portuguese population with multiple sclerosis 11 Medical and Health Sciences 1109 Neurosciences', *BMC Neurology*. BMC Neurology, 18(1), pp. 1–7. doi: 10.1186/s12883-018-1175-4.

Sporns, O. (2013a) 'Network attributes for segregation and integration in the human brain', *Current Opinion in Neurobiology*. Elsevier Ltd, 23(2), pp. 162–171. doi: 10.1016/j.conb.2012.11.015.

Sporns, O. (2013b) 'Structure and function of complex brain networks', *Dialogues in Clinical Neuroscience*, 15(3), pp. 247–262. doi: 10.31887/dcns.2013.15.3/osporns.

Staffen, W. *et al.* (2002) 'Cognitive function and fMRI in patients with multiple sclerosis: Evidence for compensatory cortical activation during an attention task', *Brain*, 125(6), pp. 1275–1282. doi: 10.1093/brain/awf125.

Stanley, M. L. *et al.* (2015) 'Changes in brain network efficiency and working memory performance in aging', *PLoS ONE*, 10(4), pp. 1–17. doi: 10.1371/journal.pone.0123950.

Stefancin, P. *et al.* (2019) 'Resting-state functional connectivity networks associated with fatigue in multiple sclerosis with early age onset', *Multiple Sclerosis and Related Disorders*. Elsevier B.V., 31(March), pp. 101–105. doi: 10.1016/j.msard.2019.03.020.

Stephan, K. E. *et al.* (2007) 'Interhemispheric integration of visual processing during task-driven lateralization', *Journal of Neuroscience*, 27(13), pp. 3512–3522. doi: 10.1523/JNEUROSCI.4766-06.2007.

Su, S. *et al.* (2017) 'Decreased global network efficiency in young male smoker: An EEG study during the resting state', *Frontiers in Psychology*, 8(SEP), pp. 1–8. doi: 10.3389/fpsyg.2017.01605.

Sunaert, S. *et al.* (1999) 'Motion-responsive regions of the human brain', *Experimental Brain Research*, 127(4), pp. 355–370. doi: 10.1007/s002210050804.

Tahedl, M. *et al.* (2018) 'Functional connectivity in multiple sclerosis: Recent findings and future directions', *Frontiers in Neurology*, 9(OCT), pp. 1–18. doi: 10.3389/fneur.2018.00828.

Tewarie, P. *et al.* (2014) 'Functional brain network analysis using minimum spanning trees in Multiple Sclerosis: An MEG source-space study', *NeuroImage*. Elsevier Inc., 88, pp. 308–318. doi: 10.1016/j.neuroimage.2013.10.022.

Thedchanamoorthy, G. *et al.* (2014) 'Node assortativity in complex networks: An alternative approach', *Procedia Computer Science*. Elsevier Masson SAS, 29, pp. 2449–2461. doi: 10.1016/j.procs.2014.05.229.

Thompson, A. J. *et al.* (2018) 'Diagnosis of multiple sclerosis: 2017 revisions of the McDonald criteria', *The Lancet Neurology*, 17(2), pp. 162–173. doi: 10.1016/S1474-4422(17)30470-2.

Tootell, R.B.H., Mendola, J.D., Hadjikhani, N.K., Ledden, P.J., Liu, Arthur.K., Reppas, J.B., Sereno, M.I. and Dale, A.M. (1997). Functional Analysis of V3A and Related Areas in Human Visual Cortex. *The Journal of Neuroscience*, 17(18), pp.7060–7078.

Tops, M. and Boksem, M. A. S. (2011) 'A potential role of the inferior frontal gyrus and anterior insula in cognitive control, brain rhythms, and event-related potentials', *Frontiers in Psychology*, 2(NOV), pp. 1–14. doi: 10.3389/fpsyg.2011.00330.

Traboulsee, A. *et al.* (2005) 'Conventional MRI Techniques in Multiple Sclerosis', *MR Imaging in White Matter Diseases of the Brain and Spinal Cord*, pp. 211–223. doi: 10.1007/3-540-27644-0_14.

Trip, S. A. and Miller, D. H. (2005) 'Imaging in multiple sclerosis', *Neurology in Practice*, 76(3). doi: 10.1136/jnnp.2005.073213.

Uddin, L.Q., Nomi, J.S., Hébert-Seropian, B., Ghaziri, J. and Boucher, O. (2017). Structure and Function of the Human Insula. *Journal of Clinical Neurophysiology*, [online] 34(4), pp.300–306. Available at: https://dx.doi.org/10.1097%2FWNP.0000000000000377.

Uddin, L. Q. (2013) 'Complex relationships between structural and functional brain connectivity', *Trends in Cognitive Sciences*. Elsevier Ltd, 17(12), pp. 600–602. doi: 10.1016/j.tics.2013.09.011.

Vaina, L. M. *et al.* (2001) 'Functional neuroanatomy of biological motion perception in humans', *Proceedings of the National Academy of Sciences of the United States of America*, 98(20), pp. 11656–11661. doi: 10.1073/pnas.191374198.

Vitorino, R. *et al.* (2016) 'Regional frontal perfusion deficits in relapsing-remitting multiple sclerosis with cognitive decline', *American Journal of Neuroradiology*, 37(10), pp. 1800–1807. doi: 10.3174/ajnr.A4824.

Walton, C., King, R., Rechtman, L., Kaye, W., Leray, E., Marrie, R.A., Robertson, N., La Rocca, N., Uitdehaag, B., van der Mei, I., Wallin, M., Helme, A., Angood Napier, C., Rijke, N. and Baneke, P. (2020). Rising prevalence of multiple sclerosis worldwide: Insights from the Atlas of MS, third edition. *Multiple Sclerosis Journal*, 26(14), pp.1816–1821.

Welton, T. *et al.* (2015) 'Reproducibility of Graph-Theoretic Brain Network Metrics: A Systematic Review', *Brain Connectivity*, 5(4), pp. 193–202. doi: 10.1089/brain.2014.0313.

Welton, T. *et al.* (2020) 'Graph Theoretic Analysis of Brain Connectomics in Multiple Sclerosis: Reliability and Relationship with Cognition', *Brain Connectivity*, 10(2), pp. 95–104. doi: 10.1089/brain.2019.0717.

Xia, M., Wang, J. and He, Y. (2013) 'BrainNet Viewer: A Network Visualization Tool for Human Brain Connectomics', *PLoS ONE*, 8(7). doi: 10.1371/journal.pone.0068910.

Online References

GAEM. (2017). *What is Multiple Esclerosis: the thousand faces disease*. [online] Available at: https://fundaciongaem.org/en/what-is-multiple-sclerosis/

National Multiple Sclerosis Society (2013). *Types of MS*. [online] National Multiple Sclerosis Society. Available at: https://www.nationalmssociety.org/What-is-MS/Types-of-MS.

Another MS Warrior. (2019). *DMT*. [online] Available at: https://anothermswarrior.com/tag/dmt/

Farnsworth, B. (2019). *iMotions*. [online] imotions. Available at: https://imotions.com/blog/eeg-vs-mri-vs-fmri-differences

Birn, R. (n.d.). *Basic physiology of fMRI: signal and noise*. [online] Available at: http://www.humanbrainmapping.org/files/2015/Ed%20Materials/OHBM15_AdvancedFMRI_Birn_Rasmus.pdf

Weisstein, E.W. (n.d.). *Graph Eccentricity*. [online] mathworld.wolfram.com. Available at: https://mathworld.wolfram.com/GraphEccentricity.html

Shaw, A. (2019). *Understanding The Concepts of Eigenvector Centrality And Pagerank*. [online] Strategic Planet. Available at: https://www.strategic-planet.com/2019/07/understanding-the-concepts-of-eigenvector-centrality-and-pagerank/.

BrainSuite. (n.d.). *bias field correction · BrainSuite*. [online] Available at: http://brainsuite.org/processing/surfaceextraction/bfc/

Nykamp, D. (n.d.). An introduction to networks - Math Insight. [online] mathinsight.org. Available at: https://mathinsight.org/network_introduction.

Appendix I

Individual F-matrices

The following matrices represent the individual ROI x ROI matrices for each participant from both groups (healthy controls and MS patients), in the V1MT run and in the BM runs.

The matrix on the left represents the pairwise Granger F-values for each connection between every two regions involved in the task, with the colorbar representing these F-values, and the matrix on the right represents the statistically significant connections, after performing the F-test ($p < 0.05$).

RUN V1MT

CNT01

CNT02

CNT03

CNT04

CNT05

CNT06

CNT07
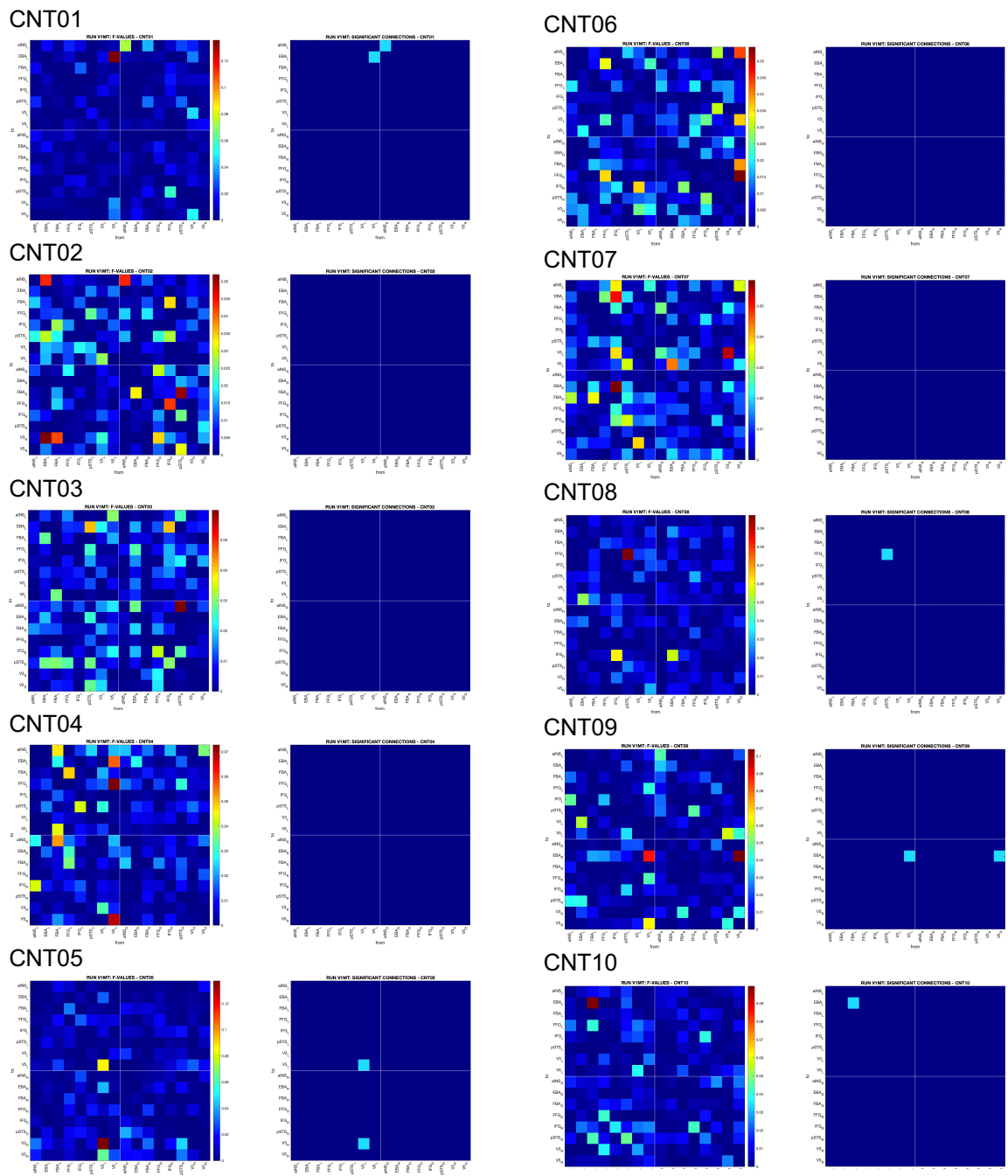
CNT08
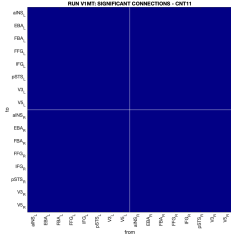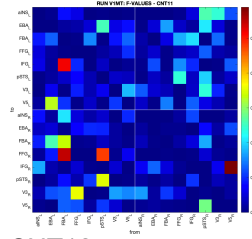
CNT09
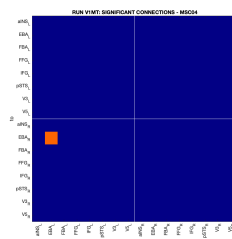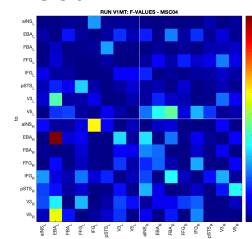
CNT10
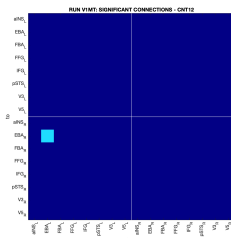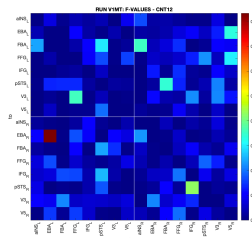
CNT11
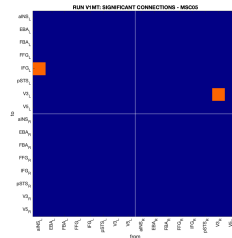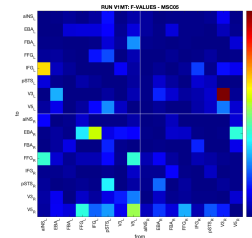
MSC04

CNT12

MSC05

CNT13
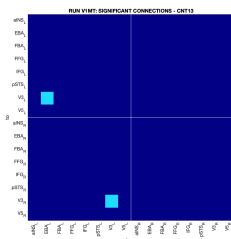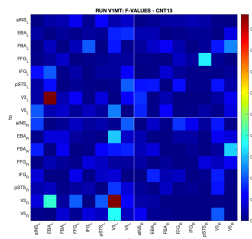
MSC06
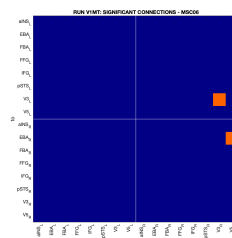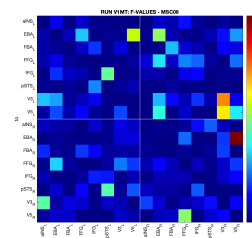
CNT14
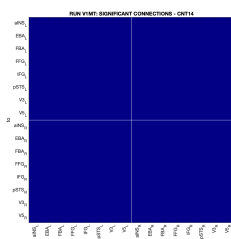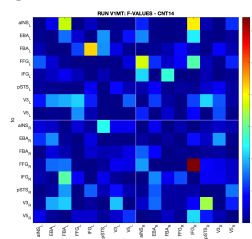
MSC07
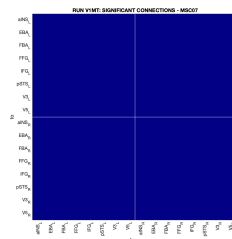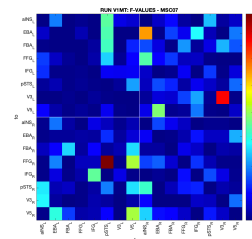
MSC01
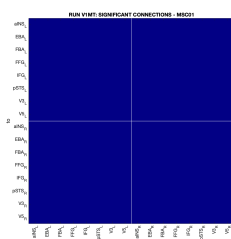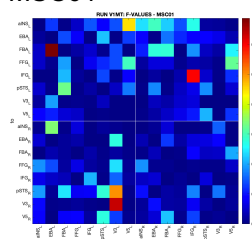
MSC08
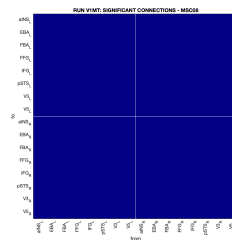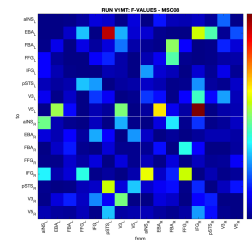
MSC02
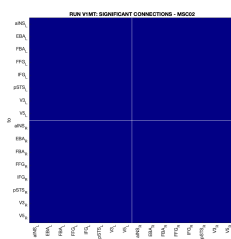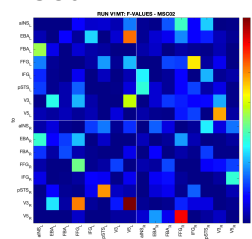
MSC09
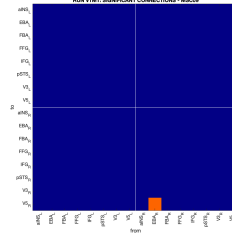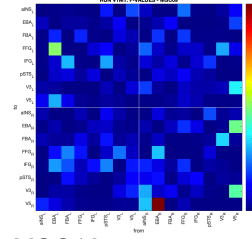
MSC03
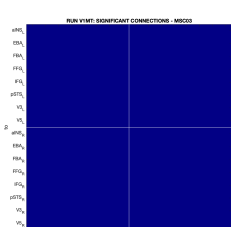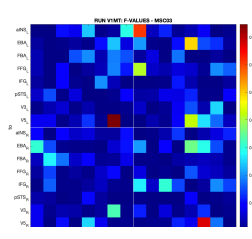
MSC10
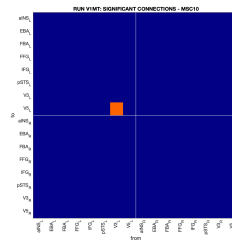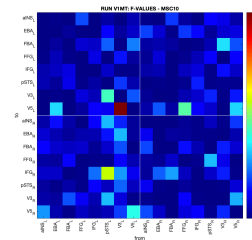
MSC11
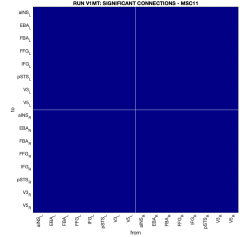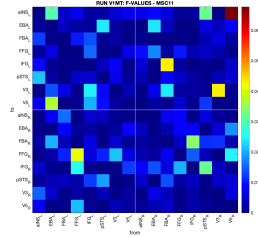
MSC14
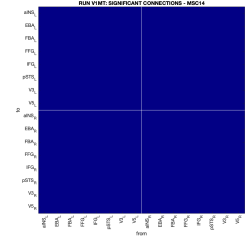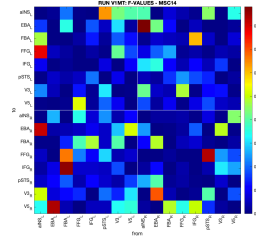
MSC12
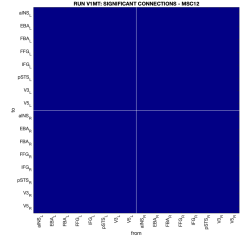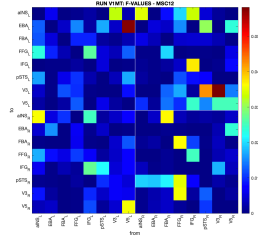
MSC15
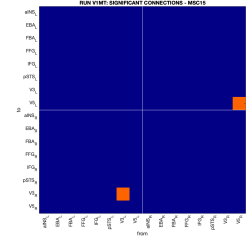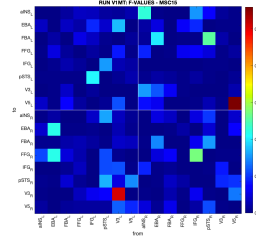
MSC13
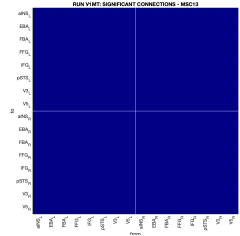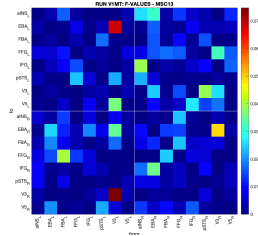
RUNS BM

CNT01
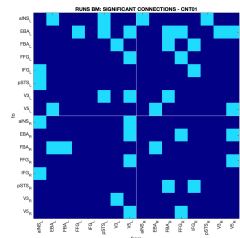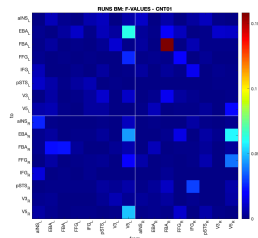
CNT04
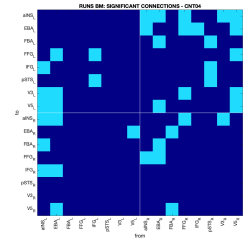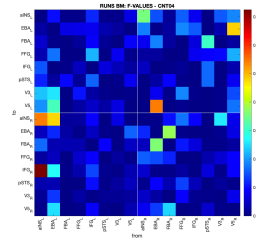
CNT02
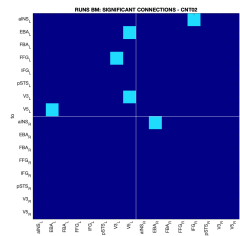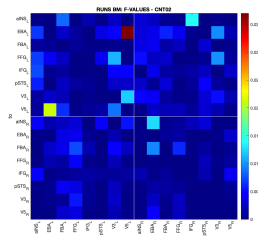
CNT05
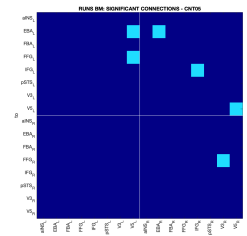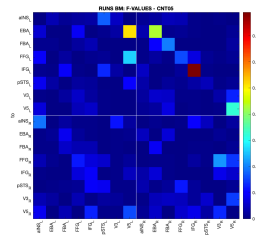
CNT03

CNT06

CNT07

CNT08

CNT09

CNT10

CNT11

CNT12

CNT13

CNT14

MSC01

MSC02

MSC03

MSC04

MSC05

MSC06

135
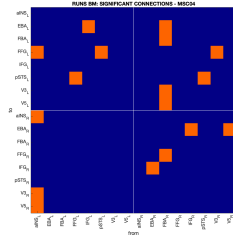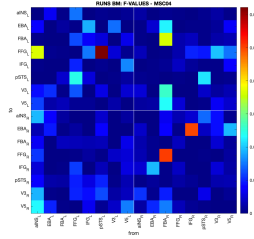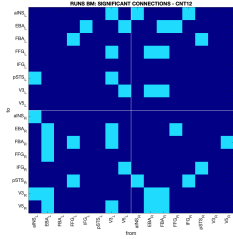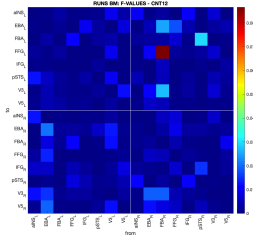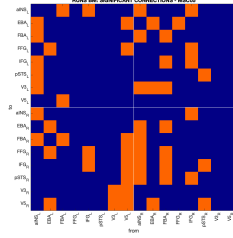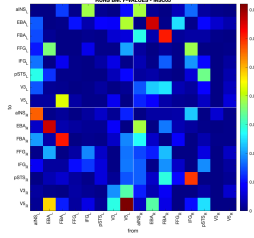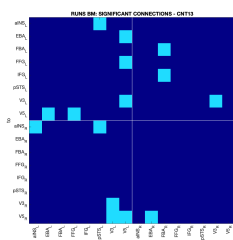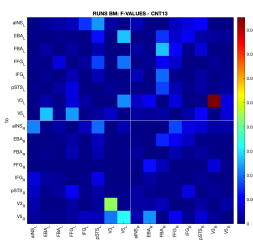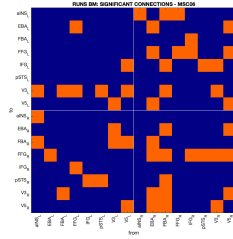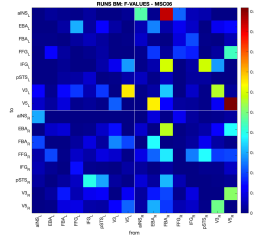
MSC07
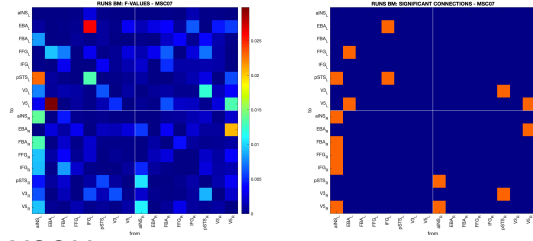
MSC12
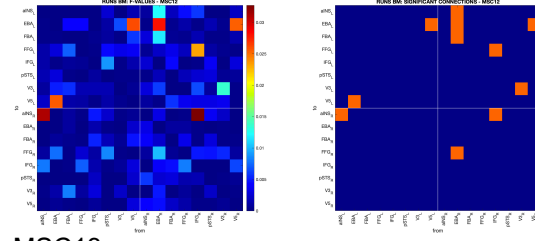
MSC08
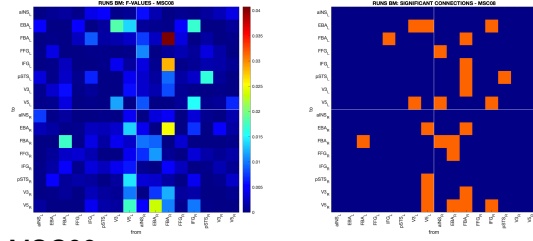
MSC13
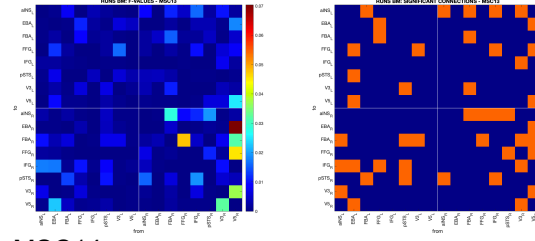
MSC09
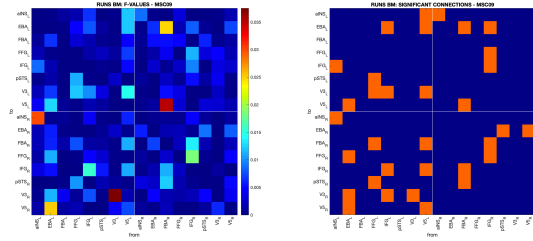
MSC14
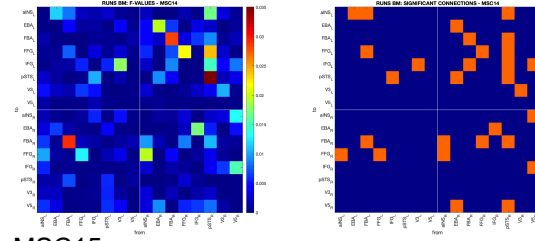
MSC10
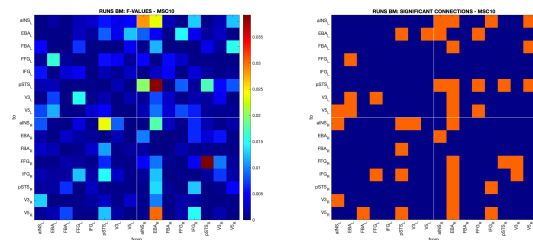
MSC15
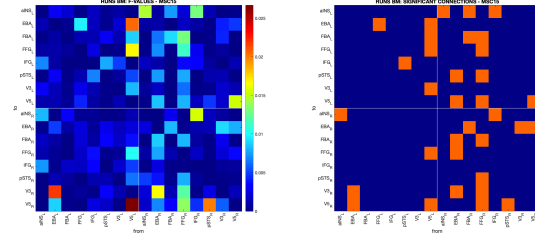
MSC11
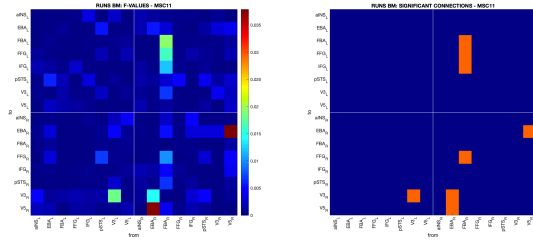
Appendix II

Significantly different nodes (between groups) – local connectivity measures

The following matrices represent the nodes and corresponding metrics that are statistically significantly different between groups, for the local measures, in the V1MT run and in the BM runs. Wilcoxon rank sum test was performed and the nodes with a p-value < 0.05 are represented in light blue. The nodes in dark blue have a p-value < 0.1 (tendency for statistical significance).

The first range of thresholds that was evaluated was 0.05 < PTh < 0.5, with steps of 0.05. Then, according to the metrics with the largest number of significantly different metrics and nodes, a new range of thresholds is chosen, with steps of 0.01.

RUN V1MT

PTh = 0.05
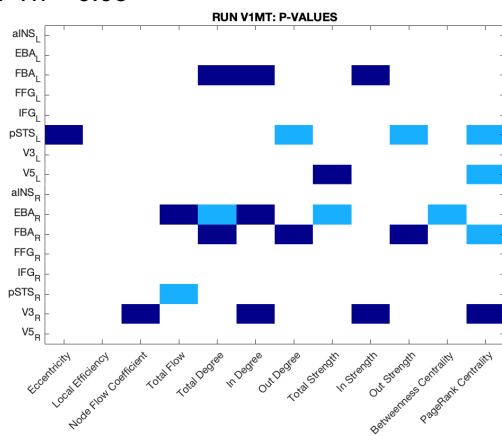
PTh = 0.15
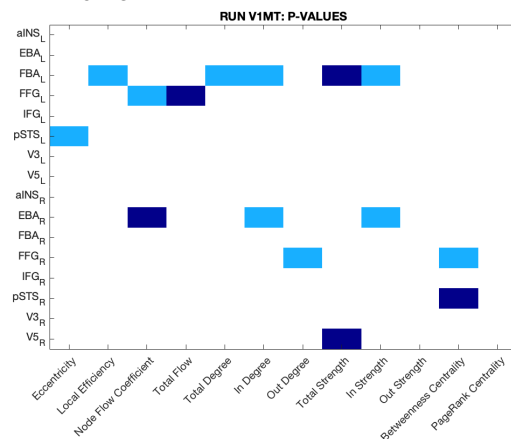
PTh = 0.1
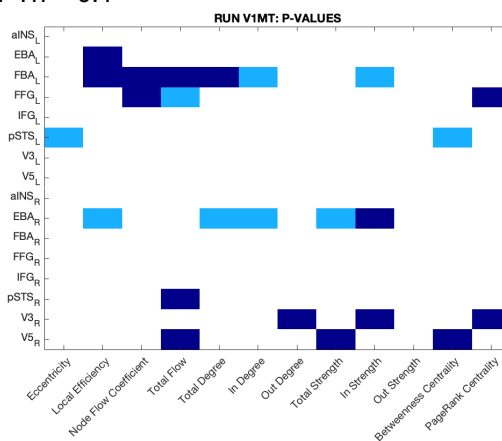
PTh = 0.2
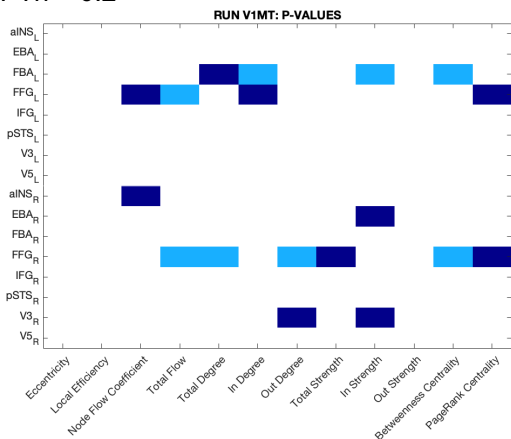
PTh = 0.25
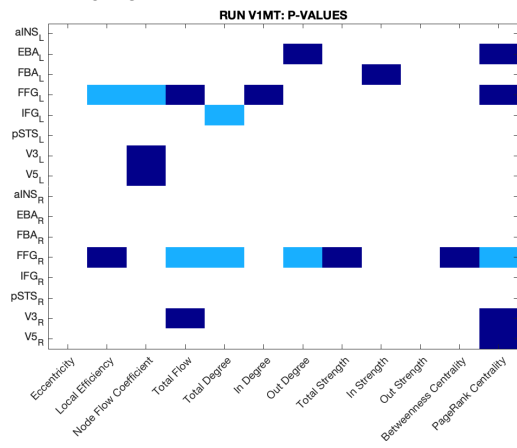
PTh = 0.4
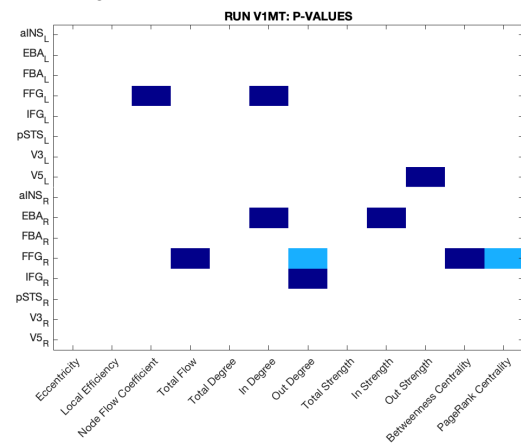
PTh = 0.3
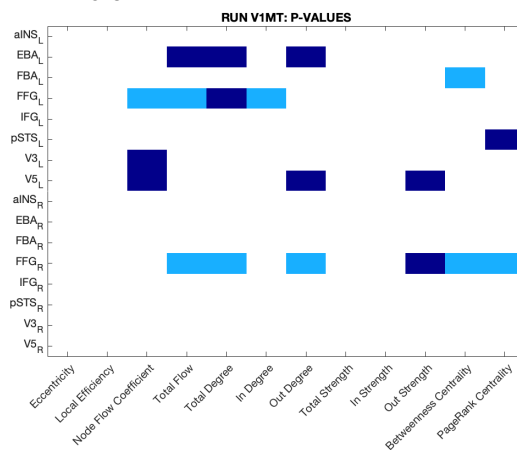
PTh = 0.45
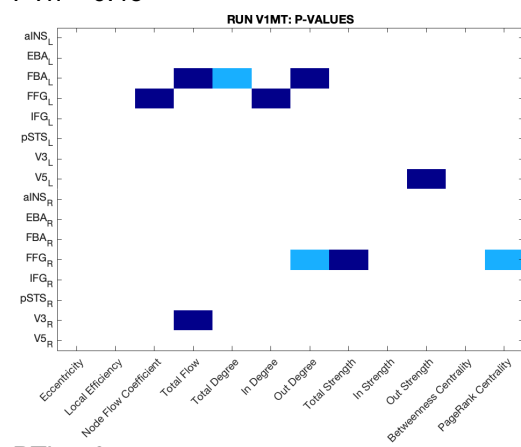
PTh = 0.35
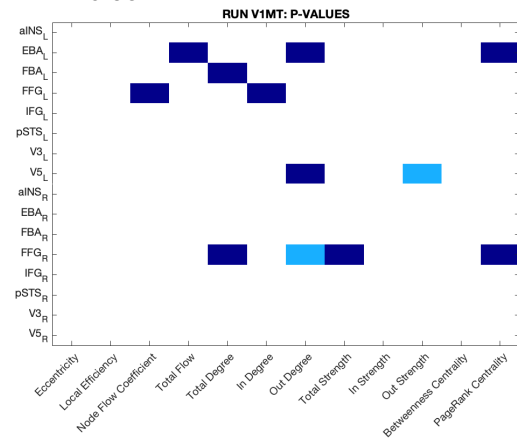
PTh = 0.5
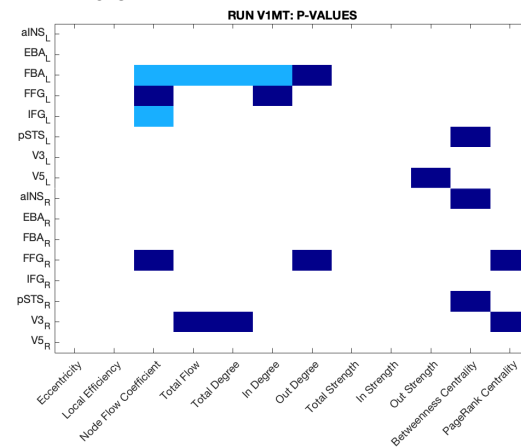
The two closest thresholds which yielded the largest number of significantly different connectivity measures and nodes were PTh = 0.1 (8 metrics and 9 nodes) and PTh = 0.15 (8 metrics and 10 nodes). These thresholds were chosen to repeat the above procedure, but now with smaller steps of 0.01.

PTh = 0.1
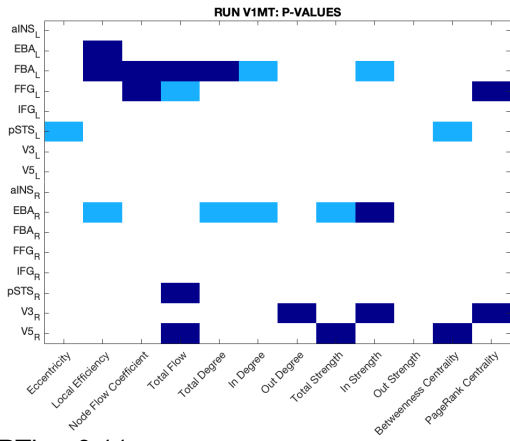
PTh = 0.14
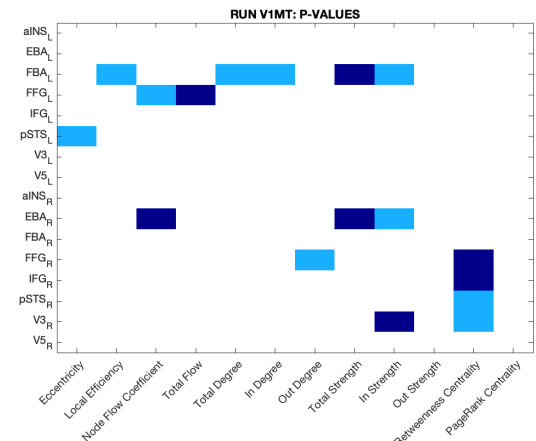
PTh = 0.11
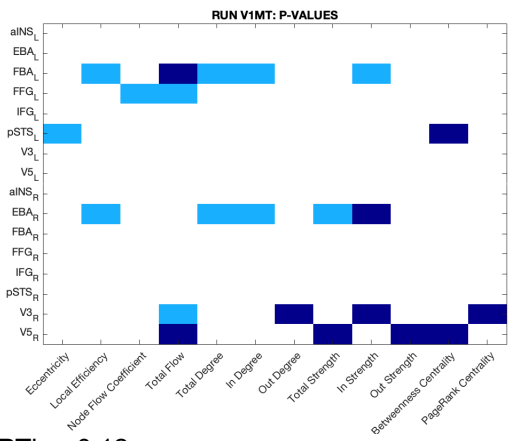
PTh = 0.15
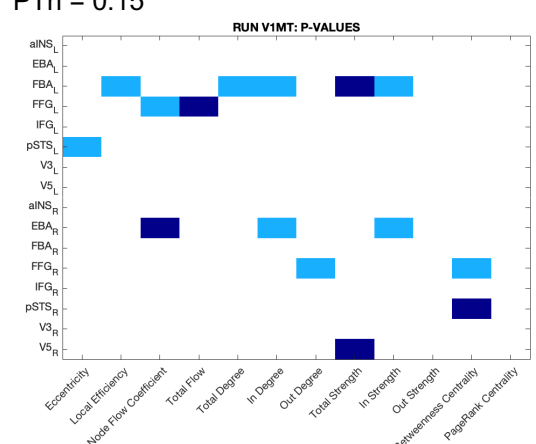
PTh = 0.12
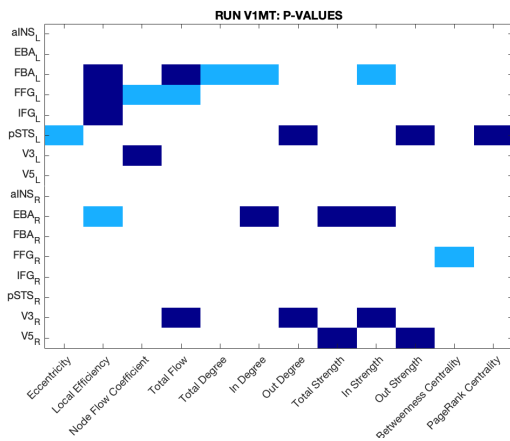
PTh = 0.13
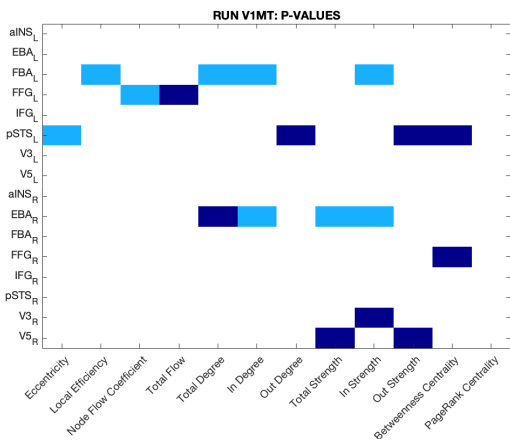
RUNS BM

PTh = 0.05
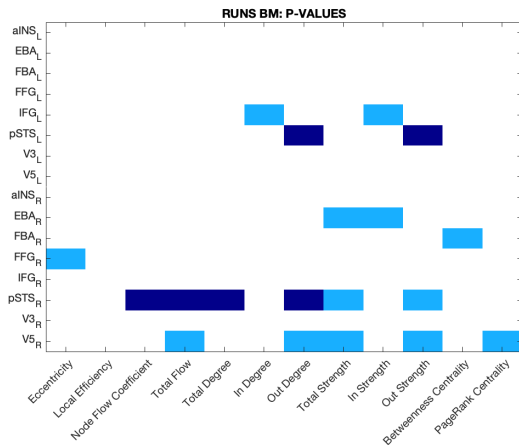
PTh = 0.1
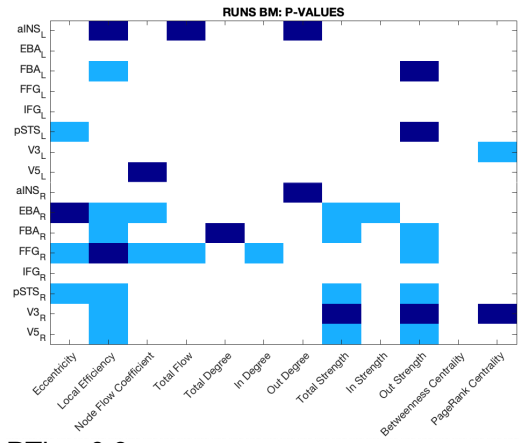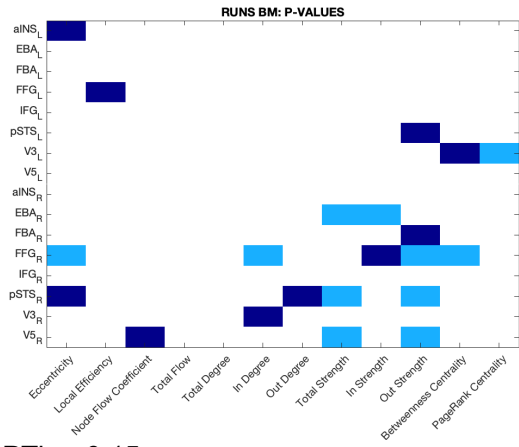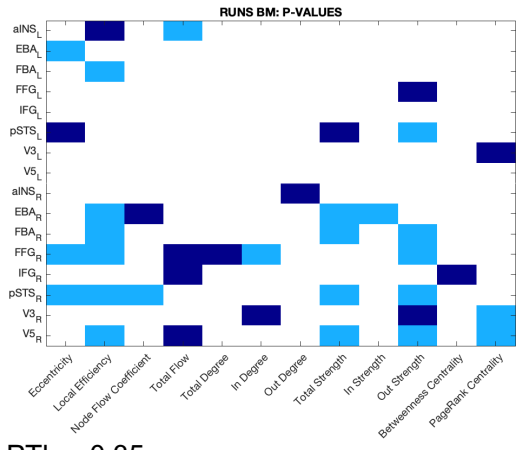
PTh = 0.15
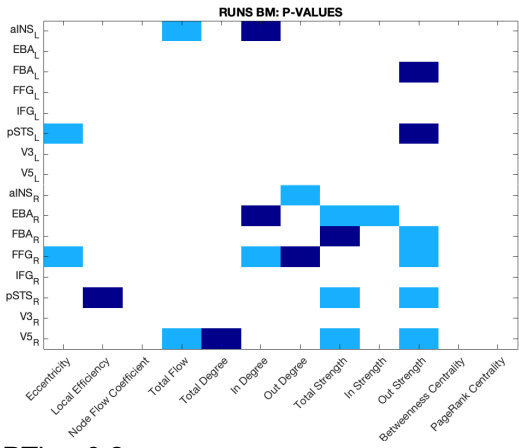
PTh = 0.2
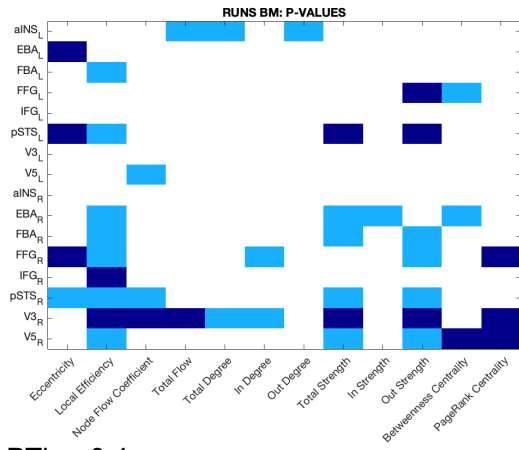
PTh = 0.25
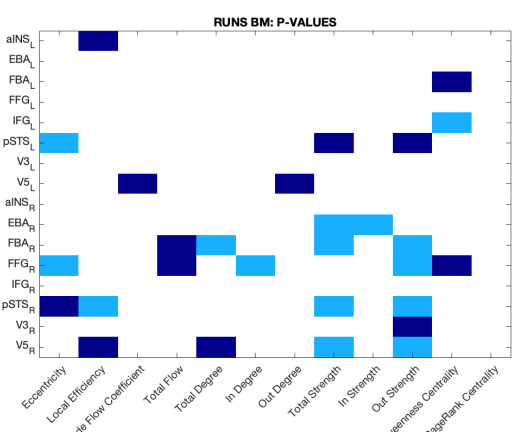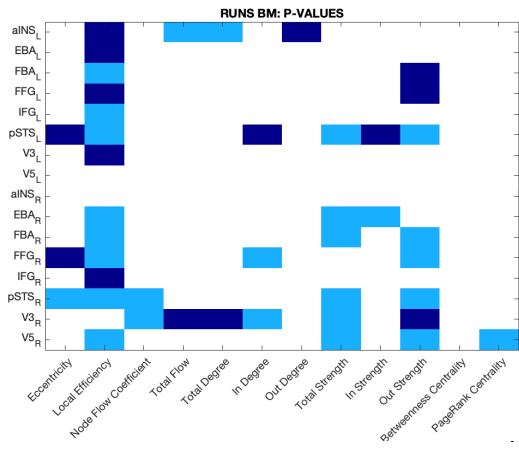
PTh = 0.3

PTh = 0.35
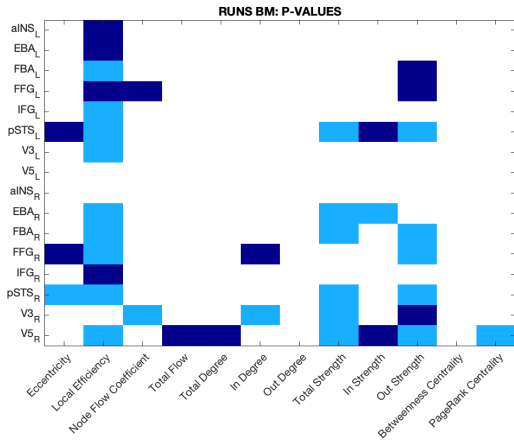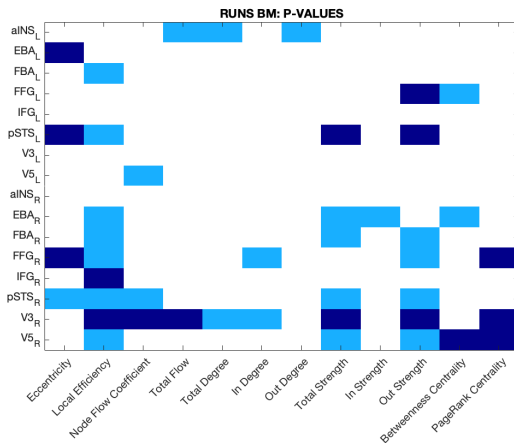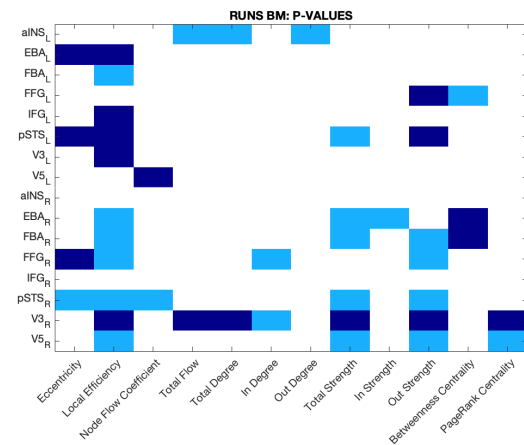

PTh = 0.4

PTh = 0.45

PTh = 0.5
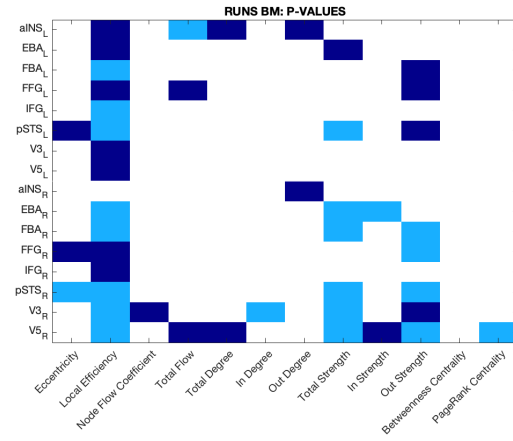
The range of thresholds with the largest number of significantly different connectivity measures and nodes was between PTh = 0.35 (which has the highest number of metrics: 11 metrics, 27 nodes) and PTh = 0.4 (which has the highest number of nodes: 10 metrics, 28 nodes). These thresholds were chosen to repeat the above procedure, but now with smaller steps of 0.01.
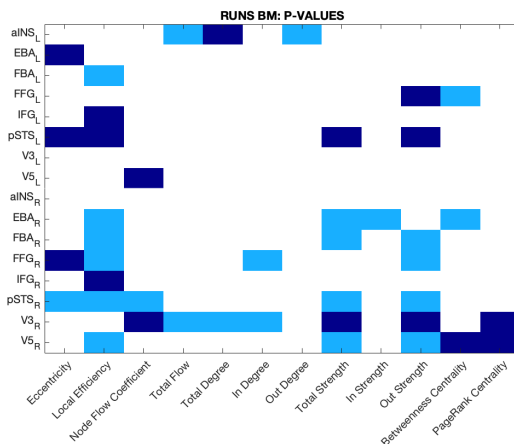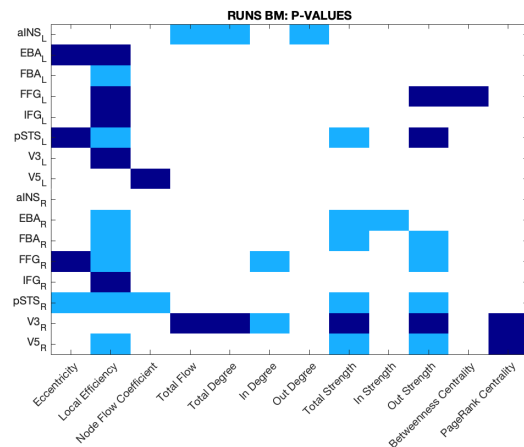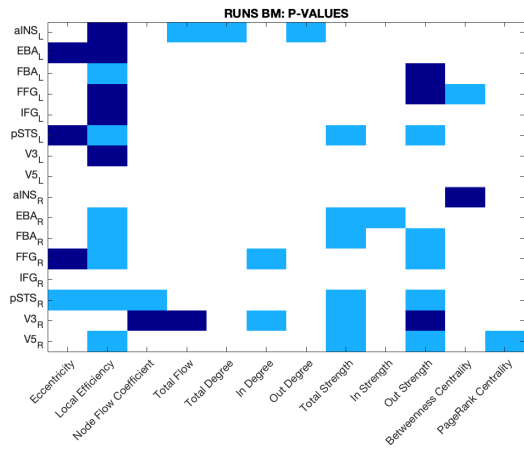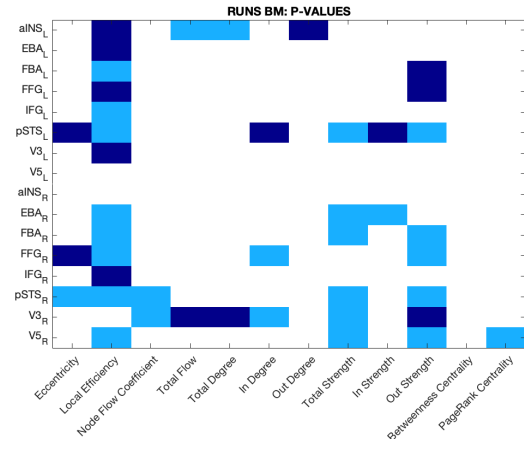
PTh = 0.35

PTh = 0.37

PTh = 0.36

PTh = 0.38

PTh = 0.39

RUNS BM: P-VALUES

PTh = 0.4

RUNS BM: P-VALUES

Appendix III

Code

All of the code developed to obtain the results can be found in the following link:
https://github.com/joanasantos13/Code-Thesis-MIEB.git

More specifically:

- extracttimecourse.m – function that extracts the average BOLD time course of the 16 regions elicited by the task.

- mvgc.m – function adapted from the *mvgc_demo* script provided by the MVGC toolbox that applies the Granger causality principles and functions.

- F_matrices.m – applies the *mvgc* function to the fMRI time courses extracted previously and obtains the matrices with F-values that represent directed functional connectivity.

- withingroup_analysis.m – calculates the mean matrices and performs within-group analysis with the F-test.

- betweengroup_analysis.m – performs between-group analysis with the Wilcoxon rank sum test.

- connectivitymeasures_run1.m
- connectivitymeasures_run2_3.m – calculates the global and local connectivity measures with BCT and performs statistical analysis of the results.

- barplots_metrics.m – constructs the barplots of section 5.7 in which the thresholds are represented in the x-axis, and the number of nodes presenting significantly different metrics between groups are in the y-axis.

- neuropsychology_run1.m
- neuropsychology_run2_3.m – performs Spearman correlation in order to find whether the F-values of connectivity are correlated with the neuropsychological tests' results of the MS patients.